University of South Bohemia in České Budějovice

Faculty of Science

Tuning carotenoid photophysics by changes in structure and local environment

Ph.D. Thesis

Emrah ÖZCAN

Supervisor: prof. RNDr. Tomáš Polívka, Ph.D.

Faculty of Science, University of South Bohemia in České Budějovice

České Budějovice 2024

This thesis should be cited as:
ÖZCAN, E., 2024: Tuning carotenoid photophysics by changes in structure and local environment. University of South Bohemia, Faculty of Science, České Budějovice, Czech Republic, 160 pp.

Annotation

This thesis investigates the complex dynamics of excited states in carotenoids, focusing on the origins and properties of certain dark states and how they are affected by external disturbances such as metal interactions, pH changes, applied voltage, and chemical modifications. Paper I demonstrates the creation of stable astaxanthin-metal complexes and their altered excited-state dynamics, revealing shortened lifetimes and enhanced ICT bands due to metal-ion interactions. Paper II explores the effect of external voltage on 8'-apo-β-carotenal, showing that applied voltage can control the ICT state amplitude and extend its lifetime. Paper III examines pH-dependent effects on crocin, finding significant pH-induced shifts and stabilization at basic pH levels. Paper IV presents the synthesis and analysis of bis-phenylhydrazone astaxanthin, highlighting its modified excited-state dynamics and the potential for organic modification to study new effects. These findings enhance our understanding of carotenoid excited states and suggest new research approaches.

Declaration

I hereby declare that I am the author of this dissertation and that I have used only those sources and literature detailed in the list of references.

Emrah ÖZCAN
České Budějovice
18.7.2024

This thesis originated from a partnership of Faculty of Science, University of South Bohemia of the Czech Republic, supporting doctoral studies in the Biophysics study programme.

Financial support

The research presented in this thesis was supported by grant from the Czech Science Foundation (19-28323X).

To my Family

Acknowledgements

The most genuine guide in life is science.

Mustafa Kemal ATATÜRK

I am deeply grateful to the many people and elements that have contributed to this work and made this thesis possible. Expressing my gratitude in words is challenging for me, but I have to acknowledge their invaluable support and assistance.

Five years ago, when I was on the brink of leaving the scientific community, a single email from Tomáš Polívka changed everything in my life. His support rekindled my passion for science and kept me in the field. I am deeply grateful and extend my heartfelt thanks to him. He not only reopened the door to science for me but has continually supported and provided opportunities to work on many fascinating projects and be part of an amazing team. His unwavering encouragement and guidance have been instrumental in my journey, and for that, I am forever thankful.

Within this remarkable team, I have met many wonderful people who have done more than just teach me about science; they have made me feel at home despite living in a foreign country. They have always been by my side, offering support and assistance with every challenge I faced. I would like to express my heartfelt gratitude to each of them: Gurkan, Ivca, Tuhin, David, Valja, Milan, Marcel, Franta, Radek, Vašek I, and Vašek II. Their kindness and camaraderie have enriched my experience beyond measure. I also want to thank Pavel; it was a pleasure to work with you in Lund, Sweden.

In navigating life's challenges and pursuing my doctoral education, I am profoundly grateful to Dr. Hasan Hüseyin Kazan, Samet Özdem, Uğur Keskin, Alparslan İzgün, and Özgür Kılıç. These friends, who have stood by me since high school, have unfailingly provided their unwavering support. I am also thankful to Nejat and Silvi, my close friends here, who have always supported me and shared many beautiful moments with me. Additionally, I extend my gratitude to all the friends I have met in Czechia for their unwavering support and companionship.

Finally, I must express my profound gratitude to the Özcan family. My heartfelt thanks go to my dear mother Lisangül Özcan, my father Bimbek Özcan, my brothers Erol and Erdem Özcan, and my sister Sedanur Özcan. They have unquestionably played the most significant role in bringing me to this point, always providing unwavering and unconditional support. Additionally, I want to extend my gratitude to Epp Maria Lililupu for her constant love and support.

Last but not least, I wanna thank me…

List of papers and author's contribution

The thesis is based on the following papers (listed chronologically):

I. **Özcan, E.,** Kuznetsova, V., Keşan, G., Fuciman, M., Litvín, R., & Polívka, T. (2023). Ultrafast excited states dynamics of metal ion complexes of the carotenoid astaxanthin. Journal of Photochemistry and Photobiology A: Chemistry, 441, 114737. (IF = 4.10)
Emrah Özcan did all experimental work and data analysis, dominantly contributed to writing the original and revised manuscript. His contribution was 75 %.

II. Keşan, G., **Özcan, E.,** Chábera, P., Polívka, T., & Fuciman, M. (2023). Time-Resolved Spectroelectrochemical Dynamics of Carotenoid 8'-apo-β-Carotenal. ChemPlusChem, 88(11), e202300404. (IF = 5.90)
Emrah Özcan participated in planning and conducting the experiments and data analysis. His contribution was 35 %.

III. **Özcan, E.,** Šímová, I., Bína, D., Litvín, R., & Polívka, T. (2024). Ultrafast spectroscopy of the hydrophilic carotenoid crocin at various pH. Physical Chemistry Chemical Physics, 26(13), 10225-10233. (IF = 3.67)
Emrah Özcan actively participated on design of the project, did most experimental work and data analysis, and dominantly contributed to writing the original and revised manuscript. His contribution was 80 %.

IV. **Özcan, E.,** Keşan, G., Chábera, P., Litvín, R., & Polívka, T. (2024). Synthesis and spectroscopic properties of carotenoid bis-phenylhydrazone astaxanthin: Extending conjugation to a C= N group. New Journal of Chemistry. (IF = 3.59)
Emrah Özcan proposed and realized the whole project, did all synthesis, spectroscopy and data analysis, and wrote the first version of the manuscript. His contribution was 90 % and he is the corresponding author of this manuscript.

The following articles by Emrah ÖZCAN, listed in chronological order, are not directly related to the author's thesis:

I. Aksoy, B. T., Keşan, G., **Özcan, E.,** Eçik, E. T., Dere, A., Karabulut, A., & Çoşut, B. (2020). Solution-processable BODIPY decorated triazine photodiodes and their comprehensive photophysical evaluation. New Journal of Chemistry, 44(5), 2155-2165. (IF = 3.59)

II. **Özcan, E.,** Aksoy, B. T., Eçik, E. T., Dere, A., Karabulut, A., Yakuphanoglu, F., & Çoşut, B. (2020). Fabrication of hybrid photodiode systems: BODIPY decorated cyclotriphosphazene covalently grafted graphene oxides. Inorganic Chemistry Frontiers, 7(16), 2920-2931. (IF = 6.10)

III. Kazan, H. H., **Özcan, E.,** Çoşut, B., Çiftçi, G. Y., & Eçik, E. T. (2020). Novel BODIPY-subphthalocyanine dyads with reasonable photodynamic therapy behaviours. New Journal of Chemistry, 44(32), 13738-13744. (IF = 3.59)

IV. Ayhan, M. M., **Özcan, E.,** Dedeoglu, B., Chumakov, Y., Zorlu, Y., & Coşut, B. (2021). Carbon (sp3) tetrel bonding mediated BODIPY supramolecular assembly via unprecedented synergy of C sp3⋯ N and C sp3⋯ F pair interactions. CrystEngComm, 23(2), 268-272. (IF = 3.75)

V. Eçik, E. T., **Özcan, E.,** Kazan, H. H., Erol, I., Şenkuytu, E., & Çoşut, B. (2021). Dual color triads: synthesis, photophysics, and applications in live cell imaging. New Journal of Chemistry, 45(22), 9984-9994. (IF = 3.59)

VI. **Özcan, E.,** Dedeoglu, B., Chumakov, Y., Zorlu, Y., Çoşut, B., & Ayhan, M. M. (2021). Modulation of supramolecular self-assembly of BODIPY tectons via halogen bonding. CrystEngComm, 23(36), 6365-6375. (IF = 3.75)

VII. **Özcan, E.,** Dedeoglu, B., Chumakov, Y., Gürek, A. G., Zorlu, Y., Çoşut, B., & Menaf Ayhan, M. (2021). Halogen-Bonded BODIPY Frameworks with Tunable Optical Features. Chemistry–A European Journal, 27(5), 1603-1608. (IF = 5.020)

VIII. Ayhan, M. M., **Özcan, E.,** Alkan, F., Çetin, M., Ün, İ., Bardelang, D., & Çoşut, B. (2022). External complexation of BODIPYs by CB [7] improves in-cell fluorescence imaging. Materials Advances, 3(1), 547-553. (IF = 5.20)

IX. **Özcan, E.,**Saglam, M. F., Kazan, H. H., Erol, I., Sengul, I. F., & Cosut, B. (2023). Indolyl imine substituted BODIPY systems; synthesis, photophysical, and biological properties. Tetrahedron, 137, 133367. (IF = 2.10)

Co-author agreement

Prof. Tomáš Polívka, the supervisor of this Ph.D. thesis, corresponding author of papers 1 and 3, and co-author of papers 2 and 4, fully acknowledges the stated contribution of Emrah Özcan to these manuscripts.

Tomáš Polívka

Digitally signed by Tomáš Polívka
Date: 2024.07.18 14:54:31 +02'00'

.....

Prof. RNDr. Tomáš Polívka, Ph.D.

Contents

1. Introduction

Pigments are important compounds in living organisms, providing color, which is a key element supporting organisms in their interaction with the surrounding environment and playing a role in their development. In addition to coloration, various pigments play essential roles in photoprotection and light collection. These pigments are found in nearly all structures of organisms, including leaves, fruits, seeds, vegetables, flowers, blood, skin, or eyes [1]. They are also often present in drugs and cosmetics [1]. As chemical compounds, the key property of pigments is their ability to absorb light in the visible region. Color arises from the properties of chromophores, where a part of incoming energy is used to promote an electron to a higher orbital while the non-absorbed energy is reflected back into the environment [2]. The classification of pigments can be based on their origins and the chemical structure of the chromophore. By origin, pigments are classified as natural or synthetic. Natural pigments are those occurring in various organisms, including plants, fungi, animals, and microorganisms, whereas synthetic pigments are produced in laboratories [3]. According to a chromophore-based classification, pigments can be sorted based on the type of their conjugated systems. These include linear carotenoids, polyenes and bilins, aromatic anthocyanins or tyrosine-based betalains, or metal-coordinated porphyrins like chlorophyll [4]. Natural pigments can further be categorized according to their structural characteristics as tetrapyrrole derivatives (such as chlorophylls and heme), isoprenoid derivatives (like carotenoids and iridoids), N-heterocyclic compounds excluding tetrapyrroles (such as purines, pterins, flavins, phenazines, phenoxazines, and betalains), benzopyrane derivatives (including anthocyanins and other flavonoid pigments), quinones (like benzoquinone, naphthoquinone, anthraquinone), and melanins [1, 2, 5].

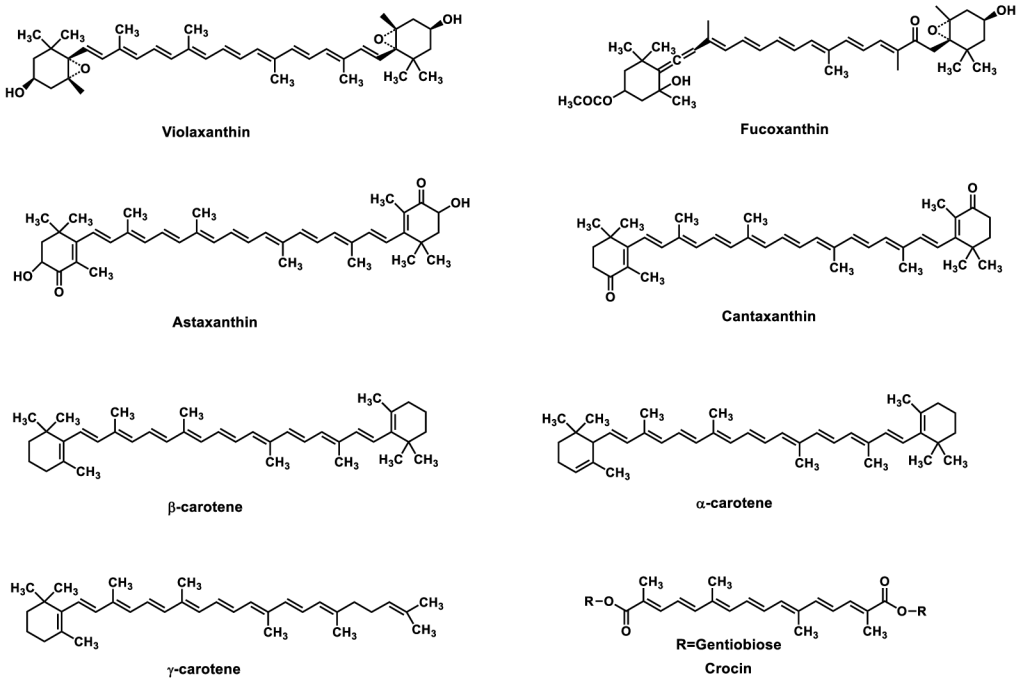

Figure 1. Structure of some common carotenoids. Data obtained from [6].

Carotenoids are widespread in nature, with approximately 1000 different types identified to date. The carotenoids are isoprenoids that contain a polyene chain with 3-15 conjugated double

bonds. This conjugated backbone defines the absorption spectrum and consequently, the color of the carotenoid. Often, the central conjugated backbone of carotenoids is functionalised, with characteristics such as cyclization at one or both ends being common. Formally, carotenoids are classified into two groups: pure hydrocarbons (carotenes) and oxygenated xanthophylls. They are synthesized in plants and microorganisms. Isopentenyl diphosphate, formed via either the mevalonate-dependent or independent pathway, leads to the formation of phytoene through a series of addition and condensation reactions. Phytoene is then converted to lycopene whose cyclization forms β-carotene and subsequent synthetic pathways form xanthophylls, such as β-cryptoxanthin, zeaxanthin, antheraxanthin, and violaxanthin or α-carotene and lutein (**Figure 1**) [6]. Actual synthetic pathways beyond phytoene vary with organisms, eventually generating the large variation of carotenoid structures [7].

Carotenoids are colored pigments, absorbing between yellow to deep red produced by all photosynthetic bacteria, algae, higher plants, cyanobacteria, and also by non-photosynthetic bacteria, fungi and yeasts. Furthermore, dietary carotenoids could change the colour of insects, birds, and marine invertebrates. The carotenoids are commercial compounds used as colorants for human food and nutritional supplements [8]. As a class of hydrocarbons, typical carotenoids consist of eight isoprenoid units joined in a head-to-tail pattern except at the centre of a carotenoid molecule. This structural organization makes these compounds symmetric as the two central methyl groups are in a 1,6-positional relationship while the remaining non-terminal groups are in a 1,5-positional relationship (**Figure 2**) [6].

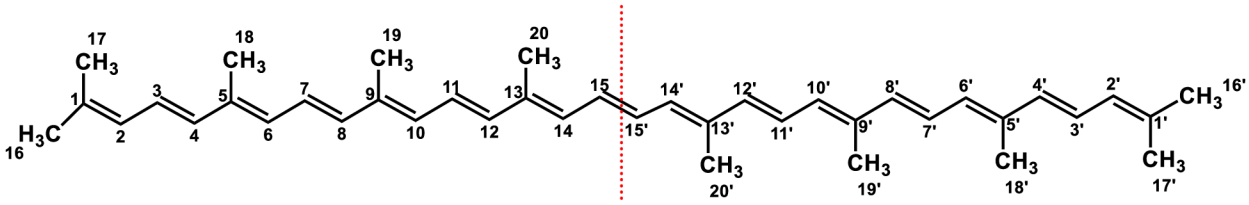

Figure 2. Structure of carotenoid lycopene. Data obtained from [6].

The backbone of the majority of carotenoids consists of a 40-carbon polyene chain (**Figure 1**). This chain could be terminated by cyclic end groups and/or complemented with functional groups containing oxygen. The structure of carotenoids determines their biological function, which is another classification style for carotenoids (**Table 1**). In addition to their absorption properties, the structure of carotenoids also gives rise to specific redox properties, forming the basis of their antioxidant function. Various end groups affect the polarity of carotenoids, leading to altered biological function through interaction with their protein or membrane environment [6, 9].

Table 1. Classification of the carotenoids. Data obtained from [6].

Basis	Sub-group	Characteristics	Example
Structure	Carotenes	Constituting carbon and hydrogen	α-carotene, β-carotene, β-cryptoxanthin
	Xanthophylls	Constituting carbon, hyrdrogen, and oxygen	lutein,zeaxanthin,violaxanthin, fucoxanthin
Cyclization	Acyclic	End group not closed	lycopene
	Alicyclic a.Monocyclic	One end group open, one closed	γ-carotene
	b. Bicyclic	Both closed	β-carotene
Structural alteration	Allenic	Continuous double bond	neoxanthin
	Acetylenic	Presence of a triple bond	alloxanthin
	Apocarotenoid	Less than 40 Carbon atoms	bixin, crocetin
	Higher carotenoid	More than 40 Carbon atoms	rhodoxanthin
Function	Primary	Required for photosynthetic process in plants	β-carotene, zeaxanthin,lutein,violaxanthin, antheraxanthin,neoxanthin
	Secondary	Presence not directly related to plant survival	α-carotene,capsanthin,bixin,lycopene, astaxanthin (carotenoids localized in fruits and flowers)

1.1. **Functions of carotenoids**

Carotenoids have been proved to have significant antioxidant activity [10]. Dietary carotenoids also display provitamin A activity, anti-cancer activity towards certain types of cancers, and preventive activity against age-related macular degeneration [11-13]. The carotenoids have been revealed as potent quenchers of singlet oxygen [14, 15]. They can react with radical species such as singlet oxygen, superoxide anion, hydrogen peroxide, nitrogen oxide, and other reactive species, primarily in various biological systems (**Figure 3**). Anti-oxidant activity is affected by the structure of the carotenoids; the number of the double bonds is correlated with the anti-oxidant activity and various substituents can affect the antioxidant activity as well. [16, 17]. In photosynthetic organisms, carotenoids perform a variety of functions. They collect and absorb light and transfer the absorbed energy to (bacterio)chlorophylls (BChl), scavenge singlet oxygen, quench BChl triplet state, dissipate the excess energy under high-light conditions, and reinforce the antenna system [18]. Carotenoids can carry out one or more of these tasks, depending on the organism.

$$^1O_2{}^* + CAR \rightarrow {}^3O_2 + {}^3CAR^* \quad \textbf{(a)}$$

$$^3CAR^* \rightarrow CAR^* + \text{heat}$$

$$ROO^* + CAR \rightarrow ROO - CAR^* \quad \textbf{(b)}$$

$$ROO - CAR^* + ROO \rightarrow ROO - CAR - ROO$$

Figure 3. Reaction of carotenoid with singlet oxygen (a) and peroxy radical (b). Data obtained from [6].

The major function of carotenoids in photosynthetic organisms is to protect the photosynthetic apparatus from excess light and to serve as light-harvesting agents. During photosynthesis, carotenoids absorb light and transfer it to chlorophylls (Chl) via singlet-singlet excitation energy transfer. This energy transfer typically occurs through the two lowest excited states, denoted as S_1 and S_2 (**Figure 4)** [19]. The efficiency of energy transfer through the S_1 and/or S_2 states is organism-dependent [20].

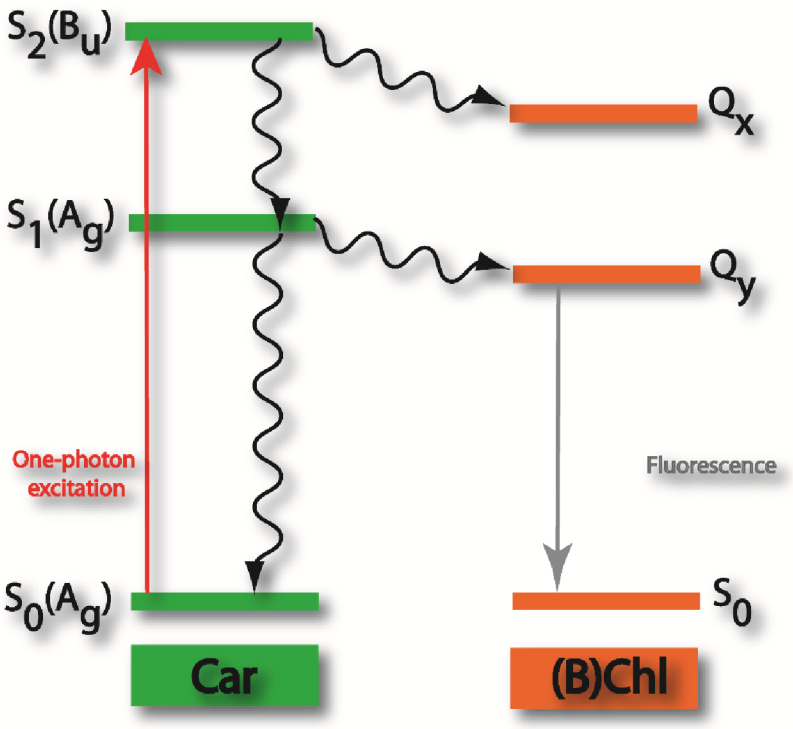

Figure 4. Energy transfer through carotenoids. Data obtained from [19].

Another important function of carotenoids in photosynthetic systems is photoprotection (**Figure 5**). This mechanism of action of carotenoids occurs towards singlet oxygen ($^1O_2$) and reactive oxygen species (ROS). These species oxidize biomolecules, resulting in tissue damage. Singlet oxygen is produced via energy transfer from an excited sensitizer to a ground state oxygen molecule ($^3O_2$). In

photosynthesis, the excited sensitizer is chlorophyll triplet state, and singlet oxygen is generated by a triplet-triplet energy transfer (1):

$$^{3}(\mathrm{B})Chl + {}^{3}O_2 \rightarrow (\mathrm{B})Chl + {}^{1}O_2 \qquad (\mathbf{1})$$

$$^{3}(\mathrm{B})Chl + Car \rightarrow (\mathrm{B})Chl + {}^{3}Car \qquad (\mathbf{2})$$

$$^{1}O_2 + Car \rightarrow {}^{3}O_2 + {}^{3}Car \qquad (\mathbf{3})$$

Carotenoids quench the chlorophyll triplet state to prevent singlet oxygen production (**2**). Singlet oxygen is also scavenged by carotenoids themselves (**3**) [19]. A more detailed description of specific carotenoids studied in this thesis follows in next chapters.

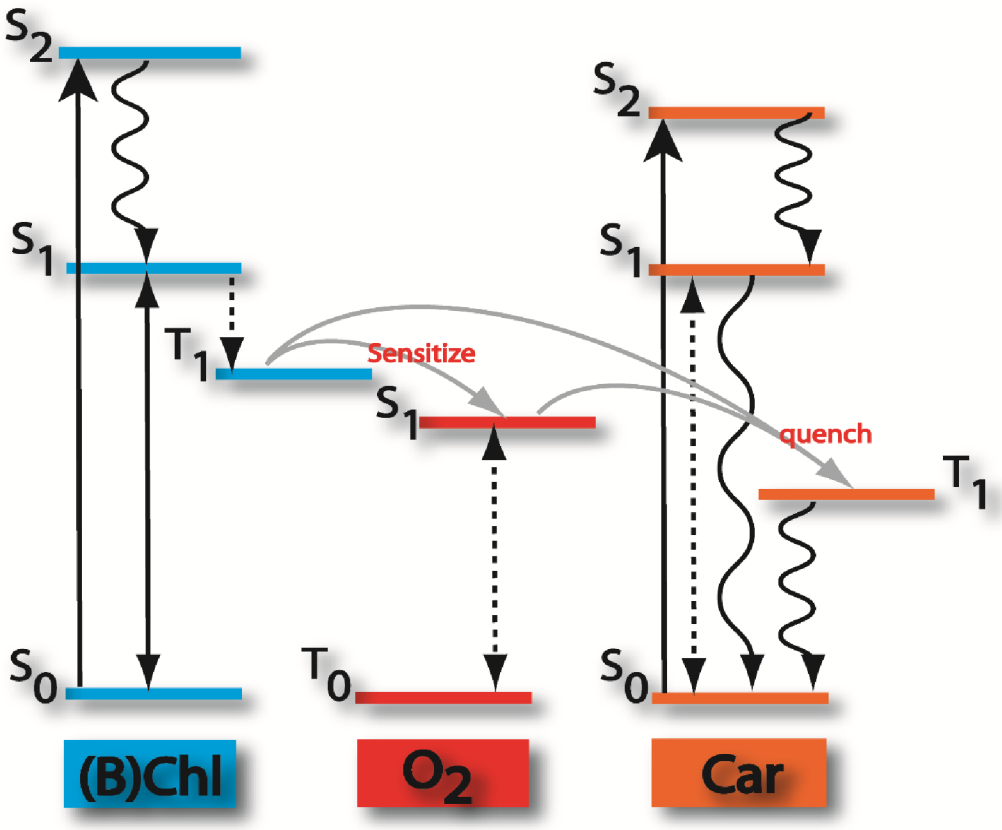

Figure 5. Energy transfer mechanism for photoprotection by carotenoids against singlet oxygen. Data obtained from [19].

1.2. Astaxanthin

Astaxanthin is a member of the xanthophylls family of oxygenated carotenoids. It is produced by freshwater microalgae, and frequently found in salmonids, crustaceans or flamingo feathers, organisms which obtain astaxanthin via diet. It is also often used as feeds for farmed fish. Astaxanthin is critical for those organisms as it promotes pigmentation and adequate growth, as well as reproduction. Owing to its remarkable antioxidant activity compared to other carotenoids, astaxanthin is favorable for preventing diseases such as cardiovascular problems, cancer, and immune

diseases [21, 22]. Astaxanthin has been reported to be more effective than other carotenoids in terms of neutralizing free radicals [23, 24]. Astaxanthin has the molecular formula $C_{40}H_{52}O_4$ with a molar mass of 596.84 g/mol [23, 25]. It has two terminal rings joined by a polyene chain. It consists of two asymmetric carbons (chiral centers) located at the 3, 3' positions of the β-ionone ring with hydroxyl group (-OH) on either end of the molecule. Hydroxyl groups may react with fatty acids forming either mono- di-esters. Astaxanthin exists in various stereoisomers (R/S isomers) such as (3S, 3'S), (3R, 3'R) and (3R, 3'S). These conformers occurs also in astaxanthin isomers and esterified forms [26, 27].

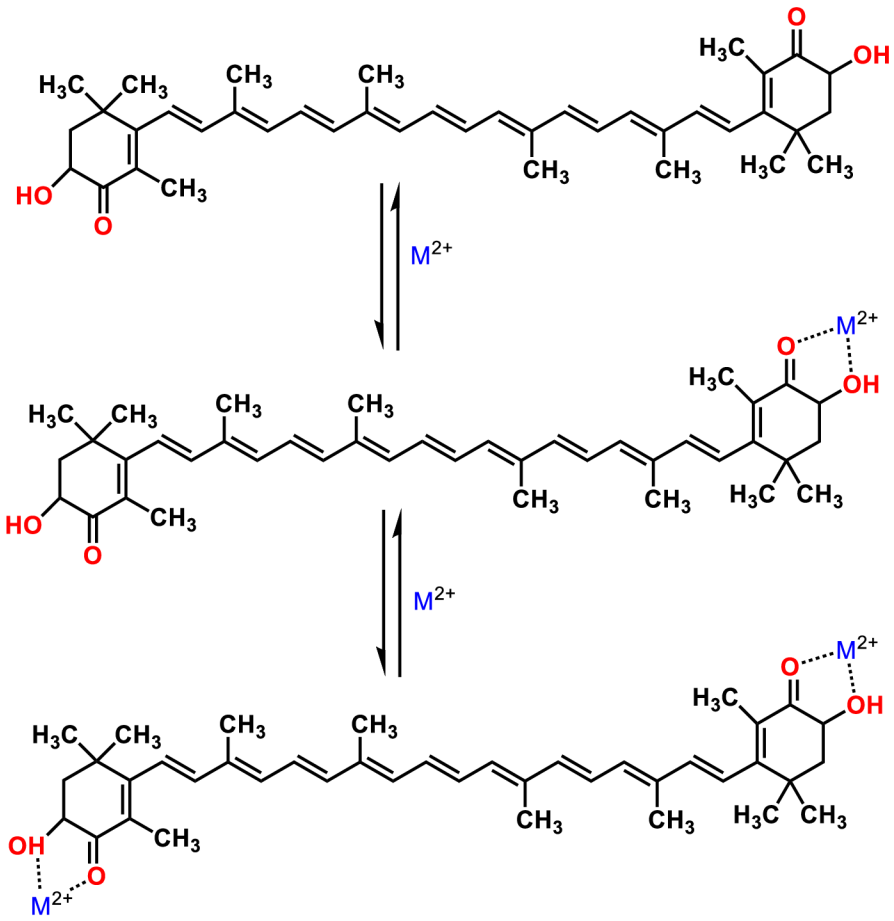

Figure 6. Complexation of astaxanthin with metals. Based on [28].

Astaxanthin has two oxygen atoms on each cyclohexene rings in the form of a keto and hydroxyl group (**Figure 6**). The keto- and hydroxyl groups at the terminal rings offer the possibility of chemical/structural modification or the formation of complexes with metal ions or with organic compounds, thereby novel types of carotenoids [28-30]. Such a tuneable modification of astaxanthin is expected to change the photophysical properties and consequently their colour [31]. The cyclohexene ring structure is similar to that of many hydroxyl quinones and α-hydroxy- ketones, having high biological activity including the ability to form chelate complexes with metal ions [28]. These compounds can also play an important role in the photoprotective action of astaxanthin and they have been shown to broaden the absorption spectra that can provide additional absorption in the visible region [28].

1.3. Crocin

Natural carotenoids are mostly hydrophobic and their activity in biological systems is limited because they aggregate in aqueous environments, causing noticeable changes in their absorption spectra [32-36]. Therefore, synthesis of water-soluble carotenoids has received a lot of attention as the aggregation may lead to loss of function [37-39]. Crocin, the digentiobiosyl ester of crocetin and one of the few important water-soluble carbonyl carotenoids, is the main natural pigment of the gardenia fruit and stigmas of saffron (**Figure 7**). Due to the water solubility, it has numerous applications such as food coloration and antioxidation [40, 41]. Saffron, derived from the stigmas of Crocus sativus, has been used for centuries in the prevention and treatment of various diseases. Therapeutic activity of saffron is predominantly owing to its major bioactive derivatives including crocin and crocetin [42]. Recent studies have shown that crocin was effective against a number of cardiovascular and central nervous system diseases [43]. It has also been used as a spice flavor and food additive, and contains anti-cancer, anti-inflammatory, anti-oxidant, hepatoprotective, and anti-diabetic benefits due to its physiological activity and safety [43-47].

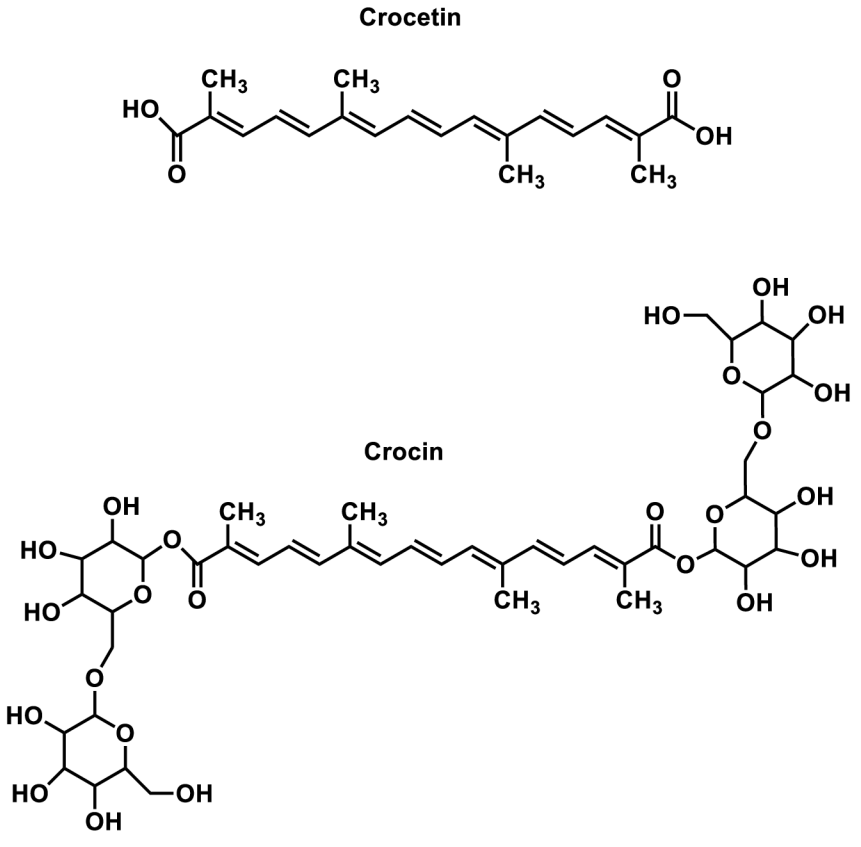

Figure 7. Chemical structure of crocetin and crocin. Based on [41]

Similarly to other carotenoids, the conjugated system of crocin consists of 7 conjugated C=C bonds, and it is extended to two symmetrically positioned C=O groups (**Figure 7**). The bulky gentiobiosyl groups do not contribute to conjugation, but they are responsible for water solubility of

crocin. Crocin has poor stability and is easily degraded under high temperature, oxidation or acidic conditions [41, 43]. Moreover, some studies have reported that high temperature and other environmental factors could break the glycosidic bond of crocin and hydrolyze crocin to crocetin. Crocetin is insoluble in water but it is water-soluble in its anionic form; thus, at basic pH, the ionized carboxyl groups significantly increase water solubility. In contrast to other carotenoids, the hydrophilic nature of crocin allows to study effect of pH on spectroscopic properties. Crocin has a good stability in the aqueous alkali solutions (pH≥9), but acidic conditions (pH<5) lead to degradation because the acidic environment destabilizes the conjugated system of crocin [43, 48-50].

1.4. 8'-apo-β-carotenal

The term "apocarotenoid" is frequently used in the carotenoid community to describe any substance produced by the cleavage of carotenoids [51, 52]. Apocarotenoids and other oxidative breakdown products of carotenoids can be produced in a variety of organisms via enzymatic or non-enzymatic mechanisms [53, 54]. Mammals contain an enzyme that catalyzes the eccentric cleavage of both provitamin A carotenoids (PAC) and non-PACs, resulting in both non-volatile apocarotenoids and volatile molecules [54]. The apocarotenoids formed by the oxidative cleavage of dietary carotenoids are gaining popularity because they may contribute to beneficial health-promoting effects through mechanisms such as cell signalling pathway intervention [55, 56]. They are found in plants, fungi, algae, and microorganisms, serving several functions [57, 58]. These include photosynthesis, responses to stress, photoprotection, and signalling. In animals and humans, intact carotenoids are thought to act as antioxidants [59]. Carotenoids are converted to apocarotenoids, such as 8'-apo-β-carotenal, via oxidative cleavage.

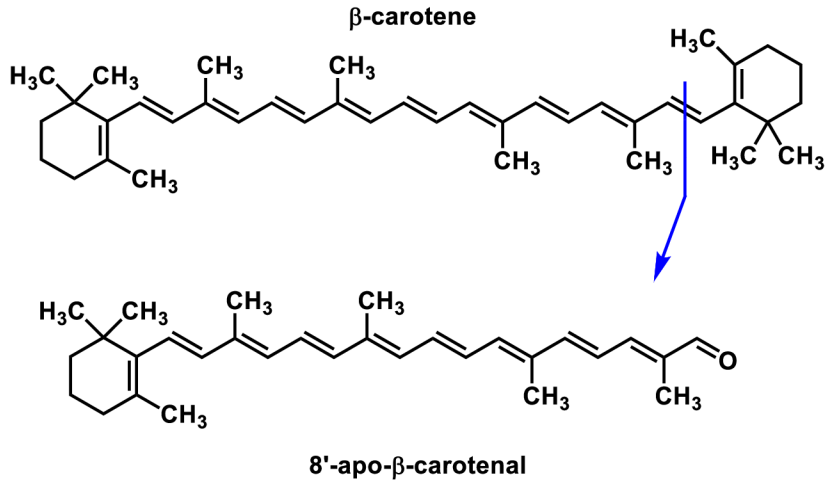

Figure 8. Central cleavages of β-carotene to 8'-apo-β-carotenal. Data obtained from [57].

This process not only generates alternative colorants like bixin but also produces volatile compounds like β-ionone [60]. 8'-apo-β-carotenal, a dark orange colorant, emerges from the oxidative

degradation of β-carotene, showcasing the intricate pathways through which carotenoids contribute to the spectrum of colors and aroma compounds in nature (**Figure 8**) [57, 60].

β-Carotene and β-apo-8’-carotenal are typically used as colorants in processed foods, including soft drinks, snacks, bread, cheese, margarine, and butter. β-Carotene, a dark red to brownish-red pigment, is unstable under light and heat, but stable throughout a wide pH range and can be used to most processed foods. 8’-apo-β-carotenal has great color intensity and can be produced in several colors, including orange, depending on the extraction solvents utilized [60]. Furthermore, 8'-apo-β-carotenal and its analogues are commonly used as synthetic models of carbonyl carotenoids due to their spectroscopic capabilities [61]. They were also used in a variety of artificial systems designed for solar energy conversion [62]. The literature includes detailed studies on the excited state dynamics [63] and electrochemical properties of 8'-apo-β-carotenal [64, 65].

2. Photophysics of Carotenoids

Since carotenoids have remarkable photoprotective and light-harvesting abilities, their photophysical properties have been extensively studied in numerous theoretical and experimental studies. The knowledge of carotenoid photophysics is still limited owing to the complicated excited-state structure, featuring both strongly allowed transitions but also dark states to which the transition from the ground state is forbidden. The understanding of carotenoid photophysics has been promoted by identification of emission spectra of polyenes, which are structurally close to carotenoids. In polyenes, the transition from ground state to the lowest excited state S_1 is symmetry forbidden, because both ground (S_0) and S_1 states have the same Ag^- symmetry. The allowed transition with lowest energy thus occur to the second excited state, S_2, which has Bu^+ symmetry (**Figure 9**). This general picture is valid for all carotenoids as their conjugated chain structure are similar [66].

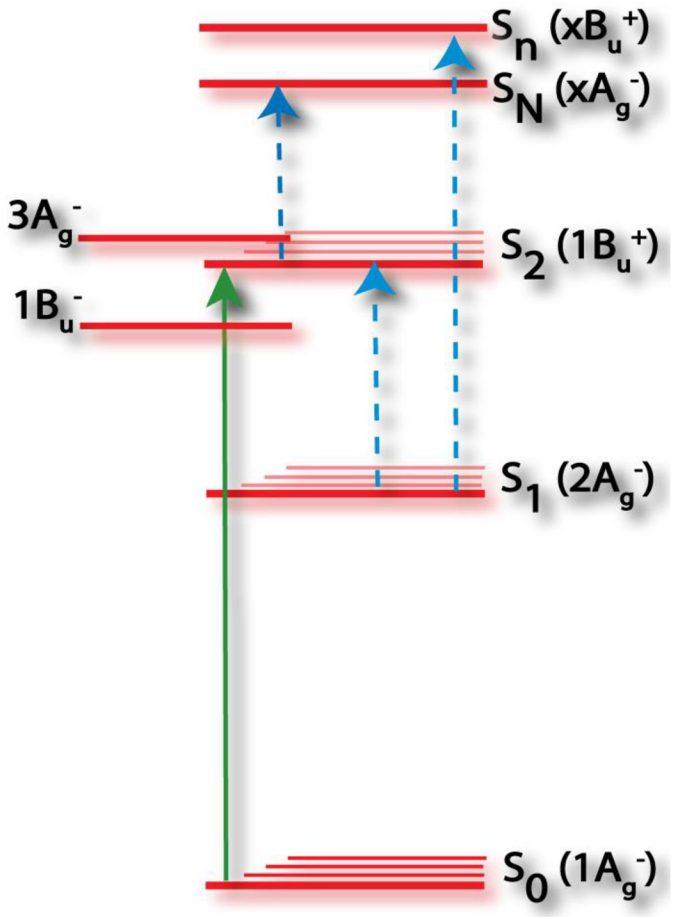

Figure 9. Energy level scheme of a carotenoid. Data obtained from [66].

It should be noted that the theory outlined above applies directly only to molecules with ideal C_{2h} symmetry. However, carotenoids are never totally symmetric, as twisting and/or bending distortions may break the symmetry, thus allowing some transitions that are formally forbidden within the ideal C_{2h} symmetry [67]. For example, the S_1-S_0 transition in carotenoids is always slightly allowed, enabling observation of a weak S_1 emission in certain carotenoids [68]. Furthermore, recent research indicates that symmetry considerations cannot solely explain the forbiddeness of some transitions in

carotenoids and additional mechanisms, such as multiply-excited character of certain states, must be taken into account when explaining the excited-state properties of carotenoids [67, 69].

In 1980s, the S_1 lifetimes of some carotenoids have been reported in organic solvents by the help of ultrafast time-resolved experiments yielding a value of a few picoseconds [70]. During the same years, sophisticated calculations of excited-state structure of polyenes have been carried out and other dark states having B_u^- and A_g^- symmetry labels were found within the S_2-S_1 gap (**Figure 9**) [71]. In carotenoids with eight or fewer C=C bonds, their fluorescence bands are associated with the S_1-S_0 transition while in longer carotenoids fluorescence is dominated by the S_2-S_0 transition. The crossover from S_1 to S_2 fluorescence could be explained by the increase in the rates of the S_1-S_0 non-radiative decay owing to the combination of smaller S_1-S_0 energy gaps and increased density of S_0-accepting modes in longer carotenoids, leading to disappearance of the S_1-S_0 fluorescence and allowing weaker S_2-S_0 fluorescence [72].

The energies of π-π * transitions of the conjugated π-system can be predicted by molecular orbital theory or the free-electron model (**Figure 10**). The model explains that the strongly-allowed low-energy transitions (S_0 to S_2) shifts to longer wavelengths with increase of the conjugation length. According to the model, energies of the S_0-S_2 transitions (ΔE) can be approximated by equation ΔE= A + B/N, where N is the number of the conjugated bonds. Thus, experimental data suggest a limit of ~700 nm (A= 14000 cm^{-1}) for the S_0-S_2 transition in infinite polyenes and carotenoids [72]. The energies of the S_0-S_2 transition also depend on the refractive index of the solvent; hence, a shift to lower energies is observed in solvents with high polarizability. Moreover, time-resolved studies of long natural carotenoids suggest the presence of additional dark states in the excited state manifold. Longer carotenoids/polyenes exhibit shorter lifetimes and more complex relaxation pathways [66]. Thus, significant theoretical challenges persist in describing the correlated, delocalized π-electrons in linear polyenes and carotenoids [73, 74].

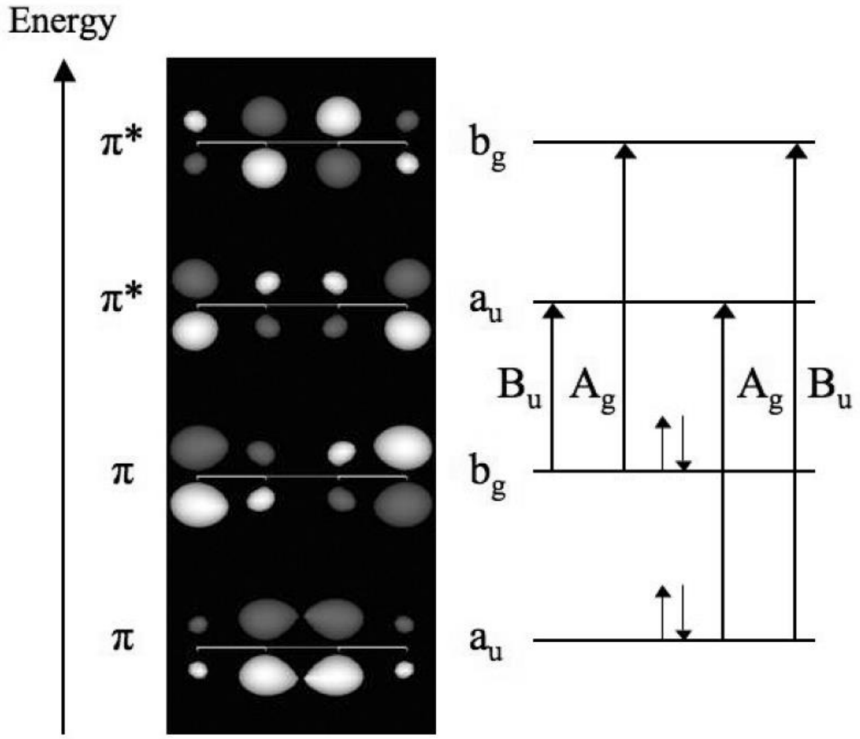

Figure 10. . The π molecular orbitals and π-π * states in butadiene. Data taken from [72].

Understanding the properties of the excited states of the carotenoids in solution is fundamental to decipher their function in the complex natural and artificial systems [75]. Below, some properties of the key electronic states of the carotenoids will be summarized.

2.1. S_2 state

The strongly allowed S_0-S_2 transition is responsible for the strong absorption of carotenoids in the blue-green spectral range [52]. This transition shows a characteristic three-peak structure associated with the three lowest vibrational levels of the S_2 state. The resolution of vibrational peaks in the absorption spectrum is an important measure since it determines certain properties of a carotenoid molecule. The vibrational peaks are well resolved for linear carotenoids, while loss of resolution is observed for carotenoids with conjugation extended to various end groups. In β-Carotene, for example, the conjugation extends to the terminal β-ionylidene rings. Conjugated double bonds located on the β-ionylidene ring are in the s-cis orientation, which is a more stable configuration. Repulsion between methyl groups on the β-ionylidene ring and hydrogen atoms on the conjugated backbone forces the β-ionylidene ring out of plane, resulting in the observed loss of vibrational resolution of the S_0-S_2 transition due to larger conformational disorder of the terminal rings [75].

The resolution of vibrational bands in non-carbonyl carotenoids is affected by carotenoid structure rather than solvent polarity. For non-carbonyl carotenoids with extended conjugation to

various end groups, similar to β-Carotene, a broader distribution of conformers typically leads to less resolved vibrational bands [76]. In contrast to non-carbonyl carotenoids, the vibrational bands of the S_0-S_2 transition of the carbonyl carotenoids, which have their conjugated system extended to a C=O group, are highly affected by solvent polarity [75, 77]. In non-polar solvents, good resolution of vibrational bands of the S_0-S_2 transition is preserved, whereas switching to a polar solvent results in significant loss of vibrational band resolution due to increased conformational disorder, so keto-carotenoids typically do not exhibit sharp vibrational bands in polar solvents [75, 78]. Furthermore, an asymmetric broadening of the S_0-S_2 transition toward lower energies is frequently observed in the absorption spectra of carbonyl carotenoids in polar solvents [20, 75].

2.2. S_1 state

When carotenoids are excited into the S_2 state, they relax to the S_1 state in a few hundred femtoseconds. The dynamics of this relaxation is viewed as S_2-S_1 internal conversion reaching the S_1 potential surface far from the S_1 energy minimum, forming a vibrationally hot S_1 state. Vibrational relaxation in the S_1 state occurs on the sub-picosecond time scale. Thus, in a pump-probe spectroscopy, upon application of the probe pulse some photons with specific energies may be absorbed from the relaxed S_1 state. This phenomenon, known as excited-state absorption (ESA) (**Figure 9),** results in a specific transient absorption band denoted as the S_1-S_N band whose decay provides insights into S_1 state relaxation dynamics, commonly used to measure S_1 lifetimes. Additionally, the bandwidth and position of the S_1-S_N band offer valuable information about properties of the conjugated chain. Vibrational relaxation in the S_1 state causes time-dependent spectral changes and its dependence on conjugation length remains unclear [79, 80]. Since the excited carotenoid rapidly relaxes to the S_1 state, the S_1 state is fundamental to understand the relaxation pathways.

The S_1 energy was unknown until new techniques and methodologies based on detection of extremely weak fluorescence [81], measurement of resonance Raman profiles [82] or measurement of the spectral profile of the S_1-S_2 transition by ultrafast spectroscopy were developed [83]. All methods targeting the S_1 energy provided experimental evidence for the dependence predicted by the theory [84]: the S_1 energy decreases with increase of the conjugation length. This has also implications for S_1 lifetimes which, via the energy gap law [85], decrease with increasing conjugation as well [75]. This relation is shown in **Table 2** for some selected carotenoids. Longer conjugation length implies shorter S_1 lifetime. This relation is essentially valid only for non-carbonyl carotenoids for which the S_1 lifetimes are independent of solvent polarity. For carbonyl carotenoids, however, solvent polarity affects the S_1 lifetime due to a coupling to an intramolecular charge transfer (ICT) state (see next chapter), thus carbonyl carotenoids have shorter S_1 lifetime in polar solvents than in non-polar solvents [70, 75, 77, 79, 86-93].

Table 2. S_1 State Lifetimes (ps) of some carotenoids.

Carotenoids	N[a]	τ_{S1}[b]	References
Lycopene	11C=C	4-4.7[c]	[79, 86, 87]
Violaxanthin	9C=C	26[c]	[88]
β-carotene	11C=C	9-11	[79, 89, 90]
Fucoxanthin	7C=C + C=O	63 (n-hexane) 21 (methanol)	[77, 91, 92]
Canthaxanthin	9C=C + 2C=O	5.2 (toluene)	[70, 75]
Astaxanthin	9C=C + 2C=O	~ 5[c]	[93]

[a]conjugation length. [b]picosecond (ps). [c]in polar and nonpolar solvents.

Detection of extremely weak S_1 fluorescence was the first method used to determine the S_1 energy. Several modifications on the standard fluorescence spectroscopy were required to obtain the fluorescence signal as the S_1 emissions of carotenoids with N>9 were very weak yielding quantum yield below the 10^{-6}. Further studies showed that the S_1 energy was less sensitive to the solvent polarizability compared to the S_2 state [94]. Another method to determine the S_1 state energy is based on resonance Raman spectroscopy. This method is based on tuning the Raman excitation over a broad spectral range. The Raman intensities of C=C stretching modes are enhanced when the electronic transition is in resonance with an electronic transition [95]. Due to extreme sensitivity of resonance Raman signal, even nearly forbidden transitions, such as the S_0-S_1 transition, could be identified. Thus, this method was used to detect not only the S_1 state but also energies of other dark states [82, 86, 96, 97]. The resonance Raman data resembles the results obtained by fluorescence, although energies obtained by fluorescence were slightly higher for longer carotenoids. Both these methods suffer from strong intensities of the allowed S_0-S_2 transition whose red edge overlaps with of the signals originating from the S_0-S_1 transition [66].

All these methods have their advantages and disadvantages in terms of both S_1 state energy and lifetime determination. However, femtosecond time-resolved spectroscopy has been widely utilized to gain information about properties of the S_1 state. A method based on measurements of the S_1-S_2 transition was developed in 1999. Since the capability of tuning the femtosecond pulses in the 1-2 μm spectral range, where the allowed S_1-S_2 transition is expected, it was possible to obtain the S_1 energies of carotenoids. This was achieved by measurements of the spectral profile of the S_1-S_2 transition. If the energies of the S_1-S_2 and S_0-S_2 transitions are known, the energy of the S_1 state can be obtained by subtracting these two values [83]. Another ultrafast time-resolved method is based on two-photon excitation (2PE) spectroscopy. A significant advantage of this method is the reduction of unwanted signals because there is no relaxation from other excited states as 2PE can directly excite the S_1 state. Quantum physics dictates that if a transition in a molecule with C_{2h} symmetry is forbidden

for a one-photon process, then this transition should be allowed for two-photon processes. This principle is harnessed by 2PE spectroscopy, which is also employed to investigate the excited states of carotenoids [68, 98, 99].

2.3. Intramolecular charge transfer (ICT) state.

In addition to the well-known S_1 and S_2 states, there are at least two other singlet states of interest. These states, namely Intramolecular Charge Transfer (ICT) and S* (as described in the following section), are usually observed under specific conditions. Despite ongoing discussions, the precise origins of these states remain unclear, inspiring considerable scientific examination [29, 100, 101].

The ICT state causes polarity-dependent behaviour in carbonyl carotenoids which have an asymmetrically positioned C=O group in conjugation. The presence of the ICT state is indicated by a new spectral band in the transient absorption spectra, which is red shifted from the S_1-S_N transition band of carotenoids [102]. The polarity-dependent lifetime of the lowest excited state is another specific indication of ICT state of carotenoids [92, 102]. Despite extensive experimental and computational efforts, exact relation between the S_1 and ICT states remains unclear. The precise molecular nature of the ICT state as well as its role in controlling the spectral and dynamic properties of polyenes and carotenoids are still mysterious. However, the literature reports emphasized that, in the presence of ICT, different models exist to explain the relationship between the S_1 and ICT states. These models are:

1) The ICT state is a separate electronic state distinct from the S_1 state (S_1 + ICT) [102-104].
2) The ICT state is strongly coupled to the S_1 state (S_1/ICT) [105-108].
3) The ICT state is indeed the S_1 state with a significant charge-transfer character (S_1 = ICT) [109, 110].
4) The ICT state is formed via the mixing of S_1 and S_2 states ((S_1 + S_2)/ICT) [100].

Recent results on 8'-apo-β-carotenal suggested that S_1-S_3 transition becomes allowed in the polar solvent, which is not allowed according to C_{2h} symmetry group of polyene chain. This would mean the S_1 state itself yields some ICT character, and the S_1-S_3 transition is then considered as the ICT-S_n transition. While these results would favor the third model [110], recent experiments on fucoxanthin using pump-dump-probe spectroscopy methods clearly demonstarted that the S_1 and ICT states exists as two separate, yet strongly coupled states that could be individually affected by the dump pulse [111, 112] pointing to the model 2 of the S_1-ICT relationship.

2.4. S* state.

Another type of dark intermediate excited state, called S*, was found for carotenoids both free in solution and bound to light-harvesting complexes [20, 75, 113-115]. A new transient absorption band was detected at the higher-energy side of the S_1-S_n transition by ultrafast transient absorption spectroscopy and subsequent global fitting [95]. This newly identified absorption band has been denoted as the S* state. The lifetime of this particular state was reported to be between 5 and 12 ps, depending on both the species of carotenoid and whether it was present in the light-harvesting complex or in organic solvent. When the carotenoid was bound to the LH1 or LH2 complex, the S* state decayed into triplet state. On the other hand, when the carotenoid was free in organic solvent, the S* state decayed to the ground state without generating a triplet state [95].

The S* state was initially defined in spirilloxanthin. According to Gradinaru et al., the S_1–S_n band of spirilloxanthin exhibits a distinct shoulder at 540 nm, and its lifetime is significantly longer than the S_1 state [20]. Initial studies suggested that S_1 and S* are two separate excited states which decay independently to the ground state, with no observed S_1–S* relaxation [75], although this concept was challenged by Berera et al. who hypothesized that a fraction of the S* population could decay to the S_1 state [116]. This S*–S_1 relaxation was also observed in non-carbonyl carotenoids at low temperatures [117] contrary to the earlier hypothesis by Wohlleben et al., whom assigned the S* state to a hot ground state populated by impulsive Raman scattering based on pump–dump–probe experiments [118, 119]. Additionally, studies by Frank et al. suggested a connection between the S* state and a twisted molecular conformation of a carotenoid molecule in the S_1 state [78, 117, 120, 121].

The origin of the S* signal remains a topic of debate. Initially, it was detected and assigned to a hot ground state [122], but this assignment was later challenged and the S* signal was instead attributed to a separate excited state [20]. Since then, multiple studies have been published supporting either the ground state[115, 123] or excited state [120, 124] hypotheses. Yet, it seems that both hot ground state and excited state contribute to the S* signal, with particular contribution depending on conjugation length: for short carotenoids (N<11), the excited state contribution dominates while a hot ground state is the key source of the S* signal for long carotenoids [125].

2.5. Carotenoid radicals

Carotenoid radicals can be generated chemically through reactions with electron acceptors, such as quinones [126] or metal ions [127-132], photochemically via photoreactions with electron acceptors [131-133] or even with solvents [134], as well as electrochemically [135-137]. Optical absorption techniques [127, 128, 130] and the electron paramagnetic resonance spectroscopy (EPR) [131, 133, 134, 138] can detect radical ions and neutral carotenoid radicals.

Firstly, due to their low oxidation potential, carotenoids serve as effective electron donors. Simultaneous electrochemical and EPR studies (SEEPR) of a series of carotenoids have shown that carotenoid radical cations are formed during the first oxidation step (Eq 1) followed by the formation of diamagnetic dications upon transfer of the second electron (Eq 2) [135]. A very essential aspect of the carotenoid radical cations is the presence of an equilibrium between the radical cation, dication and the original carotenoid in solution as given by Eq 3. The SEEPR measurements of carotenoid oxidation indicate that the following processes take place in a dichloromethane solution:

$$Car \overset{E^0_{1OX}}{\rightleftharpoons} Car^{\bullet+} + e^- \quad (1)$$

$$Car^{\bullet+} \overset{E^0_{2OX}}{\rightleftharpoons} Car^{+2} + e^- \quad (2)$$

$$Car + Car^{+2} \overset{K_{com}}{\rightleftharpoons} 2Car^{\bullet+} \quad (3)$$

Where Car is the neutral carotenoid species, $Car^{\bullet+}$ is the radical cation, and Car^{+2} is the dication. The equilibrium constant depends on the carotenoid's electron donor (cyclohexane ring or methyl end groups) or acceptor substituents (F-substituted phenyl, keto, or dicyano).

Another important feature of the carotenoid radicals is the tendency to lose a proton, H^+, to form a neutral carotenoid radical according to the following reactions:

$$Car^{+2} \overset{K_{dp}}{\rightleftharpoons} \#Car^{+} + H^+ \quad (4)$$

$$Car^{\bullet+} \overset{K'_{dp}}{\rightleftharpoons} \#Car^{\bullet} + H^+ \quad (5)$$

$$\#Car^{+} + e^- \overset{E^0_3}{\rightleftharpoons} \#Car^{\bullet} \quad (6)$$

Here $\#Car^+$ is a deprotonated cation and $\#Car^\bullet$ is a deprotonated neutral carotenoid radical [137]. The position of proton loss depends on carotenoid's terminal substituents. For β-carotene (**Figure 1**) radical cation, the deprotonation of 5-CH_3 or 4-CH_2 groups at the terminal double bond of the cyclohexene ring produces the most stable neutral radical, because of the extent of the π-conjugated system. On the other hand, deprotonation at the 9-CH_3 and 13-CH_3 methyl groups causes significant reduction of the conjugation length [139, 140].

Carotenoid radical cations are quite stable even at room temperature in anhydrous solvents at low concentrations (less than 10^{-5} M), allowing measurements of their absorption spectra. For example, the optical spectra of the radical cations of β-carotene and canthaxanthin (**Figure 1**) consist of a D_0-D_1 transition at 1425 and 1310 nm, respectively, and a D_0-D_2 transition at 990 and 885 nm, respectively. The doublet state (D) contains one unpaired electron and shows splitting of the spectral lines into a doublet. Therefore, radicals are described by D transitions in spectroscopy. The optical absorption spectra of carotenoid dications have also been reported (**Figure 11**). The molar extinction coefficients of radical cations and dications can also be determined, because they do not degrade significantly during the measurement of standard absorption spectra (<1min) [65, 141].

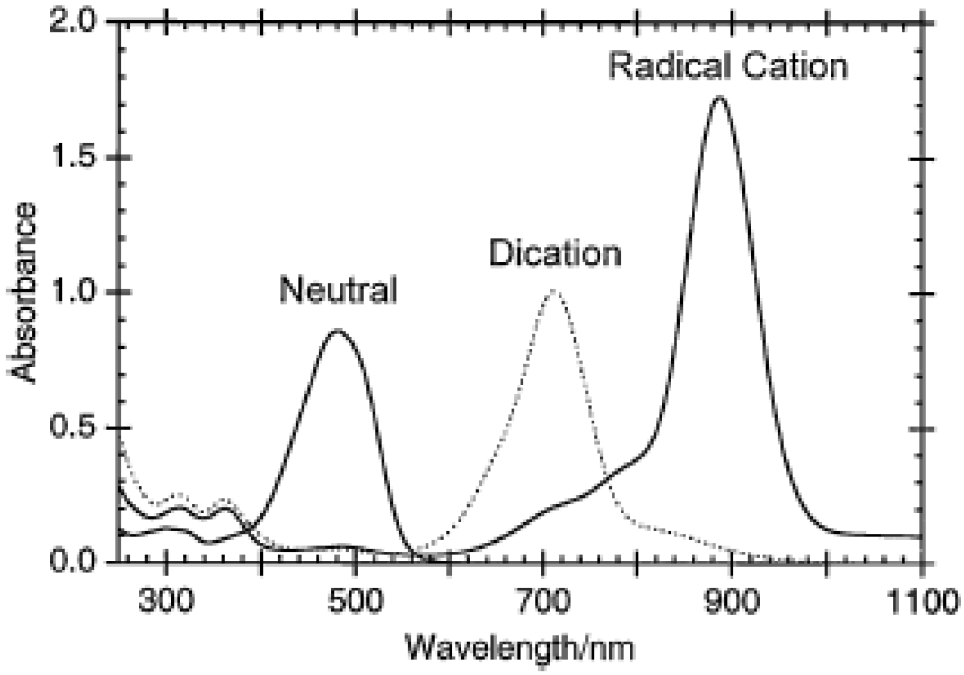

Figure 11. Absorption spectra of neutral canthaxanthin, radical cation and dication detected in dichloromethane in the presence of different concentrations of ferric chloride. Data taken from [65].

In 1984, Burton and Ingold suggested that β-carotene scavenges peroxyl radicals by addition to the conjugated system of double bonds, producing a resonance-stabilized carbon-centered radical (ROOCar$^{\bullet}$), which is a non-reactive radical [142]. This feature of carotenoid radicals is of critical importance for their application in medicine as free radicals are suggested to be an important factor contributing to the development of various diseases [143]. Another result of these experiments was the reversibility of oxygen addition to carbon-centered radicals. The following scheme for the reactions of carotenoid radicals has been proposed:

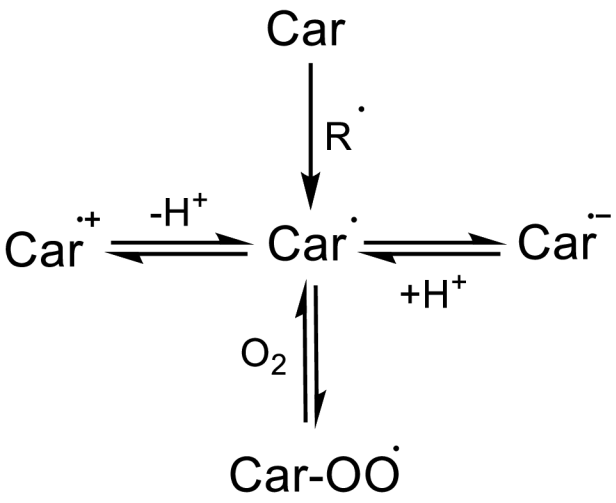

(7)

Here, Car• is a carbon-centered, resonant-stabilized radical. The major decay mechanism of carotenoid radicals in the absence of oxygen is the formation of neutral radical (#Car•) dimers [127]. On the other hand, the development of Car-OO• radicals has been thought to be a source of the pro-oxidant activity of some carotenoids [65, 144]. The role of carotenoid radicals in the antioxidant and pro-oxidant activity of carotenoids is the subject of a number of reviews and research articles in the literature [126, 138, 145-148].

2.6. Triplet state and Isomerization

Furthermore, the photophysics of carotenoids involves two additional significant processes: triplet state formation and isomerization. Though essential, these aspects are not the primary focus of this thesis. Consequently, they will be briefly summarized in this chapter.

Carotenoids are fundamental for photosynthetic organisms. In the reaction center of the photosynthesis, the carotenoids quench chlorophyll triplet states by triplet–triplet energy transfer, hence blocking the formation of toxic singlet oxygen. Moreover, even though triplet chlorophyll or singlet oxygen are formed, the carotenoids are able to quench both, resulting in dissipation of excess energy to the ground state by intersystem crossing (**See figure 5**) [149]. The lowest triplet state of the carotenoids with nine or more double bonds, which typically occur in photosynthetic organisms, is always lower in energy than singlet oxygen. Thus, the carotenoid triplet state cannot react with oxygen and generate singlet oxygen [150].Numerous reports have provided information about properties of triplet states of many C_{40} carotenoids. In these studies, triplet quantum yields, lifetimes, and molar absorption coefficients have been clarified. Determination of the concentration, formation rate, and deactivation rate of the carotenoid triplet states are crucial for determining the efficiency of carotenoids towards photosensitized oxidation [151]. Moreover, many biological and functional properties of carotenoids are associated with their triplet-excited states [152].

Since carotenoids contain multiple conjugated double bonds, numerous geometrical isomers are in principle possible. However, in nature, carotenoids accumulate mainly in the all-trans-

configuration [153, 154]. On the other hand, in several carotenoids, cis-isomers exist in considerable quantity in the human body [26, 155-157]. For example, more than 60% of total lycopene and 30% of astaxanthin are present as cis-isomers in plasma and some tissues [26, 155, 156, 158]. The isomerization is well-known chemical process of carotenoids. Some cis forms can occur naturally, as it is for the primary carotenoid precursors, phytoene and phytofluene, which occur predominantly in the cis configuration. There were a few types of cis carotenoids identified naturally, since the presence of cis double bond causes steric hindrance between neighboring groups, making it less stable. Thus, in nature, most carotenoids exist in the trans configuration, which is more stable [159]. The designations cis and trans are determined by the arrangement of the C = C double bond substituents. Thus, if the substituents are on the same side of the axis, C=C double bond is denoted as cis, while if the substituents are on opposite sides of the axis, C=C double bond is denoted as trans [159, 160].

Previous studies have shown that presence of cis-isomers can be identified based on the absorption spectrum of carotenoid, which, if a cis-isomer is present, contains characteristic spectral feature denoted as cis peak, whose relative intensity can even help to identify the cis-isomer [161, 162]. Absorption spectrum of cis carotenoids is characterized by the cis-peak absorbing between 330–350 nm. This band has the highest intensity when the double bond is located near or at the center of the chromophore [153, 163]. Furhter, cis-catrotenoids exhibit a slight hypsochromic shift and smaller extinction coefficient of the main S_0-S_2 absorption band. Thus, the cis-trans isomerization of carotenoids leads to a slight decrease of color intensity [153, 164, 165].

2.7. Photophysical properties of astaxanthin, crocin, and 8’-apo-β-carotenal

The photophysical properties of carotenoids have been extensively studied both theoretically and experimentally due to due to their photoprotective and light-harvesting abilities in biological systems. However, due to their complex excited-state structure, our understanding of carotenoid photophysics remains limited, as we explained in previous sections. In the context of this thesis, photophysical properties of three carbonyl carotenoids astaxanthin, crocin, and 8'-apo-β-carotenal, are of particular interest. **Figure 12** shows the steady-state absorption and transient absorption spectra of astaxanthin, along with a general scheme of the energy levels involved in key transitions. Some transitions, such as those involving the $1B_u^-$ and $3A_g^-$ states shown in Figure 9, are not shown in this scheme, because these transitions have never been reliably observed in an experiment. This visualization aids in understanding the photophysical properties of these three pigments while explaining their properties.

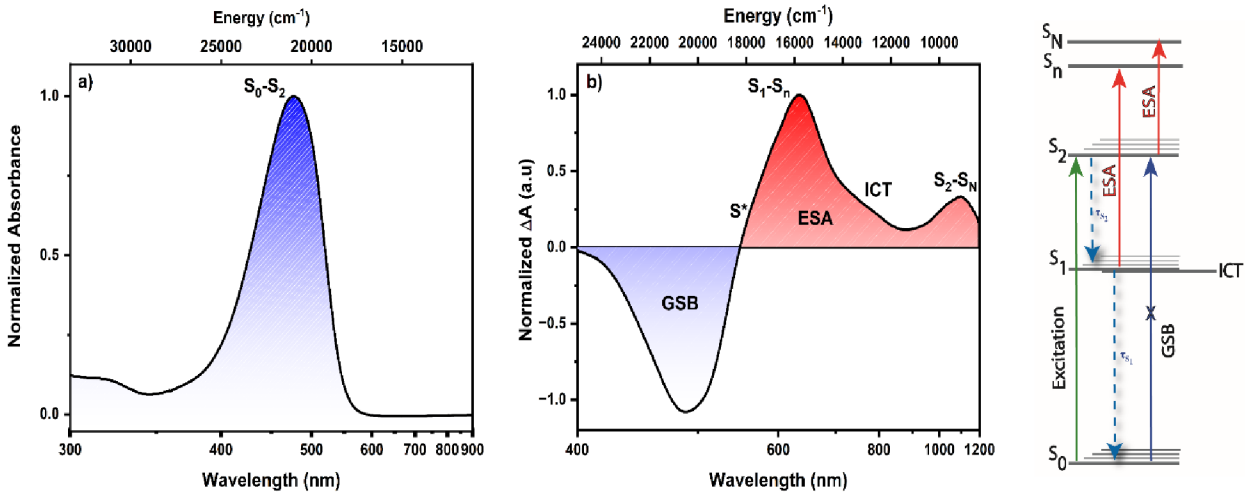

Figure 12. Normalized steady-state absorption (a) and transient absorption (b) spectra of astaxanthin. The signal from transient absorption spectroscopy experiments is typical for carotenoids, showing ground state bleaching (GSB) and excited state absorption (ESA), which consists of the S_1-S_n transition at around 600 nm, ICT state as a red shoulder of the S_1-S_n transition, S* state as a blue shoulder of the S_1-S_n transition, and the S_2-S_N transition in the NIR region. An energy level scheme of the carotenoid (right) with the typical transitions, together with relaxation pathways following photoexcitation to the S_2 state, is illustrated. Green arrows indicate excitation, red arrows represent ESA, and dashed arrows depict internal conversion.

The photophysical properties of astaxanthin has been a subject of numerous studies, as this carotenoid is readily available and is considered as a model carotenoid. The conjugated system of astaxanthin consist of 9 C=C bonds, and it is extended to two symmetrically positioned terminal cyclohexene rings featuring a conjugated C=O group and non-conjugated OH group (**Figure 6**). Absorption spectra of astaxanthin display a single broad peak, reflecting the S_0-S_2 transition, with a maximum at around 476 nm in polar solvents methanol and acetonitrile [93]. The absorption spectra of astaxanthin show a red shift in highly polarizable solvents, such as in CS_2, where the maximum occurs at 506 nm. This shift is due to a dispersion interaction between astaxanthin and solvent molecules [93, 166]. A similar red shift was observed for astaxanthin when forming metal complexes with metal ions interacting with keto and hydroxyl groups at the terminal rings of astaxanthin. (**See research section, Paper I**).

Astaxanthin belongs to the family of keto-carotenoids. These carotenoids exhibit even more complex excited-state dynamics due to the presence of the conjugated keto group, which introduces an intramolecular charge transfer (ICT) state into their excited state manifold. A number of experiments have shown that the charge transfer character increases with increasing solvent polarity. However, another important parameter is the position of the conjugated keto group. For asymmetric position of a single keto-group the ICT signal increases, but two symmetrically positioned keto groups minimize the charge transfer character of the S_1/ICT state [29]. This is precisely the case of astaxanthin, which possesses two symmetrically positioned conjugated keto groups at the terminal rings (**Figure 6**), resulting in a weak ICT signal detected across a broad range of solvents [93, 167]. Astaxanthin gives

characteristic transient absorption spectra consisting of ground state bleaching and excited state absorption (ESA) due to the S_1-S_n transition [166]. The ESA signal at early times after excitation also includes a NIR band at around 1000 nm, associated with ESA of the S_2 state. The S_1-S_n band, peaking at around 600-650 nm, fully develops within the first picosecond [29]. The weak shoulder in the 700-800 nm spectral region signals the presence of an ICT state. The ICT signal is weak because astaxanthin is a carotenoid with long conjugation and two symmetrically positioned keto groups [29]. The magnitude of the ICT signal band of astaxanthin may increase under specific circumstances, such as for example upon formation of metal complexes (**See research section, Paper I**). The excited state dynamics of astaxanthin requires at least three decay components decsribing lifetimes of excited states. The first component, whose lifetime is less than 100 fs [166], is associated with the lifetime of astaxanthin S_2 state. S_2 relaxation produces a hot S_1/ICT state that decays within a few hundred fs to the relaxed S_1 state, which has a lifetime of at around 4-5 ps [93, 167].

Crocin, the digentiobiosyl ester of crocetin and one of the few water-soluble carotenoids, features a conjugation system consisting of 7 conjugated C=C bonds extended to two symmetrically positioned C=O groups (**Figure 7**). The bulky digentiobiosyl groups do not contribute to conjugation; nevertheless, they are essential for the water solubility of crocin. The absorption spectra of crocin occur at around 450 nm in water. The vibrational bands of the S_0-S_2 transition of crocin are well resolved, with the absorption maximum assigned to the 0-1 vibrational band, while the 0-0 and 0-2 bands are located at around 460 and 415 nm, respectively [37]. The absorption maxima and resolution of vibrational bands of crocin could be influenced by factors such as solvent polarity and pH (**See research section, Paper III).**

Crocin provide characteristic carotenoid transient absorption spectra in water. Beside ground state bleaching and ESA due to the S_1-S_n transition, at early delay there is an extra ESA band in the 800-900 nm spectral region which is associated with ESA from the initially excited S_2 state [166]. A weak band in the spectral region of 600-650 nm indicates the presence of ICT state which is again weak due to the two symmetrically positioned conjugated C=O groups as in astaxanthin [29, 77]. The S_2 state decays in less than 120 fs, forming a hot S1/ICT having a 600 fs lifetime. The relaxed S_1/ICT state of crocin decays with a time constant of 58 ps in water, but becomes significantly longer (~140 ps) in methanol or 2-propanol, underscoring the polarity effect on the S_1/ICT state [37]. This characteristic pattern of crocin is significantly impacted by changes in pH **(See research section, Paper III).**

8'-apo-β-carotenal serves as a synthetic model for carbonyl carotenoids. It has eight conjugated C=C bonds, with an asymmetrically attached C=O group directly linked to the linear conjugated backbone (**Figure 8**) [110, 168]. It is often utilized in solar energy conversion systems [62] and extensively studied for its rich excited state dynamics [63] and electrochemical properties [64, 65]. The polarity-dependent behavior of 8'-apo-β-carotenal is a well-known phenomenon: transient

absorption measurements revealed that the S_1/ICT state of 8'-apo-β-carotenal has a lifetime of 25 ps in nonpolar solvent n-hexane, but it shortens to 8 ps in polar solvents like methanol or acetonitrile [38, 110]. This shortening is associated with increased amplitude of the ICT band in polar environments. The absorption spectra of 8'-apo-β-carotenal exhibit changes reflecting the typical effects induced by variations in solvent polarity observed in carotenoids with asymmetrically positioned conjugated carbonyl group. The characteristic vibrational structure of the S_0–S_2 transition of 8'-apo-β-carotenal, displaying well-resolved peaks at around 482, 455, and 432 nm in n-hexane, disappears in methanol. Instead, a broad S_0–S_2 transition lacking any hints of vibrational bands is observed. This effect is triggered by the interaction of the conjugated carbonyl group with a polar solvent, which results in an increase of conformational disorder, leading to the observed loss of vibrational structure. Additionally, the interaction involving the conjugated carbonyl group leads to an increase in absorption in the red part of the absorption spectrum, likely due to hydrogen bonding with the carbonyl oxygen [43].

Transient absorption spectra of 8'-apo-β-carotenal in the nonpolar n-hexane exhibit a narrow ESA band at 550 nm, attributable to the S_1–S_n transition. On the high-energy side of the S_1–S_n band, there is a distinct peak at 520 nm, commonly observed in many other carotenoids and typically denoted as the S* signal [48]. Additionally, weak peaks at around 650 nm, which are associated with the ICT state in asymmetrically carbonyl carotenoids are visible even in the nonpolar n-hexane. These transitions, typically forbidden in almost ideally symmetric linear carotenoids without carbonyl groups, become allowed due to the introduction of asymmetry by the conjugated carbonyl group into the system [110]. When the solvent is changed from n-hexane to methanol: relative intensity of the S_1-S_n band and S* signal decrease, while the magnitude of the ICT band increases with solvent polarity. [75, 169]. Besides influencing the transient absorption spectra of 8'-apo-β-carotenal, polarity also impacts the lifetime of the S_1/ICT state. The polarity-induced change in S_1/ICT lifetime is obvious as it exhibits a lifetime of 26 ps in n-hexane and 8 ps in methanol [110]. The relation between S_1 and ICT in 8'-apo-β-carotenal has been extensively studied. Among these studies, a novel approach involving ultrafast transient absorption spectroscopy measurements under external voltage has yielded interesting results **(See research section, Paper II).**

3. Experimental Methods and Data Analysis

Various spectroscopic methods are frequently employed to identify and determine molecular structures, as well as to investigate dynamics and energies of molecular systems. Various spectroscopic techniques are also employed to investigate pigment properties, with the aim of providing insights into the excited-state properties of individual pigments (including energies, lifetimes, and transition probabilities), as well as understanding pigment interactions in pigment-protein complexes. Each spectroscopic method is based on the interaction of radiation with matter, although the spectral range varies for different methods. The experiments reported in this thesis predominantly employ absorption and partially emission spectroscopy techniques in the VIS-NIR spectral region.This section briefly introduces the steady-state and transient absorption spectroscopies used in experiments described in this thesis. The first method, steady-state spectroscopy, provides direct information about the energy of the absorbing states, as well as steady-state molecular features such as conformation, aggregation, and more. The second method, transient absorption spectroscopy, is used to provide information about excited-state dynamics. Additionally, High-Performance Liquid Chromatography (HPLC) is utilized for further characterization and separation of pigments. Known for its high separation performance and straightforward sample handling, HPLC is recognized as an excellent method for pigment investigation. In the thesis, we have also employed spectroelectrochemistry (SEC), an experimental technique that combines electrochemistry and spectroscopy (both steady-state and time-resolved absorption), using a potentiostat and spectrometer. While electrochemical experiments provide information about redox properties of pigments, combining them with spectroscopic techniques yields insights about how the excited-state dynamics of pigments are affected under the influence of voltage.

3.1. High-Performance Liquid Chromatography

High-Performance Liquid Chromatography (HPLC), developed in the late 1960s, is now extensively used for separations and purifications of various molecules in various sectors, including pharmaceuticals, biotechnology, biochemistry, environmental science, polymers, and the food industry. HPLC enables the identification, quantification, and purification of individual components within a mixture on the basis of their molecular structure. The main components of an HPLC system include solvent reservoirs, a high-pressure pump, an injector system, a column, and a detector (**Figure 13**) [170].

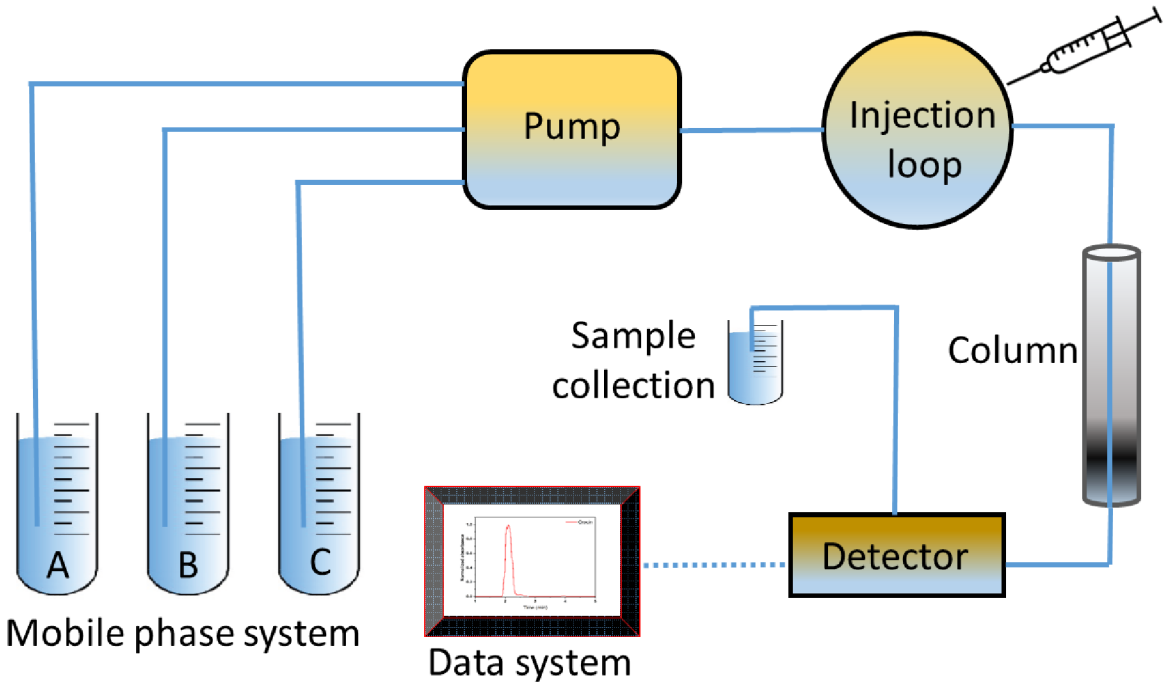

Figure 13. High-Performance Liquid Chromatography system.

The reservoirs contain mobile phase solvents, which transport the sample through the HPLC system. A mobile phase solvent is pumped through the sample injection loop, where the sample is injected into the phase stream that carries it into the high-pressure column. The reverse-phase column holds a nonpolar stationary phase, whereas the mobile-phase solvent, like mixtures of water and methanol or acetonitrile, is more polar. The reverse-phase column matrices can be functionalized with aliphatic chains such as C8, C18, or with aromatics [171]. Sample retention time varies depending on the interaction among the stationary phase, the molecules being analyzed, and the mobile phase. The more nonpolar a compound is, the longer it will be retained; hence, the elution order of the components follows a decreasing order of polarity. The detector is positioned at the outlet of the column, and its signal is transmitted to a computer, which generates the chromatogram. Various detection methods such as UV/VIS absorbance, fluorescence, or mass spectroscopy, are used in HPLC. Once the mobile phase exits the detector, the purified compound can be collected for further study [170]. Due to HPLC's high separation performance and straightforward sample handling, it serves as an excellent method for investigating pigments [172]. Consequently, this method is utilized for further sample characterization in the research sections of **Paper III and IV**.

3.2. Steady State Absorption Spectroscopy

Absorption spectroscopy is a spectroscopic method that characterizes how much light a sample absorbs as a function of wavelength. The intensity of light transmitted through the sample at a specific wavelength ((λ)) and the intensity of the incident light ($I_0(\lambda)$) are measured. Transmittance (T) is then defined as the ratio of these two intensities:

$$T = \frac{\mathrm{I}\,(\lambda)}{I_0\,(\lambda)} \qquad (1)$$

The absorbance of a homogeneous sample is then calculated using Equation 1, which is defined by the Beer-Lambert law [173]:

$$A = -logT = log\frac{I_0\,(\lambda)}{I\,(\lambda)} = c\varepsilon(\lambda)\mathrm{d} \qquad (2)$$

It is determined by the optical path of the cuvette containing the sample (d) and molar concentration (c) of the absorbing species. The extinction coefficient or molar absorptivity ε (λ) is a measure of the probability of absorption of photon at wavelength λ. The absorbance is plotted versus wavelength, and the resulting absorption spectrum provides direct information about energy of the absorbing state. A presence of isomerization, aggregation, or photo damage can also be determined by the shape of the absorption spectra. Steady-state absorption spectra are typically acquired in two variants. The first, known as a single-beam measurement, involves measuring $I_0(\lambda)$ and $I(\lambda)$ using the same beam. Two separate measurements, with and without the sample, are necessary. The second technique involves simultaneously measuring $I_0\,(\lambda)$ and (λ) using separate paths for the sample and reference beam.

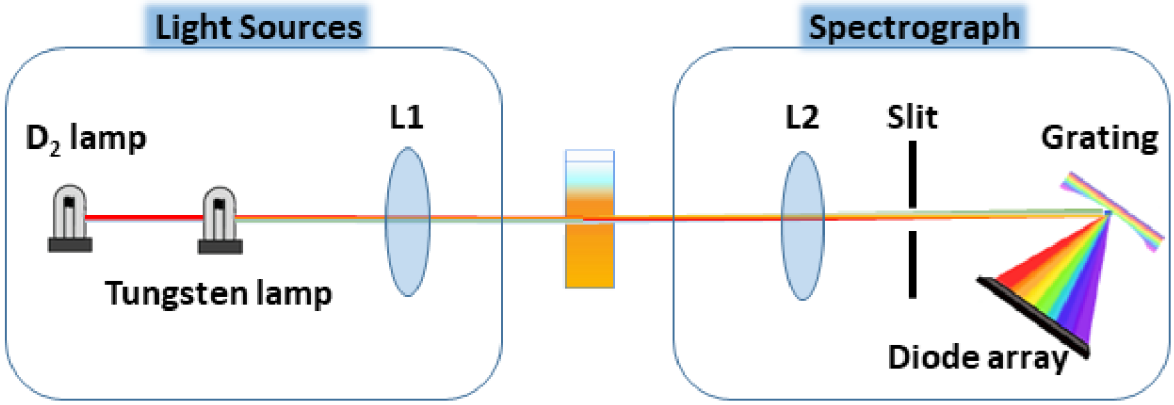

Figure 14. UV-VIS spectrophotometer.

The schematic representation of the UV-VIS spectrophotometer, utilized in our laboratory, is depicted in **Figure 14**. It comprises three main components: the light source, sample compartment, and spectrograph. The tungsten lamp emits visible and near-infrared light, while the deuterium lamp provides ultraviolet light. These two sources are optically combined to emit light in the wavelength range from 190 to 1100 nm. The collimated beam passes through the sample after being directed by lens L1. Subsequently, the lens L2 of the spectrograph focuses the beam onto the slit plane, followed by passage through the slit aperture. The holographic grating disperses the light onto a photodiode array consisting of 1024 individual photodiodes.

3.3. Femtosecond Transient Absorption Spectroscopy

A large number of biological and chemical processes occur on time scales extending up to seconds or even longer but the most fundamental photophysical processes, such as excited-state relaxation, energy and electron transfer, or isomerization typically occur on a sub-nanosecond time scales. This ultrafast timescale (femtoseconds to nanoseconds) is the time regime that is examined in experiments reported in this thesis. Thus, a spectroscopic technique with sufficient temporal resolution to follow ultrafast processes is required. Femtosecond transient absorption (pump-probe) spectroscopy has become a widely-used and useful technique to achieve this task.

The basic transient absorption spectroscopy setup in our laboratory is depicted in **Figure 15**. At first, a regenerative amplifier system (Spectra Physics) provides the primary ultrashort pulse. It generates 4.2 mJ pulses at 800 nm with a repetition rate of 1 kHz using a mode-locked Ti:Sapphire laser (MaiTai, Spectra Physics) amplified through chirped pulse amplification (Spitfire Ace, Spectra Physics), which is pumped by an Nd:YLF pump laser (Empower, Spectra Physics). The crucial step of the method involves splitting the primary pulse into two pulses, known as the pump and probe, which also gives the method its name.

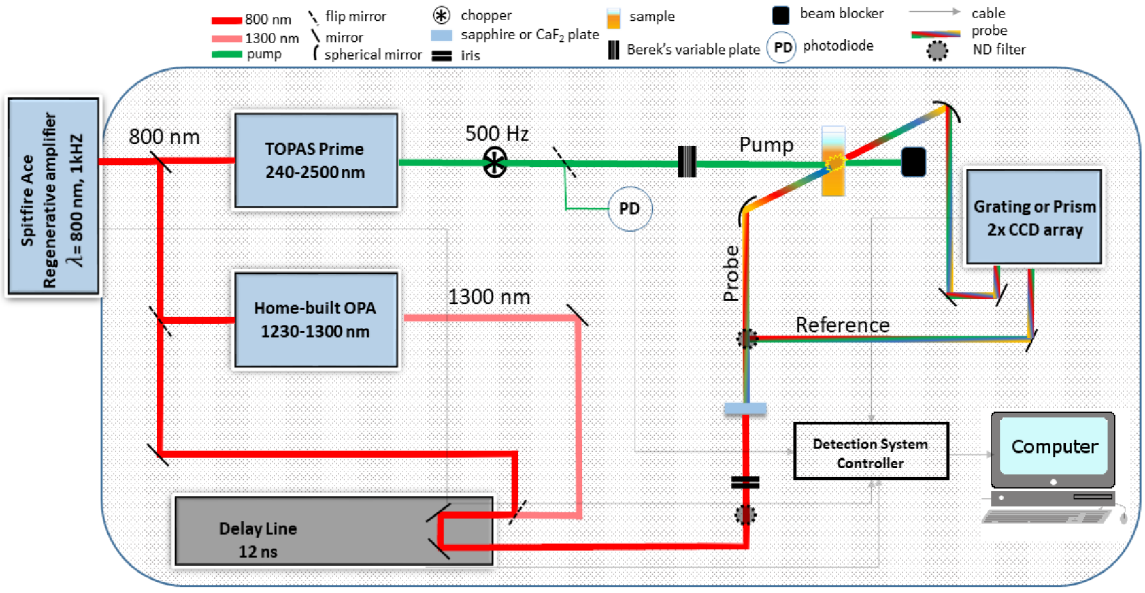

Figure 15. A simplified scheme of the pump-probe experiment in our laboratory.

The pump pulse, which serves to excite the sample and ensure that excitation occurs only in the spectral region of interest, has to be spectrally narrow. To achieve this, we utilize the optical parametric amplifier (OPA) (Topas, Light Conversion), which allows us to adjust the wavelength within the range of 240 to 2500 nm as desired. Before hitting the sample, the polarization of the pump beam is set by using a variable wave plate. In all experiments presented in the thesis a 54.7° angle between the polarization of the pump and probe pulses is used to prevent polarization effects in the sample [173]. Then the pump pulse is focused to the sample and after it excites the sample, it is eventually blocked.

The probe beam wavelength of 800 nm can either be used directly, or used to generate another wavelength in a home-built OPA, which is in our case designed to generate pulses centered at 1300 nm according to experiment details. The probe beam, either at 800 or 1300 nm is first directed to a retroreflective mirror on a translation stage (delay line), enabling us to set the required delay between pump and probe pulses, and then focused to a sapphire or calcium fluoride plate, where a white light continuum (WLC) is generated. Using 1300 nm to generate WLC allows us to measure a broader spectral region, typically extending from 400 to 1100 nm, and this configuration is also utilized in all experiments described in this thesis. The WLC is then divided into two beams, known as probe and reference beams. The probe beam is focused onto the sample using a spherical mirror, in a way that the spot size of the probe beam on the sample is smaller than that of the pump beam, ensuring probing of all excited molecules. Both probe and reference beams are detected using a double CCD detection system (Pascher Instruments) employing either a grating or prism spectrometer. The grating spectrometer covers narrowedr spectral region (about 250 nm in our case) with constant spectral resolution, while the prism spectrometer, which is mostly used in experiments described here, covers a broader spectral region (400-1200 nm). However, the drawback of the prism spectrometer is worse spectral resolution which varies over the detected spectral range. The absorption change (ΔA) for a particular delay between pump and probe (Δt) is then the difference of the ratios of the reference and probe signals at a given wavelength, measured for the excited fraction of the sample (with pump) and the non-excited fraction of the sample (without pump). A chopper in the pump beam is employed to block every second pulse, enabling alternate measurements with and without the pump pulse (Eq. 3). This approach reduces background effects and enhances the signal-to-noise ratio by compensating for laser power fluctuations.Then, the final ΔA spectrum is calculated according to Equation 3.

$$\Delta A(\Delta t, \lambda) = log\frac{I_{ref}}{I_{pp}} - log\frac{I_{ref}}{I_{np}} \qquad (3)$$

where I_{ref} is the intensity of the reference beam, I_{pp} the intensity of the probe when the excitation beam is present, and I_{np} the intensity of the probe with no excitation. The ΔA spectrum is denoted as transient absorption spectrum and contains three basic signal types: ground-state bleaching, stimulated emission and excited-state absorption **(Figure 12 section 2.7.)**

Ground-state bleaching: The probability of the absorption process depends on the number of molecules in the ground state. When the sample is excited with a pump pulse, some molecules are promoted to an excited state, reducing the number of molecules in the ground state compared to a non-excited sample. Consequently, ground-state absorption detected by the probe pulse in the excited sample is less than in the non-excited sample ($Awithpump < Awithoutpump$), resulting in a negative signal in ΔA spectra in the spectral region of ground-state absorption of the sample.

Stimulated emission: When a probe photon with appropriate energy triggers molecules in the excited state, it can induce the return of the molecule to the ground state by emitting a photon. This process is known as stimulated emission and occurs only for allowed transitions. Since the induced photon is emitted in the same direction as the probe photon, the light intensity at the detector increases due to the stimulated emission process, again leading to a negative signal in the transient absorption spectrum. The stimulated emission signal is typically red-shifted relative to the ground state bleaching observed in ΔA spectra.

Excited-state absorption: An excited sample can absorb photons with different energies than those absorbed when the sample is in the ground state. These additional absorbed photons, compared to the non-excited sample, cause a positive signal in the ΔA spectra ($Awithpump > Awithoutpump$).

There are other additional possible processes can affect the final ΔA spectrum. One of them is for example a product absorption. After a molecule is excited, photophysical or photochemical processes may lead to formation of new transient species, such as isomers or radicals, which will have absorption spectrum different from that of the parent molecule. The absorption of these products will appear as a positive signal in the ΔA spectrum

3.4. Global and Target Analysis of the Time-Resolved Data

After collecting data in a pump-probe experiment, an essential step is to analyze the data to extract dynamics of processes occurring in the studied system. The time-resolved transient absorption experiment provides a two-dimensional dataset with two axes: delay time (t) and probe wavelength (λ). A typical dataset is represented by a matrix, with the first row and column representing the measured wavelengths (λ) and times (t), respectively. The rest of the matrix contains information regarding differential absorbance at particular delay time and wavelength, ΔA(t,λ). Besides the information linked directly to the time evolution of the system after excitation, it often contains also undesired signals associated with the experiment, such as noise, chirp, or scattering that must be minimized/eliminated from the data before the fitting procedure. First, one has to subtract the background, which is accomplished by subtracting the average of several spectra before the time zero. This procedure should also remove the scattering produced by the pump beam, but in some cases, especially in highly-scattering samples, the background subtraction is not sufficient to remove the pump scattering. Then, the best alternative is to remove the spectral region of the data that contains the scattering before fitting the dataset. The last step of preparing data for fitting is the chirp correction, which occurs due to the group velocity dispersion of light as light of different wavelengths travels through optical elements at different velocities. The effect is more pronounced in the blue/UV spectral region where the dependency of the refractive index of most optical materials on the wavelength is stronger. A polynomial function is typically used to approximate the dispersion curve and correct the zero-time for chirp.

After preparation of the dataset a method of global fitting [174] has been applied to all transient absorption data collected in experiments presented in this thesis. The key feature of the global fitting method is that it fits kinetics at all wavelengths simultaneously by the same set of time constants:

$$\psi(t, \lambda_i) = \sum_{j=1}^{n} c_j(t)\epsilon_j(\lambda_i), \qquad (4)$$

where $\epsilon_j(\lambda_i)$ and $c_j(t)$ are the extinction coefficient at given wavelength and time-dependent concentration of a particular species associated with component j, respectively. The later can be written as

$$c_j(t) = \exp(-k_j t) = \exp(-\frac{t}{\tau_j}) \qquad (5)$$

where k_j and τ_j are decay rate and lifetime, respectively.

At this point, there is critical user input in predicting the basic parameters of the observed system, such as: how many states are involved, the initial guess of the lifetimes of the individual states, the relaxation and/or energy transfer scheme, etc. Evaluating all of these options is tricky, especially in the case of an unknown system, but knowledge of the system's components (for example, the lifetime of the involved carotenoid in solution) and models of energy transfer from a smaller system may usually help. The fitting model can have three basic forms, sequential, parallel, and compartmental (**Figure 16**).

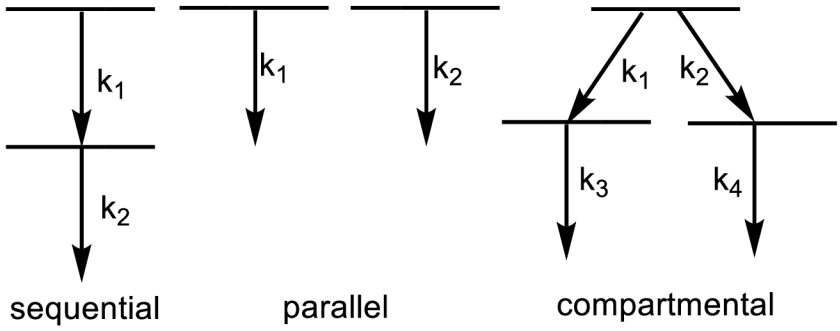

Figure 16. Possible kinetics schemes used for global (left and middle) and target (right) analysis.

In the sequential model, the population flows from the initially excited state to other states in an irreversible cascade, which can be represented as:

$$A \xrightarrow{\tau_1} B \xrightarrow{\tau_2} C \xrightarrow{\tau_3} D \ldots\ldots \qquad (6)$$

The capital letters represent individual excited state species, whereas the τ's represent the lifetimes of the particular states. The fitting then produces so-called evolution associated difference spectra (EADS). The second alternative model for data fitting is known as a parallel model. It is used when each state experiences independent mono-exponential decay, resulting in decay-associated difference spectra (DADS). The last model, known as a compartmental model or target analysis, is used

to unravel and explain systems that are too complex to be addressed using the sequential or parallel models. In the ideal situation, it consists of all possible states and energy transfer channels as indicated by the user. This approach to data fitting yields species-associated difference spectra (SADS).. For the purpose of data fitting in the papers included in this thesis, a commercial global fitting software CarpetView (Light Conversion) was used.

3.5. Spectroelectrochemistry

The basic definition of spectroelectrochemistry (SEC) is the integration of two distinct techniques: standard electrochemistry and spectroscopy. SEC provides information about chemically driven electron transfer mechanisms and redox events in a variety of molecules and other materials. SEC provides interdisciplinary advantages and may extend the scope of analysis and other applications, with a focus on topics such as analytical chemistry, materials science, biophysics, chemical biology, and more [175].

Electrochemistry is one of the oldest branches of chemistry, with applications in biology, physics, and chemistry. It has been used to study material transformation, heterogeneous electron transfer kinetics, and a wide range of chemical reactions on laboratory or industrial scales [176]. There are several electrochemical analysis modes, including amperometry, voltammetry, and electrochemical impedance spectroscopy. Electrochemistry is now a widely used scientific topic, with significant interest and practical applications in analysis, chemistry, physics, energy conversion and storage, and biology. Its applications include fuel cells, corrosion science, self-powered devices, and self-assembled coatings, among others [177-179].

Diverse spectroscopic approaches have been crucial in improving understanding across various research areas for decades, and continue to develop and improve [180, 181]. The combination of electrochemistry, which supplies the kinetic and thermodynamic processes, and spectroscopy, which supplies the molecular vibrational process, yields the SEC technique [181, 182], broadly defined as the use of spectroscopic methods to test the changes initiated by an electrochemical system in an electrochemical cell. Under potential control, spectroscopic information about electrogenerated species can be readily obtained, including electronic absorption, vibrational modes and frequencies, light emission and scattering, magnetic resonance, and circular dichroism [183-185].

Many efforts have been directed to attempts to combine the advantages of both categories of measurement, electrochemistry and spectroscopy, through the simultaneous determination of redox processes and of the associated species at each step. Typically, the spectroscopic response is monitored in situ while the electrochemical reaction is carried out under controlled conditions [181]. Unlike in ‘‘pure’’ electrochemistry or spectroscopy, there is no standard set-up in spectroelectrochemistry. The design of cells is limited by the requirements provided by the problem and/or the spectrometer [186].

There are many processes in which the starting species change oxidation state during a reaction pathway, resulting in the formation of a less stable and more reactive photoactivated species [187, 188]. First, a reactive radical intermediate is generated electrochemically. This intermediate is then promoted to a higher oxidizing or reducing potential by light. Isolating such reactive intermediates via chemical means for individual study is challenging, often necessitating the use of strong chemical oxidizing or reducing agents [189]. Furthermore, the presence of these chemical reagents in the system, unless removed, may complicate spectroscopic analysis. In contrast, electrochemistry offers an attractive method for creating reaction intermediates by controlled oxidation or reduction of the starting species. Through electrochemical means, the product of interest can be continuously generated without the need for excess chemical oxidants or reductants. Therefore, combined spectroscopy (both steady-state and time-resolved absorption) and electrochemical measurements not only offer pathways for investigating the photodynamics of reaction intermediates, but also introduce a new dynamic time dimension to the extensive field of spectroelectrochemistry [187, 190]. Because bringing the two techniques together is an area ripe for exploration, we employed SEC, which integrates electrochemistry with steady-state and time-resolved absorption spectroscopy using a potentiostat and a spectrometer. While electrochemical experiments allowed us to obtain information about the redox properties of pigments, their combination with spectroscopic techniques provided important insights into how the excited-state dynamics of pigments are affected by voltage **(See research section, Paper II).**

4. References

[1] Delgado-Vargas F., Jiménez A. R., Paredes-López O., (2000), "Natural Pigments: Carotenoids, Anthocyanins, and Betalains — Characteristics, Biosynthesis, Processing, and Stability", Critical Reviews in Food Science and Nutrition, 40 (3), 173-289.
[2] Hari R. K., Patel T. R., Martin A. M., (1994), "An overview of pigment production in biological systems: Functions, biosynthesis, and applications in food industry", Food Reviews International, 10 (1), 49-70.
[3] Bauernfeind J. C., (1981), "Natural food colors", Carotenoids as colorants and vitamin A precursors, Academic Press, New York, 1-45.
[4] Wong D. W. S., (1989), "Mechanism and theory in food chemistry", Edition, Springer.
[5] Bartley G. E., Viitanen P. V., Pecker I., Chamovitz D., Hirschberg J., Scolnik P. A., (1991), "Molecular cloning and expression in photosynthetic bacteria of a soybean cDNA coding for phytoene desaturase, an enzyme of the carotenoid biosynthesis pathway", Proceedings of the National Academy of Sciences, 88 (15), 6532-6536.
[6] Namitha K. K., Negi P. S., (2010), "Chemistry and Biotechnology of Carotenoids", Critical Reviews in Food Science and Nutrition, 50 (8), 728-760.
[7] Frank H. A., Young A., Britton G., Cogdell R. J., (2006), "The photochemistry of carotenoids", Edition, Springer Science & Business Media.
[8] Bramley P., (2003), "The genetic enhancement of phytochemicals: the case of carotenoids", Phytochemical functional foods, 253-279.
[9] Britton G., (1995), "Structure and properties of carotenoids in relation to function", The FASEB Journal, 9 (15), 1551-1558.
[10] Sies, Stahl, (2003), "Non-nutritive bioactive food constituents of plants: lycopene, lutein and zeaxanthin", International journal for vitamin and nutrition research, 73 (2), 95-100.
[11] Nagao A., During A., Hoshino C., Terao J., Olson J. A., (1996), "Stoichiometric Conversion ofall trans-β-Carotene to Retinal by Pig Intestinal Extract", Archives of Biochemistry and Biophysics, 328 (1), 57-63.
[12] Giovannucci E., (1999), "Tomatoes, Tomato-Based Products, Lycopene, and Cancer: Review of the Epidemiologic Literature", JNCI: Journal of the National Cancer Institute, 91 (4), 317-331.
[13] Landrum J. T., Bone R. A., (2001), "Lutein, Zeaxanthin, and the Macular Pigment", Archives of Biochemistry and Biophysics, 385 (1), 28-40.
[14] Boileau T. W. M., Moore A. C., Erdman J. W., (1999), "Carotenoids and vitamin A", Antioxidant status, diet, nutrition and health, 133-158.
[15] Paiva S. A. R., Russell R. M., (1999), "β-Carotene and Other Carotenoids as Antioxidants", Journal of the American College of Nutrition, 18 (5), 426-433.
[16] Krinsky N. I., Yeum K.-J., (2003), "Carotenoid–radical interactions", Biochemical and Biophysical Research Communications, 305 (3), 754-760.
[17] Kobayashi M., Sakamoto Y., (1999), "Singlet oxygen quenching ability of astaxanthin esters from the green alga Haematococcus pluvialis", Biotechnology Letters, 21 (4), 265-269.
[18] Frank H. A., Cogdell R. J., (1996), "Carotenoids in photosynthesis", Photochemistry and Photobiology, 63 (3), 257-264.
[19] Mirkovic T., Ostroumov E. E., Anna J. M., van Grondelle R., Govindjee, Scholes G. D., (2017), "Light Absorption and Energy Transfer in the Antenna Complexes of Photosynthetic Organisms", Chemical Reviews, 117 (2), 249-293.
[20] Gradinaru C. C., Kennis J. T. M., Papagiannakis E., van Stokkum I. H. M., Cogdell R. J., Fleming G. R., Niederman R. A., van Grondelle R., (2001), "An Unusual Pathway of Excitation Energy Deactivation in Carotenoids: Singlet-to-Triplet Conversion on an Ultrafast Timescale in a Photosynthetic Antenna", Proc. Natl. Acad. Sci. U. S. A., 98, 2364.
[21] Miki W., (1991), "Biological Functions and Activities of Animal Carotenoids", Pure and Applied Chemistry, 63 (1), 141-146.
[22] Higuera-Ciapara I., Felix-Valenzuela L., Goycoolea F. M., (2006), "Astaxanthin: a review of its chemistry and applications", Crit Rev Food Sci Nutr, 46 (2), 185-196.
[23] Nielsen B. R., Mortensen A., Jørgensen K., Skibsted L. H., (1996), "Singlet versus Triplet Reactivity in Photodegradation of C40 Carotenoids", Journal of Agricultural and Food Chemistry, 44 (8), 2106-2113.

[24] Nishida Y., Berg P. C., Shakersain B., Hecht K., Takikawa A., Tao R., Kakuta Y., Uragami C., Hashimoto H., Misawa N., Maoka T., (2023), "Astaxanthin: Past, Present, and Future", Marine Drugs, 21 (10).
[25] Ambati R. R., Phang S.-M., Ravi S., Aswathanarayana R. G., (2014), "Astaxanthin: Sources, Extraction, Stability, Biological Activities and Its Commercial Applications—A Review", Marine Drugs, 12 (1), 128-152.
[26] Coral-Hinostroza G. N., Ytrestøyl T., Ruyter B., Bjerkeng B., (2004), "Plasma appearance of unesterified astaxanthin geometrical E/Z and optical R/S isomers in men given single doses of a mixture of optical 3 and 3'R/S isomers of astaxanthin fatty acyl diesters", Comparative Biochemistry and Physiology Part C: Toxicology & Pharmacology, 139 (1), 99-110.
[27] Kidd P., (2011), "Astaxanthin, cell membrane nutrient with diverse clinical benefits and anti-aging potential", Altern Med Rev, 16 (4), 355-364.
[28] Polyakov N. E., Focsan A. L., Bowman M. K., Kispert L. D., (2010), "Free radical formation in novel carotenoid metal ion complexes of astaxanthin", Journal of Physical Chemistry B, 114 (50), 16968-16977.
[29] Enriquez M. M., Fuciman M., LaFountain A. M., Wagner N. L., Birge R. R., Frank H. A., (2010), "The intramolecular charge transfer state in carbonyl-containing polyenes and carotenoids", Journal of Physical Chemistry B, 114 (38), 12416-12426.
[30] Fukami H., Namikawa K., Sugiura-Tomimori N., Sumida M., Katano K., Nakao M., (2006), "Chemical Synthesis of Astaxanthin n-Octanoic Acid Monoester and Diester and Evaluation of Their Oral Absorbability", Journal of Oleo Science, 55 (12), 653-656.
[31] Shuaith N., (2015), "Synthesis and characterisation of novel astaxanthin metal complexes".
[32] Ruban A. V., Horton P., Young A. J., (1993), "Aggregation of higher plant xanthophylls: Differences in absorption spectra and in the dependency on solvent polarity", Journal of Photochemistry and Photobiology B: Biology, 21 (2), 229-234.
[33] Simonyi M., Bikádi Z., Zsila F., Deli J., (2003), "Supramolecular exciton chirality of carotenoid aggregates", Chirality, 15 (8), 680-698.
[34] Billsten H. H., Sundström V., Polívka T., (2005), "Self-Assembled Aggregates of the Carotenoid Zeaxanthin: Time-Resolved Study of Excited States", The Journal of Physical Chemistry A, 109 (8), 1521-1529.
[35] Musser A. J., Maiuri M., Brida D., Cerullo G., Friend R. H., Clark J., (2015), "The Nature of Singlet Exciton Fission in Carotenoid Aggregates", Journal of the American Chemical Society, 137 (15), 5130-5139.
[36] Wang C., Tauber M. J., (2010), "High-Yield Singlet Fission in a Zeaxanthin Aggregate Observed by Picosecond Resonance Raman Spectroscopy", Journal of the American Chemical Society, 132 (40), 13988-13991.
[37] Chábera P., Fuciman M., Razi Naqvi K., Polívka T., (2010), "Ultrafast dynamics of hydrophilic carbonyl carotenoids – Relation between structure and excited-state properties in polar solvents", Chemical Physics, 373 (1), 56-64.
[38] Sliwka H.-R., Melø T.-B., Foss B. J., Abdel-Hafez S. H., Partali V., Nadolski G., Jackson H., Lockwood S. F., (2007), "Electron- and Energy-Transfer Properties of Hydrophilic Carotenoids", Chemistry – A European Journal, 13 (16), 4458-4466.
[39] Jackson H. L., Cardounel A. J., Zweier J. L., Lockwood S. F., (2004), "Synthesis, characterization, and direct aqueous superoxide anion scavenging of a highly water-dispersible astaxanthin-amino acid conjugate", Bioorganic & Medicinal Chemistry Letters, 14 (15), 3985-3991.
[40] Francis F. J., (1987), "Lesser-Known food colorants", Food technology, 41.
[41] Pham T. Q., Cormier F., Farnworth E., Tong V. H., Van Calsteren M.-R., (2000), "Antioxidant Properties of Crocin from Gardenia jasminoides Ellis and Study of the Reactions of Crocin with Linoleic Acid and Crocin with Oxygen", Journal of Agricultural and Food Chemistry, 48 (5), 1455-1461.
[42] Hashemi M., Hosseinzadeh H., (2019), "A comprehensive review on biological activities and toxicology of crocetin", Food and Chemical Toxicology, 130, 44-60.
[43] Li D., Wu G., Zhang H., Qi X., (2021), "Preparation of crocin nanocomplex in order to increase its physical stability", Food Hydrocolloids, 120, 106415.

[44] Sun Y., Xu H.-J., Zhao Y.-X., Wang L.-Z., Sun L.-R., Wang Z., Sun X.-F., (2013), "Crocin Exhibits Antitumor Effects on Human Leukemia HL-60 Cells In Vitro and In Vivo", Evidence-Based Complementary and Alternative Medicine, 2013, 690164.
[45] Nam K. N., Park Y.-M., Jung H.-J., Lee J. Y., Min B. D., Park S.-U., Jung W.-S., Cho K.-H., Park J.-H., Kang I., Hong J.-W., Lee E. H., (2010), "Anti-inflammatory effects of crocin and crocetin in rat brain microglial cells", European Journal of Pharmacology, 648 (1), 110-116.
[46] Dar R. A., Brahman P. K., Khurana N., Wagay J. A., Lone Z. A., Ganaie M. A., Pitre K. S., (2017), "Evaluation of antioxidant activity of crocin, podophyllotoxin and kaempferol by chemical, biochemical and electrochemical assays", Arabian Journal of Chemistry, 10, S1119-S1128.
[47] Akhondzadeh Basti A., Moshiri E., Noorbala A.-A., Jamshidi A.-H., Abbasi S. H., Akhondzadeh S., (2007), "Comparison of petal of Crocus sativus L. and fluoxetine in the treatment of depressed outpatients: A pilot double-blind randomized trial", Progress in Neuro-Psychopharmacology and Biological Psychiatry, 31 (2), 439-442.
[48] Tsimidou M., Biliaderis C. G., (1997), "Kinetic Studies of Saffron (Crocus sativus L.) Quality Deterioration", Journal of Agricultural and Food Chemistry, 45 (8), 2890-2898.
[49] Carmona M., Zalacain A., Pardo J. E., López E., Alvarruiz A., Alonso G. L., (2005), "Influence of Different Drying and Aging Conditions on Saffron Constituents", Journal of Agricultural and Food Chemistry, 53 (10), 3974-3979.
[50] Zsila F., Bikádi Z., Simonyi M., (2001), "Induced chirality upon crocetin binding to human serum albumin: origin and nature", Tetrahedron: Asymmetry, 12 (22), 3125-3137.
[51] Meléndez-Martínez A. J., (2019), "An Overview of Carotenoids, Apocarotenoids, and Vitamin A in Agro-Food, Nutrition, Health, and Disease", Molecular Nutrition & Food Research, 63 (15), 1801045.
[52] Britton G., Liaaen-Jensen S., Pfander H., (2012), "Carotenoids: handbook", Edition, Birkhäuser.
[53] Britton G., Liaaen-Jensen S., Pfander H., (2008), "Carotenoids, vol. 4: natural functions", Edition, Springer Science & Business Media.
[54] Lietz G., Oxley A., Boesch-Saadatmandi C., Kobayashi D., (2012), "Importance of β,β-carotene 15,15'-monooxygenase 1 (BCMO1) and β,β-carotene 9',10'-dioxygenase 2 (BCDO2) in nutrition and health", Molecular Nutrition & Food Research, 56 (2), 241-250.
[55] Amengual J., Lobo G. P., Golczak M., Li H. N., Klimova T., Hoppel C. L., Wyss A., Palczewski K., von Lintig J., (2011), "A mitochondrial enzyme degrades carotenoids and protects against oxidative stress", Faseb j, 25 (3), 948-959.
[56] Linnewiel K., Ernst H., Caris-Veyrat C., Ben-Dor A., Kampf A., Salman H., Danilenko M., Levy J., Sharoni Y., (2009), "Structure activity relationship of carotenoid derivatives in activation of the electrophile/antioxidant response element transcription system", Free Radical Biology and Medicine, 47 (5), 659-667.
[57] Harrison E. H., (2022), "Carotenoids, β-Apocarotenoids, and Retinoids: The Long and the Short of It", Nutrients, 14 (7).
[58] Moreno J. C., Mi J., Alagoz Y., Al-Babili S., (2021), "Plant apocarotenoids: from retrograde signaling to interspecific communication", The Plant Journal, 105 (2), 351-375.
[59] Boushey C. J., Coulston A. M., Rock C. L., Monsen E., (2001), "Nutrition in the Prevention and Treatment of Disease", Edition, Elsevier.
[60] Jang W., Lee C., Suh H.-J., Lee J., (2023), "β-Carotene and β-apo-8'-carotenal contents in processed foods in Korea", Food Science and Biotechnology, 32 (11), 1501-1513.
[61] Keşan G., Özcan E., Chábera P., Polívka T., Fuciman M., (2023), "Time-Resolved Spectroelectrochemical Dynamics of Carotenoid 8'-apo-β-Carotenal", ChemPlusChem, 88 (11), e202300404.
[62] Pan J., Xu Y., Sun L., Sundström V., Polívka T., (2004), "Carotenoid and Pheophytin on Semiconductor Surface: Self-Assembly and Photoinduced Electron Transfer", Journal of the American Chemical Society, 126 (10), 3066-3067.
[63] Di Donato M., Segado Centellas M., Lapini A., Lima M., Avila F., Santoro F., Cappelli C., Righini R., (2014), "Combination of Transient 2D-IR Experiments and Ab Initio Computations Sheds Light on the Formation of the Charge-Transfer State in Photoexcited Carbonyl Carotenoids", The Journal of Physical Chemistry B, 118 (32), 9613-9630.

[64] Kispert L., Gao G., Deng Y., Konovalov V., Jeevarajan A., Jeevarajan J., Hand E. J. A. C. S., (1997), "Carotenoid radical cations, dications and radical trications", 51 (5), 572-578.
[65] Kispert L. D., Polyakov N. E., (2010), "Carotenoid Radicals: Cryptochemistry of Natural Colorants", Chemistry Letters, 39 (3), 148-155.
[66] Polivka T., Sundstrom V., (2009), "Dark Excited States of Carotenoids: Consensus and Controversy", Chem. Phys. Lett., 477, 1.
[67] Fiedor L., Heriyanto, Fiedor J., Pilch M., (2016), "Effects of Molecular Symmetry on the Electronic Transitions in Carotenoids", The Journal of Physical Chemistry Letters, 7 (10), 1821-1829.
[68] Zimmermann J., Linden P. A., Vaswani H. M., Hiller R. G., Fleming G. R., (2002), "Two-Photon Excitation Study of Peridinin in Benzene and in the Peridinin Chlorophyll a-Protein (PCP)", The Journal of Physical Chemistry B, 106 (36), 9418-9423.
[69] Wei T., Balevičius V., Polívka T., Ruban A. V., Duffy C. D. P., (2019), "How carotenoid distortions may determine optical properties: lessons from the Orange Carotenoid Protein", Physical Chemistry Chemical Physics, 21 (41), 23187-23197.
[70] Wasielewski M. R., Kispert L. D., (1986), "Direct measurement of the lowest excited singlet state lifetime of all-trans-β-carotene and related carotenoids", Chemical Physics Letters, 128 (3), 238-243.
[71] Tavan P., Schulten K., (1987), "Electronic excitations in finite and infinite polyenes", Physical Review B, 36 (8), 4337-4358.
[72] Frank H. A., Christensen R. L. (2008), "Excited electronic states, photochemistry and photophysics of carotenoids". "Carotenoids: Volume 4: Natural Functions", Springer.
[73] Šebelík V., Kloz M., Rebarz M., Přeček M., Kang E.-H., Choi T.-L., Christensen R. L., Polívka T., (2020), "Spectroscopy and excited state dynamics of nearly infinite polyenes", Physical Chemistry Chemical Physics, 22 (32), 17867-17879.
[74] Naqvi K. R., (2016), "Least-Squares Is Not the Only Yardstick for Estimating the Absorption Limit of an Infinitely Long Conjugated Chain from Spectra of Oligomers", The Journal of Physical Chemistry Letters, 7 (4), 676-679.
[75] Polivka T., Sundstrom V., (2004), "Ultrafast dynamics of carotenoid excited states - From solution to natural and artificial systems", Chem. Rev., 104, 2021.
[76] Fuciman M., Kesan G., LaFountain A. M., Frank H. A., Polivka T., (2015), "Tuning the spectroscopic properties of aryl carotenoids by slight changes in structure", Journal of Physical Chemistry B, 119 (4), 1457-1467.
[77] Zigmantas D., Hiller R. G., Sharples F. P., Frank H. A., Sundstrom V., Polivka T., (2004), "Effect of a conjugated carbonyl group on the photophysical properties of carotenoids", Physical Chemistry Chemical Physics, 6 (11), 3009-3016.
[78] Chábera P., Fuciman M., Hříbek P., Polívka T., (2009), "Effect of carotenoid structure on excited-state dynamics of carbonyl carotenoids", Physical Chemistry Chemical Physics, 11 (39), 8795-8803.
[79] Hörvin Billsten H., Zigmantas D., Sundström V., Polívka T., (2002), "Dynamics of vibrational relaxation in the S1 state of carotenoids having 11 conjugated CC bonds", Chemical Physics Letters, 355 (5), 465-470.
[80] Kuznetsova V., Southall J., Cogdell R. J., Fuciman M., Polívka T., (2017), "Spectroscopic properties of the S1 state of linear carotenoids after excess energy excitation", Chemical Physics Letters, 683, 448-453.
[81] Fujii R., Onaka K., Kuki M., Koyama Y., Watanabe Y., (1998), "The 2Ag− energies of all-trans-neurosporene and spheroidene as determined by fluorescence spectroscopy", Chemical Physics Letters, 288 (5), 847-853.
[82] Sashima T., Nagae H., Kuki M., Koyama Y., (1999), "A new singlet-excited state of all-trans-spheroidene as detected by resonance-Raman excitation profiles", Chemical Physics Letters, 299 (2), 187-194.
[83] Polivka T., Herek J. L., Zigmantas D., Akerlund H. E., Sundstrom V., (1999), "Direct observation of the (forbidden) S1 state in carotenoids", Proc. Natl. Acad. Sci. U. S. A., 96, 4914.
[84] Tavan P., Schulten K., (1987), "Electronic Excitations in Finite and Infinite Polyenes", Phys. Rev. B: Condens. Matter Mater. Phys., 36, 4337.

[85] Englman R., Jortner J., (1970), "The energy gap law for radiationless transitions in large molecules", Molecular Physics, 18 (2), 145-164.
[86] Fujii R., Inaba T., Watanabe Y., Koyama Y., Zhang J.-P., (2003), "Two different pathways of internal conversion in carotenoids depending on the length of the conjugated chain", Chemical Physics Letters, 369 (1), 165-172.
[87] Zhang J.-P., Fujii R., Qian P., Inaba T., Mizoguchi T., Koyama Y., Onaka K., Watanabe Y., Nagae H., (2000), "Mechanism of the Carotenoid-to-Bacteriochlorophyll Energy Transfer via the S1 State in the LH2 Complexes from Purple Bacteria", The Journal of Physical Chemistry B, 104 (15), 3683-3691.
[88] Keşan G., Litvín R., Bína D., Durchan M., Šlouf V., Polívka T., (2016), "Efficient light-harvesting using non-carbonyl carotenoids: Energy transfer dynamics in the VCP complex from Nannochloropsis oceanica", Biochimica et Biophysica Acta (BBA) - Bioenergetics, 1857 (4), 370-379.
[89] de Weerd F. L., van Stokkum I. H. M., van Grondelle R., (2002), "Subpicosecond dynamics in the excited state absorption of all-trans-β-Carotene", Chemical Physics Letters, 354 (1), 38-43.
[90] Nagae H., Kakitani T., Katoh T., Mimuro M., (1993), "Calculation of the excitation transfer matrix elements between the S2 or S1 state of carotenoid and the S2 or S1 state of bacteriochlorophyll", The Journal of Chemical Physics, 98 (10), 8012-8023.
[91] Frank H. A., Bautista J. A., Josue J., Pendon Z., Hiller R. G., Sharples F. P., Gosztola D., Wasielewski M. R., (2000), "Effect of the solvent environment on the spectroscopic properties and dynamics of the lowest excited states of carotenoids", Journal of Physical Chemistry B, 104 (18), 4569-4577.
[92] Keşan G., Durchan M., Tichý J., Minofar B., Kuznetsova V., Fuciman M., Šlouf V., Parlak C., Polívka T., (2015), "Different Response of Carbonyl Carotenoids to Solvent Proticity Helps To Estimate Structure of the Unknown Carotenoid from Chromera velia", The Journal of Physical Chemistry B, 119 (39), 12653-12663.
[93] Ilagan R. P., Christensen R. L., Chapp T. W., Gibson G. N., Pascher T., Polivka T., Frank H. A., (2005), "Femtosecond time-resolved absorption spectroscopy of astaxanthin in solution and in alpha-crustacyanin", J Phys Chem A, 109 (14), 3120-3127.
[94] Bondarev S. L., Knyukshto V. N., (1994), "Fluorescence from the S1(2 1Ag) state of all-trans-β-carotene", Chemical Physics Letters, 225 (4), 346-350.
[95] Hashimoto H., Uragami C., Yukihira N., Gardiner A. T., Cogdell R. J., (2018), "Understanding/unravelling carotenoid excited singlet states", Journal of The Royal Society Interface, 15 (141), 20180026.
[96] Furuichi K., Sashima T., Koyama Y., (2002), "The first detection of the 3Ag− state in carotenoids using resonance-Raman excitation profiles", Chemical Physics Letters, 356 (5), 547-555.
[97] Nagae H., Koyama Y., (2010), "Mechanism enabling the observation of the formally optically-forbidden 2Ag- and 1Bu- states in resonance-Raman excitation profiles of spheroidene in KBr disc", Chemical Physics, 373 (1), 145-152.
[98] Dick B., Hohlneicher G., (1982), "Importance of initial and final states as intermediate states in two-photon spectroscopy of polar molecules", The Journal of Chemical Physics, 76 (12), 5755-5760.
[99] Abe S., (2001), "Two-photon probe of forbidden exciton states in symmetric aggregates of asymmetric molecules", Chemical Physics, 264 (3), 355-363.
[100] Wagner N. L., Greco J. A., Enriquez M. M., Frank H. A., Birge R. R., (2013), "The nature of the intramolecular charge transfer state in peridinin", Biophysical journal, 104 (6), 1314-1325.
[101] Ehlers F., Scholz M., Schimpfhauser J., Bienert J., Oum K., Lenzer T., (2015), "Collisional Relaxation of Apocarotenals: Identifying the S* State With Vibrationally Excited Molecules in the Ground Electronic State S-0*", Phys. Chem. Chem. Phys., 17, 10478.
[102] Bautista J. A., Connors R. E., Raju B. B., Hiller R. G., Sharples F. P., Gosztola D., Wasielewski M. R., Frank H. A., (1999), "Excited state properties of peridinin: Observation of a solvent dependence of the lowest excited singlet state lifetime and spectral behavior unique among carotenoids", Journal of Physical Chemistry B, 103 (41), 8751-8758.

[103] Vaswani H. M., Hsu C.-P., Head-Gordon M., Fleming G. R., (2003), "Quantum Chemical Evidence for an Intramolecular Charge-Transfer State in the Carotenoid Peridinin of Peridinin−Chlorophyll−Protein", The Journal of Physical Chemistry B, 107 (31), 7940-7946.
[104] Papagiannakis E., Larsen D. S., van Stokkum I. H. M., Vengris M., Hiller R. G., van Grondelle R., (2004), "Resolving the Excited State Equilibrium of Peridinin in Solution", Biochemistry, 43 (49), 15303-15309.
[105] Zigmantas D., Hiller R. G., Yartsev A., Sundström V., Polívka T., (2003), "Dynamics of Excited States of the Carotenoid Peridinin in Polar Solvents: Dependence on Excitation Wavelength, Viscosity, and Temperature", The Journal of Physical Chemistry B, 107 (22), 5339-5348.
[106] Frank H. A., Bautista J. A., Josue J., Pendon Z., Hiller R. G., Sharples F. P., Gosztola D., Wasielewski M. R., (2000), "Effect of the Solvent Environment on the Spectroscopic Properties and Dynamics of the Lowest Excited States of Carotenoids", The Journal of Physical Chemistry B, 104 (18), 4569-4577.
[107] Linden P. A., Zimmermann J., Brixner T., Holt N. E., Vaswani H. M., Hiller R. G., Fleming G. R., (2004), "Transient Absorption Study of Peridinin and Peridinin−Chlorophyll a−Protein after Two-Photon Excitation", The Journal of Physical Chemistry B, 108 (29), 10340-10345.
[108] Polívka T., van Stokkum I. H. M., Zigmantas D., van Grondelle R., Sundström V., Hiller R. G., (2006), "Energy Transfer in the Major Intrinsic Light-Harvesting Complex from Amphidinium carterae", Biochemistry, 45 (28), 8516-8526.
[109] Shima S., Ilagan R. P., Gillespie N., Sommer B. J., Hiller R. G., Sharples F. P., Frank H. A., Birge R. R., (2003), "Two-photon and fluorescence spectroscopy and the effect of environment on the photochemical properties of peridinin in solution and in the peridinin-chlorophyll-protein from Amphidinium carterae", Journal of Physical Chemistry A, 107 (40), 8052-8066.
[110] Durchan M., Fuciman M., Šlouf V., Keşan G., Polívka T., (2012), "Excited-State Dynamics of Monomeric and Aggregated Carotenoid 8'-Apo-β-carotenal", The Journal of Physical Chemistry A, 116 (50), 12330-12338.
[111] Redeckas K., Voiciuk V., Vengris M., (2016), "Investigation of the S1/ICT equilibrium in fucoxanthin by ultrafast pump–dump–probe and femtosecond stimulated Raman scattering spectroscopy", Photosynthesis Research, 128 (2), 169-181.
[112] West R. G., Fuciman M., Staleva-Musto H., Sebelik V., Bina D., Durchan M., Kuznetsova V., Polivka T., (2018), "Equilibration Dependence of Fucoxanthin S1 and ICT Signatures on Polarity, Proticity, and Temperature by Multipulse Femtosecond Absorption Spectroscopy", Journal of Physical Chemistry B, 122 (29), 7264-7276.
[113] Papagiannakis E., van Stokkum I. H. M., van Grondelle R., Niederman R. A., Zigmantas D., Sundstrom V., Polivka T., (2003), "A Near-Infrared Transient Absorption Study of the Excited-State Dynamics of the Carotenoid Spirilloxanthin in Solution and in the LH1 Complex of Rhodospirillum Rubrum", J. Phys. Chem. B, 107, 11216.
[114] Papagiannakis E., Das S. K., Gall A., Van Stokkum I. H., Robert B., Van Grondelle R., Frank H. A., Kennis J. T., (2003), "Light harvesting by carotenoids incorporated into the B850 light-harvesting complex from Rhodobacter s phaeroides R-26.1: excited-state relaxation, ultrafast triplet formation, and energy transfer to bacteriochlorophyll", The Journal of Physical Chemistry B, 107 (23), 5642-5649.
[115] Wohlleben W., Buckup T., Hashimoto H., Cogdell R. J., Herek J. L., Motzkus M., (2004), "Pump-Deplete-Probe Spectroscopy and the Puzzle of Carotenoid Dark States", J. Phys. Chem. B, 108, 3320.
[116] Berera R., van Stokkum I. H. M., Kodis G., Keirstead A. E., Pillai S., Herrero C., Palacios R. E., Vengris M., van Grondelle R., Gust D., Moore T. A., Moore A. L., Kennis J. T. M., (2007), "Energy Transfer, Excited-State Deactivation, and Exciplex Formation in Artificial Caroteno-Phthalocyanine Light-Harvesting Antennas", The Journal of Physical Chemistry B, 111 (24), 6868-6877.
[117] Cong H., Niedzwiedzki D. M., Gibson G. N., LaFountain A. M., Kelsh R. M., Gardiner A. T., Cogdell R. J., Frank H. A., (2008), "Ultrafast time-resolved carotenoid to-bacteriochlorophyll energy transfer in LH2 complexes from photosynthetic bacteria", Journal of Physical Chemistry B, 112 (34), 10689-10703.

[118] Buckup T., Savolainen J., Wohlleben W., Herek J. L., Hashimoto H., Correia R. R., Motzkus M. J. T. J. o. c. p., (2006), "Pump-probe and pump-deplete-probe spectroscopies on carotenoids with N= 9–15 conjugated bonds", 125 (19), 194505.
[119] Buckup T., Hauer J., Möhring J., Motzkus M., (2009), "Multidimensional spectroscopy of β-carotene: Vibrational cooling in the excited state", Archives of Biochemistry and Biophysics, 483 (2), 219-223.
[120] Niedzwiedzki D. M., Sullivan J. O., Polivka T., Birge R. R., Frank H. A., (2006), "Femtosecond time-resolved transient absorption spectroscopy of xanthophylls", Journal of Physical Chemistry B, 110 (45), 22872-22885.
[121] Niedzwiedzki D., Koscielecki J. F., Cong H., Sullivan J. O., Gibson G. N., Birge R. R., Frank H. A., (2007), "Ultrafast dynamics and excited state spectra of open-chain carotenoids at room and low temperatures", Journal of Physical Chemistry B, 111 (21), 5984-5998.
[122] Andersson P. O., Gillbro T., (1995), "Photophysics and Dynamcis of the Lowest Excited Singlet-State in Long Substituted Polyenes With Implications to the Very Long-Chain Limit", J. Chem. Phys., 103, 2509.
[123] Lenzer T., Ehlers F., Scholz M., Oswald R., Oum K., (2010), "Assignment of Carotene S* state Features to the Vibrationally Hot Ground Electronic State", Phys. Chem. Chem. Phys., 12, 8832.
[124] Papagiannakis E., van Stokkum I. H. M., Vengris M., Cogdell R. J., van Grondelle R., Larsen D. S., (2006), "Excited-State Dynamics of Carotenoids in Light-Harvesting Complexes. 1. Exploring the Relationship between the S-1 and S* States", J. Phys. Chem. B, 110, 5727.
[125] Balevicius V., Pour A. G., Savolainen J., Lincoln C. N., Lukes V., Riedle E., Valkunas L., Abramavicius D., Hauer J., (2015), "Vibronic Energy Relaxation Approach Highlighting Deactivation Pathways in Carotenoids", Phys. Chem. Chem. Phys., 17, 19491.
[126] Polyakov N. E., Konovalov V. V., Leshina T. V., Luzina O. A., Salakhutdinov N. F., Konovalova T. A., Kispert L. D., (2001), "One-electron transfer product of quinone addition to carotenoids: EPR and optical absorption studies", Journal of Photochemistry and Photobiology A: Chemistry, 141 (2), 117-126.
[127] Gao Y., Kispert L. D., (2003), "Reaction of Carotenoids and Ferric Chloride: Equilibria, Isomerization, and Products", The Journal of Physical Chemistry B, 107 (22), 5333-5338.
[128] Gao G., Deng Y., Kispert L. D., (1997), "Photoactivated Ferric Chloride Oxidation of Carotenoids by Near-UV to Visible Light", The Journal of Physical Chemistry B, 101 (39), 7844-7849.
[129] Konovalova T. A., Kispert L. D., Konovalov V. V., (1999), "Surface Modification of TiO2 Nanoparticles with Carotenoids. EPR Study", The Journal of Physical Chemistry B, 103 (22), 4672-4677.
[130] Gao G., Deng Y., Kispert L. D., (1998), "Semiconductor Photocatalysis: Photodegradation and Trans−Cis Photoisomerization of Carotenoids", The Journal of Physical Chemistry B, 102 (20), 3897-3901.
[131] Konovalova T. A., Dikanov S. A., Bowman M. K., Kispert L. D., (2001), "Detection of Anisotropic Hyperfine Components of Chemically Prepared Carotenoid Radical Cations: 1D and 2D ESEEM and Pulsed ENDOR Study", The Journal of Physical Chemistry B, 105 (35), 8361-8368.
[132] Konovalova T. A., Gao Y., Kispert L. D., van Tol J., Brunel L.-C., (2003), "Characterization of Fe−MCM-41 Molecular Sieves with Incorporated Carotenoids by Multifrequency Electron Paramagnetic Resonance", The Journal of Physical Chemistry B, 107 (4), 1006-1011.
[133] Gao Y., Konovalova T. A., Xu T., Kispert L. D., (2002), "Electron Transfer of Carotenoids Imbedded in MCM-41 and Ti−MCM-41: EPR, ENDOR, and UV−Vis Studies", The Journal of Physical Chemistry B, 106 (42), 10808-10815.
[134] Konovalova T. A., Kispert L. D., Konovalov V. V., (1997), "Photoinduced Electron Transfer between Carotenoids and Solvent Molecules", The Journal of Physical Chemistry B, 101 (39), 7858-7862.
[135] Khaled M., Hadjipetrou A., Kispert L. D., Allendoerfer R. D., (1991), "Simultaneous electrochemical and electron paramagnetic resonance studies of carotenoid cation radicals and dications", The Journal of Physical Chemistry, 95 (6), 2438-2442.
[136] Hapiot P., Kispert L. D., Konovalov V. V., Savéant J.-M., (2001), "Single Two-Electron Transfers vs Successive One-Electron Transfers in Polyconjugated Systems Illustrated by the

Electrochemical Oxidation and Reduction of Carotenoids", Journal of the American Chemical Society, 123 (27), 6669-6677.
[137] Liu D., Gao Y., Kispert L. D., (2000), "Electrochemical properties of natural carotenoids", Journal of Electroanalytical Chemistry, 488 (2), 140-150.
[138] Polyakov N. E., Leshina T. V., Konovalova T. A., Kispert L. D., (2001), "Carotenoids as scavengers of free radicals in a fenton reaction: antioxidants or pro-oxidants?", Free Radical Biology and Medicine, 31 (3), 398-404.
[139] Focsan A. L., Bowman M. K., Konovalova T. A., Molnár P., Deli J., Dixon D. A., Kispert L. D., (2008), "Pulsed EPR and DFT Characterization of Radicals Produced by Photo-Oxidation of Zeaxanthin and Violaxanthin on Silica−Alumina", The Journal of Physical Chemistry B, 112 (6), 1806-1819.
[140] Woodall A. A., Lee S. W.-M., Weesie R. J., Jackson M. J., Britton G., (1997), "Oxidation of carotenoids by free radicals: relationship between structure and reactivity", Biochimica et Biophysica Acta (BBA) - General Subjects, 1336 (1), 33-42.
[141] Jeevarajan J. A., Wei C. C., Jeevarajan A. S., Kispert L. D., (1996), "Optical Absorption Spectra of Dications of Carotenoids", The Journal of Physical Chemistry, 100 (14), 5637-5641.
[142] Burton G. W., Ingold K. U., (1984), "β-Carotene: an Unusual Type of Lipid Antioxidant", Science, 224 (4649), 569-573.
[143] Krinsky N. I., Mayne S. T., Sies H., (2004), "Carotenoids in health and disease", Edition, CRC Press.
[144] Jørgensen K., Skibsted L. H., (1993), "Carotenoid scavenging of radicals", Zeitschrift für Lebensmittel-Untersuchung und Forschung, 196 (5), 423-429.
[145] Gao Y., Kispert L. D., Konovalova T. A., Lawrence J. N., (2004), "Isomerization of Carotenoids in the Presence of MCM-41 Molecular Sieves: EPR and HPLC Studies", The Journal of Physical Chemistry B, 108 (27), 9456-9462.
[146] Edge R., El-Agamey A., Land E. J., Navaratnam S., George Truscott T., (2007), "Studies of carotenoid one-electron reduction radicals", Archives of Biochemistry and Biophysics, 458 (2), 104-110.
[147] Jørgensen K., Skibsted L. H., (1993), "Carotenoid scavenging of radicals. Effect of carotenoid structure and oxygen partial pressure on antioxidative activity", Zeitschrift fur Lebensmittel-Untersuchung und -Forschung, 196 (5), 423-429.
[148] Palozza P., (1998), "Prooxidant Actions of Carotenoids in Biologic Systems", Nutrition Reviews, 56 (9), 257-265.
[149] Burke M., Land E. J., McGarvey D. J., Truscott T. G., (2000), "Carotenoid triplet state lifetimes", Journal of Photochemistry and Photobiology B: Biology, 59 (1), 132-138.
[150] Peterman E. J., Dukker F. M., Van Grondelle R., Van Amerongen H., (1995), "Chlorophyll a and carotenoid triplet states in light-harvesting complex II of higher plants", Biophysical journal, 69 (6), 2670-2678.
[151] Li H., Zhang P., Song X., Wang W., (2011), "Determination of Astaxanthin and Canthaxanthin Triplet Properties in Different Polarities of the Solvent by Laser Flash Photolysis", Chinese Journal of Chemistry, 29 (7), 1535-1540.
[152] Gust D., Moore T. A., Moore A. L., Jori G., Reddi E., The photochemistry of carotenoids: some photosynthetic and photomedical aspects, in: (Ed.)^(Eds.), pp. 32–47.
[153] Khoo H.-E., Prasad K. N., Kong K.-W., Jiang Y., Ismail A., (2011), "Carotenoids and Their Isomers: Color Pigments in Fruits and Vegetables", Molecules, 16 (2), 1710-1738.
[154] Honda M., Murakami K., Watanabe Y., Higashiura T., Fukaya T., Wahyudiono, Kanda H., Goto M., (2017), "The E/Z isomer ratio of lycopene in foods and effect of heating with edible oils and fats on isomerization of (all-E)-lycopene", European Journal of Lipid Science and Technology, 119 (8), 1600389.
[155] Honda M., Nakayama Y., Nishikawa S., Tsuda T., (2020), "Z-Isomers of lycopene exhibit greater liver accumulation than the all-E-isomer in mice", Bioscience, Biotechnology, and Biochemistry, 84 (2), 428-431.
[156] Limpens J., Schröder F. H., de Ridder C. M. A., Bolder C. A., Wildhagen M. F., Obermüller-Jevic U. C., Krämer K., van Weerden W. M., (2006), "Combined Lycopene and Vitamin E Treatment

Suppresses the Growth of PC-346C Human Prostate Cancer Cells in Nude Mice", The Journal of Nutrition, 136 (5), 1287-1293.
[157] Manabe Y., Komatsu T., Seki S., Sugawara T., (2018), "Dietary astaxanthin can accumulate in the brain of rats", Bioscience, Biotechnology, and Biochemistry, 82 (8), 1433-1436.
[158] Honda M., Kageyama H., Hibino T., Ichihashi K., Takada W., Goto M., (2020), "Isomerization of Commercially Important Carotenoids (Lycopene, β-Carotene, and Astaxanthin) by Natural Catalysts: Isothiocyanates and Polysulfides", Journal of Agricultural and Food Chemistry, 68 (10), 3228-3237.
[159] Penteado M. D. V. C. (2003), "Vitaminas: aspectos nutricionais, bioquímicos, clínicos e analíticos". "Vitaminas: aspectos nutricionais, bioquímicos, clínicos e analíticos".
[160] de Carvalho L. M. J., Ortiz G. M. D., de Carvalho J. L. V., Smirdele L., de Souza Neves Cardoso F., (2017), "Carotenoids in yellow sweet potatoes, pumpkins and yellow sweet cassava", Edition, IntechOpen: London, UK.
[161] Rodriguez-Amaya D. B., Kimura M., (2004), "HarvestPlus handbook for carotenoid analysis", Edition, International Food Policy Research Institute (IFPRI) Washington.
[162] Lin C. H., Chen B. H., (2003), "Determination of carotenoids in tomato juice by liquid chromatography", Journal of Chromatography A, 1012 (1), 103-109.
[163] Britton G., UV/visible spectroscopy, Carotenoids 1B: Spectroscopy, in: (Ed.)^(Eds.), Basel: Birkhauser, 1995, pp.
[164] Schieber A., Carle R., (2005), "Occurrence of carotenoid cis-isomers in food: Technological, analytical, and nutritional implications", Trends in Food Science & Technology, 16 (9), 416-422.
[165] Yuan J.-P., Chen F., (1999), "Isomerization of trans-Astaxanthin to cis-Isomers in Organic Solvents", Journal of Agricultural and Food Chemistry, 47 (9), 3656-3660.
[166] Khan T., Litvín R., Šebelík V., Polívka T., (2021), "Excited-State Evolution of Keto-Carotenoids after Excess Energy Excitation in the UV Region", ChemPhysChem, 22 (5), 471-480.
[167] Christensson N., Polivka T., Yartsev A., Pullerits T., (2009), "Photon echo spectroscopy reveals structure-dynamics relationships in carotenoids", Physical Review B, 79 (24), 245118.
[168] Berezin K. V., Nechaev V. V., (2005), "Calculation of the IR Spectrum and the Molecular Structure of β-Carotene", Journal of Applied Spectroscopy, 72 (2), 164-171.
[169] Christensen R. L., Goyette M., Gallagher L., Duncan J., DeCoster B., Lugtenburg J., Jansen F. J., van der Hoef I., (1999), "S1 and S2 States of Apo- and Diapocarotenes", The Journal of Physical Chemistry A, 103 (14), 2399-2407.
[170] Ali A. H., (2022), "High-performance liquid chromatography (HPLC): a review", Ann. Adv. Chem, 6, 010-020.
[171] Žuvela P., Skoczylas M., Jay Liu J., Bączek T., Kaliszan R., Wong M. W., Buszewski B., (2019), "Column Characterization and Selection Systems in Reversed-Phase High-Performance Liquid Chromatography", Chemical Reviews, 119 (6), 3674-3729.
[172] Litvín R., Bína D., Herbstová M., Gardian Z., (2016), "Architecture of the light-harvesting apparatus of the eustigmatophyte alga Nannochloropsis oceanica", Photosynthesis Research, 130 (1), 137-150.
[173] Lakowicz J. R., (2006), "Principles of fluorescence spectroscopy", Edition, Springer.
[174] van Stokkum I. H. M., Larsen D. S., van Grondelle R., (2004), "Global and Target Analysis of Time-Resolved Spectra", Biochim. Biophys. Acta, Bioenerg., 1657, 82.
[175] Zhai Y., Zhu Z., Zhou S., Zhu C., Dong S., (2018), "Recent advances in spectroelectrochemistry", Nanoscale, 10 (7), 3089-3111.
[176] Rackus D. G., Shamsi M. H., Wheeler A. R., (2015), "Electrochemistry, biosensors and microfluidics: a convergence of fields", Chemical Society Reviews, 44 (15), 5320-5340.
[177] Sheng T., Xu Y.-F., Jiang Y.-X., Huang L., Tian N., Zhou Z.-Y., Broadwell I., Sun S.-G., (2016), "Structure Design and Performance Tuning of Nanomaterials for Electrochemical Energy Conversion and Storage", Accounts of Chemical Research, 49 (11), 2569-2577.
[178] Zhang W., Lai W., Cao R., (2017), "Energy-Related Small Molecule Activation Reactions: Oxygen Reduction and Hydrogen and Oxygen Evolution Reactions Catalyzed by Porphyrin- and Corrole-Based Systems", Chemical Reviews, 117 (4), 3717-3797.

[179] Goswami S., Matula A. J., Rath S. P., Hedström S., Saha S., Annamalai M., Sengupta D., Patra A., Ghosh S., Jani H., Sarkar S., Motapothula M. R., Nijhuis C. A., Martin J., Goswami S., Batista V. S., Venkatesan T., (2017), "Robust resistive memory devices using solution-processable metal-coordinated azo aromatics", Nature Materials, 16 (12), 1216-1224.
[180] Compton R. G., Spectroelectrochemistry. Edited by Wolfgang Kaim and Axel Klein, in: (Ed.)^(Eds.), Wiley Online Library, 2008, pp.
[181] Kaim W., Fiedler J., (2009), "Spectroelectrochemistry: the best of two worlds", Chemical Society Reviews, 38 (12), 3373-3382.
[182] Heineman W. R., (1978), "Spectroelectrochemistry. Combination of optical and electrochemical techniques for studies of redox chemistry", Analytical Chemistry, 50 (3), 390A-402A.
[183] Ooka H., Takashima T., Yamaguchi A., Hayashi T., Nakamura R., (2017), "Element strategy of oxygen evolution electrocatalysis based on in situ spectroelectrochemistry", Chemical Communications, 53 (53), 7149-7161.
[184] Bubrin M., Schweinfurth D., Ehret F., Záliš S., Kvapilová H., Fiedler J., Zeng Q., Hartl F., Kaim W., (2014), "Structure and Spectroelectrochemical Response of Arene–Ruthenium and Arene–Osmium Complexes with Potentially Hemilabile Noninnocent Ligands", Organometallics, 33 (18), 4973-4985.
[185] Martín-Yerga D., Pérez-Junquera A., Hernández-Santos D., Fanjul-Bolado P., (2017), "Time-Resolved Luminescence Spectroelectrochemistry at Screen-Printed Electrodes: Following the Redox-Dependent Fluorescence of [Ru(bpy)3]2+", Analytical Chemistry, 89 (20), 10649-10654.
[186] Bond A. M., (2002), "Broadening electrochemical horizons: principles and illustration of voltammetric and related techniques", Edition, Oxford University Press, USA.
[187] Goia S., Turner M. A. P., Woolley J. M., Horbury M. D., Borrill A. J., Tully J. J., Cobb S. J., Staniforth M., Hine N. D. M., Burriss A., Macpherson J. V., Robinson B. R., Stavros V. G., (2022), "Ultrafast transient absorption spectroelectrochemistry: femtosecond to nanosecond excited-state relaxation dynamics of the individual components of an anthraquinone redox couple", Chemical Science, 13 (2), 486-496.
[188] Pitman C. L., Miller A. J. M., (2014), "Molecular Photoelectrocatalysts for Visible Light-Driven Hydrogen Evolution from Neutral Water", ACS Catalysis, 4 (8), 2727-2733.
[189] Liu J., Lu L., Wood D., Lin S., (2020), "New Redox Strategies in Organic Synthesis by Means of Electrochemistry and Photochemistry", ACS Central Science, 6 (8), 1317-1340.
[190] Lee K. J., Elgrishi N., Kandemir B., Dempsey J. L., (2017), "Electrochemical and spectroscopic methods for evaluating molecular electrocatalysts", Nature Reviews Chemistry, 1 (5), 0039.

Research Section

5. Paper I

Ultrafast excited states dynamics of metal ion complexes of the carotenoid astaxanthin

Özcan, E., Kuznetsova, V., Keşan, G., Fuciman, M., Litvín, R., & Polívka, T. (2023). Journal of Photochemistry and Photobiology A: Chemistry, 441, 114737. https://doi.org/10.1016/j.jphotochem.2023.114737

Abstract

Carotenoids are natural compounds with multiple functions in biological systems. They exhibit rich photophysics that can be modified by changes in properties of their local environments. Here we present time-resolved spectroscopy data from complexes resulting from interaction of the carotenoid astaxanthin with Zn^{2+} and Cu^{2+} ions. The astaxanthin-metal complexes exhibit significant alteration of their excited-state dynamics, resulting in enhancement of the charge transfer character of the lowest excited state, S_1/ICT. The S_1/ICT lifetime of pure astaxanthin, 4.4 ps, is shortened to 3.9 ps and 2.6 ps for astaxanthin-Zn and astaxanthin-Cu complex, respectively. The lifetime shortening is attributed to prolongation of effective conjugation caused by interaction of metal ions with keto oxygen at the terminal rings of astaxanthin. The significant shortening of the S_1/ICT lifetime of astaxanthin-Cu complex also results in observation of the S* signal, which is likely due to a hot ground state generated by rapid depopulation of excited states.

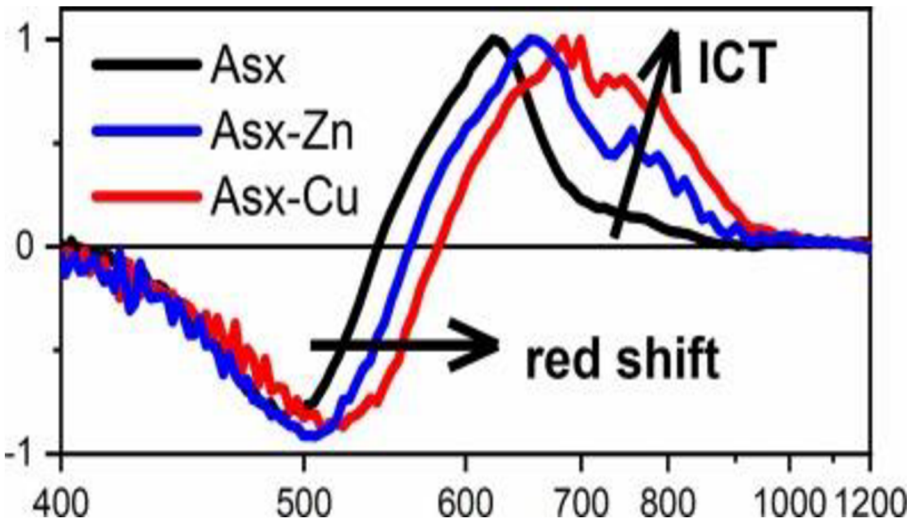

Keywords: Carotenoids, Metal complexes, Ultrafast spectroscopy, Charge transfer state.

5.1. Introduction

Photophysical and photochemical properties of carotenoids have been a subject of numerous studies as these pigments play important role in many photo-driven reactions in biological systems. Besides their well-known function as light-harvesting pigments in photosynthesis [1, 2], they are the key molecules involved in photoprotection. Here they act at a broad range of timescales extending from ultrafast (picosecond) quenching of singlet excited states of chlorophylls [3–6] to (sub)nanosecond quenching of (bacterio)chlorophyll triplets [7,8], and even slower, microsecond, quenching of singlet oxygen or other reactive oxygen species [9–14]. The variety of carotenoid functions together with their rich excited-state dynamics [15] makes these molecules attractive subjects of spectroscopic studies. A large number of carotenoids have been identified in nature, but much less have been studied in detail by advanced spectroscopic methods. The most studied are especially plant carotenoids lutein, zeaxanthin and violaxanthin due to their key role in light-harvesting and photoprotection in plants [5], the keto-carotenoids fucoxanthin and peridinin due to their large abundance in nature and excellent light-harvesting capacity [16–21], as well as linear carotenoids from purple bacteria, such as neurosporene, spheroidene or lycopene [22–24].

Another intensely studied carotenoid is astaxanthin (Asx). Although it does not play a role in light-harvesting and it is rather known as natural colorant giving color to the lobster carapace [25], flamingo feathers [26], or as an essential dietary nutrient for salmon playing role on its growth and survival [27,28], it is also a highly efficient antioxidant [26,29,30] with promising positive effects on human health [31,32]. Asx belongs to the family of keto-carotenoids which have their conjugated C=C backbone extended to C=O group. These carotenoids exhibit even more complex excited-state dynamics as the presence of the conjugated keto group introduces an intramolecular charge transfer (ICT) state into their excited state manifold.

The excited states of all carotenoids are in the simplest picture described by two excited states: the strongly absorbing S_2 state and the low-lying excited state S_1, for which the one-photon transition from the ground state S_0 is forbidden [15]. For keto-carotenoids, a polar environment stabilizes the ICT state that is coupled to the dark S_1 state, forming a state usually denoted as S_1/ICT state [33], which can be viewed as a double-well potential separated by a small barrier allowing fast equilibration between the S_1-like and ICT-like potential minima [34,35]. The presence of the ICT state is readily detected by characteristic bands in transient absorption spectrum; the ICT-like transition is for most carotenoids significantly red-shifted from the S_1-Sn band and amplitude ratio between S_1-Sn and ICT-like bands is a measure of degree of charge transfer character of the coupled S_1/ICT state [18, 21]. Even though the two bands typically exhibits the same time evolution, they are associated with two minima of the complicated S_1/ICT potential surface as evidenced by pump-dump-probe experiments [34, 35].

A number of experiments have shown that the charge transfer character increases with increasing solvent polarity, but another important parameter is the position of the conjugated keto group. For asymmetric position of a single keto-group the ICT signal increases but two symmetrically positioned keto groups minimize the charge transfer character of the S_1/ICT state [36]. This is precisely the case of Asx which has two symmetric conjugated keto groups at the terminal rings (Fig. 1), resulting in a weak ICT signal detected in a broad range of solvents [37, 38].

Asx has also been reported to form complexes with metal ions with the most likely Asx-metal interaction points being the hydroxy and keto groups at the terminal rings [39–41], suggesting they could also affect the ICT state properties. Asx complexes binding Cu^{2+}, Ca^{2+}, Zn^{2+}, and Fe^{2+} were reported and confirmed by NMR and optical spectroscopy [39, 40]. In absorption spectra, the metal binding induced a red shift causing extension of absorption spectrum to nearly 600 nm. Alternatively, in dichloromethane, Asx radical was generated [39]. These studies demonstrated feasibility of formation of stable Asx-metal complexes, but they did not provide information about effect of metal binding on excited-state properties of Asx.

Here we have prepared astaxanthin-Cu^{2+} (Asx-Cu) and astaxanthin-Zn^{2+} (Asx-Zn) complexes characterized by red-shifted absorption spectrum in methanol. Further, we apply femtosecond transient absorption spectroscopy to examine in detail the excited-state properties of these complexes. Since no spectroscopic studies targeting possible effects of complexation with metals on excited-state properties of astaxanthin have been carried out so far, we compare the data taken for Asx-metal complexes with those measured for pure Asx in methanol solution. We show that interaction with metal ions enhances the charge transfer character of the S_1/ICT state and lengthens the effective conjugation of Asx.

5.2. Material and Methods

5.2.1. Sample preparation

For sample preparation methanol (UV grade, VWR), copper sulfate (Sigma Aldrich), copper chloride (Merck), zinc perchlorate hexahydrate (Alfa Aesar), and astaxanthin (Sigma Aldrich) were used as obtained except for zinc perchlorate hexahydrate which was dried at 300°C overnight to prepare anhydrous zinc perchlorate. Stock solutions of Asx (16×10^{-6} M), copper chloride ($CuCl_2$; 1×10^{-2} M), copper sulfate ($CuSO_4$; 1×10^{-3} M) and zinc perchlorate ($Zn(ClO_4)_2$; 1×10^{-3} M) were prepared in 50 ml of dry methanol. All stock solutions were maintained in dark at 4°C for two days to check the stability of the solutions. Then, Asx and metal salts were mixed in different molar ratios (Asx/Metals of 1:1, 1:2, 1:5, 1:10, 1:20, 1:50, 1:100, 1:200) in 10 ml-glass bottles individually and kept in dark at room temperature. Absorption spectra of the samples were regularly measured in UV–VIS spectrometer (Shimadzu UV-2600) in a 10-mm pathlength quartz cuvette to monitor long time (up to 750 h) changes in absorption spectra (Supporting Information Fig. S1). The samples with various molar

ratios were tested for stability and Asx-metal complex formations and the molar ratios with the best performance (1:5 for Asx/CuCl2, 1:100 for Asx/CuSO4 and Asx/ ZnClO4) were selected for spectroscopic experiments (Supporting Information Fig. S1).

5.2.2. Transient absorption spectroscopy

Transient absorption measurements were carried out with an experimental setup using a modular laser system consisting of a Ti: sapphire regenerative amplifier (Spitfire Ace-100F, Spectra-Physics, USA) seeded with a Ti:sapphire oscillator (MaiTai SP, Spectra-Physics, USA), and pumped by Nd:YLF laser (Empower 30, Spectra-Physics, USA). The laser system produces ~100 fs pulses centered at 800 nm at a 1-kHz repetition rate. The output was divided into excitation and probe beams by a beam splitter. The excitation beam was generated by an optical parametric amplifier (TOPAS Prime, Light Conversion, Lithuania). The probe pulses were generated by sending the 800 nm beam to a home-built OPA to produce a 1300 nm output that was focused to a 2-mm CaF_2 plate. A white-light continuum beam covers the 400–1200 nm spectral region. To minimize chirp and chromatic aberration, the white-light beam was collimated by an off-axis parabolic mirror and split by a broadband 50/50 beam splitter to reference and probe beams. The probe beam was focused by a 150 mm spherical mirror to the sample where it overlapped with the excitation beam. Probe and reference beams were dispersed in a prism spectrograph (Pascher Instruments, Sweden) and detected by a double CCD array allowing to measure in the whole 400–1200 nm spectral region. The spectrometer was calibrated before each experiment by placing a multiple oxide filter (WCT 2065, Avian Technologies, USA) into the white light beams in front of an entrance slit. The pump polarization was set at magic angle (54.7°) relative to the probe. The pump photon density at the sample was kept below 10^{14} photon. cm^{-2}. $pulse^{-1}$.

5.2.3. Data analysis

The resulting spectro-temporal data sets were analyzed using a global fitting software (CarpetView, Light Conversion, Lithuania). To visualize the excited-state dynamics, it was assumed that the excited system evolves according to a sequential, irreversible scheme. Each component in the sequential scheme represents individual excited-state species, and the spectral profile of each species is called evolution-associated difference spectrum (EADS). The spectra were chirp corrected using the correction routine within the same software.

5.3. Results

Absorption spectra of Asx and its metal complexes in methanol are shown in Fig. 1. Asx in methanol has an absorption spectrum with a single broad peak, reflecting the S_0-S_2 transition, with a maximum at 476 nm in agreement with previous reports [37]. When Asx is mixed with appropriate amount of $CuCl_2$ or $Zn(ClO_4)_2$, Asx-metal complexes are formed. The formation of the complex is associated with a red shift of the absorption maximum, to 504 nm for Asx-Cu and to 488 nm for Asx-

Zn complexes. The time evolution of the complex formation is shown in Supporting Information Fig. S1. Formation of the Asx-Cu complex by using $CuSO_4$ was also tested with essentially the same results as for $CuCl_2$. Formation of the Asx-Cu complex from $CuSO_4$ requires larger concentration of $CuSO_4$ than when $CuCl_2$ is used (Supporting Information Fig. S1). The formation of the Asx-metal complexes induces some decrease of absorbance (the concentration of Asx is identical for the black and red absorption spectra in Fig. 1). However, the area under the main absorption band decreases by less than 10% upon complexation for both Cu and Zn complexes, indicating that the transition dipole moment associated with the S_0-S_2 transition is only marginally changed. Absorption spectra of the complexation reactions also show clear isosbestic points, indicating the stability of Asx during the reactions (Supporting Information Fig. S1).

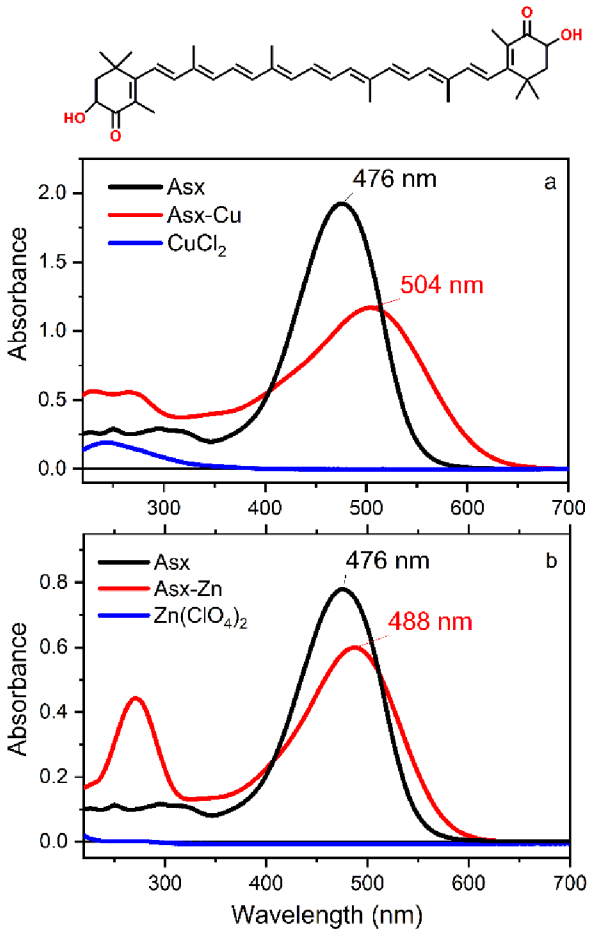

Figure 1. Absorption spectra in methanol. (a) 16 µM Asx (black), Asx-Cu complex produced by mixing of 16 µM Asx and 80 µM $CuCl_2$ (red), and 80 µM $CuCl_2$ (blue). (b) 6.15 µM Asx (black), Asx-Zn complex produced by mixing of 6.15 µM Asx and 0.615 mM of $Zn(ClO_4)_2$ (red), and 0.615 mM of $Zn(ClO_4)_2$ (blue). Structures of Asx are also shown.

The decrease of absorbance thus likely results from larger conformational disorder induced by complexation, generating broader distribution of the S_0-S_2 transition energies. Apart from the red shift of the main absorption band, some changes upon forming of complexes are observed also in the

UV part of the spectrum. A new band in UV is observed for Asx-Cu complex at 270 nm, and for Asx-Zn complex this band becomes intense, reaching ~75% of the main absorption band amplitude (Fig. 1). It should be noted that this band is not the *cis*-peak, which for Asx in methanol occurs at around 370 nm [42], thus the 270 nm band is not related to a possible isomerization upon complex formation. The mechanism of such an enhancement of the UV absorption band upon complexation with Zn^{2+} remains unknown. While Asx radical formation was identified in experiments using Asx and $CuCl_2$ in dichloromethane [39], no such reaction occurs for our Asx and $CuCl_2$ mixture in methanol. Onset of absorption of Asx radical cation is around 700 nm [39]. Fig. S2 (Supporting Information) shows absorption spectra of all our samples in the 200–1100 nm spectral region. No absorption occurs at wavelengths >700 nm, excluding the possibility of Asx cation radical formation.

Transient absorption spectra at different delays after excitation are shown in Fig. 2. Asx in methanol gives characteristic carotenoid spectra consisting of ground state bleaching and excited state absorption (ESA) due to the S_1-S_n transition. The ESA signal at early time after excitation (0.15 ps) also includes a NIR band at 1030 nm that is associated with ESA of the S_2 state [43]. The S_1-S_n band, peaking at 620 nm in agreement with earlier studies of Asx in methanol [37], is fully developed within the first picosecond. The weak shoulder in the 700–800 nm spectral region signals the presence of an ICT state. The ICT signal is weak because Asx is a carotenoid with long conjugation and two symmetrically positioned keto groups [36].

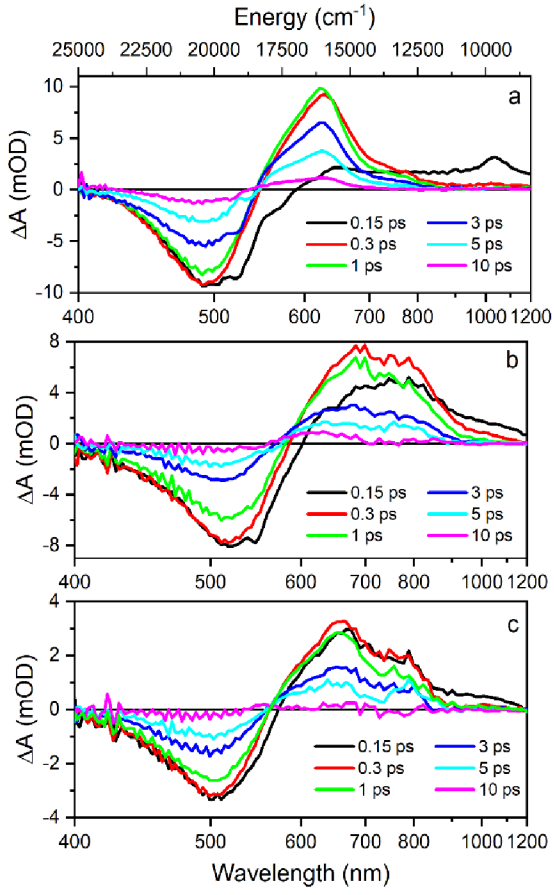

Figure 2. Transient absorption spectra of a) Asx, b) Asx-Cu, c) Asx-Zn in methanol after the excitation at 525 nm (Asx) and 555 nm (Asx-metal complexes). The spectra were measured at the time delays indicated in the panels.

The formation of Asx-metal complexes induces some changes in transient absorption spectra. Expectedly, both ground state bleaching and S_1-S_n ESA are red-shifted, reflecting the red shift of ground state absorption spectra upon complexation with metals. The S_1-S_n bands have maxima at 660 and 690 nm for Asx-Zn and Asx-Cu complexes, respectively. The ESA signal at 0.15 ps after excitation does not have the distinct S_2 ESA band in NIR, but the S_1-related ESA is clearly there already at 0.15 ps, signaling faster S_2 decay than in Asx in methanol. Nevertheless, the most important change is enhancement of the signal associated with the ICT state. The weak shoulder observed for Asx in methanol (Fig. 2a) is amplified to a band at 775 nm reaching about 50% of the main S_1-S_n maximum for Asx-Zn complex (Fig. 2c). For Asx-Cu complex, the ICT band at 790 nm has amplitude nearly equal to the S_1-S_n band (Fig. 2b). The data measured for the Asx-Cu complex generated by reaction with CuSO4 (Supporting Information, Fig. S3) does not differ from that shown in Fig. 2b.

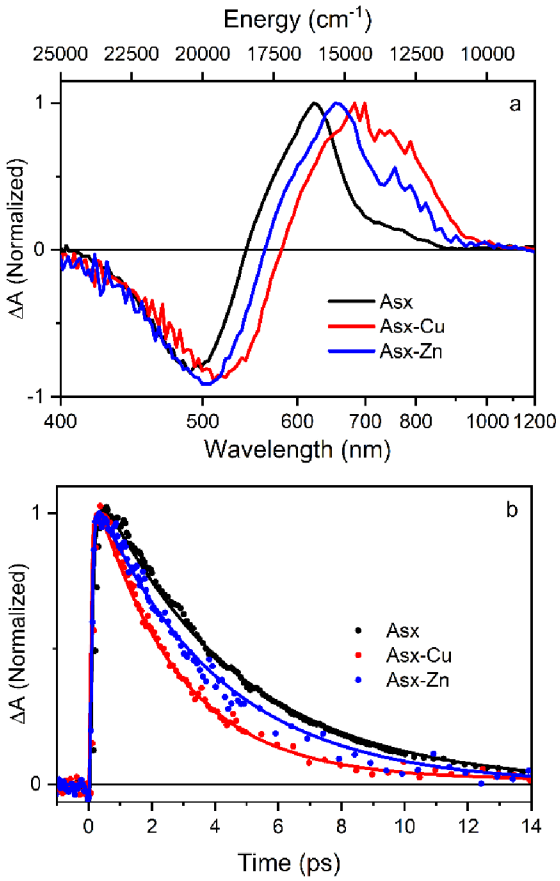

Figure 3. a) Normalized transient absorption spectra of Asx (black), Asx-Cu (red), Asx-Zn (blue) in methanol. The spectra were measured at 1 ps after excitation at 525 nm (Asx) and 555 nm (Asx-metal). b) Normalized kinetics measured at the S_1-S_n maximum of compounds in methanol. The probing wavelengths are 620, 650, and 680 nm for Asx, Asx-Zn and Asx-Cu, respectively. Kinetics are normalized to maximum.

The transient absorption spectra at 1 ps after excitation of all three samples are compared in Fig. 3a. The increase of magnitude of the ICT band as well as the red shift when going from Asx to Asx-Zn and to Asx- Cu complex is obvious. The kinetics measured at the maximum of the S_1-S_n band (Fig.

3b) decay faster for Asx-metal complexes. It is well known that magnitude of the ICT band in transient absorption spectra inversely correlates with the S_1/ICT lifetime thus the shortening of the S_1/ICT lifetime could be associated with the increased charge transfer character of the S_1/ICT state in Asx-metal complexes [18, 21].

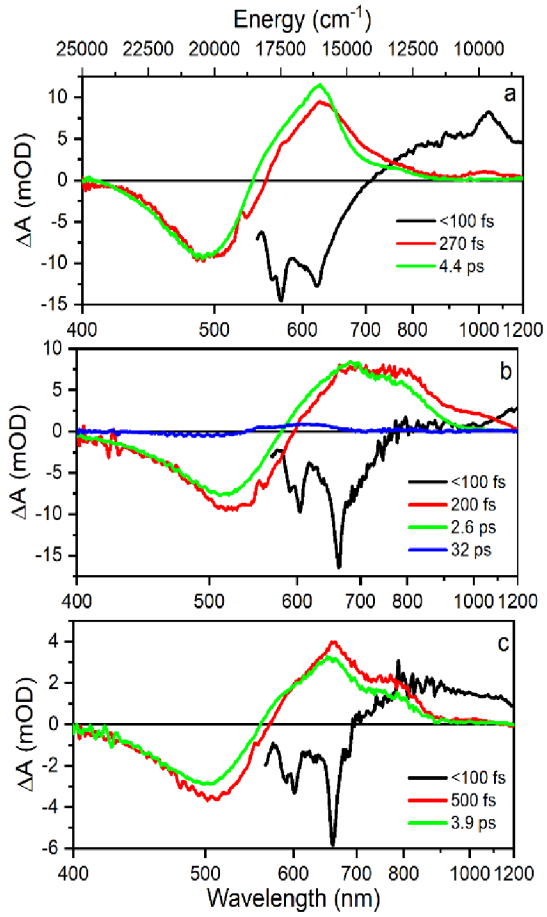

Figure 4. EADS obtained from global fitting of data recorded for a) Asx, b) Asx-Cu, c) Asx-Zn complexes in methanol.

Global fitting analysis was applied to determine the excited state lifetimes. The results are summarized in Fig. 4. For Asx in methanol, the first EADS, whose lifetime is at the limit of our time resolution, has features characteristic of the excited Asx S_2 state. The second EADS is related to the hot S_1/ICT state that decays within 270 fs to the relaxed S_1 state whose EADS has a lifetime of 4.4 ps. This pattern of Asx excited state dynamics agrees with results reported earlier [37, 38]. For Asx-metal complexes, the picture is qualitatively similar, but lifetimes of individual components differ. For Asx-Zn complex, the EADS associated with hot S_1 state has longer lifetime, suggesting slower relaxation of the hot S_1/ICT state, but the S_1/ICT EADS lifetime is shorter than in Asx, yielding 3.9 ps. The Asx-Cu complex has even shorter S_1/ICT lifetime, 2.6 ps, as expected also from kinetics shown in Fig. 3b). A longer but weak EADS with 32 ps lifetime having a shape typical for the S* signal is obtained exclusively for the Asx-Cu complex.

5.4. Discussion

The data presented in the previous section demonstrate that the photophysical properties of astaxanthin are influenced by the presence of $CuCl_2$, $CuSO_4$ and $Zn(ClO_4)_2$ in methanol. The absorption band exhibits a red shift comparable to that reported for Asx-metal complexes earlier [39]. Similar red shift was observed also for other carotenoids interacting with TiO_2 nanoparticles [45]. Thus, the observed changes are consistent with formation of Asx-metal complexes. Interestingly, interaction of Asx in ethanol with $CuCl_2$ was reported to enhance isomerization of Asx [46]. Since the isomerization reaction was achieved under different conditions (>30:1 $CuCl_2$: Asx molar ratio was needed to see the cis-peak while molar ratio 5:1 was used here) and in different solvent, our data show that tuning the actual conditions can prevent the isomerization reaction and produce a stable Asx-Cu complex. Thus, we conclude that the red shift of absorption spectrum is due to the complexation of Asx with metal ions. The exact origin of the red shift upon complexation with metals is unknown, but since red shift of carotenoid absorption is observed in highly-polarizable solvents such as DMSO or CS_2 where it is due to dispersion interaction between Asx and solvents [37,43], it is conceivable that the metal ions can change the local polarizability. Alternatively, prolongation of the effective conjugation length due to the binding of the metal ions at the respective ends of the conjugation chain [39–41] may also cause the red shift of absorption spectrum. Given the large molar excess of metal salts in our samples, it is reasonable to expect that metal ions interact with both terminal rings of Asx.

To test this hypothesis, we have estimated the Asx/Cu stoichiometry by the Job plot method [40, 47, 48]. The data (Fig. S4, Supporting Information) suggests that the Asx:Cu molar ratio is far less than 1:1, supporting our assumption that both terminal rings of each Asx should be in contact with the metal ions. Even though the Job plot does not give the 1:2 ratio either, the maximum at 0.4 suggests the 1:2 ratio is the dominant binding mode [40, 48]. Due to very slow assembly of Asx-Zn complexes (Fig. S1, Supporting Information) this test could not be carried out for Asx-Zn complex.

Another important question is whether our samples contain a mixture of free Asx and Asx-metal complexes. To address this question, we have carried out an additional transient absorption experiment with 500 nm excitation. Free Asx has a substantial absorption at 500 nm (Fig. 1) but negligible absorption at 555 nm used to excite Asx-metal complexes. Since the excited-state properties of free Asx differ from those obtained for Asx-metal complexes (Fig. 3), if there is any free Asx present, the data measured after 500 and 555 nm excitations should differ. A direct comparison of 500 and 555 nm data is shown in Fig. 5, demonstrating that the transient absorption spectra are indeed different after 500 and 555 nm excitations. The S_1-S_n band obtained after 500 nm excitation peaks at 650 nm, thus blue-shifted from the band observed after 555 nm excitation. Yet, the amplitude of the ICT band is not changed indicating that the charge transfer character of the S_1/ICT state remains unchanged upon change of excitation wavelength.

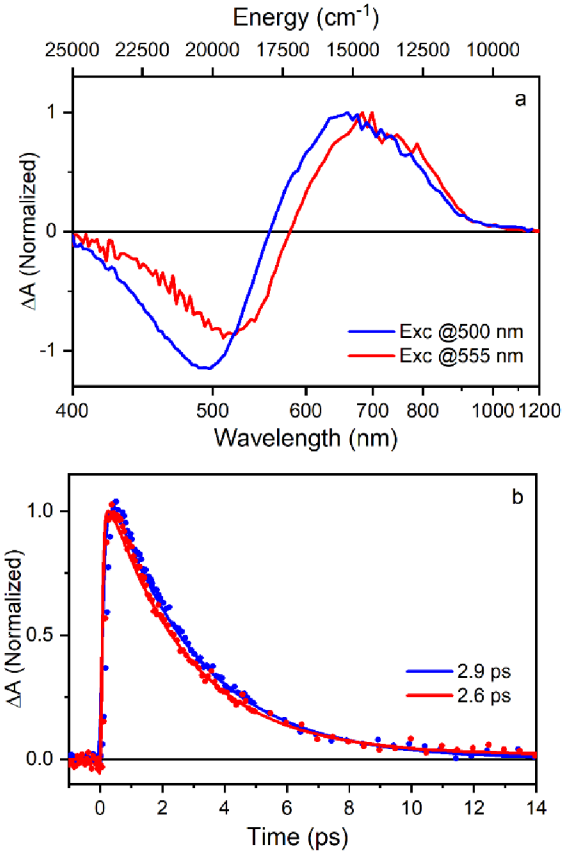

Figure 5. a) Comparison of normalized transient absorption spectra of Asx-Cu in methanol at 1 ps measured after excitation at 500 nm (blue) and 555 nm (red), b) Kinetics measured at the S_1-S_n maximum of Asx-Cu in methanol. The probing wavelengths are 665 and 680 nm for excitation at 500 and 555 nm, respectively. Kinetics are normalized to maximum.

The comparison of kinetics measured at the maxima of the respective S_1-S_n bands (Fig. 5b) shows that the S_1/ICT lifetime remains nearly the same upon change of excitation wavelength, further confirming that the excited state properties of the molecules excited at 500 nm are essentially identical to those excited at 550 nm. The S_1/ICT lifetime after both excitations is much shorter than 4.4 ps observed for free Asx (Fig. 4a). The same pattern is observed for Asx-Zn (Supporting Info, Fig. S5). Absence of a decay component associated with free Asx after 500 nm excitation confirms that there is very little (if any) free Asx, meaning that nearly all Asx molecules form complexes with either Cu or Zn in the Asx-metal samples. The difference in transient absorption spectra then reflects some inhomogeneity in the sample that is likely related to a conformational disorder that is enhanced by interaction of metal with Asx.

5.4.1. Excited-state dynamics of the Asx-metal complexes

While steady-state spectroscopic properties of some Asx-metal complexes were described earlier [39], no data on excited state dynamics of such complexes have been reported so far. Our data show that the formation of Asx-metal complexes significantly affects the excited state dynamics as

well as properties of the lowest excited state. Besides the red shift of the S_1-S_n band, which mirrors the shift of absorption spectra, interaction with metal ions results in markedly shorter S_1/ICT lifetime as well as in enhancement of the ICT band. These effects are pronounced especially for the Asx-Cu complex, which may indicate stronger interaction of Cu^{2+} ion with Asx compared to Zn^{2+} whose interaction with Asx also results in effects mentioned above, but in much lesser extent. It is known that enhancement of the charge transfer character of the S_1/ICT usually leads to a shortening of the S_1/ICT lifetime [18, 21], but there is also evidence that this correlation weakens with lengthening of the conjugation length [18, 21, 49, 50]. Typically, keto carotenoids with sub-10 ps S_1/ICT lifetime do not show further S_1/ICT shortening even though the ICT bands are enhanced in polar solvents as reported for e.g., spheroidenone [18,21]. Thus, the Asx S_1/ICT lifetime reduction from 4.4 to 2.6 ps upon formation of the Asx-Cu complex is uncommon. For long keto carotenoids, the S_1/ICT lifetime reduction could be rather caused by lengthening of the effective conjugation. In this case, the interaction of Asx with metals results in a presence of metal ion close to the conjugated keto group at the terminal ring [41], which may affect the effective conjugation. We note it mirrors the effect reported for astalysine, a water-soluble astaxanthin ester which exhibited essentially the same S_1/ICT lifetime reduction when switching from the moderately polar 2-propanol (4.4 ps) to the highly polar water (2.2 ps) [44].

It is known that the S_1 lifetimes of linear carotenoids exhibit linear dependence on 1/N (N–conjugation length) if plotted on logarithmic scale [51]. Such dependence is shown in Fig. 6. The S_1/ICT lifetimes of our complexes are included in the graph, allowing to estimate their effective conjugation length. While the effective conjugation of Asx is ~11, it is prolonged to 11.2 and 11.8 for Asx-Zn and Asx-Cu complexes. The observed shortening of the S_1/ICT lifetime upon interaction with metal ions to Asx is thus interpreted here as a result of lengthening of effective conjugation length. It also reflects a stronger interaction of Cu^{2+} compared to Zn^{2+} as the S_1/ICT lifetime of Asx-Zn is closer to pure Asx. However, the data clearly show that ICT band in transient absorption spectra is enhanced in Asx-metal complexes. Further, the amplitude of the ICT band increases in the order Asx, Asx-Zn and Asx-Cu, again suggesting the stronger interaction of Cu^{2+} and Asx.

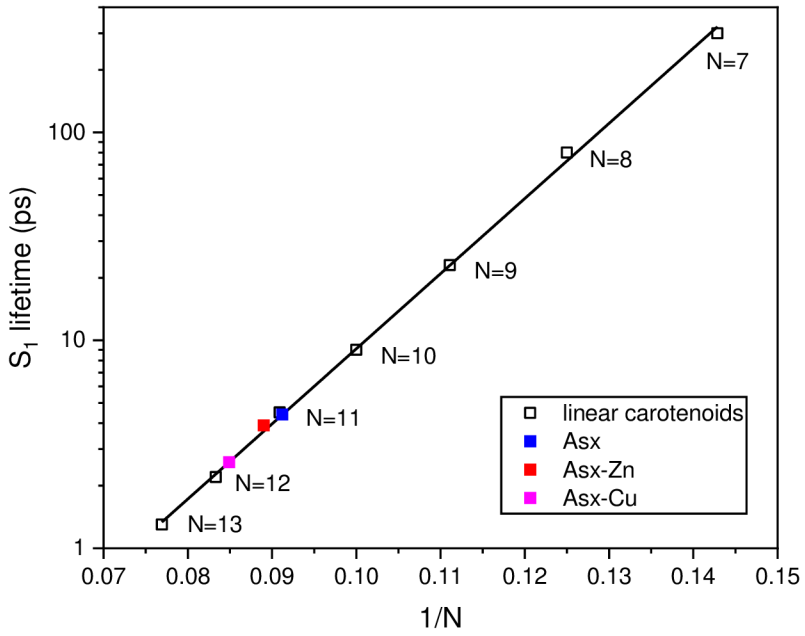

Fig. 6. N-dependence of the S1 lifetime for linear carotenoids (open symbols). The values for Asx and Asx-metal complexes are given in colors. The S1 lifetimes of linear carotenoids are taken from Ref [15].

This means that interaction of the metal ions with the terminal rings of Asx enhances the charge transfer character of the S_1/ICT state. This effect often occurs due to increased asymmetry of charge distribution [36], but this is unlikely the case here, because our Job plot analysis shows that metal ions likely interact with both terminal rings of Asx, thus no significant asymmetry should be induced by this interaction. We also note that for carotenoids with long conjugation the keto group at the terminal ring does not enhance the ICT band in transient absorption spectra even in asymmetrical position, as it is obvious in echinenone [50]. Thus, the precise mechanism of the ICT enhancement observed in Asx-metal complexes remains unclear. It is likely that direct interaction of metal ions with the keto oxygen induces changes in electron distribution, leading to the observed enhancement of the ICT band, while much weaker interactions with solvent molecules cannot induce comparable effect.

Finally, we note that in the Asx-Cu complex we have also identified a long-lived component (32 ps, blue EADS in Fig. 4b), which is clearly the S* signal, a heavily discussed feature reported in numerous carotenoids that is interpreted either as a separate excited state [52] or as a hot ground state [53, 54]. No such component was found for Asx or Asx-Zn. Earlier reports did not identify any S* signal for Asx in methanol, acetonitrile or CS_2 [37], but a weak S* component with a 33 ps lifetime, thus essentially identical to the one we observe here for Asx-Cu, was reported for Asx in DMSO [55]. An S* component was also identified for astalysine, though its lifetime was considerably shorter, 7 ps [44]. Recent studies show that at least for long carotenoids in solution the S* signal is most likely related to a hot ground state [56], and its decay reflects cooling of the hot ground state by transferring energy to solvent [57]. Here, the significant shortening of the S_1/ICT lifetime of Asx-Cu implies that

about 18000 cm^{-1} of energy pumped into the Asx-Cu S_2 state (excitation at 555 nm) returns to the ground state within less than 3 ps. This inevitably makes the ground state hot, resulting in the observed S* signal. The same applies for astalysine [44] and different S* lifetimes then reflect different vibrational properties of the ground state and/or different properties of the solvent shell.

5.5. Conclusions

In this work, we have demonstrated that astaxanthin-metal complexes exhibiting a long-term stability can be prepared in methanol. Stability of these complexes allowed to apply transient absorption spectroscopy to explore their excited states in detail. We have applied ultrafast transient absorption spectroscopy to explore excited states of stable astaxanthin-metal complexes. The interaction of Asx with metal ions has changed the excited-state properties of astaxanthin significantly, thereby opening a possibility of tuning excited state properties of this keto-carotenoid that is otherwise resistant to such changes as its excited state lifetime remains constant in a broad range of solvents [37, 38, 53]. Such tuning of excited-state properties is an important tool for understanding the carotenoid excited state dynamics, especially the relation between the carotenoid structure and mechanism of fast energy dissipation, which could be directly related to some biological functions of carotenoids [55]. The results show that even long keto-carotenoids are prone to alteration of their excited-state properties if the perturbation of their local environment is strong enough, which is here achieved by interaction of metal ions with their terminal rings.

The observed changes in excited-state dynamics induced by Asx-metal interaction, shortening of lifetime due to lengthening of effective conjugation and increase of the charge transfer character of the S_1/ICT state, also suggest a decrease of the S_1/ICT energy. Since a low-lying carotenoid acceptor state is a necessary condition for effective photoprotection by carotenoids [5, 58], our results show that placing a charge at the terminal rings may further enhance photoprotective actions of Asx. Effective photoprotection by Asx has been successfully demonstrated in main light harvesting antenna of plants, LHCII, from mutant tobacco producing exclusively astaxanthin [59]. The results indicate that tailoring binding sites in a way allowing interaction with the conjugated keto oxygen at terminal rings of Asx may further enhance the quenching. Thus, our results further widen the possibilities of using Asx, which is a readily available carotenoid, in either artificial or modified natural light-harvesting and/or photoprotective systems.

Acknowledgements

The authors thank Hristina Staleva-Musto and Hana Velanov´a for their help during the initial stages of the project. Financial support was provided by the grant 19-28323X from the Czech Science Foundation.

5.6. Supporting Information

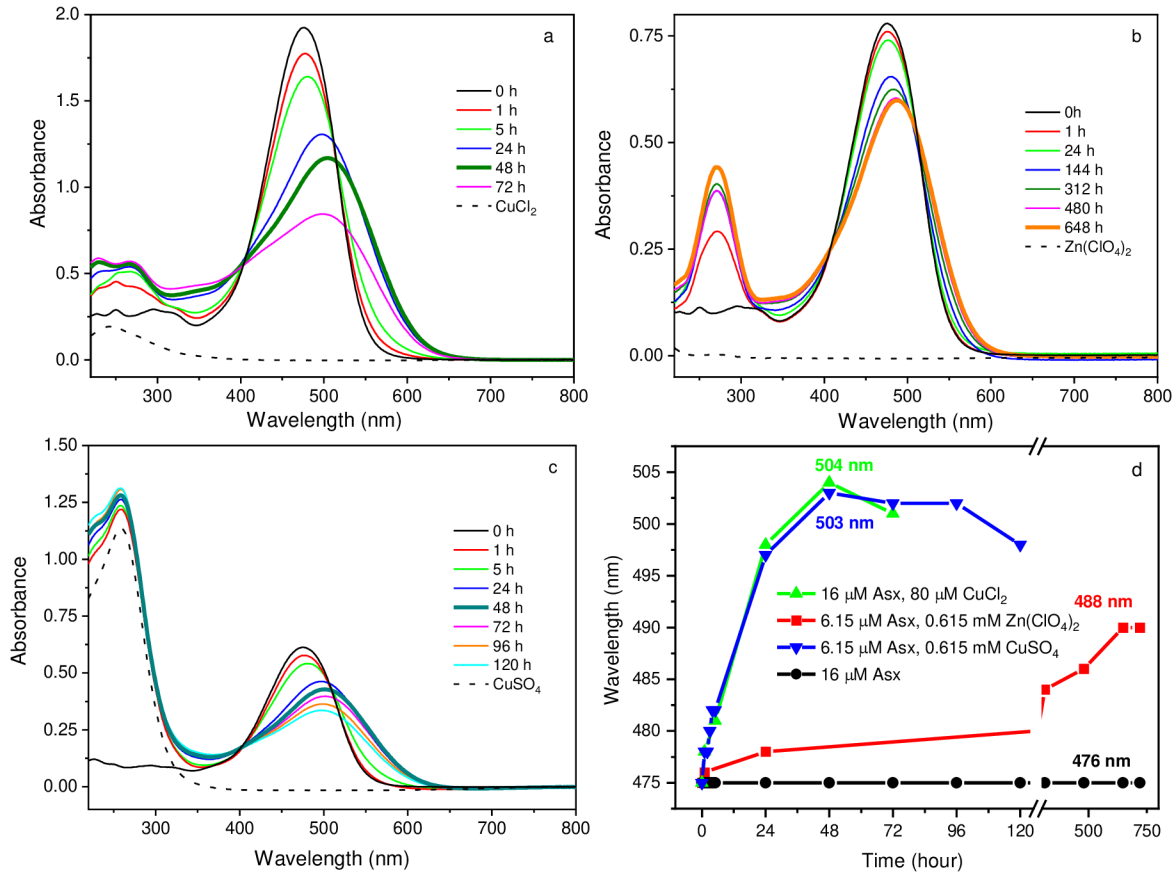

Figure S1. Time dependence of absorption spectra measured in dark at room temperature. Time zero corresponds to the absorption spectrum of Asx in methanol prior to addition of the compound initializing the formation of Asx-metal complex. (a) Formation of Asx-Cu complex,16 µM Asx, added 80 µM of $CuCl_2$, (b) Formation of Asx-Zn complex, 6.15 µM Asx, 0.615 mM of $Zn(ClO_4)_2$, (c) Formation of Asx-Cu complex, 6.15 µM Asx, 0.615 mM of $CuSO_4$. In panels a-c, the thick line corresponds to the absorption spectrum of the sample used for transient absorption experiments. The black dotted line shows absorption of 80 µM $CuCl_2$ (a), 0.615 mM $Zn(ClO_4)_2$ (b), and 0.615 mM $CuSO_4$ (c) in methanol. Note than while for Asx-Zn complex in (b) the absorption band at 270 nm is associated with the formation of the complex, in (c) the strong band at 260 nm is solely due to the absorption of $CuSO_4$. (d) Time evolution of the absorption maximum for all three samples. Pure Asx in methanol is shown as a reference sample to demonstrate the stability of astaxanthin in methanol.

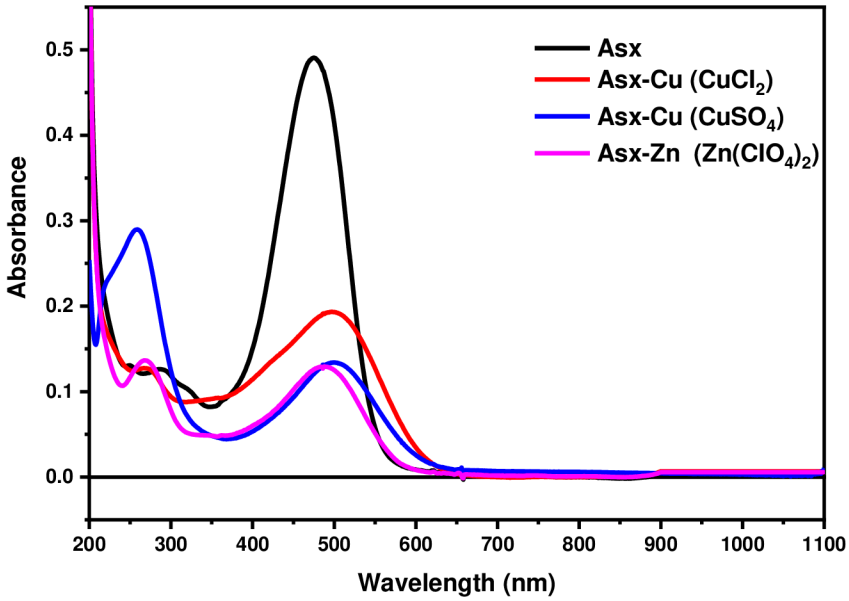

Figure S2. Full absorption spectra of Asx and its metal complexes demonstrating absence of any Asx radicals which have strong absorption band in the 850-1050 nm spectral region.

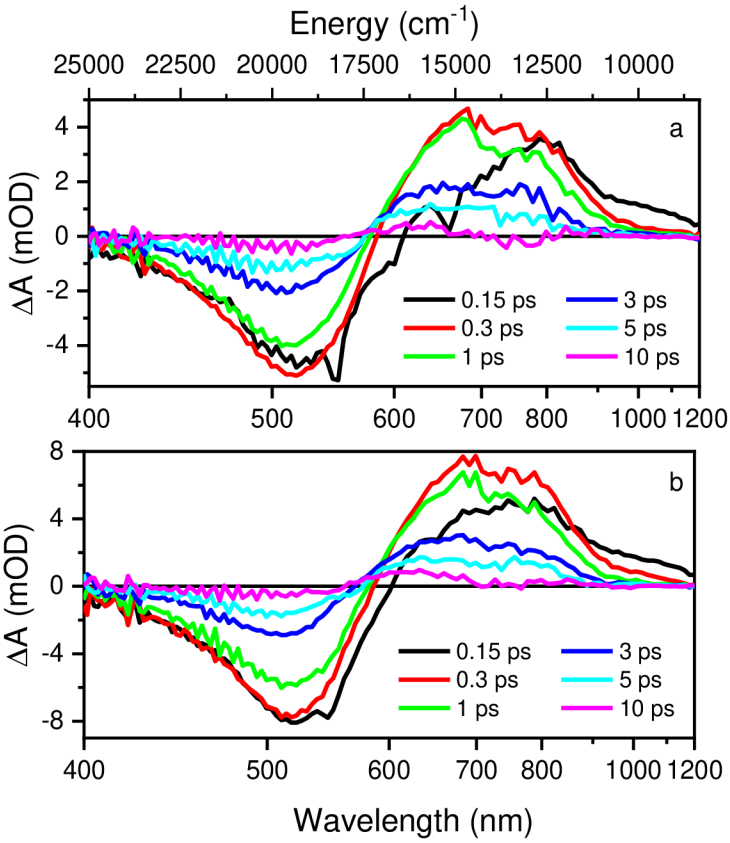

Figure S3. Comparison of transient absorption spectra of Asx-Cu complexes produced by interaction of Asx with $CuSO_4$ (a) or $CuCl_2$ (b) in methanol. Excitation wavelength at 555 nm, spectra were measured at time delays indicated in the panels.

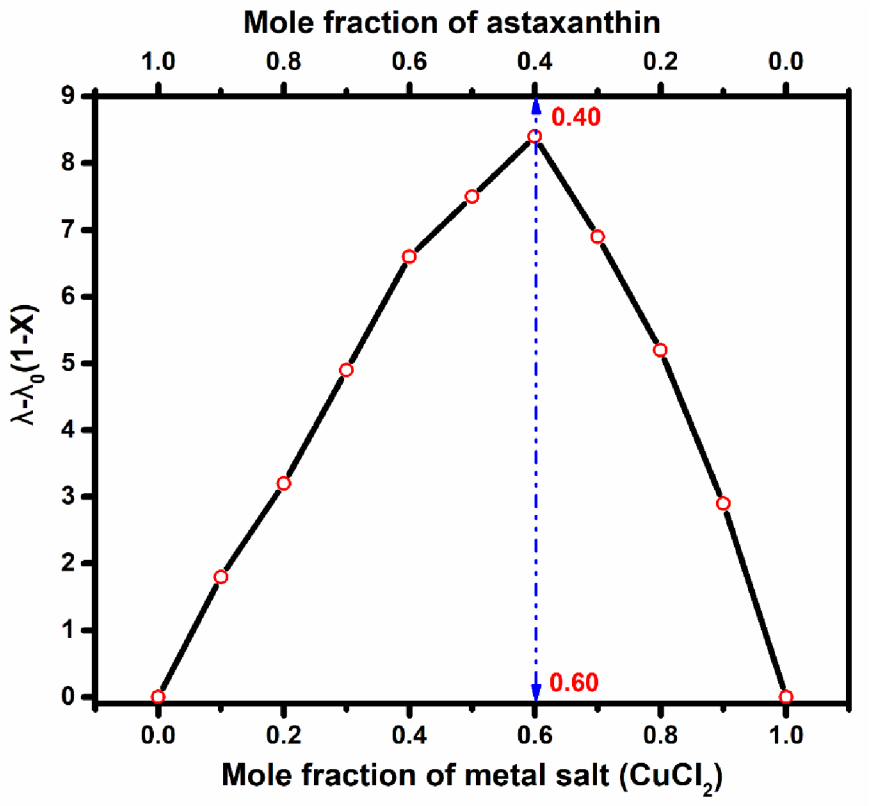

Figure S4. Job plot of complex formation of Asx and $CuCl_2$ with an Astaxanthin/Cu^{2+} molar ratio of 1:2. The continuous variation method was employed to determine stoichiometry between Asx and $CuCl_2$. Solutions of astaxanthin (16 µM) and $CuCl_2$ (16 µM) were prepared in separate volumetric flasks. Then, eleven sample solutions containing the astaxanthin and metal salts were prepared in various ratios (10:0 to 0:10 v/v) in a total volume of 3 mL. The absorption spectra of samples with various molar ratios were measured in a 10-mm path-length quartz cuvette. The relative shift of absorption maximum was recorded, and a graph was created using the formula $\lambda - \lambda_0 (1-X)$, where λ is absorption maximum of each molar ratio, λ_0 is absorption maximum of pure astaxanthin, and X represents the mole fraction. The resulting Job plot has maximum for the mole fraction of metal and astaxanthin 0.6 and 0.4, respectively, indicating the 1:2 Asx:Cu binding stoichiometry.

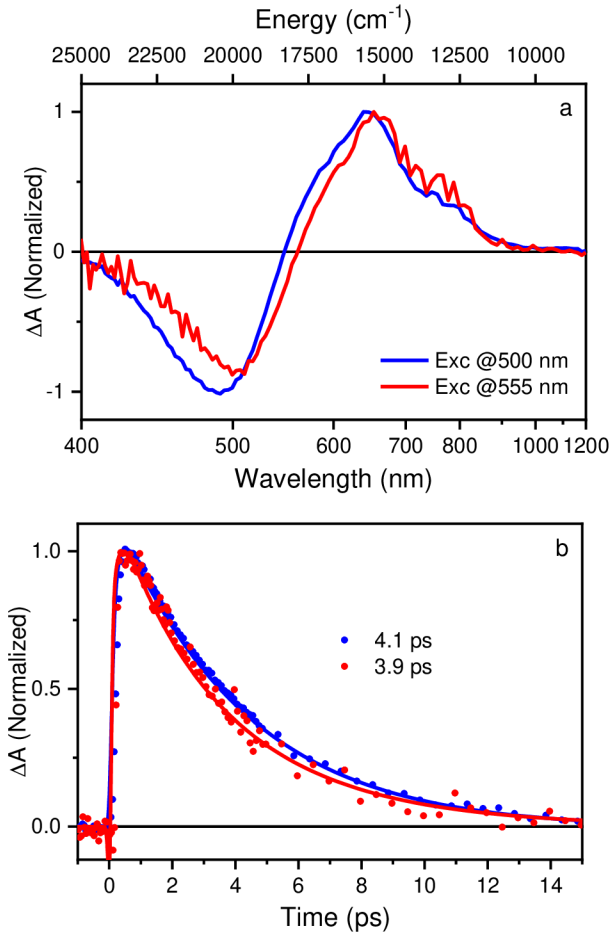

Figure S5. a) Comparison of normalized transient absorption spectra of Asx-Zn in methanol at 1 ps measured after excitation at 500 nm (blue) and 555 nm (red). b) Kinetics measured at the S_1-S_n maximum of Asx- Zn in methanol. The probing wavelengths are 645 and 650 nm for excitation at 500 and 555 nm, respectively. Kinetics are normalized to the maximum.

5.7. Additional data not included in the article

One of the key tasks in this project was to prepare stable metal complexes in solution. Therefore, we started our investigation by looking into the earlier studies carried out by Hana Velanová and Hristina Staleva-Musto within a bachelor student project [60], as well as the literature, especially Polyakov's article [39]. First, we tried different amounts of metal complexes mixed with astaxanthin in a methanol solution and heated the mixture, a protocol tested earlier [60], but the astaxanthin quickly degraded. The reason is that carotenoids may degrade at elevated temperature, and the excess amount of metal likely further increases the degradation. However, astaxanthin has also been reported to form complexes with metal ions, suggesting they could also affect the ICT state properties, as reported by Polyakov et al. Astaxanthin complexes binding with Cu^{2+}, Ca^{2+}, Zn^{2+}, and Fe^{2+} were reported and confirmed by NMR and optical spectroscopy. In the absorption spectra, the metal binding induced a red shift, causing an extension of the absorption spectra. Therefore, we started to prepare our complexes in methanol, for metal complexes which has been successfully prepared in

ethanol according to the literature, at room temperature using different amounts of metals. For this purpose, we used an equivalent system and tested each metal in 1:1, 1:2, 1:5, 1:10, 1:20, 1:50, 1:100, and 1:200 molar ratios to observe the effect of the amount of metals. The tests resulted in optimal molar ratios, which differ for different metals as it is obvious from FigS1 of Supporting information.

In addition to the successfully obtained metal complexes reported in our article, the same experiments were carried out using different metals and their different counter ions. The results are shown in Figures D1-D4. These metals and their corresponding counter ions did not exhibit any variations in their absorption spectra. This suggests that they did not form complexes with astaxanthin.

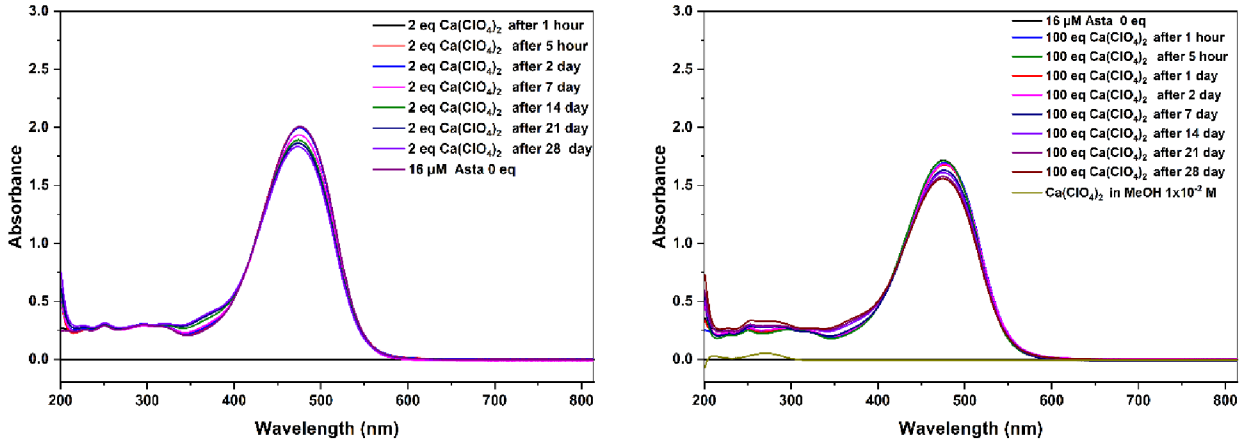

Figure D1. Time dependence of absorption spectra measured in dark at room temperature. Formation of Asxanthin-$Ca(ClO_4)_2$ complex 2 and 100 eq.

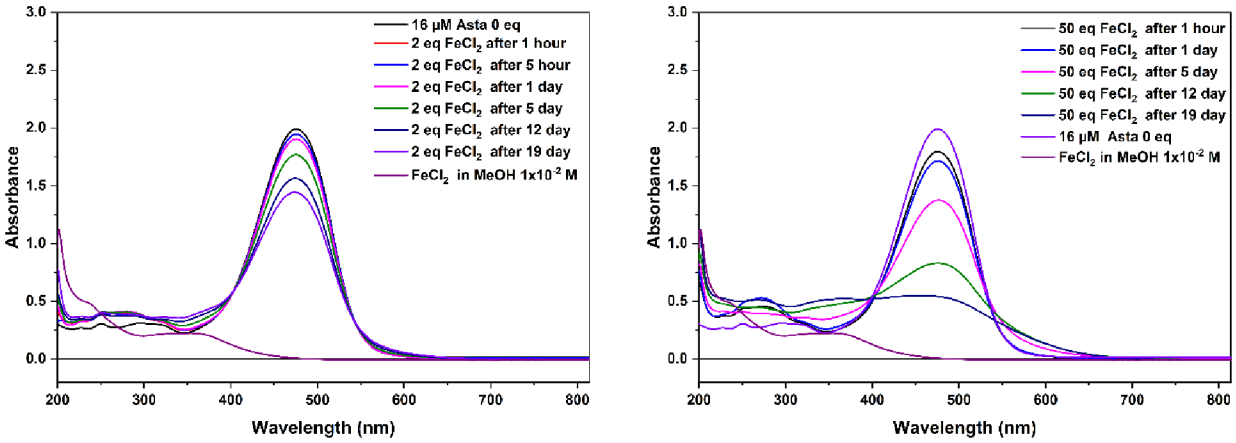

Figure D2. Time dependence of absorption spectra measured in dark at room temperature. Formation of Asxanthin-$FeCl_2$ complex 2 and 50 eq.

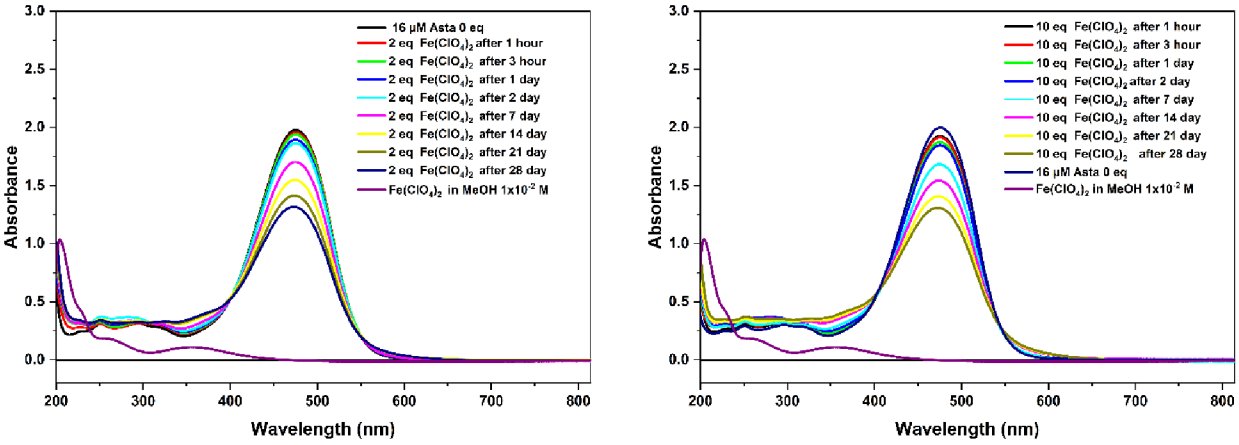

Figure D3. Time dependence of absorption spectra measured in dark at room temperature. Formation of Asxanthin-$Fe(ClO_4)_2$ complex 2 and 10 eq.

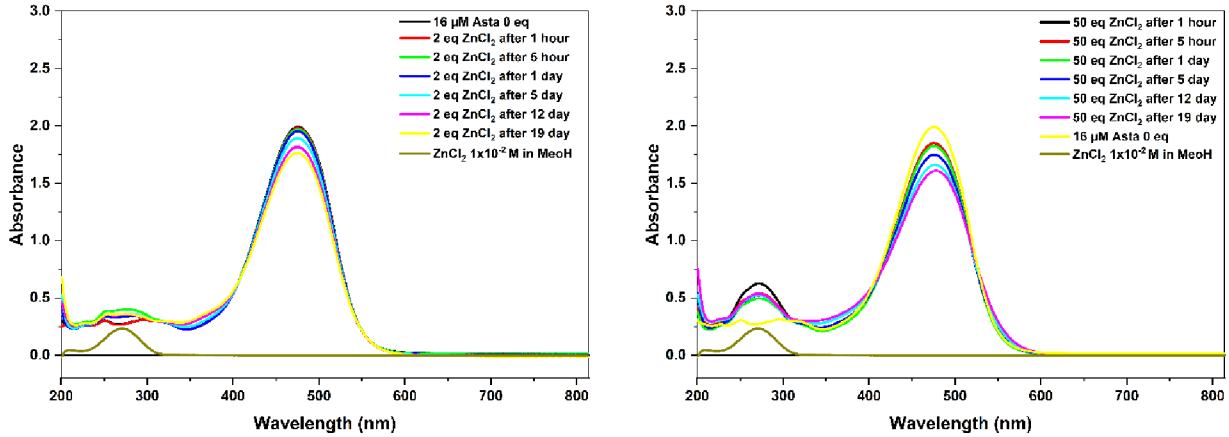

Figure D4. Time dependence of absorption spectra measured in dark at room temperature. Formation of Asxanthin-$ZnCl_2$ complex 2 and 50 eq.

5.8. References

[1] T. Polívka, H.A. Frank, Molecular factors controlling photosynthetic light harvesting by carotenoids, Acc. Chem. Res. 43 (2010) 1125–1134, https://doi.org/ 10.1021/ar100030m.

[2] R. Croce, H. van Amerongen, Light harvesting in oxygenic photosynthesis: Structural biology meets spectroscopy, Science 369 (2020) eaay2058, https://doi.org/10.1126/science.aay2058.

[3] A.V. Ruban, R. Berera, C. Ilioaia, I.H. van Stokkum, J.T. Kennis, A.A. Pascal, H. van Amerongen, B. Robert, P. Horton, R. van Grondelle, Identification of a mechanism of photoprotective energy dissipation in higher plants, Nature 450 (2007) 575–578, https://doi.org/10.1038/nature06262.

[4] N.E. Holt, D. Zigmantas, L. Valkunas, X.P. Li, K.K. Niyogi, G.R. Fleming, Carotenoid cation formation and the regulation of photosynthetic light harvesting, Science 307 (2005) 433–436, https://doi.org/10.1126/science.1105833.

[5] H. Staleva, J. Komenda, M.K. Shukla, V. Slouf, R. Kana, T. Polivka, R. Sobotka, Mechanism of photoprotection in the cyanobacterial ancestor of plant antenna proteins, Nat. Chem. Biol. 11 (2015) 287–291, https://doi.org/10.1038/nchembio.

[6] C.D.P. Duffy, A.V. Ruban, Dissipative pathways in the photosystem-II antenna in plants, J. Photochem. Photobiol. B, Biol. 152 (2015) 215–226, https://doi.org/10.1016/j.jphotobiol.2015.09.011.

[7] T.G. Monger, R.J. Cogdell, W.W. Parson, Triplet states of bacteriochlorophyll and carotenoids in chromatophores of photosynthetic bacteria, Biochim. Biophys. Acta. 449 (1976) 136–153, https://doi.org/10.1016/0005-2728(76)90013-X.

[8] Z. Kvícalova, J. Alster, E. Hofmann, P. Khoroshyy, R. Litvín, D. Bína, T. Polívka, J. Psencík, Triplet–triplet energy transfer from chlorophylls to carotenoids in two antenna complexes from dinoflagellate Amphidinium carterae, Biochim. Biophys. Acta-Bioenerg. 2016 (1857) 341–349, https://doi.org/10.1016/j.bbabio.2016.01.008.

[9] H.A. Frank, R. Cogdell, Photochem. Photobiol. 63 (1996) 252–326.

[10] C.S. Foote, Y.C. Chang, R.W. Denny, Chemistry of singlet oxygen. X. Carotenoid quenching parallels biological protection, J. Am. Chem. Soc. 92 (1970) 5216–5218, https://doi.org/10.1021/ja00720a036.

[11] T.W. Boileau, A.C. Moore, J. W. Erdman, diet, nutrition, health, Carotenoids and vitamin A, (1999) 133-158.

[12] S.A.R. Paiva, R.M. Russell, β-Carotene and other carotenoids as antioxidants, J. Am. Coll. Nutr. 18 (1999) 426–433, https://doi.org/10.1080/ 07315724.1999.10718880.

[13] N.I. Krinsky, K.J. Yeum, Carotenoid-radical interactions, Biochem. Biophys. Res. Commun. 305 (2003) 754–760, https://doi.org/10.1016/S0006-291X(03)00816-7.

[14] M. Kobayashi, Y. Sakamoto, Singlet oxygen quenching ability of astaxanthin esters from the green alga Haematococcus pluvialis, Biotechnol. Lett. 21 (1999) 265–269, https://doi.org/10.1023/A:1005445927433.

[15] T. Polivka, V. Sundstrom, Ultrafast dynamics of carotenoid excited states – From solution to natural and artificial systems, Chem. Rev. 104 (2004) 2021, https://doi.org/10.1021/cr020674n.

[16] D. Zigmantas, R.G. Hiller, V. Sundstr¨om, T. Polívka, Carotenoid to chlorophyll energy transfer in the peridinin–chlorophyll-a–protein complex involves an intramolecular charge transfer state, Proc. Natl. Acad. Sci. U.S.A. 99 (2002) 16760–16765, https://doi.org/10.1073/pnas.262537599.

[17] J.A. Bautista, R.E. Connors, B.B. Raju, R.G. Hiller, F.P. Sharples, D. Gosztola, M. R. Wasielewski, H.A. Frank, Excited state properties of peridinin: Observation of a solvent dependence of the lowest excited singlet state lifetime and spectral behavior unique among carotenoids, J. Phys. Chem. B 103 (1999) 8751–8758, https://doi.org/10.1021/jp9916135.

[18] H.A. Frank, J.A. Bautista, J. Josue, Z. Pendon, R.G. Hiller, F.P. Sharples, D. Gosztola, M.R. Wasielewski, Effect of the solvent environment on the spectroscopic properties and dynamics of the lowest excited states of carotenoids, J. Phys. Chem. B 104 (2000) 4569–4577, https://doi.org/10.1021/jp000079u.

[19] D. Kosumi, T. Kusumoto, R. Fujii, M. Sugisaki, Y. Iinuma, N. Oka, Y. Takaesu, T. Taira, M. Iha, H.A. Frank, H. Hashimoto, Ultrafast excited state dynamics of fucoxanthin: excitation energy dependent intramolecular charge transfer dynamics, Phys. Chem. Chem. Phys. 13 (2011) 10762–10770, https://doi.org/10.1039/C0CP02568B.

[20] S. Shima, R.P. Ilagan, N. Gillespie, B.J. Sommer, R.G. Hiller, F.P. Sharples, H. A. Frank, R.R. Birge, Two-photon and fluorescence spectroscopy and the effect of environment on the photochemical properties of peridinin in solution and in the peridinin-chlorophyll-protein from Amphidinium carterae, J. Phys. Chem. A 107 (2003) 8052–8066, https://doi.org/10.1021/jp022648z.

[21] D. Zigmantas, R.G. Hiller, F.P. Sharples, H.A. Frank, V. Sundstrom, T. Polivka, Effect of a conjugated carbonyl group on the photophysical properties of carotenoids, Phys. Chem. Chem. Phys. 6 (2004) 3009–3016, https://doi.org/10.1039/B315786E.

[22] H. Cong, D.M. Niedzwiedzki, G.N. Gibson, A.M. LaFountain, R.M. Kelsh, A. T. Gardiner, R.J. Cogdell, H.A. Frank, Ultrafast time-resolved carotenoid tobacteriochlorophyll energy transfer in LH2 complexes from photosynthetic bacteria, J. Phys. Chem. B 112 (2008) 10689–10703, https://doi.org/10.1021/jp711946w.

[23] T. Polívka, T. Pullerits, H.A. Frank, R.J. Cogdell, V. Sundstr¨om, Ultrafast formation of a carotenoid radical in LH2 antenna complexes of purple bacteria, J. Phys. Chem. B. 108 (2004) 15398–15407, https://doi.org/10.1021/jp0483019.

[24] D.M. Niedzwiedzki, P.L. Dilbeck, Q. Tang, E.C. Martin, D.F. Bocian, C.N. Hunter, D. Holten, New insights into the photochemistry of carotenoid spheroidenone in light-harvesting complex 2 from the purple bacterium Rhodobacter sphaeroides, Photosynth. Res. 131 (2017) 291–304, https://doi.org/10.1007/s11120-016-0322-2.

[25] D. Loco, F. Buda, J. Lugtenburg, B. Mennucci, The dynamic origin of color tuning in proteins revealed by a carotenoid pigment, J. Phys. Chem. Lett. 9 (2018) 2404–2410, https://doi.org/10.1021/acs.jpclett.8b00763.

[26] I. Higuera-Ciapara, L. Felix-Valenzuela, F.M. Goycoolea, Astaxanthin: a review of its chemistry and applications, Crit. Rev. Food. Sci. Nutr. 46 (2006) 185–196, https://doi.org/10.1080/10408690590957188.

[27] R. Christiansen, O. Lie, O.J. Torrissen, Growth and survival of Atlantic salmon, Salmo salar L., fed different dietary levels of astaxanthin. First-feeding fry, Aquac. Nutr. 1 (1995) 189–198, https://doi.org/10.1111/j.1365-2095.1995.tb00043.x.

[28] Y. Cao, L. Yang, X. Qiao, C. Xue, J. Xu, Dietary astaxanthin: an excellent carotenoid with multiple health benefits, Crit. Rev. Food. Sci. Nutr. (2021) 1–27, https://doi.org/10.1080/10408398.2021.1983766.

[29] W. Miki, Biological functions and activities of animal carotenoids, Pure Appl. Chem. 63 (1991) 141–146, https://doi.org/10.1351/pac199163010141.

[30] Y.M. Naguib, Antioxidant activities of astaxanthin and related carotenoids, J. Agric. Food. Chem. 48 (2000) 1150–1154, https://doi.org/10.1021/jf991106k.

[31] S. Fakhri, F. Abbaszadeh, L. Dargahi, M. Jorjani, Astaxanthin: A mechanistic review on its biological activities and health benefits, Pharmacol. Res. 136 (2018) 1–20, https://doi.org/10.1016/j.phrs.2018.08.012.

[32] A. Donoso, J. Gonzalez-Duran, A.A. Munoz, P.A. Gonzalez, C. Agurto-Munoz, Therapeutic uses of natural astaxanthin: An evidence-based review focused on human clinical trials, Pharmacol. Res. 166 (2021), 105479, https://doi.org/10.1016/j.phrs.2021.105479.

[33] D. Zigmantas, R.G. Hiller, A. Yartsev, V. Sundstrom, T. Polivka, Dynamics of excited states of the carotenoid peridinin in polar solvents: Dependence on excitation wavelength, viscosity, and temperature, J. Phys. Chem. B 107 (2003) 5339–5348, https://doi.org/10.1021/jp0272318.

[34] K. Redeckas, V. Voiciuk, M. Vengris, Investigation of the S1/ICT equilibrium in fucoxanthin by ultrafast pump–dump–probe and femtosecond stimulated Raman scattering spectroscopy, Photosynth. Res. 128 (2016) 169–181, https://doi.org/10.1007/s11120-015-0215-9.

[35] R.G. West, M. Fuciman, H. Staleva-Musto, V. Sebelik, D. Bina, M. Durchan, V. Kuznetsova, T. Polivka, Equilibration dependence of fucoxanthin S1 and ICT signatures on polarity, proticity, and temperature by multipulse femtosecond absorption spectroscopy, J. Phys. Chem. B 122 (2018) 7264–7276, https://doi.org/10.1021/acs.jpcb.8b04217.

[36] M.M. Enriquez, M. Fuciman, A.M. LaFountain, N.L. Wagner, R.R. Birge, H.A. Frank, The intramolecular charge transfer state in carbonyl-containing polyenes and carotenoids, J. Phys. Chem. B 114 (2010) 12416–12426, https://doi.org/10.1021/jp106113h.

[37] R.P. Ilagan, R.L. Christensen, T.W. Chapp, G.N. Gibson, T. Pascher, T. Polivka, H. A. Frank, Femtosecond time-resolved absorption spectroscopy of astaxanthin in solution and in alpha-crustacyanin, J. Phys. Chem. A 109 (2005) 3120–3127, https://doi.org/10.1021/jp0444161.

[38] N. Christensson, T. Polivka, A. Yartsev, T. Pullerits, Photon echo spectroscopy reveals structure-dynamics relationships in carotenoids, Phys. Rev. B 79 (2009), 245118, https://doi.org/10.1103/PhysRevB.79.245118.

[39] N.E. Polyakov, A.L. Focsan, M.K. Bowman, L.D. Kispert, Free radical formation in novel carotenoid metal ion complexes of astaxanthin, J. Phys. Chem. B 114 (2010) 16968–16977, https://doi.org/10.1021/jp109039v.

[40] C.S. Chen, S.H. Wu, Y.Y. Wu, J.M. Fang, T.H. Wu, Properties of astaxanthin/Ca2+ complex formation in the deceleration of cis/trans isomerization, Org. Lett. 9 (2007) 2985–2988, https://doi.org/10.1021/ol0709533.

[41] E. Hernandez-Marin, A. Barbosa, A. Martínez, The metal cation chelating capacity of astaxanthin. Does this have any influence on antiradical activity? Molecules. 17 (2012) 1039–1054, https://doi.org/10.3390/molecules17011039.

[42] K. Holtin, M. Kuehnle, J. Rehbein, P. Schuler, G. Nicholson, K. Albert, Determination of astaxanthin and astaxanthin esters in the microalgae Haematococcus pluvialis by LC-(APCI)MS and characterization of predominant carotenoid isomers by NMR spectroscopy, Anal. Bioanal. Chem. 395 (2009) 1613–1622, https://doi.org/10.1007/s00216-009-2837-2.

[43] T. Khan, R. Litvín, V. ˇSebelík, T. Polívka, Excited-state evolution of ketocarotenoids after excess energy excitation in the UV region, ChemPhysChem 22 (2021) 471–480, https://doi.org/10.1002/cphc.202000982.

[44] P. Chabera, M. Fuciman, K. Razi Naqvi, T. Polívka, Ultrafast dynamics of hydrophilic carbonyl carotenoids – Relation between structure and excited-state properties in polar solvents, Chem. Phys. 373 (2010) 56–64, https://doi.org/10.1016/j.chemphys.2010.01.007.

[45] J. Pan, G. Benko, Y.H. Xu, T. Pascher, L.C. Sun, V. Sundstrom, T. Polivka, Photoinduced electron transfer between a carotenoid and TiO2 nanoparticle, J. Am. Chem. Soc. 124 (2002) 13949–13957, https://doi.org/10.1021/ja0279186.

[46] L. Zhao, F. Chen, G. Zhao, Z. Wang, X. Liao, X. Hu, Isomerization of transastaxanthin induced by copper(II) ion in ethanol, J. Agric. Food. Chem. 53 (2005) 9620–9623, https://doi.org/10.1021/jf0517750.

[47] P. Job, Job's method of continuous variation, Ann. Chim. 9 (1928).

[48] J.S. Renny, L.L. Tomasevich, E.H. Tallmadge, D.B. Collum, Method of continuous variations: applications of job plots to the study of molecular associations in organometallic chemistry, Angew. Chem. Int. Ed. Engl. 52 (2013) 11998–12013, https://doi.org/10.1002/anie.201304157.

[49] S. Stalke, D.A. Wild, T. Lenzer, M. Kopczynski, P.W. Lohse, K. Oum, Solventdependent ultrafast internal conversion dynamics of n' -apo-β-carotenoic-n' -acids (n= 8, 10, 12), Phys. Chem. Chem. Phys. 10 (2008) 2180–2188, https://doi.org/10.1039/B720037D.

[50] P. Chabera, M. Fuciman, P. Hˇríbek, T. Polívka, Effect of carotenoid structure on excited-state dynamics of carbonyl carotenoids, Phys. Chem. Chem. Phys. 11 (2009) 8795–8803, https://doi.org/10.1039/B909924G.

[51] M. Fuciman, G. Kesan, A.M. LaFountain, H.A. Frank, T. Polivka, Tuning the spectroscopic properties of aryl carotenoids by slight changes in structure, J. Phys. Chem. B 119 (2015) 1457–1467, https://doi.org/10.1021/jp512354r.

[52] C.C. Gradinaru, J.T.M. Kennis, E. Papagiannakis, I.H.M. van Stokkum, R.J. Cogdell, G.R. Fleming, R.A. Niederman, R. van Grondelle, An unusual pathway of excitation energy deactivation in carotenoids: singlet-to-triplet conversion on an ultrafast timescale in a photosynthetic antenna, Proc. Natl. Acad. Sci. U. S. A. 98 (2001) 2364, https://doi.org/10.1073/pnas.051501298.

[53] T. Buckup, J. Savolainen, W. Wohlleben, J.L. Herek, H. Hashimoto, R.R. Correia, M.J.T.J.o.c.p. Motzkus, Pump-probe and pump-deplete-probe spectroscopies on carotenoids with N= 9–15 conjugated bonds, J. Chem. Phys. 125 (2006), 194505, https://doi.org/10.1063/1.2388274.

[54] T. Lenzer, F. Ehlers, M. Scholz, R. Oswald, K. Oum, Assignment of carotene S* state features to the vibrationally hot ground electronic state, Phys. Chem. Chem. Phys. 12 (2010) 8832, https://doi.org/10.1039/B925071A.

[55] M. Fuciman, M. Durchan, V. Slouf, G. Kesan, T. Polivka, Excited-state dynamics of astaxanthin aggregates, Chem. Phys. Lett. 568 (2013) 21–25, https://doi.org/ 10.1016/j.cplett.2013.03.009.

[56] V. Balevi˘cius, D. Abramavicius, T. Polívka, A. Galestian Pour, J. Hauer, A unified picture of S* in carotenoids, J. Phys. Chem. Lett. 7 (17) (2016) 3347–3352.

[57] V. Balevi˘cius Jr, T. Wei, D. Di Tommaso, D. Abramavicius, J. Hauer, T. Polívka, C. D.P. Duffy, The full dynamics of energy relaxation in large organic molecules: from photo-excitation to solvent heating, Chem. Sci. 10 (2019) 4792–4804, https://doi.org/10.1039/C9SC00410F.

[58] P.L. Dilbeck, Q. Tang, D.J. Mothersole, E.C. Martin, C.N. Hunter, D.F. Bocian, D. Holten, D.M. Niedzwiedzki, Quenching capabilities of long-chain carotenoids in light-harvesting-2 complexes from rhodobacter sphaeroides with an engineered carotenoid synthesis pathway, J. Phys. Chem. B. 120 (2016) 5429–5443, https://doi.org/10.1021/acs.jpcb.6b03305.

[59] N. Liguori, P. Xu, I.H.M. van Stokkum, B. van Oort, Y. Lu, D. Karcher, R. Bock, R. Croce, Different carotenoid conformations have distinct functions in lightharvesting regulation in plants, Nat. Commun. 8 (2017) 1994, https://doi.org/10.1038/s41467-017-02239-z.

[60] Velanová, H.: Formation of complexes of astaxanthin with metal ions and their basic spectroscopic characterization. Bc. Thesis, Faculty of Science, University of South Bohemia, České Budějovice, Czech Republic. 2019

6. Paper II

Time-Resolved Spectroelectrochemical Dynamics of Carotenoid 8’-apo-β-Carotenal

Keşan, G., Özcan, E., Chábera, P., Polívka, T., & Fuciman, M. (2023). Time-Resolved Spectroelectrochemical Dynamics of Carotenoid 8’-apo-β-Carotenal. ChemPlusChem, 88(11), e202300404.

https://doi.org/10.1002/cplu.202300404

Abstract

This work examines the influence of applied external voltage in bulk electrolysis on the excited-state properties of 8'-apo-β-carotenal in acetonitrile by steady-state and ultrafast time-resolved absorption spectroscopy. The data collected under bulk electrolysis were compared with those taken without applied voltage. The steady-state measurements showed that although intensity of the S_0-S_2 absorption band varies with the applied voltage, the spectral position remain nearly constant. Comparison of transient absorption spectra shows that the magnitude of the ICT-like band decreases during the experiment under applied voltage condition, and is associated with a prolongation of the S_1/ICT-like lifetime from 8 ps to 13 ps. Furthermore, switching off the applied voltage resulted in returning to no-voltage data within about 30 min. Our results show that the amplitude of the signal associated with the ICT state can be tuned by applying an external voltage.

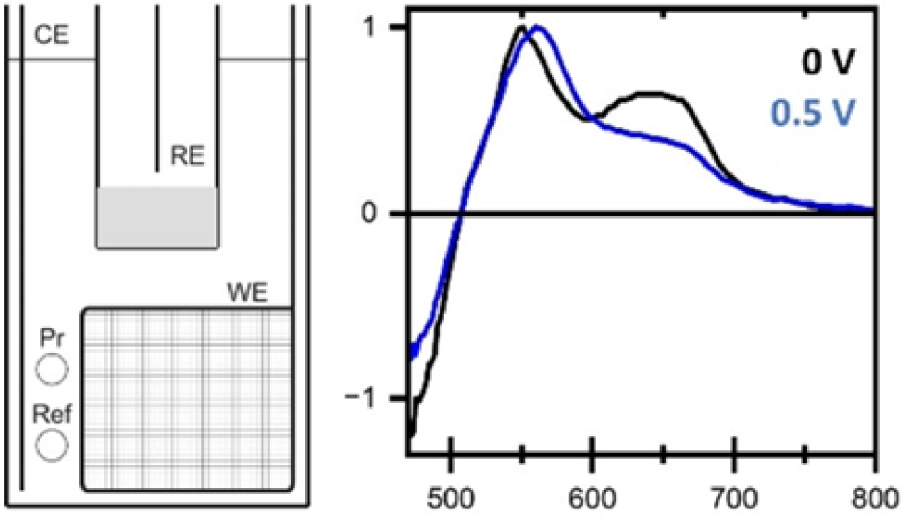

Keywords: Carotenoid, Cyclic voltammetry, 8'-apo-β-carotenal, Spectroelectrochemistry, Transient absorption

6.1. Introduction

Carotenoids are natural pigments that have key functions in photosynthetic organisms. As light-harvesting pigments, they absorb light in the blue-green spectral range, which is not accessible by Chlorophylls (Chls) and Bacteriochlorophylls (BChls) and transfer the absorbed energy to Chls and/or BChls.[1–4] The energy transfer efficiency depends on molecular structure of the bound carotenoid as well as on carotenoidprotein interaction.[1,4,5] Besides light harvesting, carotenoids act as electron donors in electron transfer (ET) processes.[6] To gain more information about photosynthetic systems and artificially designed molecular systems involving carotenoids, it is important to understand excited states, photophysics and electrochemical properties of carotenoids. Thus, several techniques such as fluorescence,[7,8] resonance Raman,[9,10] two-photon,[11–13] and transient absorption spectroscopy have been employed to obtain information about excited states and photophysics of carotenoids. Cyclic and square-wave voltammetry are extensively used for characterization of oxidoreductive reactions of carotenoids.[14,15]

Excited states of carotenoids are usually described by a simplified three-level scheme.[16] While the S_0-S_1 transition is forbidden for one-photon transition, the S_0-S_2 transition of carotenoids is fully allowed and responsible for a strong absorption band in the blue-green spectral region. In this three level scheme, upon excitation of the S_2 state the S_1 state is populated via S_2-S_1 internal conversion in less than 300 fs. The lifetime of the S_1 state depends on conjugation length of carotenoids.[16] Yet, carotenoids with a conjugated carbonyl group, denoted as carbonyl carotenoids, have attracted a lot of attention due to adding another dimension to the rich photophysics of carotenoids. If their conjugation extends to the asymmetrically positioned C=O group, an intramolecular charge transfer (ICT) state appears, which is another dark state with a charge-transfer character.[17,18] The spectroscopic properties of this state depend on polarity and proticity of the environment.[19–23] The ICT state is manifested in transient absorption spectra as a band that is red-shifted from the S_1-S_n band as well as by a weak stimulated emission in the near-IR region.[18] The ICT state couples to the S^1 state, forming a state usually denoted as S_1/ICT[12,17,24,25] resulting in shortening of the S_1/ICT state lifetime in polar environment.[16,20,26,27]

Carotenoid 8'-apo-β-carotenal and its analogues are widely used as synthetic models of carbonyl carotenoids because of their availability for spectroscopic experiments. They were also used in various artificial systems aimed for solar energy conversion.[6,28,30] Excited state dynamics[31–36] and electrochemical properties[14,37–39] of 8'-apo-β-carotenal were in details described earlier. Transient absorption measurements showed that the S_1 state of 8'-apo-β-carotenal has a lifetime of 25 ps in nonpolar solvent *n*-hexane, but it is shortened to 8 ps in polar solvents such as methanol or acetonitrile.[31,32,40] This shortening is associated with increased amplitude of the ICT band in polar environments. Cyclic voltammetry data obtained for 8'-apo-β-carotenal showed two well-separated

anodic peaks corresponding to two sequential single electron oxidations in the range between around 0.5 V and 1 V versus SCE in dichloromethane.[14]

Here we examine excited state dynamics of 8'-apo-β-carotenal by ultrafast time-resolved absorption spectroscopy as a function of applied external voltage in an electrochemical cell. Time-resolved spectroelectrochemistry method has been so far applied to nanocrystals,[41] semiconductors[30] and thin films,[28] but this experimental approach has not yet been applied to carotenoids. We have applied time-resolved absorption in combination with electrochemistry to study excited state dynamics of 8'-apo-β-carotenal in acetonitrile to reveal the effect of applied voltage on the ICT state. This integrated approach allows us to decipher the fundamental energy landscape governing the behaviour of 8'-apo-β-carotenal, with implications spanning fields such as materials science and photophysics, where precise control of excited states is of paramount importance. The results show that the amplitude of the ICT state in transient absorption spectrum as well as associated polarity-induced effects can be tuned by applying external voltage.

6.2. Results

6.2.1. Cyclic voltammetry

Electrochemical properties of carotenoids, including 8'-apo-β-carotenal, have been extensively investigated.[14,37–39] It has been shown that the electrochemical reaction mechanisms of carotenoids obtained by cyclic voltammetry (CV) are related to their structures such as number of conjugated double carbon bonds or presence of a carbonyl group, solvents, switch potentials and scan rate. Figure 1 displays CV of 8'-apo-β- carotenal in acetonitrile recorded from 1 to -1 V at the scan rate of 0.1 V/s versus Ag/Ag^+ reference electrode.

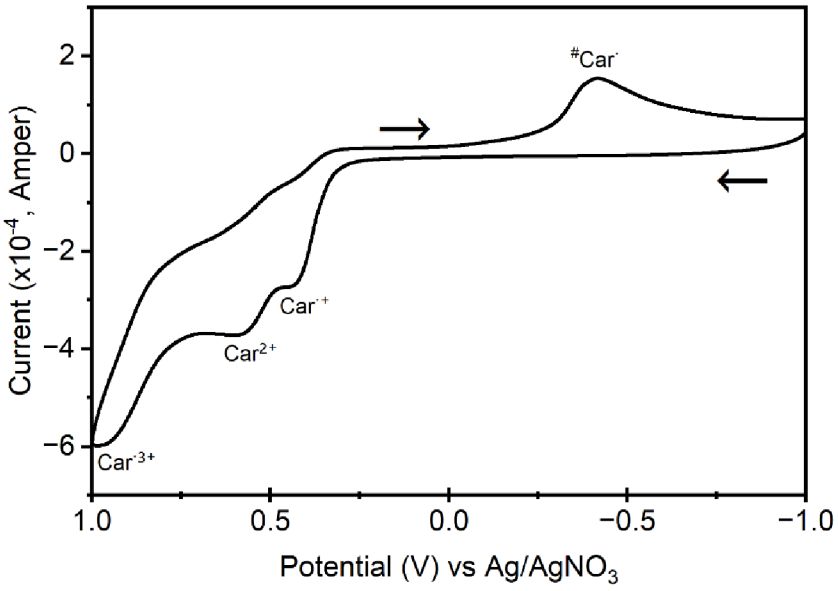

Figure 1. Cyclic Voltammogram of 1 mM 8'-apo-β-carotenal in 0.1 M TBAHFP/acetonitrile solution at the scan rate of 0.1 V/s.

During thenegative scan (1 to +1 V), the first peak is due to the first oxidation of a neutral 8'-apo-β-carotenal resulting in radical cations (Car•$^{+}$), and the second peak represents oxidation of Car•$^{+}$ forming dications (Car^{2+}). The third peak at higher potential could be attributed to the formation of the radical trication.[38] After switching direction of potential at 1 V, during the positive scan, the weak reduction peak corresponds to a reduction of Car^{2+}. The strong peak around -0.4 V can be assigned to formation of neutral radical (#Car•) which is formed by either reduction of cation (#Car^{+}) generated by reduction of Car^{2+}, or by deprotonation of Car•$^{+}$.[42] The oxidation potentials of 8'-apo-β-carotenal presented here differ from earlier presented data[14,37–39] due to using both different solvent and reference electrode solution.

6.2.2. Steady state spectroelectrochemistry

Absorption spectrum of 0.1 mM 8'-apo-β-carotenal in 0.01 M acetonitrile/TBAHFP solution is shown in Figure 2 (black spectrum). Like other carbonyl carotenoids in a polar solvent,[15] 8'-apo-β-carotenal in the TBAHFP/acetonitrile solution has a broad absorption spectrum, lacking vibrational bands (Figure 2a, black) and peaking at ~455 nm in agreement with previous reports.[31–34]

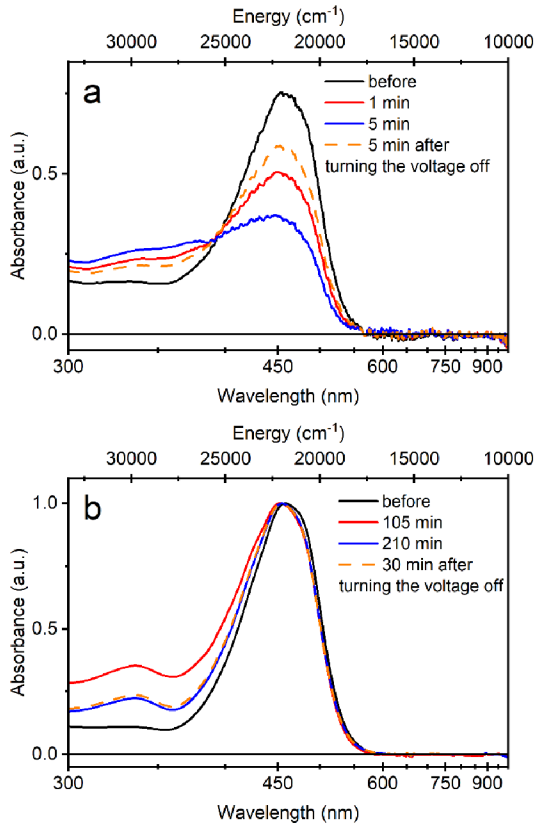

Figure 2. Comparison of absorption spectra of 0.1 mM 8'-apo-β-carotenal in 0.01 M TBAHFP/acetonitrile solution in applied voltage of 0.5 V. (a) The spectra were recorded at various times during 5 min of bulk electrolysis (at 1 min and 5 min; red and blue spectra, respectively) and 5 min after stopping voltage (orange dashed spectrum). (b) The normalized spectra were recorded at various times during 210 min bulk electrolysis (at 105 min and 210 min; red and blue spectra, respectively) and 30 min after turning voltage off (orange dashed line). The black absorption line in the figures is spectrum measured before the bulk analysis.

To test the effect of TBAHFP, we compared that spectrum with 0.1 mM 8'-apo-β-carotenal in pure acetonitrile (Figure S1 Supp. Information). The spectra are identical, demonstrating that the addition of TBAHFP to acetonitrile does not influence the spectroscopic properties of 8'-apo-β-carotenal in acetonitrile.

Our aim was to modify the sample condition by applying the voltage, while still maintaining the neutral carotenoid as the dominant species in the sample. For bulk electrolysis (BE) we chose 0.5 V to strike a balance between providing sufficient electrochemical perturbation to investigate the ICT state while maintaining conditions that are conducive to the stability of the molecule and prevention of unwanted side reactions.

Steady-state absorption profiles of 8'-apo-β-carotenal in TBAHFP/acetonitrile solution recorded at various times during BE are shown in Figure 2 and compared with standard absorption spectrum (black). Figure 2a shows that magnitude of the absorption band after application of the voltage quickly (order of tens of seconds) decreases and after ca 5 minutes reaches its minimum (Figure 2a, blue spectrum). After turning off the voltage, part of the absorption band magnitude recovers (Figure 2a, dashed line spectrum). The observed decrease of absorption band amplitude may be caused by a change in oscillator strength of the S_0-S_2 transition of neutral carotenoid molecules during BE. Also, a presence of isosbestic point indicates that a certain fraction of molecules is converted to a species absorbing in UV, which is possibly due to a degradation, producing species with shorter conjugation. This is likely the reason why the amplitude of absorption spectrum is not fully reversible.

Figure 2b shows normalized steady-state absorption profile during bulk electrolysis at 210 min and a spectrum taken 30 minutes after switching the voltage off, to mirror the experimental scheme used in the transient absorption experiment. (See Time-resolved spectroelectrochemistry section below). The normalized spectrum recorded at 105 min (Figure 2b, red spectrum), and even the spectrum 30 min after turning the voltage off remains nearly the same as the spectrum measured before applying the voltage (Figure 2a, black spectrum). These results indicate that neither TBAHFP nor the applied voltage of 0.5 V affect the S_2 state energy of 8'-apo-β-carotenal in acetonitrile. No carotenoid radical formation has been observed during the measurement. As opposed to the case of dichloromethane solvent where radical formation has been observed. (See Supporting Information Figure S2.)

6.2.3. Time-resolved spectroelectrochemistry

Figure 3 provides an overview of the results obtained from standard (**TA-I** and **TA-IV**) and spectroelectrochemical timeresolved transient absorption measurements (**TA-II** and **TA-III**) during BE of 0.1 mM 8'-apo-β-carotenal in 0.01 M TBAHFP/ acetonitrile solution. The transient absorption spectra taken at 1 ps after excitation are shown in Figure 3a. To distinguish the effect of BE on excited-state dynamics of 8'-apo-β-carotenal, a standard time-resolved transient absorption measurement,

TA-I, was carried out first for 15 minutes in the same electrochemical cell prior to applying the voltage (Figure 3a, black line). The excited-state bands peaking at 550 nm and 643 nm correspond to the S_1-S_n and ICT-S_n transition, respectively, in agreement with previous reports.[31–34] Since the S_1 and ICT states of carbonyl carotenoids are coupled, forming a potential surface with S_1 and ICT minima,[26,27] the two bands, denoted as the S_1-like and ICT-like bands correspond to transition from the S_1 and ICT minima of the S_1/ICT potential surface.

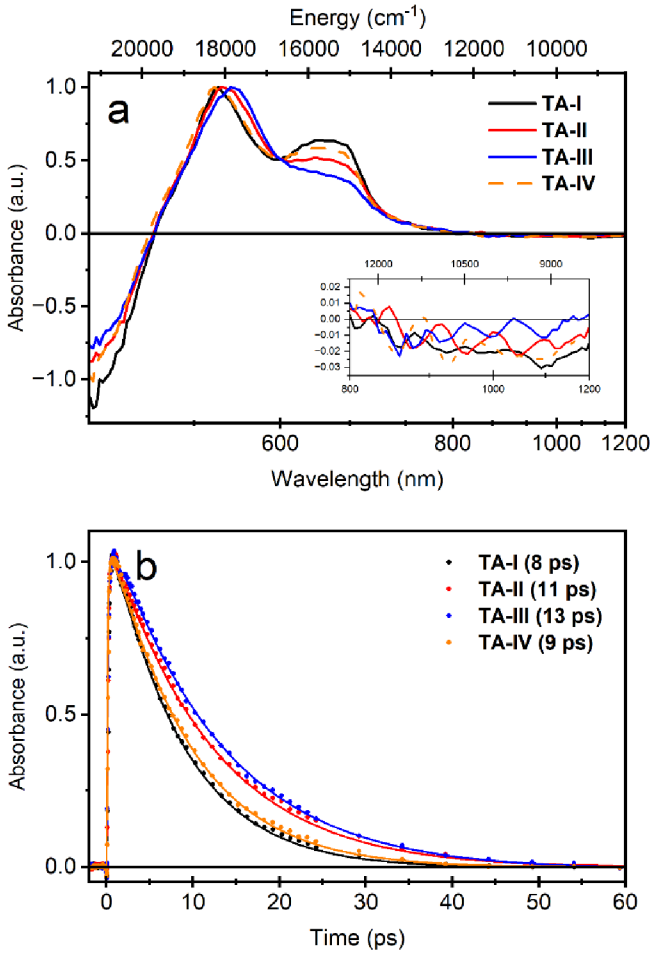

Figure 3. (a) Normalized transient absorption spectra taken at 1 ps after excitation of 0.1 mM 8'-apo-β-carotenal, 0.01 M TBHFP in acetonitrile: prior to applied voltage (TA-I), measured from 90 min to 105 min after applied voltage of 0.5 V (TA-II), measured from 150 min to 210 min after applied voltage of 0.5 V (TA-III), and measured between 15 and 30 min after turning off voltage (TA-IV). Inset shows the zoom view in the range 800 and 1200 nm, the region of stimulated emission associated with ICT state, b) Normalized kinetic traces measured at the S1-SN maxima. The fits obtained from global fitting analyses are demonstrated by solid lines. S1/ICT lifetimes are given in parentheses. Excitation wavelength was 490 nm.

The positions of the S1-like and ICT-like bands measured in **TA-II** and **TA-III** (Figure 3a, red and blue spectra) show that the S_1-like band is slightly broadened and red-shifted to the longer wavelengths by ~6 to ~10 nm compared to **TA-I**. Morever, amplitude of the ICT-like band has decreased significantly in **TA-II** and **TA-III** data. Importantly, these changes are reversible as

demonstrated by measurements taken 15 min after turning the voltage off (**TA-IV**). The transient absorption spectrum **TA-IV** (Figure 3a, orange dashed spectrum) has the S_1-like band and ICT-like band almost restored compared to the original data before switching on the voltage (**TA-I**). Transient absorption spectra at various delays, for all datasets present here, are shown in Supporting Information Figure S3.

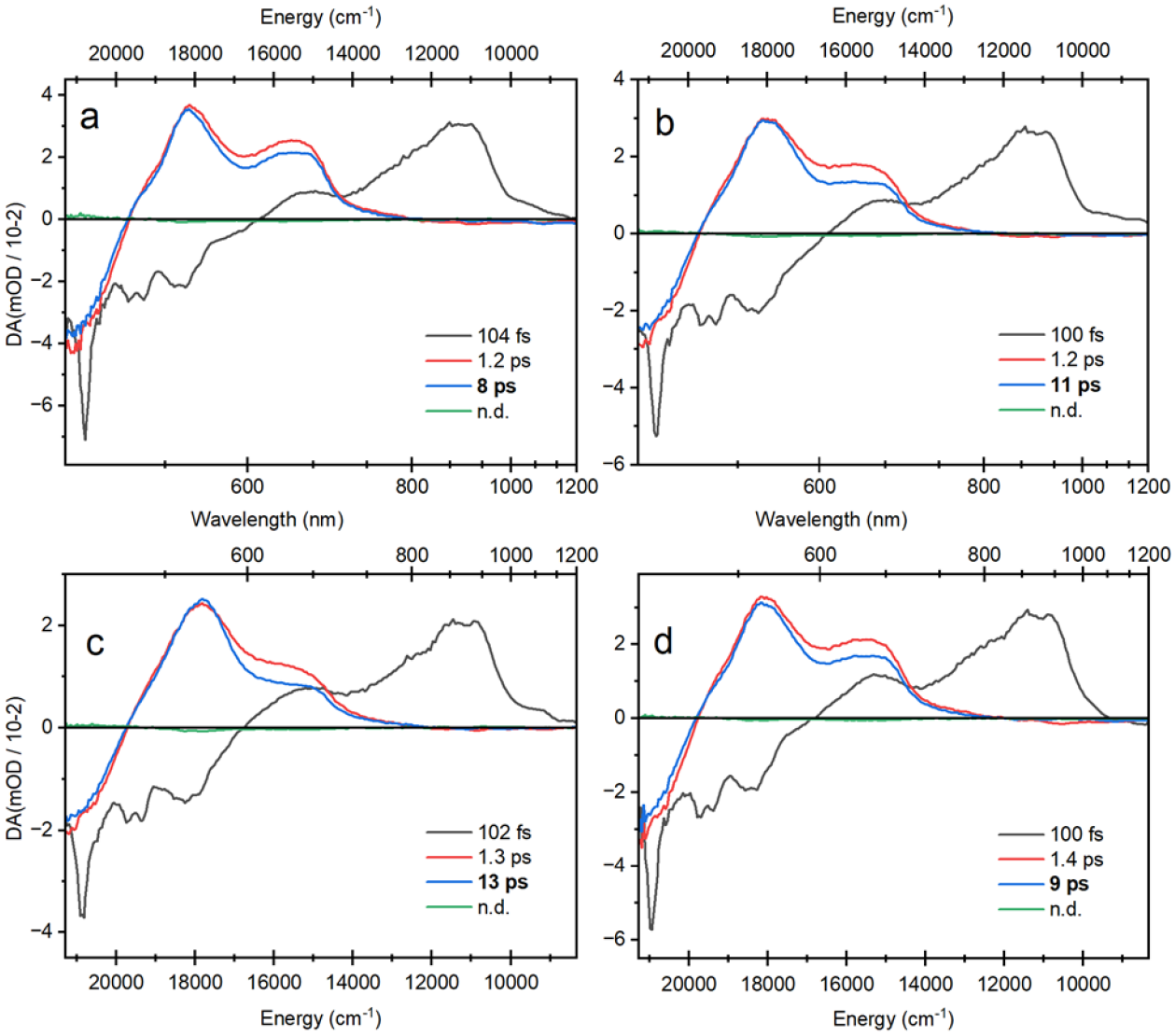

Figure 4. EADS obtained from global fitting analyses for 8'-apo-β-carotenal in TBAHFP/acetonitrile solution (a) TA-I, (b) TA-II, (c) TA-III, and (d) TA-IV. Each spectral components is assigned its lifetime from global analysis, with exception of non-decaying components (n.d.). We provide the n.d. components as an evidence that there are no long-lived photoproducts (e. g. due to photo-damage of the sample) that would affect the dynamics.

Another spectroscopic marker of the presence of a conjugated C=O group in carbonyl carotenoids besides the polarity-induced ICT-like transition is a weak stimulated emission band in the near-IR region.[18] The inset in Figure 3 shows that there has been a slight rise and drop in amplitude of the weak negative signal corresponding to the ICT stimulated emission mirroring the changes in magnitude of the ICT-like transition. This observation confirms that the charge transfer character of the S_1/ICT state of 8'-apo-β-carotenal, as well as the overall excited-state dynamics are influenced by the applied external voltage during BE.

Thus, the applied voltage affects the properties of the S_1/ICT state of 8'-apo-β-carotenal. This observation is further supported by the S_1/ICT lifetimes probed at the maximum of the S_1-like transition (Figure 3b). The S_1/ICT lifetime of 8'-apo-β-carotenal in TBAHFP/acetonitrile solution (Figure 3b, black) obtained from global fitting is about 8 ps, which matches previously reported data.[31,34] Under applied voltage, however, the S_1/ICT lifetime is prolonged to about 11 ps (Figure 3b, red) and further to 13 ps for the data set **TA-III** (Figure 3b, blue). The kinetic trace of the data set **TA-IV** proves the reversibility of the system as the S_1/ICT lifetime is recovered to 9 ps (Figure 3b, orange dashed), thus nearly matching the **TA-I** kinetics. The increase of the S_1/ICT lifetime is complemented by a decrease of the ICT-like band amplitude (Figure 3a and b).

To gain more information about excited-state dynamics of 8'-apo-β-carotenal during BE, we have applied a global fitting analysis to the data obtained from transient absorption experiment by assuming a sequential model of excited-state dynamics. The evolution-associated difference spectra (EADS), which correspond to the individual excited-state species in the sequential model, are shown in Figure 4. For all data sets, three time components were required to fit the data (Figure 4). The fastest EADS (black), for all panels in Figure 4, corresponds to the decay of the S_2 state as evidenced by the characteristic S_2-S_N band in the 800–1000 nm spectral region. The S_2 state decay is the same for all data sets (~100 fs), further confirming that the S_2 state is not affected by the applied voltage. The second EADS (red), which has a lifetime of around 1.2 ps, is due to the relaxation of a hot S_1/ICT state as well as the S_1-ICT equilibration. The final EADS corresponds to the relaxed S_1/ICT state of 8'-apo-β-carotenal, and only this EADS exhibits lifetime dependence on the applied voltage. For **TA-I** (Figure 4a), the S_1/ICT lifetime is 8 ps in agreement with the data reported for 8'-apo-β-carotenal in a polar solvent earlier.[31–34] Applying the voltage prolongs the S_1/ICT lifetime to 11 ps (**TA-II**, Figure 4b) and further to 13 ps (**TA-III**, Figure 4c). Figure 4d shows EADS obtained from data measured after switching off the voltage (**TA-IV**). The obtained lifetimes prove reversibility of the voltage-induced processes.

6.3. Discussion

From Figure 3 we can see that applying voltage of 0.5 V in BE reduces magnitude of the ICT band in TA spectra and increases the S_1/ICT state lifetime. Often, these effects are manifestation of polarity decrease of environment surrounding the carotenoid.[19,22] Change of polarity is also complemented by changes visible in steady-state absorption spectra. However, BE has negligible effect on absorption spectra (Figure 2) that would be attributable to change of polarity, and we can hardly expect that voltage 0.5 V could notably alter solvent polarity.

Looking at steady-state absorption spectra of 8'-apo-β-carotenal in acetonitrile/TBAHFP solution (Figure 2) during BE at 0.5 V we do not observe any hint of spectral features that could be associated with carotenoid radical $Car^{\bullet+}$ formation. In acetonitrile, the $Car^{\bullet+}$ is likely unstable and quickly loses another electron forming dication Car^{2+}, a hint of which we can observe within the first five minutes

of BE as a weak absorption band in the 580–650 nm spectral region (Figure 2a), while it diminishes in long term experiment (105 to 210 min, Figure 2b). The formation of Car^{2+}, we assume, is a negligible process leading to depletion of radical cations $Car^{\bullet+}$, due to setting the voltage just before the second wave where the Car^{2+} is formed (Figure 1). The competing and more probable process that reduces concentration of $Car^{\bullet+}$ is formation of neutral radical #Car• via deprotonation.[42]

Thus, the presence of various charged and neutral species in the sample affects the excited-state properties of neutral 8'-apo-β-carotenal as evidenced by change of the S_1/ICT lifetime as well as the amplitude of the ICT band. Both these changes are consistent with decrease of the CT character of the S_1/ICT state 8'-apo-β-carotenal.[17,20] Observation of variation of the CT character of the S_1/ICT state upon BE implies that the local environment of neutral 8'-apo-β-carotenal must alter the S_1-ICT coupling which is the key parameter determining the degree of the CT character of the S_1/ICT state.[18,26,27]

As shown by Redeckas et. al.[26] and West et. al.,[27] dumping the ICT state and disturbing the S_1/ICT population ratio is followed by rapid (units of ps) re-equilibration of populations of the states. Moreover, this equilibration is intramolecular, not due to interaction between two carotenoid molecules. It suggests that any individual molecule that is in S_1 state can transit to ICT state. Environment surrounding the molecule affects the magnitude of barrier between S_1 and ICT minima of the S_1/ICT potential surface and thus changing the equilibration rate, the common S_1/ICT lifetime and overall S_1/ICT population ratio. We hypothesize that processes during BE create assorted mixture of ions (TBA^+, HFP^-), and radicals ($Car^{\bullet+}$, #Car•) which can affect the barrier between S_1 and ICT state and effectively change the S_1/ICT population ratio in advantage of S_1 state of a neutral carotenoid.

6.4. Conclusions

The excited state dynamics of 8'-apo-β-carotenal were investigated in acetonitrile during the bulk electrolysis and results were compared with the standard measurements without applied voltage. During BE with applied voltage of 0.5 V we observed significant change of S_1/ICT state ratio in advantage to the S_1 state and increase of the S_1/ICT state lifetime as compared with the system without applied voltage.

6.5. Experimental Section

6.5.1. Cyclic voltammetry

Cyclic voltammetry (CV) measurements were carried out using CH Instrument Electrochemical Workstation (CHI600E) with a standard three-electrode electrochemical system in a 1 mm spectroelectrochemical cuvette (Scheme S1, in Supporting Information). The commercial (ALS Japan) Pt Gauze electrode, Pt wires and Ag wires were used as a working, counter, and reference electrodes, respectively. For sample preparation, a 0.1 M tetrabutylammonium hexafluorophosphate (TBAHFP)

electrolyte solution was prepared in dry acetonitrile. Then, 8'-apo-β-carotenal was added to 0.1 M TBAHFP/acetonitrile at a concentration of 0.1 M. For quasi reference electrode solution, $AgNO_3$ was dissolved in 0.1 M TBAHFP/acetonitrile solution at concentration of 0.01 M. The final molar ratios of 8'-apo-β-carotenal and TBAHFP was 1: 100, and 1:10 for $AgNO_3$ and TBAHFP.

6.5.2. Steady-state absorption spectroscopy

Absorption spectra of the sample were measured on the UV-VIS spectrometer (Shimadzu UV-2600) with integrated three-electrode electrochemical system. The concentration of 8'-apo-β-carotenal in the TBAHFP/acetonitrile solution was adjusted to 0.1 mM by diluting with pure acetonitrile. Therefore, the final concentration of the sample was 0.1 mM 8'-apo-β-carotenal in 0.01 TBAHFP/acetonitrile solution. The same procedure was applied to the reference electrode solution. The aim was to maintain the same molar ratio among 8'-apo-β-carotenal, TBAHFP and $AgNO_3$ in acetonitrile as in cyclic voltammetry measurements. An external voltage of 0.5 V was used to observe any changes in steady-state absorption of 8'-apo-β-carotenal under continuously applied bulk electrolysis for short time (up to 5 min) and long time (up to 210 min). Then, to test the recovery of the sample, the applied voltage was turned off in both experiments. The absorption spectra were recorded at various times during the BE and after turning the applied voltage off.

6.5.3. Transient absorption spectroscopy

Time-resolved transient absorption (TA) measurements were performed with a three-electrode electrochemical system integrated to the ultrafast spectrometer. The femtosecond spectrometer consists of a Ti:Sapphire regenerative amplifier (Spitfire Ace-100F, Spectra-Physics, USA) seeded with a Ti:Sapphire oscillator (MaiTai SP, Spectra-Physics, USA), and pumped by Nd:YLF laser (Empower 30, Spectra-Physics, USA). The output beam, 100 fs pulses with wavelength centered at 800 nm at a 1-kHz repetition rate, was divided into excitation and probe beams by a beam splitter. The excitation beam was generated by an optical parametric amplifier (TOPAS Prime, Light Conversion, Lithuania) centered at 490 nm. The probe beam was a broadband white-light continuum beam (470 to 1200 nm) generated by focusing 1300 nm output generated in a home-built OPA to a 2-mm Sapphire plate. The white-light continuum beam was further divided into reference and probe beams by a broadband 50/50 beam splitter. Probe and reference beams were dispersed in a prism spectrograph (Pascher Instruments, Sweden) and detected by a pair of linear CCD arrays allowing to measure the whole 400–1200 nm spectral region. The spectrometer was calibrated before the experiment by placing a multiple oxide filter (WCT 2065, Avian Technologies, USA) into the white light beams in front of CCD arrays. The pump polarization was set at a magic angle (54.7°) relative to the probe beam polarization.

TA measurements were classified into three parts; before applied voltage (TA-I), under the continuously applied voltage of 0.5 V (TA-II and TA-III), and after turning the applied voltage off (TA-

IV). TA-I, standard TA measurement, was carried for 15 min as a reference to further experiments. Immediately after this measurement, the voltage of 0.5 V was applied to the sample and maintained up to 210 min continuously. During the BE, the second, TA-II, and third, TA-III, TA data sets were collected; from 90 min after starting applied voltage to 105 min, and from 150 min to 210 min, respectively. The fourth TA data set, TA-IV, was measured from 15 min after turning voltage off to 30 min.

6.5.4. Data analysis

Global fitting procedure was applied to chirp-corrected data set using the CarpetView fitting software (Light Conversion, Lithuania), assuming the excited system evolves according to a sequential and irreversible scheme which corresponds to individual excited-state species called evolution-associated difference spectra (EADS). OriginPro software was used for visualizing the results.

Acknowledgements

The authors thank Alireza Honarfar, František Adamec and Ivana Šímová for their help during the experiments. Financial support was provided by the Czech Science Foundation, grant No. 19-28323X and by Laselab Europe, project ID: LLC002273.5.6

6.6. Supporting Information

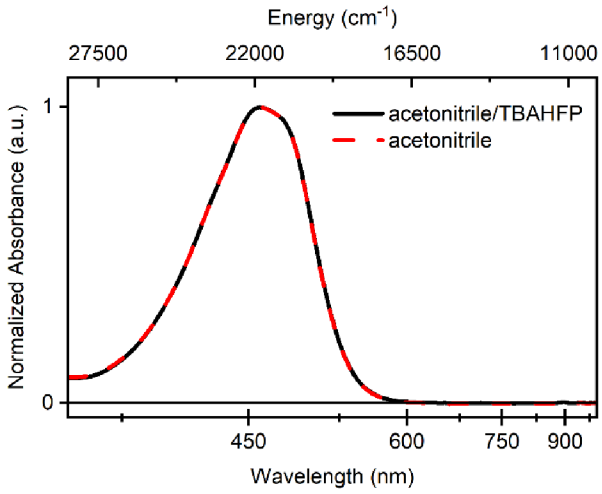

Figure S1. Comparison of normalized absorption spectra of 0.1 mM 8'-apo-β-carotenal in 0.01 M acetonitrile/TBAHFP solution (black) and in pure acetonitrile (red).

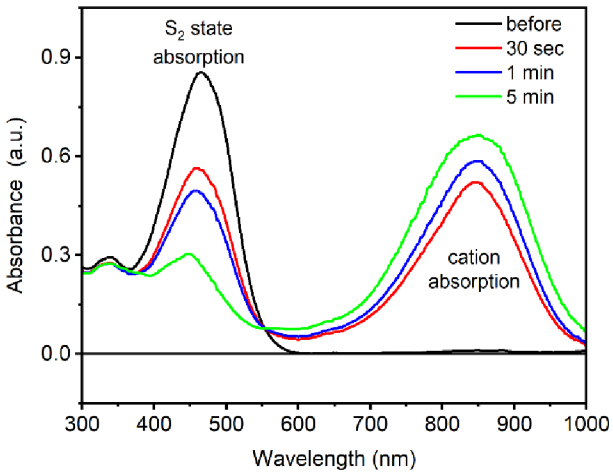

Figure S2. Comparison of absorption spectra of 0.1 mM 8′-apo-β-carotenal in 0.01 M TBAHFP/dichloromethane solution with applied voltage of 0.5 V. The spectra were recorded at various times during 5 min of bulk electrolysis. The black absorption spectrum in the graph was measured before bulk electrolysis.

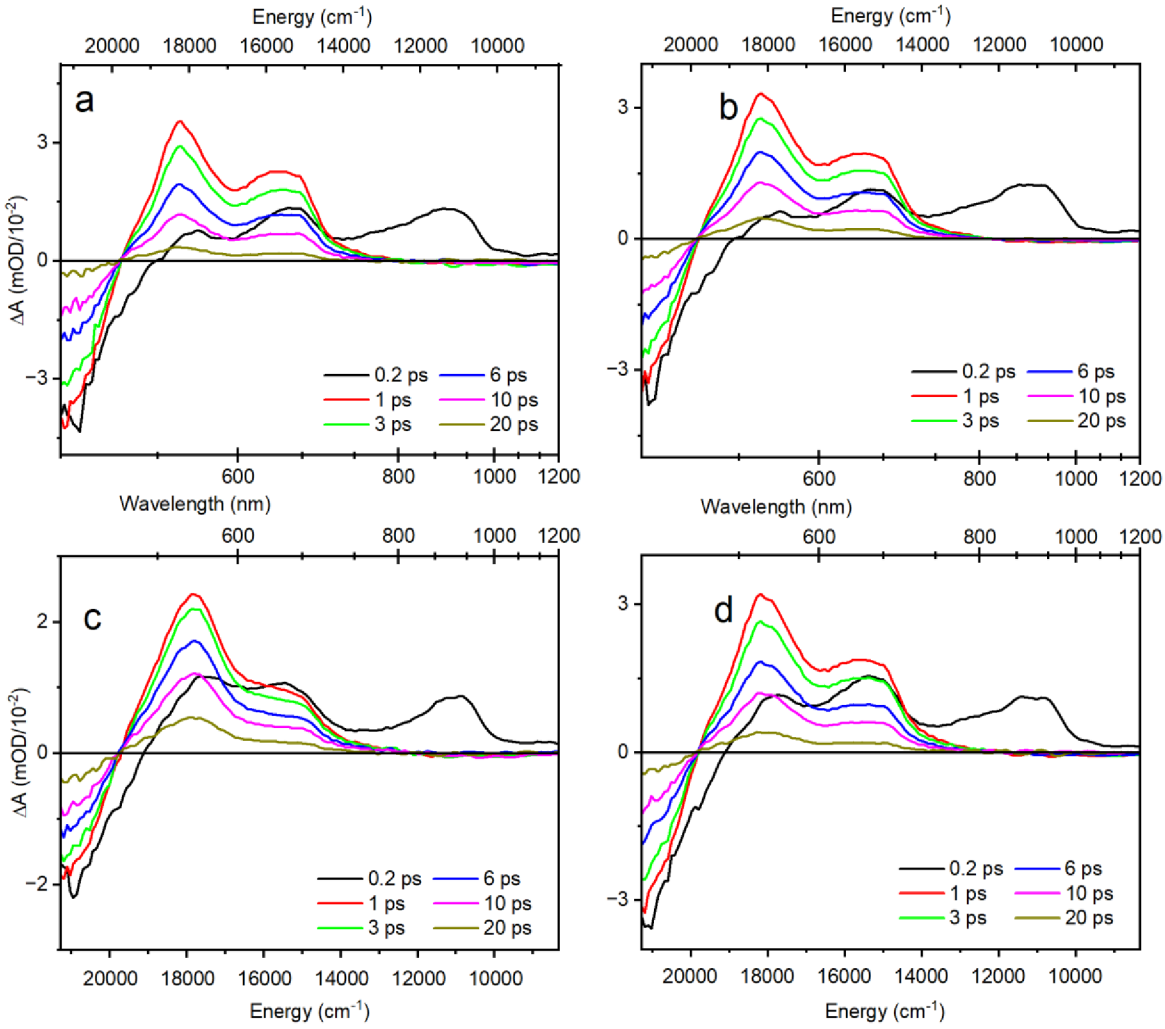

Figure S3. Transient absorption spectra of 0.1 mM 8′-apo-β-carotenal in 0.01 M acetonitrile/TBAHFP solution at different delay times. (a) Prior application of voltage, TA-I, (b) 90 min after applied voltage of 0.5 V up to 105 min, TA-II, (c) 150 min after applied voltage of 0.5 V up to 210 min, TA-III, and (d) 15 min after switching off the voltage up to 30-minutes, TA-IV.

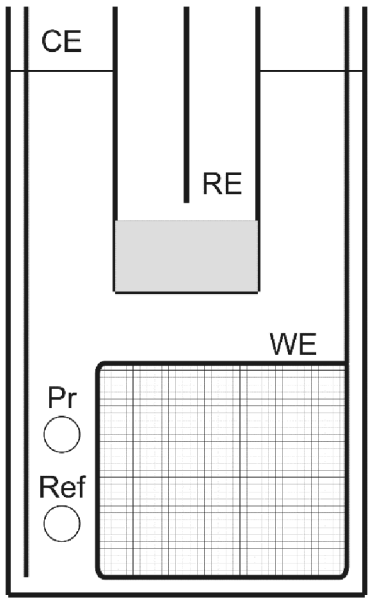

Scheme S1. The illustration of a three-electrode electrochemical system which is used for all spectroscopic methods in the manuscript. CE: counter electrode (Pt wire), RE: reference electrode (Ag wire in $AgNO_3$/TBAHFP/acetonitrile solution), WE: working electrode (gauze Pt wire). The circles indicate positions of beams during transient absorption measurements. Pr: pump and probe beams, Ref: reference beam. Steady-state absorption spectra were measured through gauze working electrode.

6.7. References

[1] T. Polívka, H. A. Frank, Acc. Chem. Res. 2010, 43, 1125–1134.

[2] G. D. Scholes, G. R. Fleming, A. Olaya-Castro, R. Van Grondelle, Nat. Chem. 2011, 3, 763–774.

[3] H. Hashimoto, Y. Sugai, C. Uragami, A. T. Gardiner, R. J. Cogdell, J. Photochem. Photobiol. C 2015, 25, 46–70.

[4] R. Croce, H. van Amerongen, Science 2020, 369, eaay2058.

[5] T. Mirkovic, E. E. Ostroumov, J. M. Anna, R. van Grondelle, Govindjee, G. D. Scholes, Chem. Rev. 2017, 117, 249–293.

[6] J. Pan, G. Benkö, Y. Xu, T. Pascher, L. Sun, V. Sundström, T. Polívka, J. Am. Chem. Soc. 2002, 124, 13949–57.

[7] V. Chynwat, H. A. Frank, Chem. Phys. 1995, 194, 237–244.

[8] R. Fujii, T. Ishikawa, Y. Koyama, M. Taguchi, Y. Isobe, H. Nagae, Y. Watanabe, J. Phys. Chem. A 2001, 105, 5348–5355.

[9] B. Robert, Photosynth. Res. 2009, 101, 147–155.

[10] M. J. Llansola-Portoles, A. A. Pascal, B. Robert, J. R. Soc. Interface 2017, 14, DOI 10.1098/rsif.2017.0504.

[11] D. Kosumi, T. Kusumoto, R. Fujii, M. Sugisaki, Y. Iinuma, N. Oka, Y. Takaesu, T. Taira, M. Iha, H. A. Frank, H. Hashimoto, Chem. Phys. Lett. 2009, 483, 95–100.

[12] P. A. Linden, J. Zimmermann, T. Brixner, N. E. Holt, H. M. Vaswani, R. G. Hiller, G. R. Fleming, J. Phys. Chem. B 2004, 108, 10340–10345.

[13] V. Šebelík, V. Kuznetsova, H. Lokstein, T. Polívka, J. Phys. Chem. Lett. 2021, 12, 3176–3181.

[14] D. Liu, Y. Gao, L. D. Kispert, J. Electroanal. Chem. 2000, 488, 140–150.

[15] D. Niedzwiedzki, J. F. Rusling, H. A. Frank, Chem. Phys. Lett. 2005, 415, 308–312.

[16] T. Polívka, V. Sundström, Chem. Rev. 2004, 104, 2021–2071.

[17] H. A. Frank, J. A. Bautista, J. Josue, Z. Pendon, R. G. Hiller, F. P. Sharples, D. Gosztola, M. R. Wasielewski, J. Phys. Chem. B 2000, 104, 4569–4577.

[18] D. Zigmantas, T. Polivka, R. G. Hiller, A. Yartsev, V. Sundstrom, J. Phys. Chem. A 2001, 105, 10296–10306.

[19] J. A. Bautista, R. E. Connors, B. B. Raju, R. G. Hiller, F. P. Sharples, D. Gosztola, M. R. Wasielewski, H. A. Frank, J. Phys. Chem. B 1999, 103, 8751–8758.

[20] D. Zigmantas, R. G. Hiller, F. P. Sharples, H. A. Frank, V. Sundström, T. Polívka, Phys. Chem. Chem. Phys. 2004, 6, 3009–3016.

[21] D. M. Niedzwiedzki, N. Chatterjee, M. M. Enriquez, T. Kajikawa, S. Hasegawa, S. Katsumura, H. A. Frank, J. Phys. Chem. B 2009, 113, 13604–13612.

[22] G. Keşan, M. Durchan, J. Tichý, B. Minofar, V. Kuznetsova, M. Fuciman, V. Šlouf, C. Parlak, T. Polívka, J. Phys. Chem. B 2015, 119, 12653–12663.

[23] E. Ragnoni, M. Di Donato, A. Iagatti, A. Lapini, R. Righini, J. Phys. Chem. B 2015, 119, 420–432.

[24] D. Zigmantas, R. G. Hiller, A. Yartsev, V. Sundström, T. Polívka, J. Phys. Chem. B 2003, 107, 5339–5348.

[25] T. Polívka, I. H. M. van Stokkum, D. Zigmantas, R. van Grondelle, V. Sundström, R. G. Hiller, Biochemistry 2006, 45, 8516–26.

[26] K. Redeckas, V. Voiciuk, M. Vengris, Photosynth. Res. 2016, 128, 169–181.

[27] R. G. West, M. Fuciman, H. Staleva-Musto, V. Šebelík, D. Bína, M. Durchan, V. Kuznetsova, T. Polívka, J. Phys. Chem. B 2018, 122, 7264–7276.

[28] F. G. Gao, A. J. Bard, L. D. Kispert, J. Photochem. Photobiol. A 2000, 130, 49–56.

[29] J. Xiang, F. S. Rondonuwu, Y. Kakitani, R. Fujii, Y. Watanabe, Y. Koyama, H. Nagae, Y. Yamano, M. Ito, J. Phys. Chem. B 2005, 109, 17066–77.

[30] J. Pan, Y. Xu, L. Sun, V. Sundström, T. Polívka, J. Am. Chem. Soc. 2004, 126, 3066–3067.

[31] F. Ehlers, D. A. Wild, T. Lenzer, K. Oum, J. Phys. Chem. A 2007, 111, 2257–2265.

[32] M. Kopczynski, F. Ehlers, T. Lenzer, K. Oum, J. Phys. Chem. A 2007, 111, 5370–5381.

[33] F. Ehlers, T. Lenzer, K. Oum, J. Phys. Chem. B 2008, 112, 16690–16700.

[34] M. Durchan, M. Fuciman, V. Šlouf, G. Keşan, T. Polívka, J. Phys. Chem. A 2012, 116, 12330–12338.

[35] Y. Pang, G. R. Fleming, Phys. Chem. Chem. Phys. 2010, 12, 6782–6788.

[36] M. Di Donato, M. S. Centellas, A. Lapini, M. Lima, F. Avila, F. Santoro, C. Cappelli, R. Righini, J. Phys. Chem. B 2014, 118, 9613-9630..

[37] Y. Deng, G. Gao, Z. He, L. D. Kispert, J. Phys. Chem. B 2000, 104, 5651–5656.

[38] L. D. Kispert, G. Gao, Y. Deng, V. Konovalov, A. S. Jeevarajan, J. A. Jeevarajan, E. Hand, Acta Chem. Scand. 1997, 51, 572–578.

[39] L. D. Kispert, N. E. Polyakov, Chem. Lett. 2010, 39, 148–155.

[40] Z. He, D. Gosztola, Y. Deng, G. Gao, M. R. Wasielewski, L. D. Kispert, J. Phys. Chem. B 2000, 104, 6668–6673.

[41] A. Honarfar, P. Chabera, W. Lin, J. Meng, H. Mourad, G. Pankratova, L. Gorton, K. Zheng, T. Pullerits, J. Phys. Chem. C 2021, 125, 14332–14337.

[42] A. L. Focsan, S. Pan, L. D. Kispert, J. Phys. Chem. B 2014, 118, 2331–2339.

7. Paper III

Ultrafast spectroscopy of the hydrophilic carotenoid crocin at various pH

Özcan, E., Šímová, I., Bína, D., Litvín, R., & Polívka, T. (2024). Ultrafast spectroscopy of the hydrophilic carotenoid crocin at various pH. Physical Chemistry Chemical Physics, 26(13), 10225-10233.

https://doi.org/10.1039/D4CP00665H

Abstract

This study delves into the pH-dependent effects on the excited-state behavior of crocin, a hydrophilic carotenoid with diverse functions in biological systems. Steady-state spectroscopy demonstrates notable changes in absorption and fluorescence spectra, characterized by a pH-dependent blue shift and altered resolution of vibrational bands. Transient absorption spectra further elucidate these effects, highlighting a significant blue shift in the S_1–S_n peak with increasing pH. Detailed kinetic analysis shows the pH dependent dynamics of crocin's excited states. At pH 11, a shortening of effective conjugation is observed, resulting in a prolonged S_1/ICT lifetime. Conversely, at pH 9, our data suggest a more complex scenario, suggesting the presence of two distinct crocin species with different relaxation patterns. This implies structural alterations within the crocin molecule, potentially linked to the deprotonation of hydroxyl groups in crocin and/or saponification at high pH.

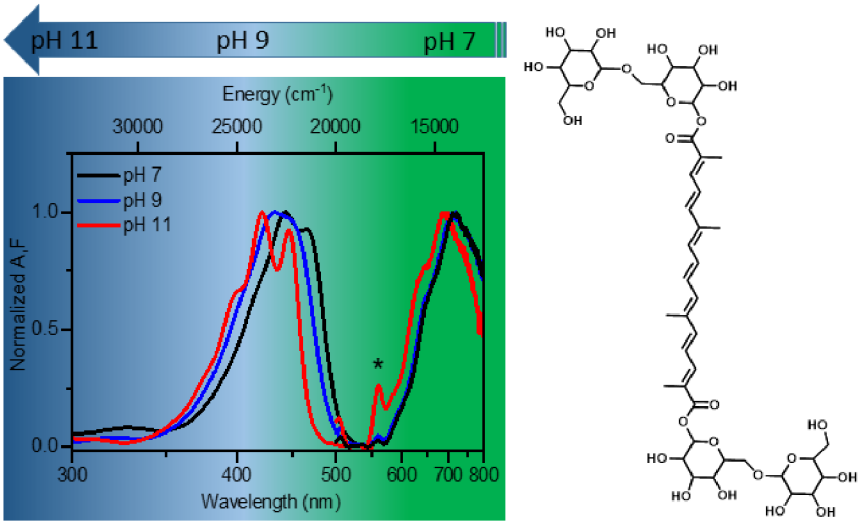

Keywords: Carotenoids, Crocin, Ultrafast spectroscopy, Excited states, pH-dependence.

7.1. Introduction

Photophysical and photochemical properties of carotenoids, abundant natural pigments, have been extensively investigated in a variety of theoretical and experimental studies due to their photoprotective[1] and light-harvesting[2,3] abilities in biological systems. The wide range of carotenoid functions, including quenching of singlet-excited states of chlorophylls,[4–7] chlorophyll triplets[8,9] and antioxidation achieved by scavenging singlet oxygen or other reactive oxygen species,[10–15] as well as their rich excited-state dynamics make these molecules attractive for spectroscopic studies.[16] However, because of the complicated excited-state structure, our understanding of carotenoid photophysics is still limited.

Using the simplest description of excited states of all carotenoids, they exhibit two excited states: the strongly absorbing S_2 state and the low-lying excited state, S_1. The transition from the ground state, S_0, to the lowest excited state, S_1, is forbidden due to the multiply-excited character of the S_1 state.[17] Thus, the lowest energy one-photon transition from the ground state occurs to the S_2 state, which then relaxes to the S_1 state that is readily monitored by its characteristic S_1–S_n band in transient absorption spectra.[18,19] This general picture is valid for all carotenoids as their photophysical properties are predominantly determined by the conjugated C=C double bond chain structure, which is similar for all carotenoids.[17]

Nevertheless, carbonyl carotenoids having a conjugated C=O group exhibit polarity-dependent behavior, which is explained by the presence of an additional electronic state in the excited-state manifold, the intramolecular charge transfer (ICT) state. The presence of the ICT state can be easily detected by characteristic bands in the transient absorption spectrum. The ICT-like transition is red-shifted from the S_1–S_n band and the amplitude ratio between the two bands indicates the degree of charge transfer character of the coupled S_1/ICT state.[20,21] A polar environment stabilizes the ICT state, which may be described as a double-well potential separated by a small barrier, allowing rapid equilibration between the S_1-like and ICT-like potential minima.[22,23] Numerous studies have indicated that the charge transfer increases with the solvent polarity, and the position of the conjugated keto group is also crucial. The ICT signal increases when a single keto group is positioned asymmetrically, whereas two symmetrically positioned keto groups minimize the charge transfer character of the S_1/ICT state.[24,25]

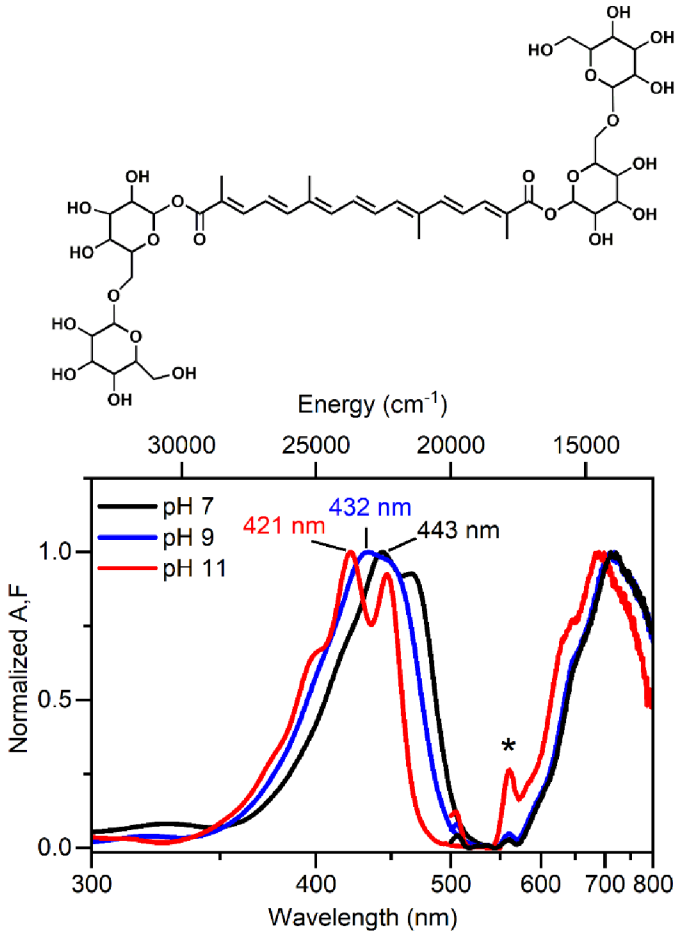

Fig. 1 Normalized steady state absorption and fluorescence spectra of crocin in buffer solutions with different pH at room temperature. The emission band marked by asterisk is due to the Raman band of water. Molecular structure of crocin is also shown.

Natural carotenoids are mostly hydrophobic, and they aggregate in aqueous environments, causing noticeable changes in their spectroscopic properties.[26–30] Therefore, synthesis of water-soluble carotenoids has received a lot of attention as the aggregation may lead to loss of function.[31–33] Crocin, the digentiobiosyl ester of crocetin and one of the few important water-soluble carbonyl carotenoids, is the main natural pigment of the gardenia fruit and stigmas of saffron. Due to its water solubility, crocin has numerous applications as a food colorant and antioxidant.[34,35]

The conjugated system of crocin consists of 7 conjugated C=C bonds, and it is extended to two symmetrically positioned C=O groups (Fig. 1). The bulky gentiobiosyl groups do not contribute to conjugation, but they are responsible for water solubility of crocin. Crocin degrades under high temperature, oxidation, or acidic conditions.[35,36] Moreover, some studies have reported that high temperature and other environmental factors could break the glycosidic bond of crocin and hydrolyze crocin to crocetin.[36–38]

In contrast to other carotenoids, the hydrophilic nature of crocin allows to study effect of pH on spectroscopic properties. Crocin has a good stability in the aqueous alkali solutions (pH≥9), but acidic conditions (pH<5) lead to degradation because the acidic environment destabilizes the conjugated system of crocin.[36,39] Excited state dynamics of crocin in water is faster than in alcohols:

the S_1/ICT state lifetime decreases from ~140 ps in methanol or 2-propanol to 60 ps in water.[31] No data addressing the effect of pH on excited state properties of crocin or other water-soluble carotenoids are available so far.

Here, we applied ultrafast transient absorption spectroscopy to compare excited-state properties of crocin at different pH. Since crocin is unstable at acidic conditions (pH≤5), we have focused on neutral (pH 7) and basic (pH 9 and pH 11) conditions. The results indicate a shortening of effective conjugation at pH 11. The behaviour at pH 9 crocin was more complicated, suggesting a presence of more than one species in the sample.

7.2. Material and Methods

7.2.1. Sample preparation

Crocin (PhytoLab), citric acid (anhydrous, Fluka), sodium hydrogen phosphate (anhydrous, Lachner), sodium carbonate (anhydrous, Lachner), sodium hydrogen carbonate (anhydrous, Lachner), were used as obtained for sample preparation. Stock solutions of crocin ($5x10^{-5}$ M), citric acid ($C_6H_8O_7$; 0.1 M), sodium hydrogen phosphate (Na_2HPO_4; 0.2 M), sodium carbonate (Na_2CO_3; 0.1 M), and sodium hydrogen carbonate ($NaHCO_3$; 0.1 M) were prepared in 20 ml of deionized water. All stock solutions were kept in the dark at 4 °C for two days to check the stability of the solutions. The salts were then mixed in various volumes to prepare different buffer solutions (pH 3, 5, 7, 9 and 11) according to the buffer reference center (Sigma Aldrich) and checked with a pH meter (Orion star A111, Thermo Fisher). Then, crocin and buffer solutions (pH 3, 5, 7, 9, and 11) were mixed 1:1 (volume) in 10 ml glass bottles individually and kept in the dark at room temperature. Absorption spectra of the samples were regularly measured using UV-VIS spectrometer (Shimadzu UV-2600) in a 10-mm path length quartz cuvette to monitor long time (up to 552 hours) changes in absorption spectra. The samples in various buffer solutions, tested for stability and pH effects, were selected for transient absorption experiments (Fig. S1, ESI†).

7.2.2. Transient absorption spectroscopy

Transient absorption measurements were performed with an experimental setup using a modular laser system consisting of a Ti:sapphire regenerative amplifier (Spitfire Ace-100F, Spectra-Physics, USA) seeded with a Ti:sapphire oscillator (MaiTai SP, Spectra-Physics, USA), and pumped by a Nd:YLF laser (Empower 30, Spectra-Physics, USA). The laser system generates B100 fs pulses centered at 800 nm at a repetition rate of 1 kHz. The output is separated into excitation and probe beams by a beam splitter. The excitation beam was generated by an optical parametric amplifier (TOPAS Prime, Light Conversion, Lithuania). The probe pulses were produced by passing the 800 nm beam through a home-built OPA, which produced a 1300 nm output that was focused on a 3-mm CaF_2 plate, generating a white-light continuum beam that covers the 400–900 nm spectral region. To minimize chirp and chromatic aberration, the white-light beam was collimated by an off-axis parabolic mirror and split

into reference and probe beams by a broadband 50/50 beam splitter. The probe beam was focused by a 250 mm spherical mirror to the sample where it overlapped with the excitation beam. Probe and reference beams were dispersed in a prism spectrograph (Pascher Instruments, Sweden) and detected by a double CCD array allowing to measure in the whole 400–900 nm spectral region. Before each experiment, the spectrometer was calibrated by placing a multiple oxide filter (WCT 2065, Avian Technologies, USA) into the white light beams in front of an entry slit. The mutual polarization of excitation and probe beams was set to the magic angle (54.7°). The excitation photon density at the sample was kept below 10^{14} photon cm^{-2} $pulse^{-1}$.

7.2.3. Data analysis

A global fitting software was used to analyze the resulting spectro-temporal data sets (CarpetView, Light Conversion, Lithuania). To visualize the excited-state dynamics, we assumed that the excited system evolves sequentially and irreversibly. Each component in the sequential scheme represents individual excited-state species, and the spectral profile of each species is called the evolution-associated difference spectrum (EADS). EADS provide the information about the time evolution of the studied system, although they do not necessarily represent the spectral profiles of the individual excited state species in a complex system. The spectra were chirp-corrected using the same software's correction routine.

7.2.4. Fluorescence measurements

Fluorescence emission and excitation spectra were measured on Horiba Fluorolog 3.2.2. spectrofluorimeter in 1x1 cm cuvettes. Both emission and excitation spectra were corrected for spectral sensitivity of the detector and excitation lamp emission spectrum. Time-resolved fluorescence was measured using FluoTime 300 instrument (PicoQuant, Germany) with excitation at 481 nm provided with a laser diode module LDH-P-C-485 (PicoQuant). Data were analyzed globally by iterative reconvolution as implemented in the FluoFit software (PicoQuant). Decay-associated spectra were corrected for detector spectral sensitivity.

7.3. Results

7.3.1. Steady-state spectroscopy

Absorption spectra of crocin in different buffer solutions pH (7, 9, and 11) are shown in Fig. 1. The absorption maximum of crocin occurs at 443 nm in pH 7. Since the vibrational bands of S_0–S_2 transitions are well resolved, the absorption maximum can be assigned to the 0–1 vibrational band, while the 0–0 and 0–2 bands are located at 466 and 415 nm, respectively, which is in good agreement with previous report.[31] The absorption maximum of crocin blue shifts with increasing pH, peaking at 432 nm for pH 9 and at 421 nm for pH 11. Furthermore, the resolution of vibrational bands changes as pH increases. At pH 9, the resolution of vibrational bands is lost and the 0–0 band is visible only as a shoulder. Upon increasing pH to 11, however, the resolution of vibrational bands is restored and is

even significantly better than at neutral pH (Fig. 1). We have also tested the stability of crocin at low pH. In agreement with earlier reports,[36] at acidic conditions, crocin degrades within a few hours (Fig. S2, ESI†). Thus, transient absorption experiments were conducted only for pH range 7–11.

Fluorescence spectra of crocin at different pH (7, 9, and 11) are also shown in Fig. 1. The large Stokes shift exceeding 200 nm indicates that fluorescence occurs from the S_1 state. This is consistent with the known fact that carotenoids with nine or more conjugated C=C bonds show primarily fluorescence associated with the S_2–S_0 transition, while for shorter carotenoids, the fluorescence is dominated by the S_1 emission.[40] Crocin, which has seven C=C bonds, thus shows S_1 emission bands between 600 and 800 nm. While fluorescence of crocin at pH 11 peaking at 690 nm mirrors the pH-induced blue shift and better resolution of vibrational bands of the absorption spectrum, the emission maximum at pH 9 (710 nm) is nearly identical to that at neutral pH (715 nm).

The fluorescence spectra were fitted by a set of Gaussian peaks to determine the S_1 energy of crocin at different pH. The fitting results are shown in Fig. S3 (ESI†). This analysis identifies the emission maximum as corresponding to the 0–2 vibronic transition, in agreement with earlier reports.[40] The location of the 0–0 band allows to estimate the S_1 energy of crocin. The extracted values of the S_1 energy are ~16670 cm^{-1} (600 nm) at pH 7, ~16750 cm^{-1} (597 nm) at pH 9, and ~17070 cm^{-1} (586 nm) at pH 11. We have also measured fluorescence excitation spectra at the S_1 emission maximum. As shown in Fig. S4 (ESI†), these exhibit excellent agreement with the absorption spectra.

7.3.2. Transient absorption spectroscopy

Transient absorption spectra at different delays after excitation are shown in Fig. 2. The excitation wavelength was chosen to excite the lowest vibrational bands of the S_0–S_2 transition, 470 nm for pH 7, 450 nm for pH 9 and 11, respectively. Regardless of the pH, the data provide characteristic carotenoid transient absorption spectra that include ground state bleaching and excited state absorption (ESA) due to the S_1–S_n transition. At early delays (0.15 ps) there is an extra ESA band in the 800–900 nm spectral region, which is associated with ESA from the initially excited S_2 state.[41] Besides the dominant S_1–S_n transition, a weak band in the spectral region of 600–650 nm indicates the presence of an ICT state. The ICT signal is weak for crocin due to its symmetrically positioned conjugated C=O groups which minimize the charge transfer character of the coupled S_1/ICT state as demonstrated also for other carbonyl carotenoids.[21,25]

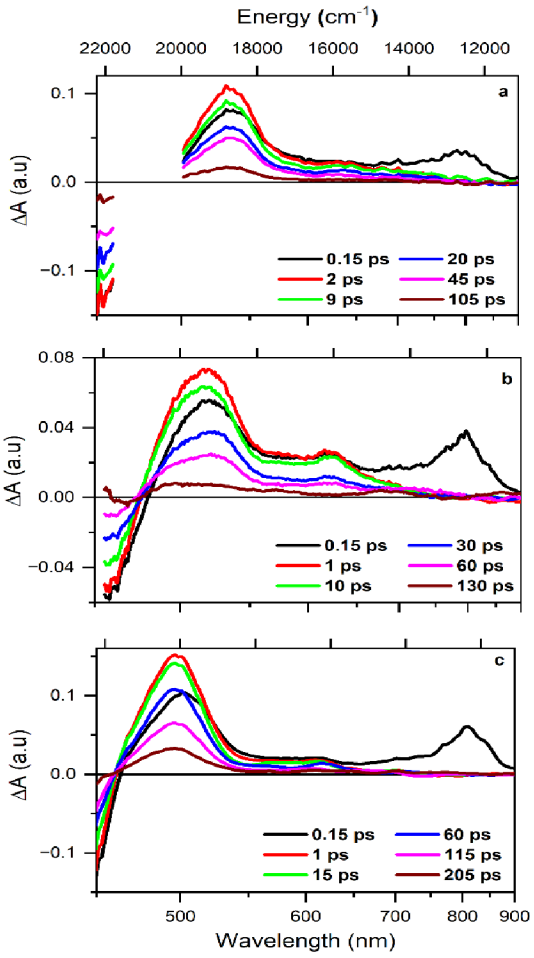

Fig. 2 Transient absorption spectra of crocin in (a) pH 7, (b) pH 9 and (c) pH 11 buffer solutions after excitation at 470 (pH 7) and 450 nm (pH 9 and 11). The spectra were measured at the time delays indicated in the panels.

Although the general features observed in transient absorption spectra are comparable, data recorded at different pH reveal changes in energetics and dynamics. To visualize these changes, Fig. 3 compares normalized transient absorption spectra of crocin in all buffer solutions. When going from pH 7 to pH 11, the S_1–S_n maximum (Fig. 3a) shifts from 532 nm at pH 7, which matches data reported earlier for crocin in water,[31] to 498 nm at pH 11, mirroring the blue shift observed in absorption spectra (Fig. 1). At pH 9, the S_1–S_n band peaks at 518 nm. Interestingly, the ICT signal remains weak at all pH, but it is clearly enhanced at pH 9 in comparison to pH 7 and pH 11. Besides the changes in the S_1–S_n band, the ESA signal associated with the S_2–S_N band exhibits a slight red shift at pH 11 as it peaks at 810 nm while 800 nm maximum is observed at other pH values (Fig. 3b). Excited state dynamics was monitored by kinetics measured at the maximum of the S_1–S_n band (Fig. 4). As seen there, the lifetime of the the S_1/ICT state is significantly affected by pH, increasing in the order pH 9–pH 7–pH 11.

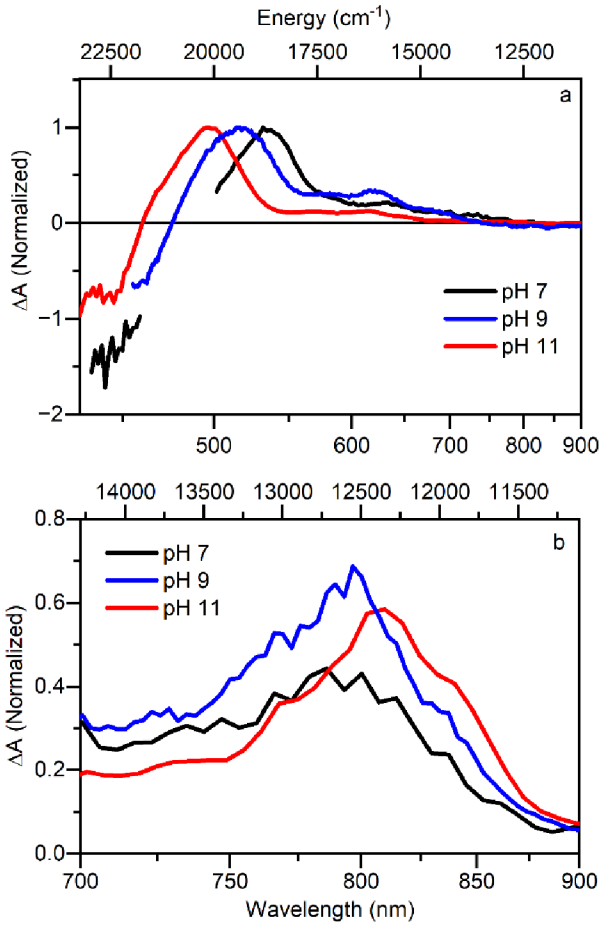

Fig. 3 a) Normalized TA spectra of crocin in pH (7, 9 and 11) buffer solutions measured at 5 ps. (b) Transient absorption spectra in the NIR spectral region measured at 150 fs. The spectra are normalized to the S_1–S_n maximum signal at 150 fs. The spectra were measured after excitation at 470 (pH 7) and 450 nm (pH 9 and 11).

Global fitting analysis was employed to obtain the lifetimes of the excited states and the results are shown in Fig. 5. For pH 7 data, three time components were required to fit the data. The first EADS, which decays on a sub-120 fs timescale, is generated upon excitation and is dominated by the characteristic S_2–S_N band as well as negative signal below 600 nm due to the S_2 stimulated emission. These markers assign the first EADS to the S_2 state whose lifetime reaches the limit of our time resolution. The second EADS is related to the hot S_1/ICT state that at pH 7 decays within 610 fs to form the EADS of relaxed S_1/ICT state.

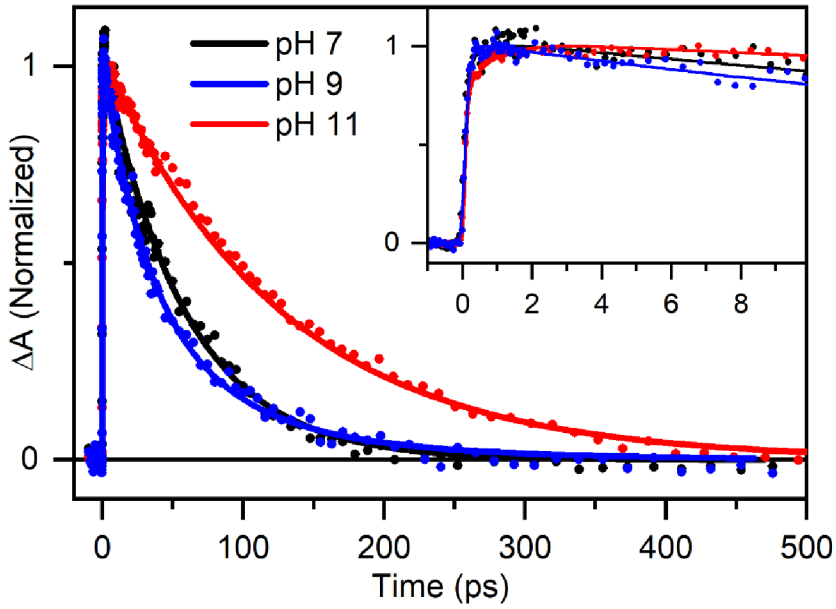

Fig. 4 Normalized kinetics measured at the maximum of the S_1–S_n band of crocin at pH (7, 9, and 11) buffer solutions. The probing wavelengths were 532, 518, and 498 nm for pH 7, 9, and 11, respectively. Excitation was at 470 nm (pH 7) and 450 nm (pH 9 and 11). Inset shows magnification of the first 10 ps. Kinetics are normalized to maximum. Solid lines represent fits obtained from global fitting analysis.

This EADS has a characteristic profile of the relaxed S_1/ICT state and decays with a time constant of 58 ps (Fig. 5a). This pattern of the excited state dynamics of crocin at pH 7 agrees with that obtained for crocin in water reported earlier.[31] For pH 11, the overall picture is similar to pH 7, but lifetimes of the individual components differ. The relaxation of hot S_1/ICT state is slightly longer at pH 11, 815 fs, the last EADS corresponding to the S_1/ICT lifetime is significantly prolonged at pH 11, yielding 126 ps (Fig. 5c).

For the data measured at pH 9 after excitation at 450 nm, the relaxation pattern is different, because fitting data to three-time components failed (Fig. S5b, ESI†). In contrast to pH 7 and 11, four decay components are needed to obtain a good fit at pH 9 (Fig. 5b). The first two EADS correspond to the S_2 state decay and relaxation of hot S_1/ICT state as they do at pH 7 and 11, but two components with lifetimes of 24 and 60 ps are needed to fit the decay of the S_1/ICT state. The additional 24 ps component, which is the reason for the fastest decay kinetics of the S_1/ICT state at pH 9 (Fig. 4), exhibits larger amplitude of the ICT band.

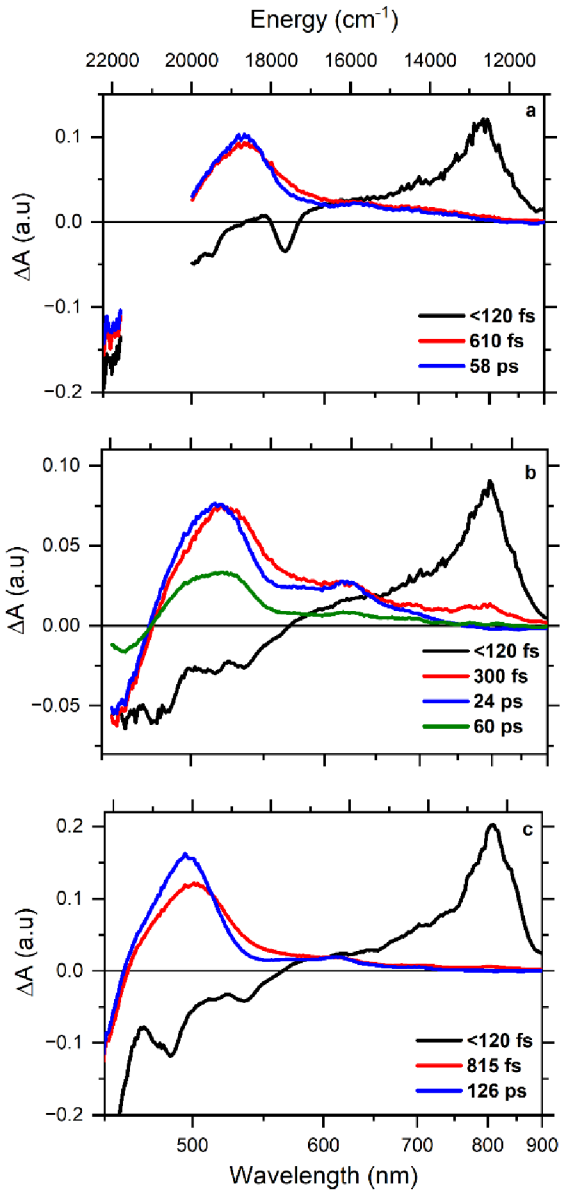

Fig. 5 EADS obtained from global fitting of crocin data in buffer solutions of (a) pH 7, (b) pH 9, and (c) pH 11.

It is noteworthy that the 60 ps component has a lifetime comparable to that obtained for the S_1/ICT lifetime at pH 7. Since changing pH from 7 to 9 resulted in a blue shift of absorption spectra, we have measured data at pH 9 also with excitation of the red absorption edge at 470 nm. This dataset can be readily fitted with three components whose lifetimes are nearly identical to those obtained from fitting data measured at pH 7 (Fig. S5, ESI†). Further evidence for the presence of two species at pH 9 is provided by direct comparison of transient absorption spectra measured after 470 and 450 nm excitation at pH 9 (Fig. S6, ESI†). The S_1–S_n maximum after excitation at 450 nm is at 518 nm, while it is red-shifted to 526 nm after 470 nm excitation. It is still blue-shifted from 534 nm observed for the S_1–S_n maximum of crocin at pH 7, but crocin molecules at pH 9 excited at 470 nm have clearly spectroscopic properties like those of crocin at pH 7. Thus, crocin at pH 9 apparently consists of two species, one has spectroscopic properties comparable with crocin at pH 7, while the other is blue

shifted, has shorter S_1/ICT lifetime and increased ICT band in transient absorption spectrum. Excitation at 470 nm excites only the "pH 7-like" species, while when the sample at pH 9 is excited at 450 nm, both species are excited resulting in additional decay component associated with the blue-shifted species.

7.3.3. Time-resolved fluorescence spectroscopy

Since we could detect the S_1 emission in fluorescence spectra, we have also applied time-resolved fluorescence spectroscopy to confirm the S_1/ICT lifetimes obtained from transient absorption. The results obtained for all buffered solutions of crocin are shown in Fig. 6. Even visual inspection of the decays shows that the fluorescence lifetime increases with increasing pH, matching the results obtained from transient absorption spectroscopy.

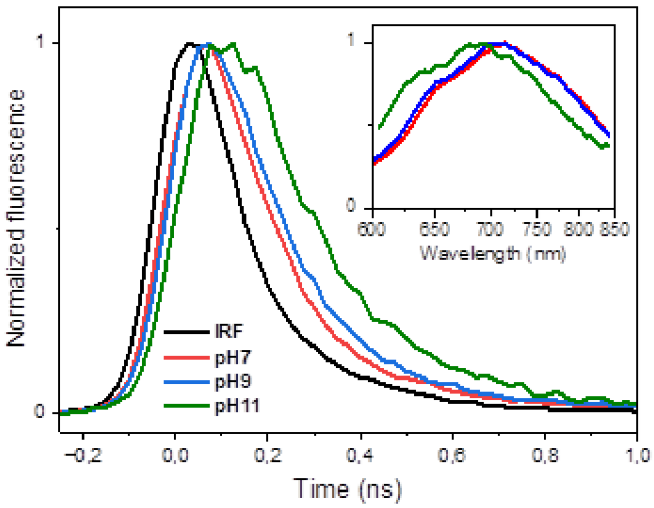

Fig. 6 Time-resolved fluorescence spectra and kinetics of crocin in buffer solutions (ex: 481 nm). Inset shows the S_1 emission spectra. Kinetics were measured at the emission maximum.

The fluorescence decays were measured in the wavelength range of 600 to 840 nm and globally fitted. The resulting decay-associated spectra (DAS) are also shown in Fig. 6. The DAS obtained from fitting fluorescence decays matches the steady-state fluorescence spectra, confirming that the emission originates from the S_1 state. The fitted lifetimes at pH 11 (110 ps) and pH 7 (50 ps) are in reasonable agreement with the S_1/ICT lifetimes acquired from the global fitting analysis of transient absorption data. Due to limited time resolution, the fluorescence decay at pH 9 captures only the slower (~60 ps) component, while the 24 ps lifetime identified in transient absorption data remains unresolved in fluorescence decay.

7.4. Discussion

The spectroscopic data presented in the previous section demonstrate that the photophysical properties of crocin are significantly impacted by changes in pH. The absorption spectra of crocin exhibited a blue shift and alterations in the resolution of vibrational bands with increasing pH. The effect of pH is mirrored in emission from the S_1 state, which also exhibit a significant shift in relation

to the absorption maxima (Fig. 1). The presence of S_1 emission is in line with a relatively short conjugation of crocin, consisting of 7 C=C and 2 C=O groups, resulting in effective conjugation length of N~8. The pH-induced changes are also reflected in transient absorption spectra, where a ~34 nm blue shift of the S_1–S_n peak is observed when going from pH 7 to pH 11, while a somewhat intermediate behaviour occurs at pH 9. Interestingly, the ICT signal is slightly enhanced at pH 9 compared to pH 7 and pH 11, and the decay rates of the S_1/ICT state are also significantly affected by pH (Fig. 3 and 4).

Remarkably, the pH-induced changes in decay rates are reminiscent of those reported when crocin was exposed to solvents with different polarity. The S_1/ICT lifetime of crocin at pH 11 is 126 ps and it is shortened to 60 ps at pH 7. Nearly the same change is observed when going from crocin in 2-propanol (140 ps) to water (60 ps).[31] Thus, one may ask whether the pH change somehow reproduces the polarity effects on excited state properties. However, besides the solvent polarity, hydrogen-bonding capacity of the solvent also play a role, as evidenced by different S_1/ICT lifetimes measured in H_2O and D_2O (60 and 95 ps, respectively).[31] Further inspection of data presented here (pH-induced effects) and those reported by Chabera et al.[31] (polarity-induced effects) reveals more differences. First, the 38 nm shift of the S_1 ESA band produced upon pH change from 7 to 11 (Fig. 3a) is significantly larger than that observed when going from water (532 nm) to methanol or 2-propanol (516 nm). The same is valid for pH- and polarity-induced shifts of the steady-state absorption spectra: a blue shift of more than 20 nm occurs when switching from pH 7 to pH 11 (Fig. 1) while only an 11 nm shift is observed between water and methanol. Moreover, the resolution of the vibrational bands at pH 7 (Fig. 1) is much better than for absorption spectrum of crocin in methanol or 2-propanol.[31]

These results indicate that although the conjugated keto groups play a crucial role in both the polarity- and pH-induced effects on crocin, leading to tunability of excited state properties, these two effects have distinct origins. Clearly, pH does not induce any changes in polarity; instead, as indicated by a slow reaction induced by the pH change (Fig. S1, ESI†), the pH-induced effects are rather related to some structural changes in crocin. This is also underscored by the fact that at intermediate conditions used in our experiments, pH 9, the effect on crocin excited states is the strongest, and dynamics more complicated, resulting in an additional component with significantly shorter lifetime of 24 ps.

Spectroscopic properties of crocin in a pH 7 buffer are identical to those reported for crocin in water earlier[31] and we will not discuss them in detail further. Briefly, the large polarity and high proticity of water, resulting in a strong interaction of water molecules with the conjugated keto groups of crocin, shorten the S_1/ICT lifetime and red shift both absorption and transient absorption spectra compared to crocin dissolved in alcohols. Yet, no increase of the ICT band in transient absorption spectrum is observed, due to the symmetrical position of the keto-groups.[24]

At pH 11, the observed spectroscopic changes, prolonging of the S_1/ICT lifetime and blue shift of both absorption and transient absorption spectra suggest shortening of the effective conjugation length. Crocin's conjugated system consists of seven conjugated C=C bonds, and it is extended to two symmetrically positioned C=O groups. The significant increase of resolution of vibrational bands in absorption spectrum (Fig. 1) may suggest that the presumed decrease of effective conjugation could be associated with removal of keto groups from conjugation, because keto-carotenoids typically do not exhibit sharp vibrational bands in polar solvents.[24] To test this hypothesis, we compare our data with those reported for crocetindial, which has the same conjugated system as crocin, and 8,8'-diapocarotene-8,8'-diol (see ESI† Fig. S7 for structures), which has the keto groups replaced by two symmetrically positioned OH groups that do not contribute to the conjugation length.[31] If the two keto groups of crocin are removed at pH 11, one should observe spectroscopic properties similar to 8,8'-diapocarotene-8,8'-diol in methanol since for a carotenoid without a conjugated keto-group, the solvent polarity has minimal influence on spectroscopic properties.[20,24] However, the data reported by Enriquez et al.[25] on 8,8'-diapocarotene-8,8'-diol show that its absorption and transient absorption spectra peak at ~425 nm (0–0 band) and ~475 nm, respectively, thus significantly blue-shifted from crocin at pH 11 (447 and 496 nm). Moreover, the S_1 lifetime of 8,8'-diapocarotene-8,8'-diol is 450 ps, which is significantly longer than the 126 ps obtained for crocin at pH 11 (Fig. 5c).

These comparisons imply that crocin at pH 11 has an effective conjugation length longer than 7, which would correspond to the situation when the C=O bonds are not in conjugation. An effective conjugation longer than 7 is also indicated by the S_1 energy obtained from the fluorescence spectra: the S1 energy of 17 000 cm^{-1} is lower than expected for a carotenoid with N = 7 whose S_1 energy should be higher than 18 000 cm^{-1}.[17] It is therefore obvious that the keto groups are not isolated from the conjugated backbone of crocin, but their effect is somehow diminished at pH 11.

A possible explanation of this effect can be traced in pH-dependent behaviour of the parent molecule, crocetin (see ESI† Fig. S7, for structure). Crocetin has two carboxyl (COOH) groups terminating the conjugation. These groups deprotonate at high pH, resulting in ionization of the carboxylic group (COO–) associated with a slight change in properties of the C=O bond.[39,42] Since the carboxylic group is esterified in crocin (crocin is a gentiobiosyl diester of crocetin), such effect cannot occur in crocin. However, at pH 11 a fraction of OH groups located at the gentiobiosyl moieties will be deprotonated. This leads to shifts of bonds which may eventually diminish the influence of the C=O groups on spectroscopic properties.

Alternatively, it is known that treating esterified carotenoids with KOH leads to saponification.[43] Thus, high pH may induce the saponification reaction also in crocin, resulting in removal of the gentiobiosyl groups of crocin and formation of crocetin. Feasibility of this hypothesis is supported by irreversibility of the changes induced by pH 11 (ESI† Fig. S8) and by absorption

spectrum of crocetin in a water-based buffer at pH 8.5,[39] which is very similar to that we observe at pH 11 for crocin here. To test this hypothesis, we have run HPLC of crocin at different pH. The results, shown in ESI† (Fig. S9 and S10) indeed confirm that increasing pH induces irreversible structural changes of crocin. A new species, which is less polar than crocin, is identified supporting the hypothesis of saponification of crocin to crocetin at pH 11. At this pH, the carboxyl groups of crocetin are deprotonated, resulting in "weakening" the double bond character of the keto group which will then contribute less to conjugation. This explains the observed blue shift, as the effective conjugation length would decrease with increasing pH, leading to the longer lifetime of crocin at pH 11. The presumably weaker conjugation of the C=O group at pH 11 is also in line with the observed enhancement of the vibrational bands resolution in the absorption spectrum, as this feature is directly related to the degree of conjugation of the C=O group.[25]

At pH 9, the picture is even more complicated. To fit transient absorption data, one extra component is needed and excitation at 450 and 470 nm gives different spectral profile of the S_1–S_n band (Fig. S6, ESI†). This suggests that at pH 9 the sample contains two crocin species exhibiting slightly different relaxation patterns. It is tempting to assign these two species existing at intermediate pH 9 to those observed at pH 7 and pH 11, especially because after very long exposure of crocin to pH 9, its absorption spectrum eventually settles to that measured at pH 11 (Fig. S1 and inset, ESI†). However, this is clearly not the case as (1) we do not detect any time component attributable to the crocin species at pH 11, and (2) absorption spectrum at pH 9 loses the vibrational structure.

Instead, crocin seems to be composed of two ground state species at pH 9. The existence of two species is also confirmed by HPLC which however indicates that minor species (about 25%) is like that observed at pH 11 (Fig. S9, ESI†). This is not confirmed by transient absorption spectroscopy as we do not detect any features (vibrationally resolved absorption spectra and/or long lifetime) attributable to the species observed at pH 11. The mismatch could be caused by the experimental conditions under which HPLC is measured. Due to the limits of HPLC experiment the pH 9 and pH 11 samples must be neutralized to pH 7 prior to HPLC. Thus, while HPLC provides clear evidence that pH change generates structural changes, the species identified by HPLC cannot be directly compared with those measured in transient absorption as the experimental conditions are different.

Transient absorption data rather indicate that at pH 9 there is a species absorbing at the red edge of absorption spectrum; this one is similar to crocin at pH 7 as evidenced by data obtained after 470 nm excitation (Fig. S5c and d, ESI†). The other species, however, exhibits a blue shift of absorption spectrum with diminished resolution of vibrational structure, shorter S_1/ICT lifetime (24 ps), and enhanced ICT band in the transient absorption spectrum. All these features indicate that this extra species generated at pH 9 has enhanced ICT character of the S_1/ICT state, which typically occurs due to increased asymmetry of electron distribution in the excited state.[25] Thus, we hypothesize that at pH 9 there is a substantial fraction of crocin molecules, for which only one C=O group is affected,

introducing asymmetry to electron distribution in an otherwise symmetric crocin molecule. The effect is likely the same as that described above for pH 11, but since the reaction at pH 9 is much slower, it generates substantial population of asymmetric crocin molecules. We note, however, that for a completely asymmetric molecule (having only one conjugated C=O group) a significantly stronger ICT band should be observed as previously demonstrated by Enriquez et al.[25] Thus, as a result of the pH-induced reaction (deprotonation of hydroxy groups or saponification), the degree of asymmetry must be somewhat weaker than in the entirely asymmetric molecule, which is likely caused by the weaker conjugation of the C=O group as described above.

7.5. Conclusions

We conclude that pH markedly affects spectroscopic properties of crocin. Increase of pH causes partial deprotonation of hydroxy groups in the non-conjugated parts of crocin, which eventually leads to structural changes in the crocin molecule. A saponification most likely occurs at high pH, transforming crocin to crocetin, affecting the properties of the two conjugated C=O groups. Besides the excited state dynamics, pH also markedly affects crocin stability. While acidic pH leads to a rapid degradation of crocin, basic pH stabilizes the crocin molecule (Fig. S1, ESI†), in agreement with earlier reports on crocetin.[39]

Acknowledgements

Financial support was provided by the grant 19-28323X from the Czech Science Foundation and institutional support RVO 60077344.

7.6. Supporting Information

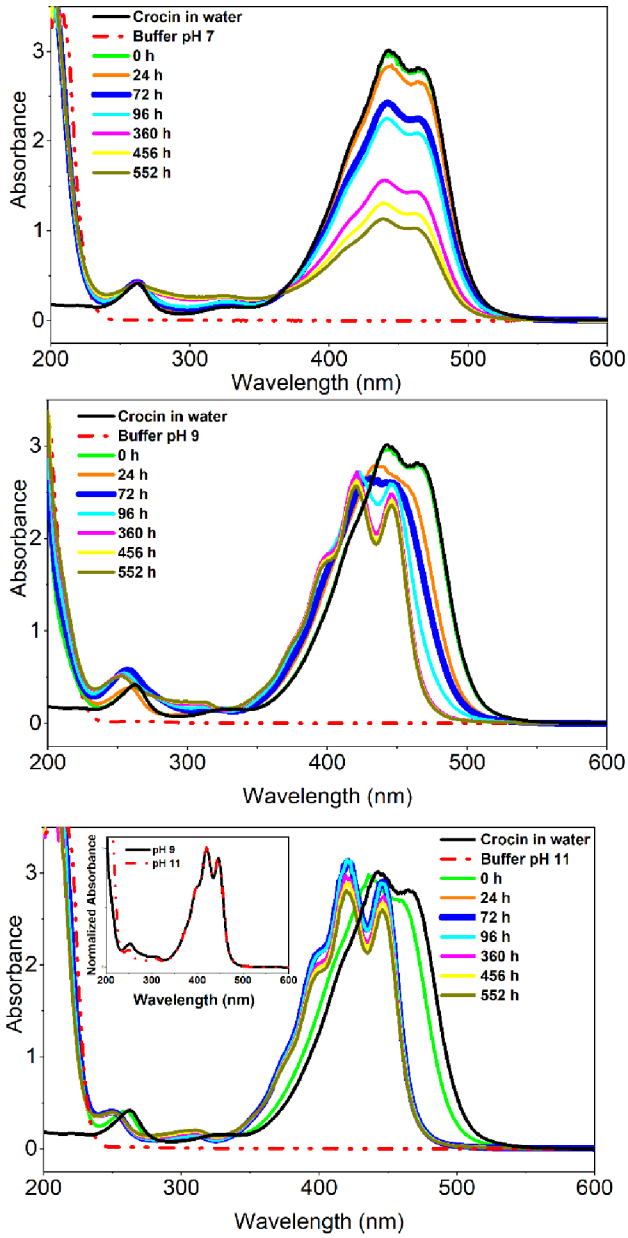

Figure S1. Absorption spectra and their time evolution over an extended period of time. The thick lines represent the samples used for transient absorption measurements. The time dependence of the absorption spectra for 25 µM Crocin in water (pH ~ 6.5) and 0.1 M pH 7, 9, and 11 buffer solutions was measured in the dark at room temperature. The zero times correspond to Crocin's initial absorption spectra in water and at pH 7, 9, and 11. The red dotted line illustrates the absorption of 0.1 M buffer solutions. In the pH 11 inset, normalized absorption spectra of Crocin in pH 9 (black line) and pH 11 (red dotted line) are presented at 552 hours.

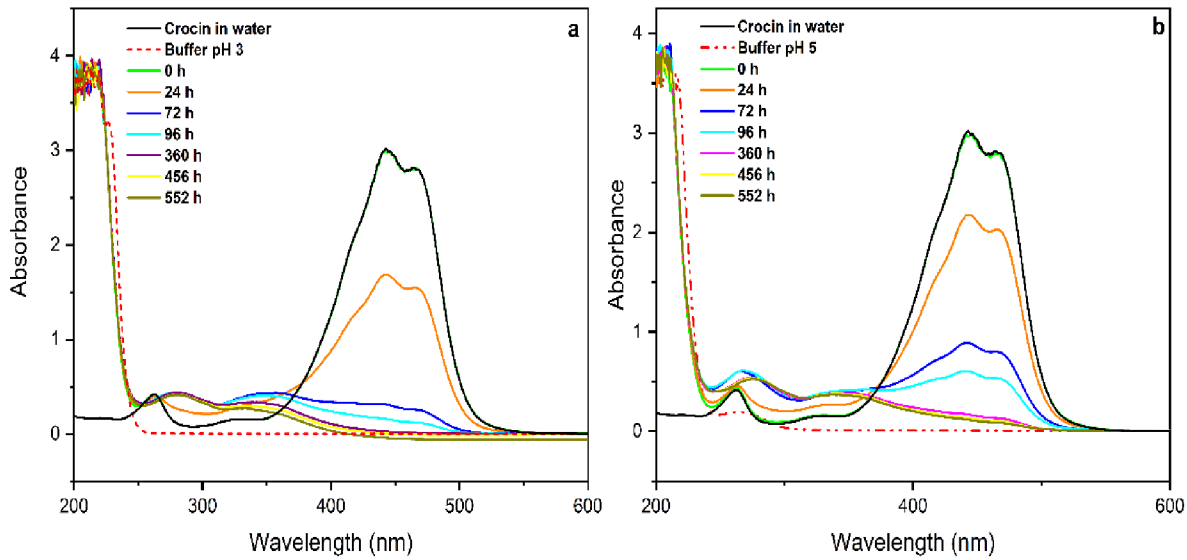

Figure S2. The stability of crocin under acidic conditions. The graph illustrates absorption spectra and their temporal evolution over an extended period of time. The time-dependent absorption spectra for 25 µM Crocin in water (pH ~ 6.5) and 0.1 M a) pH 3 and b) pH 5 buffer solutions were measured in the dark at room temperature. The zero times align with Crocin's initial absorption spectra in water and at pH 3 and 5. The red dotted line on the graph represents the absorption of 0.1 M buffer solutions.

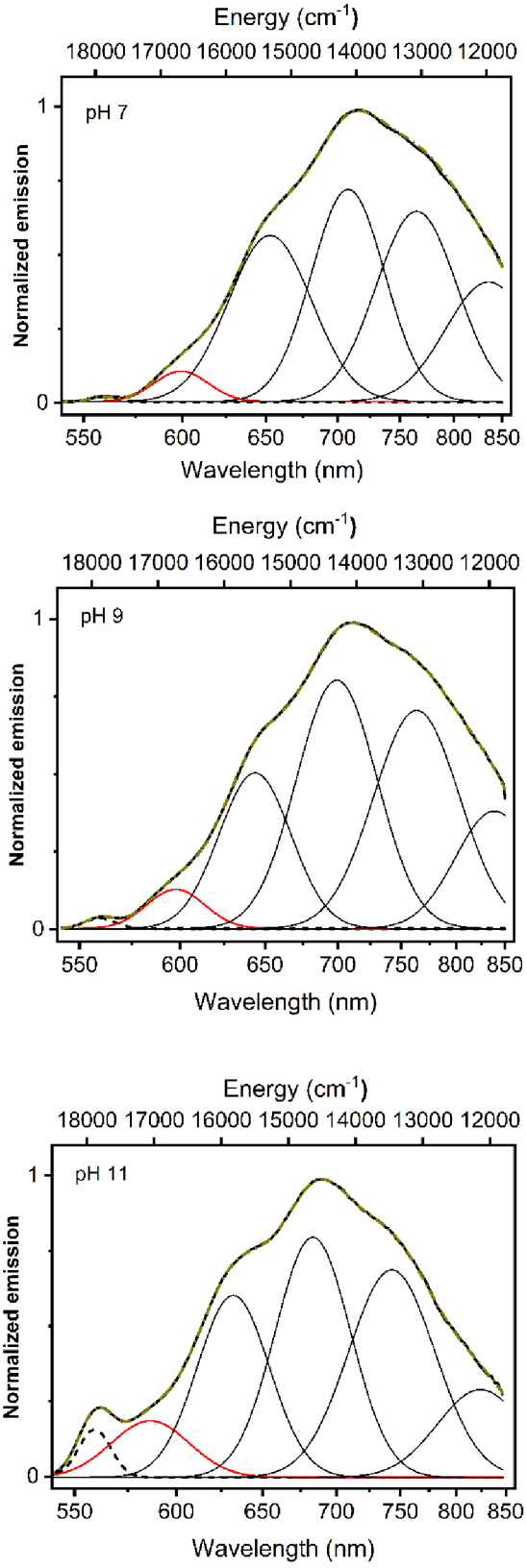

Figure S3. The Gaussian fits of emission spectra of crocin in pH 7, 9, and 11 (Ex: 470 nm). The red Gaussian corresponds to the 0-0 band.

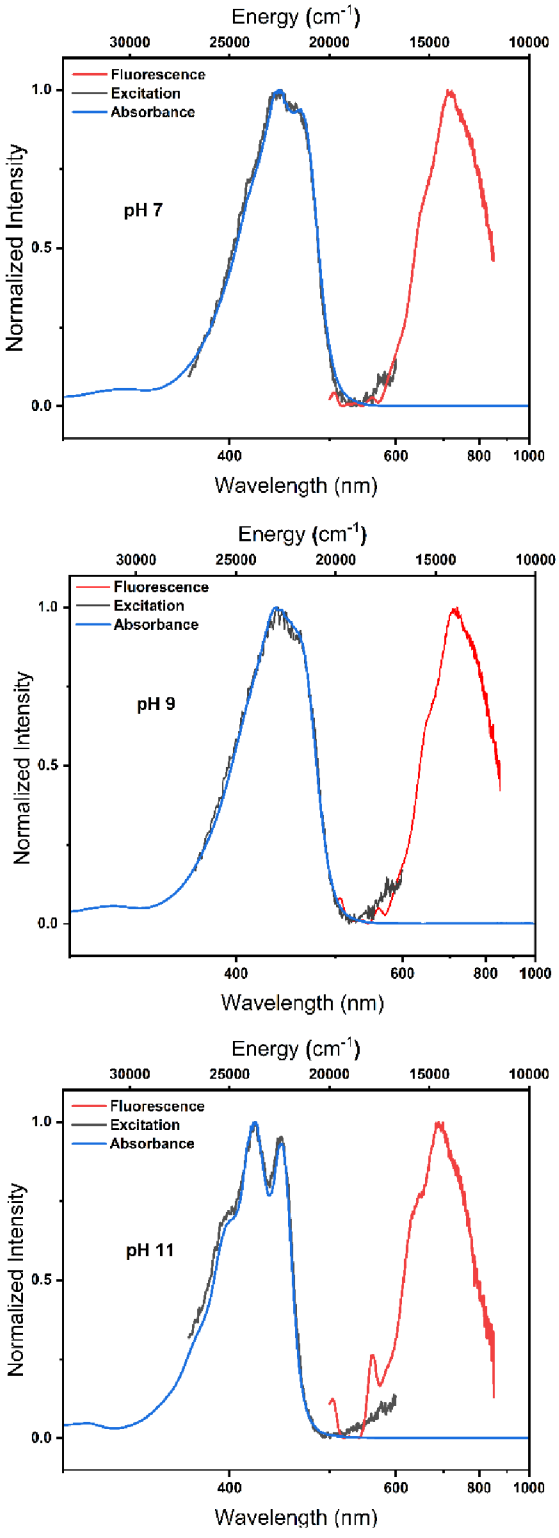

Figure S4. Absorption, emission, and excitation spectrum of crocin in pH 7, 9, and 11. All spectra were normalized and the excitation wavelength for emission spectra is 470 nm. Excitation spectra were recorded at the emission maximum.

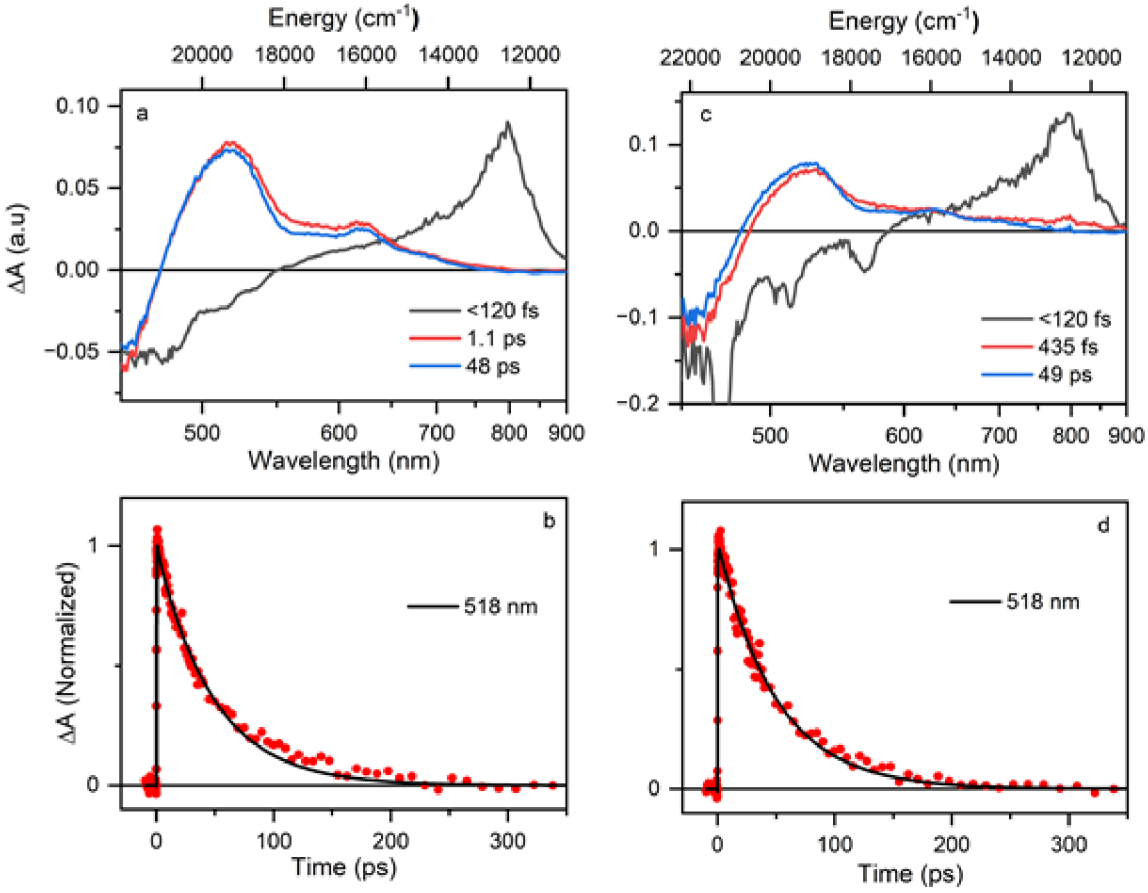

Figure S5. Left: EADS and kinetics of crocin at pH 9 excited at 450 nm fitted to three components (not enough). Right: EADS and kinetics of crocin at pH 9 excited at 470 nm – three components are enough.

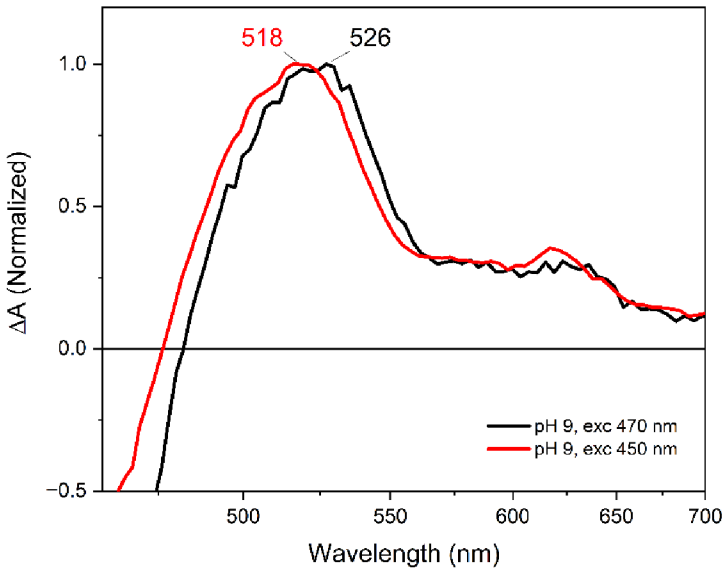

Figure S6. Comparison of transient absorption spectra for three fit components at pH 9, measured after 470 nm (black) and 450 nm (red) excitations at 5 ps.

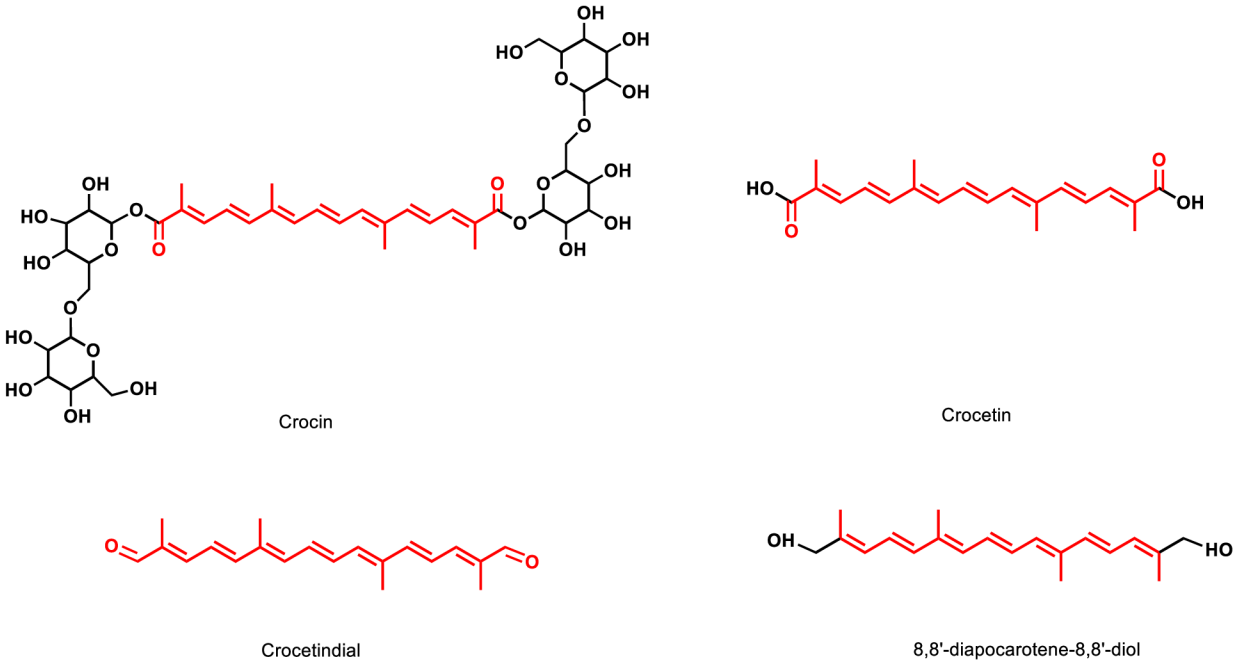

Figure S7. The molecular structure of crocin and similar molecules, which are discussed in the main text. The conjugation length of the molecules is represented in red.

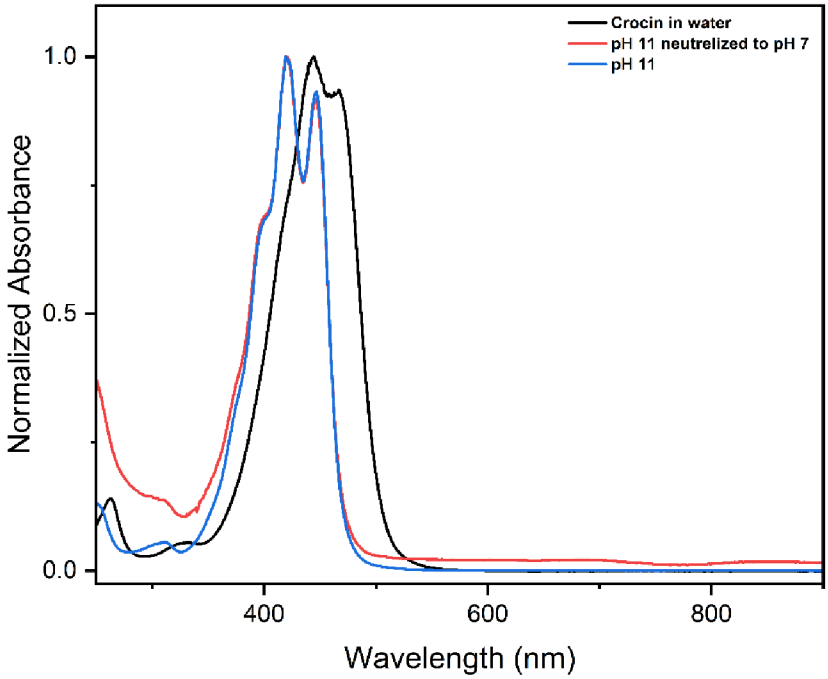

Figure S8. Normalized absorption spectra of crocin in water (black), crocin in pH 11 buffer solution (blue), and crocin neutralized from pH 11 to pH 7 using buffers.

7.6.1. High-performance liquid chromatography (HPLC) analysis of crocin at different pH

Sample heterogeneity was assessed by reverse-phase HPLC, using a Waters Alliance HPLC system with PDA 2998 detector (Waters, USA). Pigments were separated on a reverse phase Nova-Pak C18 column (3.9 × 300 mm, 4 µm, silica-based, end-capped; Waters, USA) using a linear gradient elution. A tertiary solvent system used was as follows: solvent A (80:20 methanol: 0.5 M ammonium acetate (aq., pH 7.2), v/v), solvent B (90:10 acetonitrile: water, v/v), solvent C (100% ethyl acetate). The gradient consists of injection into 100 % solvent A, followed by a ramp to 100 % solvent B within 4 minutes. The gradient follows by a transition to 20 % solvent B and 80 % solvent C in 14 minutes.[44] The flow rate was 1 ml min^{-1}. The method was used because it is suitable for many carotenoids and well established in our laboratory. Samples were injected in a water-based buffer as indicated elsewhere in the text. Samples from high pH were neutralized prior to injection by dilution with buffer with pH 7 due to the limits of the used HPLC column. Samples from pH 9 and pH 11 were neutralized after two days of reaction to be comparable to the conditions during the optical spectroscopy experiments.

The HPLC chromatogram of crocin (Fig. S9) shows one broad peak immediately at the front of the elution, at ~ 2.1 min. No other components were detected in the sample. Sample treated by pH 11 consisted of one major component at ~ 2.7 min (the void volume peak at 2.1 min is prominent in these data due to the low concentration of the injected sample). The spectrum of this component is virtually identical to bulk spectra of crocin at pH 11 (Fig. S10). The chromatogram of crocin treated at pH 9 contains two major peaks. The first one, at 2.25 min, forms 77 % of the sample and has a spectrum similar to crocin but blue-shifted by 11 nm to 429 nm. The second peak in pH 9-treated sample is identical with that from the pH 11 sample. Based on these data it can be concluded that crocin treated by pH 11 for two days is converted to another, less polar, species. Saponification of the glycoside side-chains of crocin is one of the possible origins of this species. Identity of the intermediate species in the sample at pH 9 is not clear. Since it is less polar than crocin at pH 7 and more polar that the species identified at pH 11, it is feasible that at pH 9 due to very slow saponification reaction there is a substantial fraction of monoesters. Such asymmetric molecule could explain some spectroscopic features of crocin at pH 9, but we note that its absorption spectrum does not indicate a presence of an asymmetric keto-group thus the picture is more complicated.

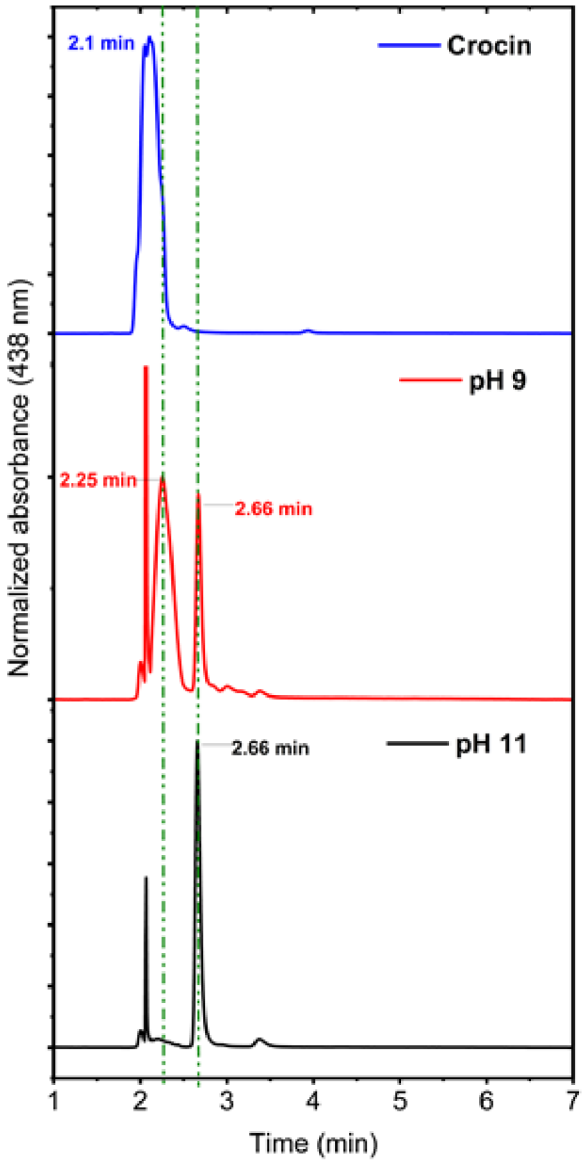

Figure S9. HPLC chromatograms of crocin (blue), crocin in pH 9 neutralized to pH 7 (red), and crocin in pH 11 neutralized to pH 7 (black). Elution times of identified peaks are shown in the graph.

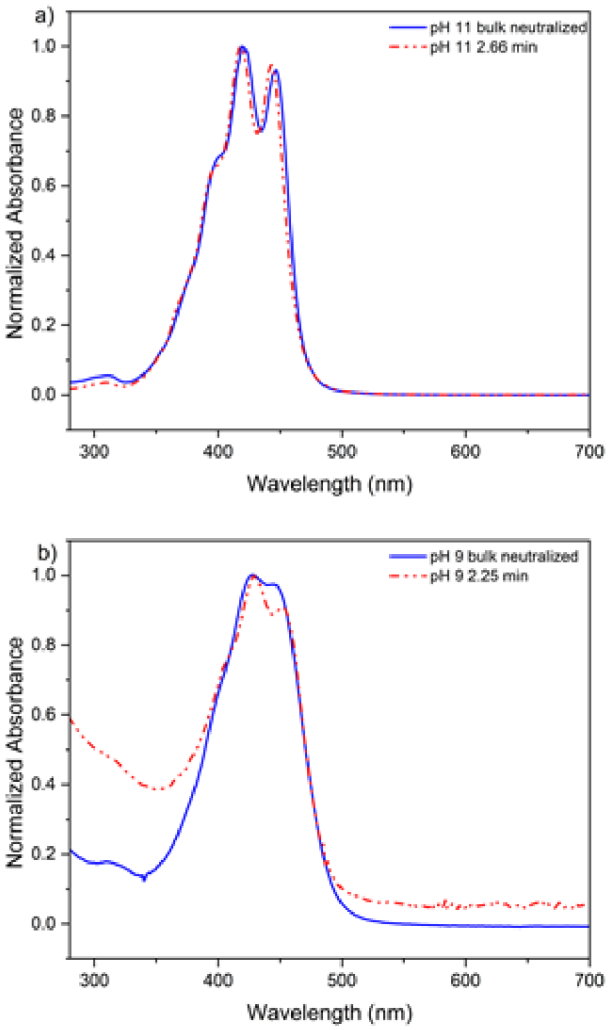

Figure S10: Comparison of normalized absorption spectra of crocin at a) pH 11 (neutralized to pH 7, shown in blue), and HPLC peak at 2.66 min of the pH 11 sample (show in red dotted line). b) pH 9 (neutralized to pH 7, shown in blue), and HPLC peak at 2.65 min of the pH 9 sample (show in red dotted line). The red spectra are extracted from HPLC data.

7.7. References

1. K. K. Namitha and P. S. Negi, Crit. Rev. Food Sci. Nutr., 2010, 50, 728–760.

2. T. Polivka and H. A. Frank, Acc. Chem. Res., 2010, 43, 1125–1134.

3. R. Croce and H. van Amerongen, Science, 2020, 369, 2058.

4. A. V. Ruban, R. Berera, C. Ilioaia, I. H. van Stokkum, J. T. Kennis, A. A. Pascal, H. van Amerongen, B. Robert, P. Horton and R. van Grondelle, Nature, 2007, 450, 575–578.

5. N. E. Holt, D. Zigmantas, L. Valkunas, X.-P. Li, K. K. Niyogi and G. R. Fleming, Science, 2005, 307, 433–436.

6. H. Staleva, J. Komenda, M. K. Shukla, V. Slouf, R. Kana, T. Polivka and R. Sobotka, Nat. Chem. Biol., 2015, 11, 287–291.

7. C. D. P. Duffy and A. V. Ruban, J. Photochem. Photobiol., B, 2015, 152, 215–226.

8. T. G. Monger, R. J. Cogdell and W. W. Parson, Biochim. Biophys. Acta, 1976, 449, 136–153.

9. Z. Kvıcalova, J. Alster, E. Hofmann, P. Khoroshyy, R. Litvin, D. Bina, T. Polivka and J. Psencik, Biochim. Biophys. Acta, Bioenerg., 2016, 1857, 341–349.

10. H. A. Frank and R. J. Cogdell, Photochem. Photobiol., 1996, 63, 257–264.

11. C. S. Foote, Y. C. Chang and R. W. Denny, J. Am. Chem. Soc., 1970, 92, 5216–5218.

12. T. W. Boileau, A. C. Moore and J. J. A. S. Erdman, J. Antioxid. Act., 1999, 133–158.

13. S. A. R. Paiva and R. M. Russell, J. Am. Coll. Nutr., 1999, 18, 426–433.

14. N. I. Krinsky and K.-J. Yeum, Biochem. Biophys. Res. Commun., 2003, 305, 754–760.

15. M. Kobayashi and Y. Sakamoto, Biotechnol. Lett., 1999, 21, 265–269.

16. D. Zigmantas, T. Polı´vka, P. Persson and V. Sundstro¨m, Chem. Phys. Rev., 2022, 3, 041303.

17. T. Polivka and V. Sundstrom, Chem. Rev., 2004, 104, 2021.

18. T. Polivka and V. Sundstro¨m, Chem. Phys. Lett., 2009, 477, 1–11.

19. M. R. Wasielewski and L. D. Kispert, Chem. Phys. Lett., 1986, 128, 238–243.

20. H. A. Frank, J. A. Bautista, J. Josue, Z. Pendon, R. G. Hiller, F. P. Sharples, D. Gosztola and M. R. Wasielewski, J. Phys.Chem. B, 2000, 104, 4569–4577.

21. D. Zigmantas, R. G. Hiller, F. P. Sharples, H. A. Frank, V. Sundstrom and T. Polivka, Phys. Chem. Chem. Phys., 2004, 6, 3009–3016.

22. K. Redeckas, V. Voiciuk and M. Vengris, Photosynth. Res., 2016, 128, 169–181.

23. R. G. West, M. Fuciman, H. Staleva-Musto, V. Sebelik, D. Bina, M. Durchan, V. Kuznetsova and T. Polivka, J. Phys. Chem. B, 2018, 122, 7264–7276.

24. P. Chabera, M. Fuciman, P. Hribek and T. Polivka, Phys. Chem. Chem. Phys., 2009, 11, 8795–8803.

25. M.M. Enriquez, M. Fuciman, A. M. LaFountain, N. L. Wagner, R. R. Birge and H. A. Frank, J. Phys. Chem. B, 2010, 114, 12416–12426.

26. A. V. Ruban, P. Horton and A. J. Young, J. Photochem. Photobiol., B, 1993, 21, 229–234.

27. M. Simonyi, Z. Bikadi, F. Zsila and J. Deli, Chirality, 2003, 15, 680–698.

28. H. H. Billsten, V. Sundstrom and T. Polivka, J. Phys. Chem. A, 2005, 109, 1521–1529.

29. A. J. Musser, M. Maiuri, D. Brida, G. Cerullo, R. H. Friend and J. Clark, J. Am. Chem. Soc., 2015, 137, 5130–5139.

30. C. Wang and M. J. Tauber, J. Am. Chem. Soc., 2010, 132, 13988–13991.

31. P. Chabera, M. Fuciman, K. Razi Naqvi and T. Polıvka, Chem. Phys., 2010, 373, 56–64.

32. H.-R. Sliwka, T.-B. Melo, B. J. Foss, S. H. Abdel-Hafez, V. Partali, G. Nadolski, H. Jackson and S. F. Lockwood, Chem. – Eur. J., 2007, 13, 4458–4466.

33. H. L. Jackson, A. J. Cardounel, J. L. Zweier and S. F. Lockwood, Bioorg. Med. Chem. Lett., 2004, 14, 3985–3991.

34. F. J. Francis, Food Technol., 1987, 41, 62–68.

35. T. Q. Pham, F. Cormier, E. Farnworth, V. H. Tong and M.-R. Van Calsteren, J. Agric. Food Chem., 2000, 48, 1455–1461.

36. D. Li, G. Wu, H. Zhang and X. Qi, Food Hydrocolloids, 2021, 120, 106415.

37. M. Tsimidou and C. G. Biliaderis, J. Agric. Food Chem., 1997, 45, 2890–2898.

38. M. Carmona, A. Zalacain, J. E. Pardo, E. Lopez, A. Alvarruiz and G. L. Alonso, J. Agric. Food Chem., 2005, 53, 3974–3979.

39. F. Zsila, Z. Bikadi and M. Simonyi, Tetrahedron: Asymmetry, 2001, 12, 3125–3137.

40. R. L. Christensen, M. Goyette, L. Gallagher, J. Duncan, B. DeCoster, J. Lugtenburg, F. J. Jansen and I. van der Hoef, J. Phys. Chem. A, 1999, 103, 2399–2407.

41. T. Khan, R. Litvin, V. Sebelik and T. Polivka, ChemPhysChem, 2021, 22, 471–480.

42. K. M. Thompson, W. P. Griffith and M. Spiro, J. Chem. Soc., Faraday Trans., 1993, 89, 4035–4043.

43. R. K. Saini and Y.-S. Keum, Food Chem., 2018, 240, 90–103.

44. R. Litvín, D. Bína, M. Herbstová and Z. Gardian, Photosynth. Res., 2016, 130, 137-150.

8. Paper Ⅳ

Synthesis and spectroscopic properties of carotenoid bis-phenylhydrazone astaxanthin: Extending conjugation to a C=N group

Özcan, E., Keşan, G., Chabera, P., Litvín, R., & Polivka, T. (2024). Synthesis and spectroscopic properties of carotenoid bis-phenylhydrazone astaxanthin: Extending conjugation to a C= N group. New Journal of Chemistry.

https://doi.org/10.1039/D4NJ02282C

Abstract

We report on synthesis and detailed spectroscopic characterization of bis-phenylhydrazone astaxanthin (BPH-Asx), a derivative of astaxanthin (Asx), in which the conjugated carbonyl group of Asx is replaced by a conjugated C=N bond. BPH-Asx was successfully synthesized and characterized using various spectroscopic techniques, revealing subtle changes in absorption spectra and significant alterations in excited-state dynamics compared to Asx. The results reveal a shortened S_1 lifetime, 1.4 ps for BPH-Asx compared to 5 ps for Asx, indicating a significant impact on its excited-state dynamics. Since no polarity-induced effect was observed for BPH-Asx, the changes induced by the conjugated C=N group are due to prolongation of effective conjugation. Moreover, the identification of a distinctive S* signal with a 3 ps lifetime in BPH-Asx underscores the relation between effective conjugation and presence of the S* signal that is not detected in Asx.

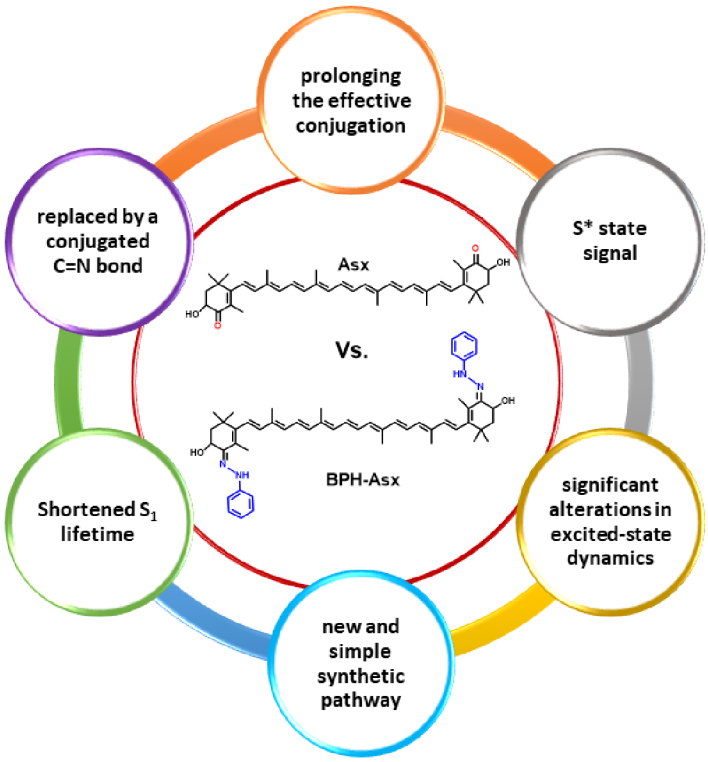

8.1. Introduction

Carotenoids are class of natural pigments with extraordinary photoprotective[1] and light-harvesting[2, 3] abilities in biological systems. Moreover, their rich excited-state dynamics[4] as well as capacity to engage in various functions, such as quenching of singlet-excited states of chlorophylls[5-8], chlorophyll triplets[9, 10], and antioxidation achieved by scavenging singlet oxygen or other reactive oxygen species[11-16] emphasize their importance in both biology and chemistry. Due to their important roles in light-induced processes, photophysical and photochemical properties of carotenoids have been frequently studied; however, owing to the complicated excited-state structure and dynamics, gaps in understanding the carotenoid photophysics still remain.

According to the basic description of the excited states of all carotenoids, two states are highlighted: strongly absorbing S_2 state and lower-lying S_1 state, to which a one-photon transition from the ground state (S_0) is forbidden due to the multiply-excited character[17]. Thus, the lowest energy one-photon transition from the ground state occurs to the S_2 state, which relaxes to the S_1 state whose properties are readily monitored via its characteristic S_1-S_n band in transient absorption spectra[18, 19]. This general picture is valid for all carotenoids and their conjugated C=C bond chain structures, common in all carotenoids, primarily determine their photophysical properties[17].

Beyond this three-state model (S_0, S_1 and S_2), other states have been identified. In keto-carotenoids, featuring conjugated C=O bond in their structure, an intramolecular charge transfer (ICT) state coupled to the dark S_1 state is stabilized in a polar environment, resulting in a state commonly referred as the S_1/ICT[20, 21]. The presence of the ICT state is easily detected by characteristic bands in the transient absorption spectrum. The ICT-like transition is red-shifted from the S_1-S_n band for most keto-carotenoids. The amplitude ratio between the S_1-S_n and ICT-like bands serves as a measure of degree of charge transfer character of the coupled S_1/ICT state[20, 21]. Numerous investigations have demonstrated that the degree of charge transfer character is proportional to solvent polarity but the conjugation length and position of the conjugated keto group are also crucial factors. The ICT signal increases for short keto-carotenoids having a single keto group positioned asymmetrically while the charge transfer nature of the S_1/ICT state is minimized for long ones with two keto groups positioned symmetrically[20, 22, 23]. This is for example the case of astaxanthin (Asx), one of the widely studied keto-carotenoids, which has two symmetric conjugated keto (C=O) groups at the terminal rings, resulting in only a weak ICT signal detected in a broad range of solvents[24-26].

Another state known as S* has been identified in carotenoids with long conjugation. The S* signal is typically demonstrated as a distinct blue shoulder at the S_1-S_n band, and its lifetime is longer than that of the S_1 state[27]. The origin of the S* signal is still a matter of debate. The first detection of the S* signal assigned it to a hot ground state[28], but this assignment was later challenged and the S* signal was instead attributed to a separate excited state[27]. Since then, numerous studies favoring either ground state[29, 30] or excited state[31, 32] hypothesis have been reported. Yet, it seems that both hot

ground state and excited state contribute to the S* signal, with particular contribution depending on conjugation length: while for short conjugation (N<11) the excited state contribution dominates, a hot ground state is the key source of the S* signal for long carotenoids[33].

Since excited state dynamics of carotenoids depends on the structure of the conjugated system, synthetic carotenoids with various modifications of the conjugated chain helped to understand some aspects of carotenoid photophysics. These modifications often focused on synthesis of carotenoids with a conjugation length longer than that of natural carotenoids. Such approach, involving a synthesis of □-carotene analogs with 15 or even 19 C=C bonds (in contrast to 11 in natural □-carotene), led to the first observation of the S* signal[28]. Series of synthetic carotenoids with varying conjugation lengths later helped to understand excited-state dynamics of □-carotene[34], zeaxanthin[35] or keto-carotenoids peridinin[36] and fucoxanthin[37].

Besides synthesis of carotenoid series with the same structure but different conjugation lengths, chemical modifications of carotenoids have also targeted various functional groups involved in conjugation in order to test their role in excited-state dynamics. To this end, alterations of the allene group of peridinin[38] or fucoxanthin[39] were used to test the effect of the allene group on ICT state of these keto-carotenoids. Similarly, symmetry of peridinin was modified by 'moving' the lactone ring along the main conjugated chain[40]. Many synthetic carotenoids have been introduced in the past few decades including those having non-natural atoms such as sulfur, nitrogen, or phosphorus in their structure[41]. Yet, excited state dynamics of these carotenoids has not been studied, apart from two exceptions featuring nitrogen atoms in their structure. First, ultrafast dynamics of all-trans-7',7'-dicyano-7'-apo-□-carotene[42], demonstrating strong effect of the cyano groups on excited state lifetime. Second, astaxanthin (Asx) esterified by the amino acid lysine, synthesized to make Asx water soluble, was subjected to ultrafast transient absorption spectroscopy[43].

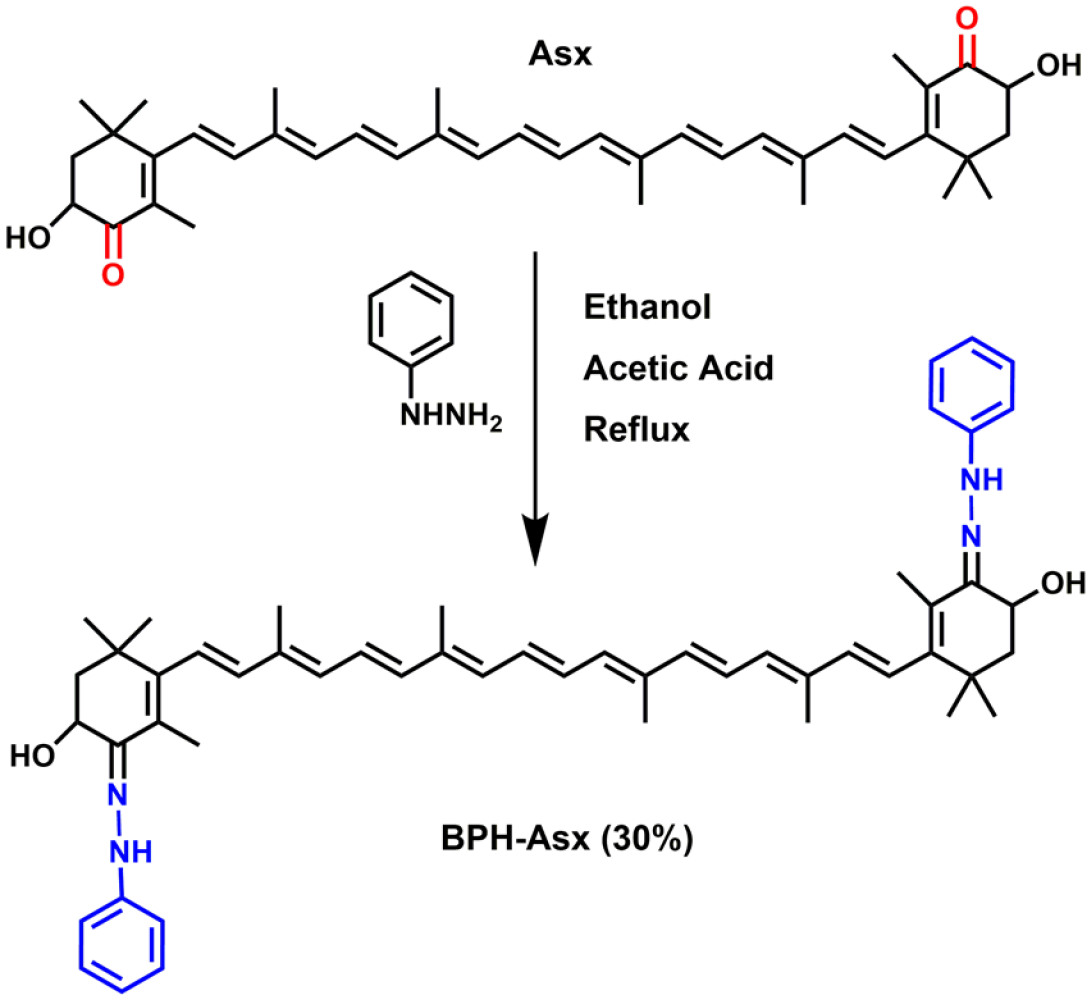

Scheme 1. Synthetic pathway of bis-phenylhydrazone astaxanthin (BPH-Asx).

Asx is a subject of chemical modification also in this study. It has two oxygen atoms on each cyclohexene rings in the form of a keto (C=O) and hydroxyl (C-OH) group. These groups at terminal rings offer a possibility of chemical/structural modification of Asx, synthesizing novel carotenoids[44-46]. Since such modification of Asx, especially that modifying the keto group, is expected to change the photophysical properties, it is an ideal tool to explore features of excited states of the Asx. More specifically, by the synthesis of novel carotenoids (Scheme 1), we can obtain astaxanthin whose conjugated C=O group, the expected generator of the ICT state, is modified to some other functional group. Such modification could figure out whether a carbonyl group is needed for observation of spectroscopic features related to the ICT state.

Here, we report on synthesis of a novel astaxanthin derivative named bis-phenylhydrazone astaxanthin (BPH-Asx) which instead of conjugated C=O group has C=N bond in conjugation. We have conducted a detailed study of its photophysical properties that were investigated by ultrafast time-resolved transient absorption spectroscopy. The data showed that Asx could be successfully modified, resulting in stable BPH-Asx, which has significantly different spectroscopic properties compared to Asx.

8.2. Experimental Section

8.2.1. Materials and Methods

Astaxanthin (Sigma Aldrich, ≥97%, HPLC), phenylhydrazine (Merck, ≥97%, for synthesis), ethanol (Penta, ≥97%, GC), glacial acetic acid (Lachner, 99.8 G.R.), acetonitrile (Acn, Fluka, ≥99.9%, HPLC), benzene (Fluka, ≥99.5%, GC), methanol (Merck, ≥99.9%, HPLC), and dichloromethane (Dcm, Merck, ≥99.9%, GC) were used as obtained without further purification. Reactions were monitored by thin layer chromatography using Merck TLC Silica gel 60 with DCM/methanol (1/1, v/v) as the eluent. Mass spectra were acquired in linear modes with average of 50 shots on a Bruker Daltonics Microflex mass spectrometer equipped with a nitrogen UV-Laser operating at 337 nm. ESI-MS detection was conducted on a Bruker QqTOF compact instrument operated using Compass Control 4.0 software (Bruker Daltonics, Germany). Compass DataAnalysis 4.4 (Build 200.55.2969) (Bruker Daltonics, Germany) software was used for data processing. NMR spectra (^{1}H and ^{13}C NMR) were recorded for all compounds in $CDCl_3$ by a Varian INOVA 500 MHz spectrometer using TMS as internal reference. High-performance liquid chromatography (HPLC) was performed using a Waters Alliance HPLC system with a PDA 2998 detector (Waters, USA). The compounds were injected in methanol and separated on a reverse phase Nova-Pak C18 column (3.9 × 300 mm, 4 µm, silica-based, end-capped; Waters, USA) using a linear gradient elution. A tertiary solvent system used was as follows[47]: solvent A (80:20 methanol: 0.5 M ammonium acetate (aq., pH 7.2 v/v)), solvent B (90:10 acetonitrile: water), solvent C (100% ethyl acetate). The flow rate was 1 ml min^{-1}. Absorption spectra of the samples were measured in a 10-mm path length quartz cuvette using UV-VIS spectrometer (Shimadzu UV-2600). Fluorescence spectra were measured in 3x3 mm quartz cells using Horiba Fluorolog-3 spectrometer, using Xe arc lamp, double monochromators and a photomultiplier detector at right angle detection geometry.

8.2.2. Synthesis of bis-phenylhydrazone astaxanthin (BPH-Asx)

Astaxanthin 10 mg (0.017 mmol), excess phenylhydrazine 7.34 mg (0.068 mmol) and a few drops of glacial acetic acid in ethanol (25 mL) were heated at reflux overnight. The resulting precipitate was filtered and washed with cold ethanol (100 mL). As the TLC of the solid part was clear, no further separation was applied. BPH-Asx was obtained as an orange-red color powder (4 mg, 30%). MALDI TOF (m/z) (Fig.S1) Calc. 776.50, Found: 776.998 $[M+H]^+$; ESI-MS (Fig. S1): $C_{52}H_{63}N_4O_2$ $[M^+]$ calculated 775.4945, found: 775.4936 m/z. ^{1}H NMR (Fig.S2; 500 MHz, $CDCl_3$) δ 9.61 (2H, NH, j), 7.24 (4H, Ar-CH, h), 7.12 (d, *J*=8,0 Hz, 4H, Ar-CH, h), 6.84 (t, *J*=7.6 Hz, 2H, Ar–CH, g), 6.66 (t, *J*= 14.9 Hz, 4H, alkene H, f), 6.42 (d, *J*= 14.9 Hz, 2H, alkene H, f), 6.29–6.22 (m, 8H, alkene H, f), 5.30 (s, 2H, CH, e) 4.83 (s, 2H, OH, d), 2.10 (s, 4H, CH2, c), 1.99–2.00 (s, 12H, CH_3, b), 1.13–1.25 (s, 18H, CH_3, a) ppm. ^{13}C NMR (Fig. S3, 125 MHz, $CDCl_3$) δ 150.3, 138.4, 137.5, 136.7, 135.1, 130.3, 129.6, 129.1, 128.5, 128.3, 126.8, 124.3, 114.4, 68.5, 53.8, 30.8, 30.2, 27.5, 26.4, 21.9 ppm. FT-IR (Fig. S4; ATR, cm^{-1}) υ=3300 cm^{-1} (NH), υ=1750 cm^{-1} (C=N), υ=1251 cm^{-1} (C-N), υ=1500-1600 cm^{-1} (C=O).

8.2.3. Transient absorption spectroscopy

Transient absorption (TA) spectroscopy was measured using an in-house build setup, based on a Solstice ACE (Spectra Physics) laser amplifier system that produces ~60 fs pulses at a central wavelength of 796 nm at 4 kHz repetition rate. The amplifier output is divided into two parts that each pump an optical parametric amplifier (TOPAS-C, Light Conversion). One generates the pump beam while the other produces a NIR beam (1360 nm) that is focused onto a 3 mm CaF_2 crystal to generate a supercontinuum probe beam. The delay between pump and probe pulses is introduced by a computer-controlled delay stage (Aerotech, 10 ns) placed in the probe beam path. After supercontinuum generation the probe pulses are split into two parts: the former being focused to ~100 µm spot size and overlapping with the pump pulse in the sample volume, and the latter serving as a reference. After passing the sample the probe beam is collimated again and relayed onto the entrance aperture of a prism spectrograph. Both beams are then dispersed onto a double photodiode array, each holding 512 elements (Pascher Instruments). The intensity of excitation pulses was set to 230 □W, yielding excitation density of 6.5×10^{13} photons/pulse/cm^2 photons/pulse/cm^2. Mutual polarization between pump and probe beams was set to the magic angle (54.7°) by placing a Berek compensator in the pump beam. Time-resolution of the setup after dispersion correction is estimated to be ≤100 fs. The measured samples, placed in a 1-mm pathlength optical cuvette, were translated after each scan to avoid photodegradation. To check for stability of each sample steady-state absorption spectra were measured before and after experiments.

8.2.4. Data Analysis

The resulting spectro-temporal data sets were analyzed by a global fitting software (CarpetView, Light Conversion, Lithuania). It was assumed that the excited system evolves irreversibly and sequentially to visualize the excited-state dynamics. Each component of the sequential scheme illustrates an individual excited-state species, and the spectral profile of each species is called the evolution-associated difference spectrum (EADS). The same software was used for chirp-correction of the spectra.

8.3. Results

8.3.1. Synthesis and structural characterization

BPH-Asx was successfully prepared by using the procedure described in literature[48]. The synthesis procedure of BPH-Asx is detailed in Scheme 1. The BPH-Asx was synthesized by the condensation reaction of commercially available Asx and phenylhydrazine in ethanol and in the presence of a catalytic amount of glacial acetic acid. After reaction reflux overnight, solid BPH-Asx was obtained with a reasonable yield (30%) by just washing with cold EtOH/MeOH to remove excess/unreacted phenylhydrazine. The BPH-Asx obtained without further purification appeared as an orange-red solid.

The successful condensation of Asx with phenylhydrazine to produce the desired target compound, BPH-Asx, was confirmed by using various spectroscopic techniques.

The molecular ion peak of the BPH-Asx was determined by the MALDI-TOF mass spectrometer as 776.998 m/z, which is in good agreement with the predicted structure and further confirmed by ESI-MS (Fig.S1). The novel BHP-Asx structure was further supported by comparing its ^{1}H NMR spectroscopic data with that of commercially available Asx (Fig. S2). The proposed chemical structures for both compounds were confirmed by analysis of both aromatic and aliphatic protons. Specifically, in the case of BPH-Asx, additional resonances of aromatic benzene protons at 7.24 and 7.12 (10H, g and h), along with a new resonance of NH (2H, j) proton at 9.61 ppm, were identified. The presence of these additional characteristic protons strongly supports the structural confirmation of BPH-Asx. In the ^{13}C NMR spectrum, the aromatic carbons of the BHP-Asx were marked between 150.3 and 114.41 and the aliphatic carbons signals were seen between the 68.59 and 21.98 ppm regions of the spectra (Fig. S3). FT-IR spectroscopy is a useful and effective method for investigating structural changes in molecules and we compare the FT-IR spectra of BPH-Asx and Asx in Figure S4. In the FT-IR spectrum of BPH-Asx, distinctive peaks were observed at 3300 cm^{-1} corresponding to the NH stretching vibrations, 1750 cm^{-1} indicate of the C=N stretching vibrations, and 1251 cm^{-1} were attributed to the C-N stretching vibrations. Notably, in comparison to astaxanthin, BPH-Asx exhibited these new characteristic peaks and the absence of the strong peak at 1660 cm^{-1} associated with the C=O stretching vibrations. These spectral structural differences between BPH-Asx and Asx further confirm the proposed structure and alterations of functional groups.

Asx and its modified derivative BPH-Asx were analyzed by HPLC for further characterization (Fig S5). The chromatogram of Asx consists of a single broad peak at 11.1 min, identified as all-trans Asx[49]. The chromatogram of BPH-Asx exhibits five peaks, occurring at longer retention times compared to Asx. The highest peak at 12.9 minutes (81%) was identified as BPH-Asx. Two minor peaks at 13.9 minutes (6%), 14.1 minutes (6%) showed absorbance bands around 380 nm (Fig. S6) and likely correspond to cis-isomers of BPH-Asx[49]. Presence of small amount of some unidentified Asx-related species was indicated by a minor peak at 12.2 minutes (3%). The last minor peak at 15.6 minutes (4%) showed significantly red-shifted absorbance (Fig. S6) indicating significantly longer effective conjugation in the ground state. This could be caused by the *s-trans* configuration of the terminal rings making the whole conjugation linear including the two C=N groups (Scheme 1).

8.3.2. Steady-State and Transient Absorption Spectroscopy

Absorption spectra of Asx and BPH-Asx in Acetonitrile (Acn) and Dichloromethane (Dcm) are depicted in Fig 1. The absorption maximum of Asx is at 476 nm in Acn with a single broad peak, reflecting the S_0-S_2 transition, in agreement with previous reports on Asx in this solvent[25]. The absorption maximum of Asx red shifts with increasing solvent polarizability, peaking at 486 nm in Dcm. For BPH-Asx, absorption spectra in both solvents exhibit a small red shift compared to Asx: the

absorption maxima are at 483 and 488 nm in Acn and Dcm, respectively. A slightly broader distribution of the S_0-S_2 transition energies is observed for BPH-Asx, but overall the comparison of absorption spectra suggests that the transition dipole moment associated with the S_0-S_2 transition undergoes only modest changes upon change from Asx to BPH-Asx. The properties of the S_0–S_2 transition are further confirmed by fluorescence spectra shown in Fig. S7. The weak fluorescence originates from the S_2 state in agreement with data reported on Asx earlier.[50] The solvent induced red-shift of fluorescence spectrum is larger for Asx than for BPH-Asx, mirroring the behavior of absorption spectra.

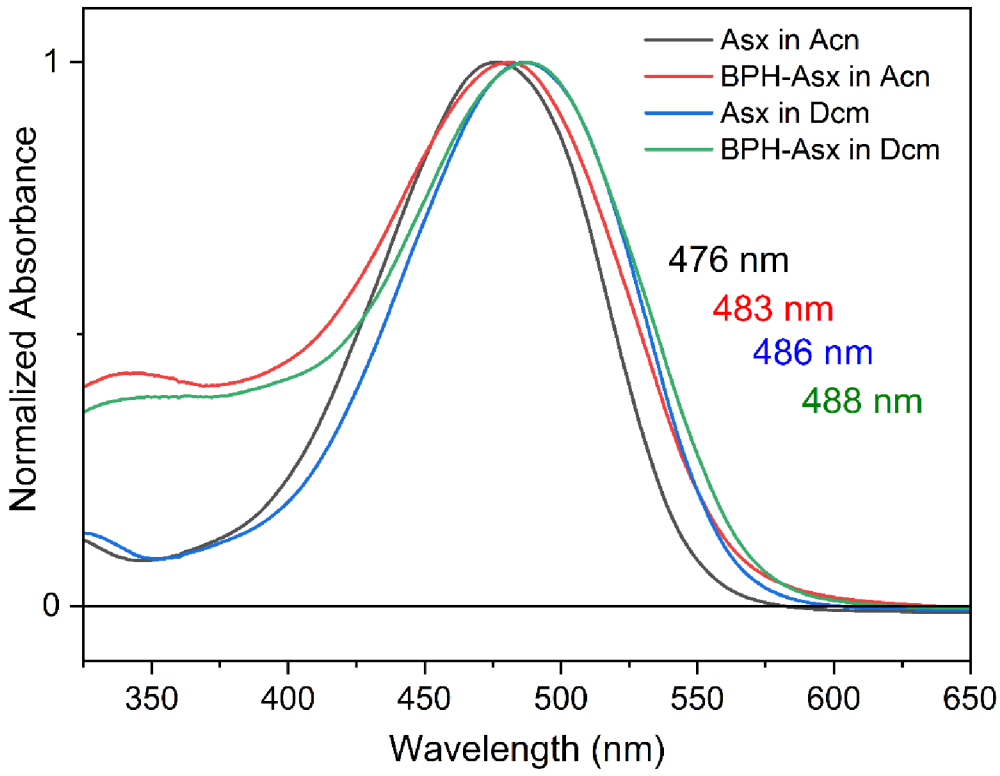

Figure 1. Steady state absorption spectra of Asx and BPH-Asx in acetonitrile and dichloromethane.

Transient absorption spectra at different time delays following excitation are shown in Figure 2. The excitation wavelength was at 500 nm for Asx and BPH-Asx in both solvents, intended to excite the molecules just below the maximum of the S_0-S_2 transition. The data provide characteristic carotenoid transient absorption spectra, comprising ground state bleaching and excited state absorption (ESA) attributed to the S_1-S_n transition for both Asx and BPH-Asx. The S_1-S_n band of Asx in Acn, peaking at 629 nm, is consistent with previous studies,[25] fully forming within the first picosecond. In Dcm, the S_1-S_n peak shifts to 642 nm (Fig 2a and b). In addition to the dominant S_1-S_n transition, a weak band in the 700-800 nm spectral region indicates the presence of an ICT state. The ICT signal is weak for Asx due to its symmetrically positioned conjugated C=O groups that minimize the charge transfer character of the coupled S_1/ICT state as has been also demonstrated for other carbonyl carotenoids[22]. The 800-900 nm spectral region exhibits an additional ESA band at early delays (0.15 ps), which is linked to the ESA from the initially excited S_2 state[51].

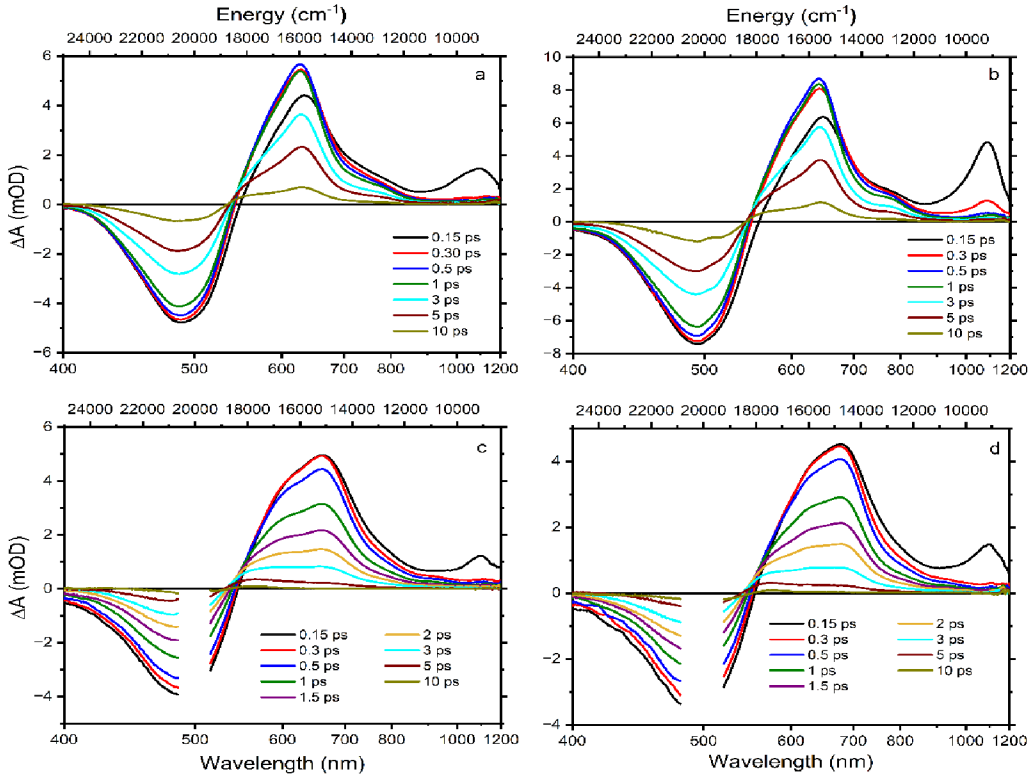

Figure 2. Transient absorption spectra of Asx in Acn (a), Asx in Dcm (b), BPH-Asx in Acn (c), and BPH-Asx in Dcm (d). The delay times after 500 nm excitation are indicated in each panel. The color-coding is the same in all panels.

Although the general features observed in the transient absorption spectra of both carotenoids look similar, the modification of the conjugated chain from Asx to BPH-Asx induces some changes in the transient absorption spectra. As expected, both the ground state bleaching and S_1-S_n ESA exhibit a red shift, reflecting the observed difference in the ground state absorption spectra. The S_1-S_n bands of BPH-Asx have maxima at 642 nm and 681 nm in Acn and Dcm, respectively (Fig 2c and d). Besides the changes in the S_1-S_n band, the ESA signal associated with the S_2-S_N band of BPH-Asx at 0.15 ps after excitation did not show any shift but had less amplitude comparing to Asx. The signal associated with the ICT state is much less pronounced in BPH-Asx as it nearly disappears in both solvents. However, this can be partly due to a broader S_1-S_n band of BPH-Asx, resulting in a weak ICT band hidden under the dominant S_1-S_n transition, which extends to 800 nm for BPH-Asx. To visualize these changes, Fig. 3a compares normalized transient absorption spectra at 1 ps after excitation of both compounds in both solvents.

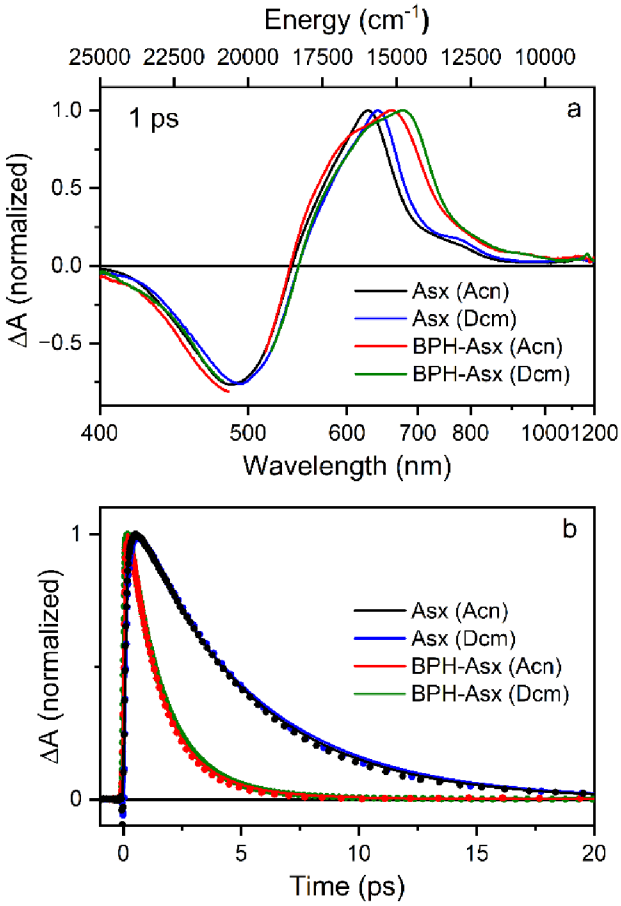

Figure 3. (a) Normalized transient absorption spectra of Asx and BPH-Asx in both solvents. The spectra were measured at 1 ps after excitation at 500 nm for all compounds/solvents. (b) Normalized kinetics measured at the S_1-S_n maximum for each sample. The solid lines represent fits obtained from global fitting analysis.

The decrease in the magnitude of the ICT band, along with the red shift observed when going from Asx to BPH-Asx, is evident. Excited state dynamics was monitored by kinetics measured at the maximum of the S_1-S_n band (Fig. 3b). The decay is significantly faster for BPH-Asx compared to Asx, while there is no change for both compounds with respect to solvent polarity.

Excited state lifetimes were determined using a global fitting analysis, and the results are summarized in Fig. 4. For both compounds, three decay components are sufficient to obtain good fits. The first EADS for Asx in both solvents show features typical of the excited Asx S_2 state, and its lifetime is at sub-100 fs time scale, reaching the limit of our time resolution. The second EADS has already typical features of the S_1-S_n band except the increased amplitude at the low energy side of the band, which is characteristic of a hot S_1/ICT state[52].

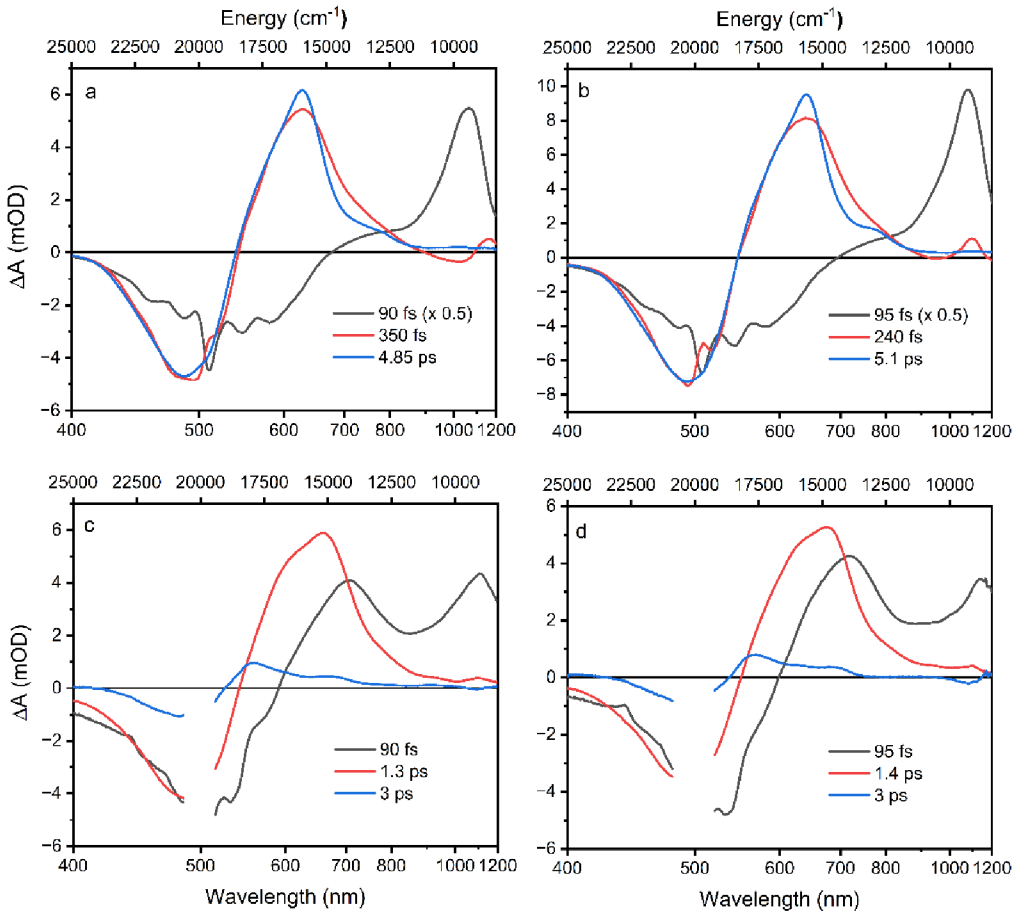

Figure 4. EADS obtained from global fitting of Asx in Acn (a), Asx in Dcm (b), BPH-Asx in Acn (c), and BPH-Asx in Dcm (d).

Decay of the hot S_1/ICT state occurs within a few hundred femtoseconds, differing slightly between Acn (350 fs) and Dcm (240 fs) and yields EADS of the relaxed S_1/ICT state. This EADS exhibits the characteristic profile of the relaxed S_1/ICT state and decays with a time constant of 4.85 ps (Acn) and 5 ps (Dcm). This pattern of the excited state dynamics of Asx in Acn agrees with the results obtained earlier[25, 52].

For BPH-Asx, three decay components provide a good fit, but the individual EADS differ from those obtained for Asx. The first EADS with sub-100 fs lifetime clearly contains features associated with both S_2 state (the ESA signal peaking around 1100 nm) and the hot S_1/ICT state. This implies that S_2 and hot S_1/ICT decays are both very short and occur on a comparable time scale, preventing separation of their contributions with our time resolution. Then, the second EADS corresponds to the relaxed S_1/ICT state, which has a lifetime of 1.3 ps in Acn and 1.4 ps in Dcm. In contrast to Asx, however, global fitting of BPH-Asx reveals EADS with a lifetime longer than the S_1/ICT state.

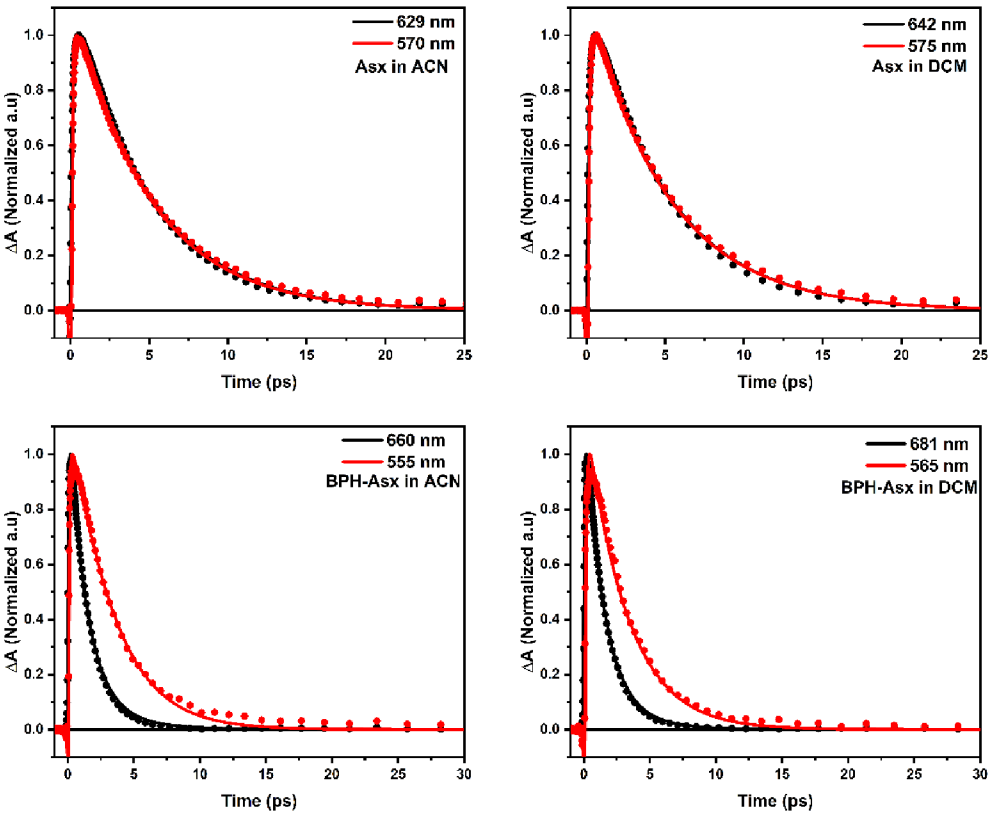

Figure 5. Comparison of normalized kinetics measured at the S_1 (black) and S* (red) maximum bands of Asx and BPH-Asx in polar and non-polar solvents. The lines represent fits obtained from global fitting analysis.

This EADS (blue in Fig. 4c and 4d) has a spectral shape characteristic of an S* signal, which is typically indicated by a distinct blue shoulder at the S_1-S_n band, with a longer lifetime compared to the S_1 state[27]. Here, the S* EADS has a lifetime of 3 ps. To further visualize the difference, we compared kinetics measured at the peak maxima of S_1/ICT and S* bands for both Asx and BPH-Asx (Fig.5). The kinetics clearly demonstrate that while the kinetics of Asx are identical, BPH-Asx exhibits a slower decay of the S* signal compared to the S_1/ICT decay in both Acn and Dcm, as expected.

8.4. Discussion

A straightforward chemical reaction of Asx with phenylhydrazine and acetic acid in ethanol produced stable BPH-Asx with ~30% yield, demonstrating a successful synthesis of a first carotenoid with a conjugated C=N group. Formally, structure of the conjugated system of BPH-Asx is the same as for Asx except the C=O groups of Asx, located symmetrically at both terminal rings, are replaced by C=N groups in BPH-Asx. This allows to study the effect of replacement of the C=O group by the C=N group on spectroscopic properties directly. The presence of keto-groups in Asx generates a featureless absorption spectrum, most likely due to enhanced conformational disorder in the ground state produced by a broad distribution of end ring torsions. The relevant carotenoid without these conjugated keto-groups (zeaxanthin) has absorption spectrum with clearly resolved vibrational bands, proving the importance of the keto-groups in forming the featureless absorption spectrum. The same apparently happens when the keto groups are replaced by the C=N group: the overall shape of the

main absorption band is very similar, though the absorption spectrum of BPH-Asx is slightly broader, suggesting further enhancement of conformational disorder. Furthermore, absorption maximum of BPH-Asx is red-shifted by a few nanometers which is the first indication of changes of spectroscopic properties induced by the conjugated C=N group. Solvent polarity has minimal effect on absorption spectrum of BPH-Asx, which is in striking contrast to the dicyano-apo-carotene, another carotenoid featuring nitrogen atoms in conjugation[42].

While the changes in absorption spectra are rather subtle, more pronounced changes occur in excited state dynamics. The red shift of BPH-Asx is enhanced in transient absorption spectra reflecting the S_1-S_n band, but the most significant effect of the conjugated C=N group is on the S_1/ICT lifetime. Even though the ICT band amplitude is not enhanced in BPH-Asx, the S_1/ICT lifetime drops from ~5 ps (Asx) to ~1.4 ps (BPH-Asx). Since the S_1/ICT lifetimes are essentially identical in Dcm and Acn (Fig. 4), the shortening can hardly be associated with solvent polarity. To verify this, we have measured additional data for both carotenoids in non-polar benzene (Fig. S8 and S9). The data clearly show that further decrease of solvent polarity does not have any effect on spectroscopic properties. The S_1/ICT lifetime is the same in benzene and Acn, proving that the observed shortening of the S_1/ICT lifetime is not due to solvent polarity, but it rather indicates a prolongation of effective conjugation length for BPH-Asx.

The effective conjugation length can be determined by comparison of the S_1/ICT lifetime with that of carotenes[53]. The S_1/ICT lifetime of Asx, ~5 ps, is comparable to that of the linear lycopene with N=11. Shortening of the S_1/ICT lifetime to 1.4 ps (BPH-Asx) suggests effective conjugation of ~13. This implies that the conjugated C=N groups contribute to the total conjugation length significantly more than the C=O groups. Another support for explanation of the observed changes in spectroscopic properties solely by prolongation of the effective conjugation is detection of the S* signal exclusively in BPH-Asx. The blue shoulder (S*) of the S_1-S_n band decaying slower than the main S_1-S_n band (Fig. 5) is a feature reported exclusively for carotenoids with N>11[33]. Though the origin of this signal is not completely clear, recent studies have showed that for these long carotenoids the S* signal is likely due to a hot ground state populated by fast decay of the S_1 state[33]. Thus, the distinct lifetimes of the S* and S_1/ICT signals, 3 and 1.4 ps provide further support for explanation of the differences between spectroscopic properties of Asx and BPH-Asx by prolongation of the effective conjugation.

To identify possible origin of the proposed prolongation of effective conjugation, we have examined both molecules by calculations using density functional theory. The structures were optimized using the B3LYP level of theory with 6-31g(d,p) basis set. Since the prolongation of the effective conjugation in carotenoids with conjugation extended to terminal rings is often associated with twisting of the end rings resulting in planarization of the conjugated system[53], we have focused on dihedral angles between the terminal rings and the main conjugation chain. For the relaxed ground state structures of Asx and BPH-Asx *in vacuo* we have obtained values of -38.5° and -43.7° (see Fig.

S10 for relaxed structures). These values are close to those reported for Asx earlier[54] and indicate that planarization of BPH-Asx cannot be the reason for prolongation of the conjugation length. Thus, a different mechanism must operate here, likely related to the properties of the conjugated C=N group that is further connected to other, non-conjugated part of the phenylhydrazone group. Even though non-conjugated groups usually do not contribute to the effective conjugation length, for some keto-carotenoids, electron distribution in the excited state has been affected by non-conjugated groups, resulting in a change of excited-state properties[54]. It is likely that comparable mechanism works also here as there is only mild change (small red-shift of absorption spectrum) of spectroscopic properties in the ground state, but significant change occurs for the lowest excited state, somehow mimicking the behaviour reported in ref. 54.

Longer effective conjugation length of BPH-Asx and no effect of solvent polarity on its excited states is in striking contrast with another carotenoid involving a nitrogen atom in conjugated system, dicyano-apo-carotene, which exhibits a strong dependence of excited state properties on solvent polarity as its S_1 lifetime varies by an order of magnitude from 11.7 ps in 3-methylpentane to 1.9 ps in Acn[42]. This is due to a significant charge transfer character of the excited state, because dicyano-apo-carotene has two C≡N groups but both located at the same side of the molecule, generating large asymmetry in the electron distribution along the conjugated chain. BPH-Asx in contrast, has two C=N groups positioned symmetrically at ends of the conjugated chain, preventing asymmetry in electron distribution which is the source of polarity-induced effects on excited state dynamics[20-23]. Instead, adding two symmetric phenylhydrazone groups extends the electron distribution along the conjugated chain, making the effective conjugation of BPH-Asx longer than of Asx.

In conclusion, we have demonstrated that the carotenoid astaxanthin can be successfully modified with organic compounds via a new and simple synthetic pathway, adding non-native groups to the astaxanthin conjugated system, which may provide a basis for synthesis of further non-natural carotenoids. The modification of Asx presented here results in significant changes of photophysical properties, opening a way to study effects that are not present in natural carotenoids. This approach may help to shed more light on complicated structure of carotenoid excited states as well as on intricate relaxation pathways involving dark excited states, eventually contributing to a deeper understanding of complex photophysical properties of carotenoids.

Acknowledgements

The research leading to these results has received funding from the Czech Science Foundation (grant 19-28323X), and LASERLAB-EUROPE (grant agreement no. 871124, European Union's Horizon 2020 research and innovation programme). EO further thanks Gebze Technical University for technical support in enabling mass spectroscopy, NMR, and FTIR measurements, and Profs. Bünyemin Çoşut and İbrahim Fazıl Şengül for their help and support. The authors thank to Petr Štěpnička and Martin Štícha from Charles University for their help with ESI-MS measurements.

8.5. Supporting Information

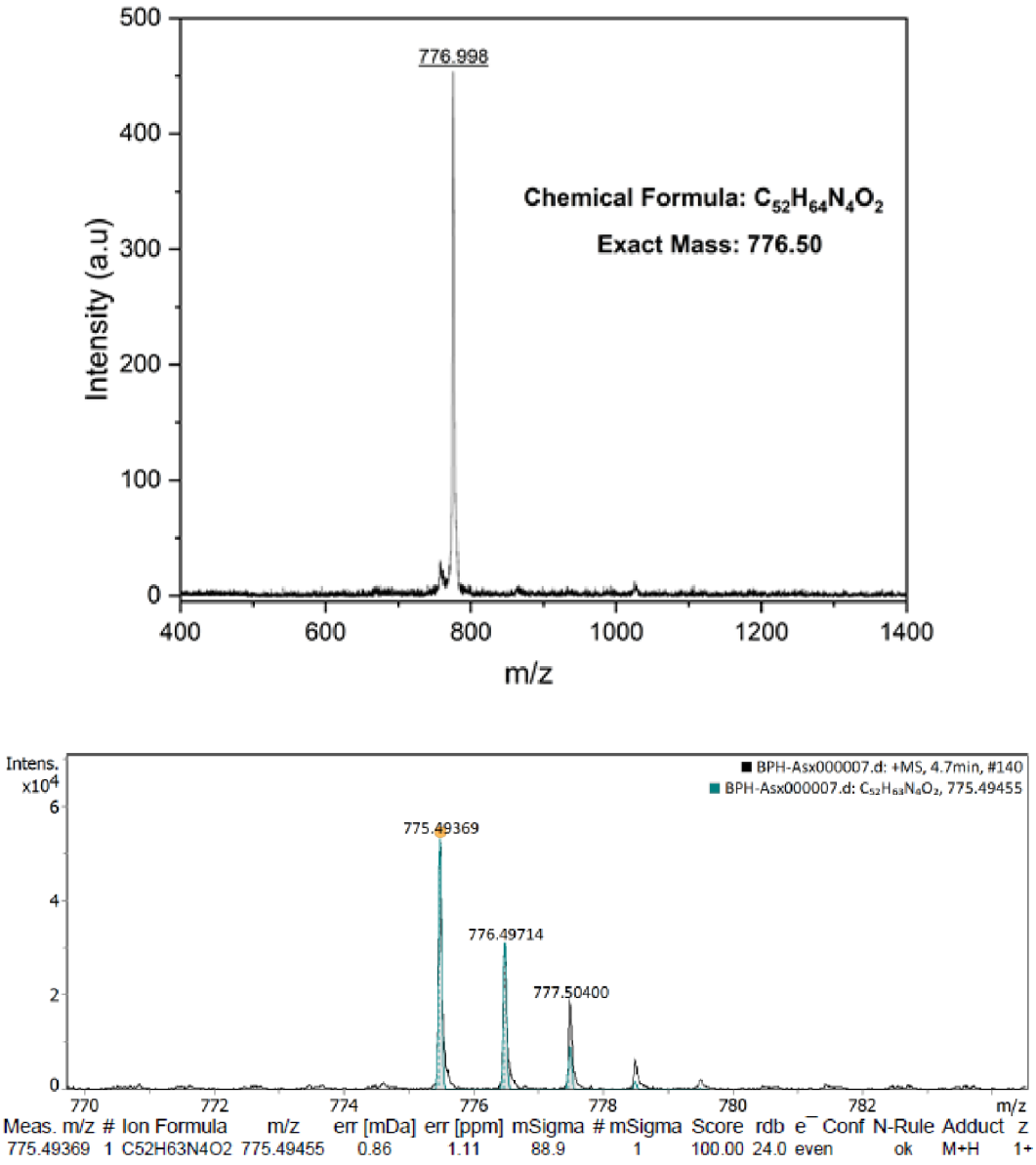

Figure S1: Positive ion and linear mode MALDI TOF-MS spectrum of BPH-Asx. Bottom: ESI-MS Spectrum of BPH-Asx demonstrating difference between experimental and calculated mass of 1.1 ppm.

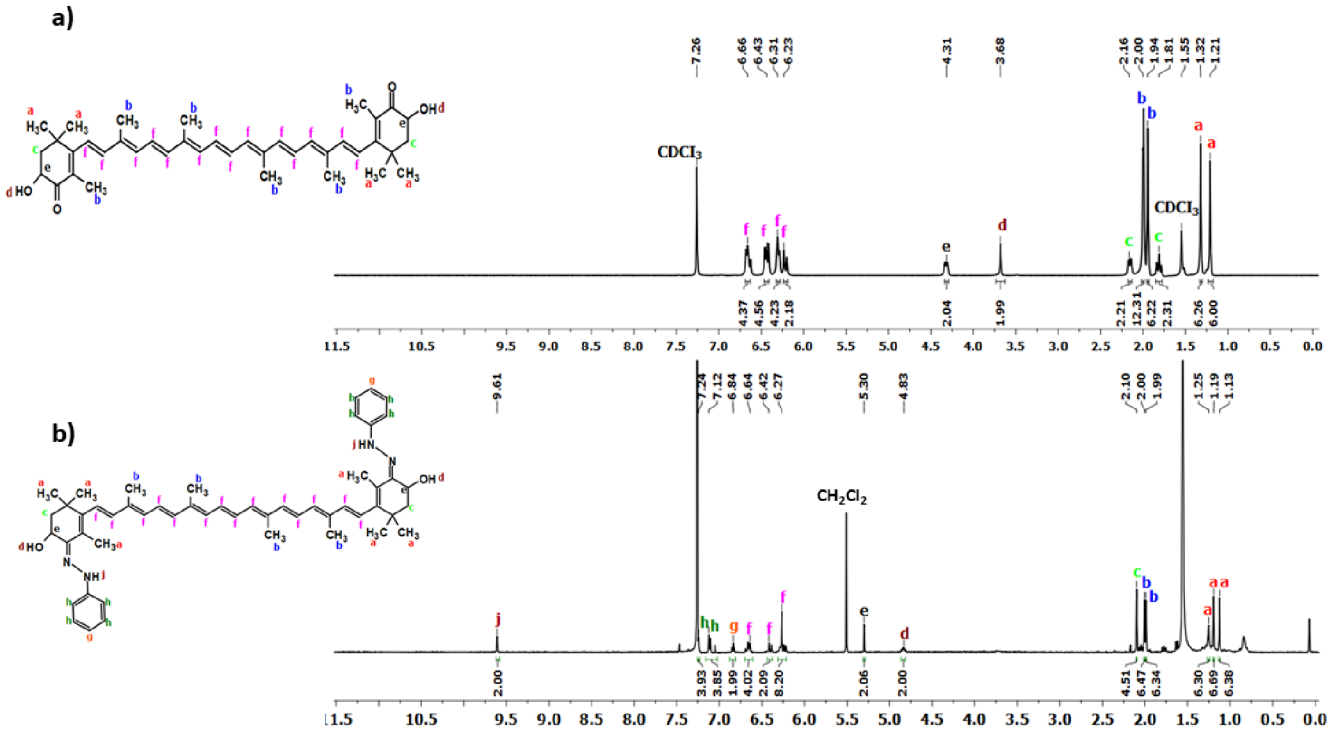

Figure S2: ^{1}H NMR Spectrum of a) Asx b) BPH-Asx in $CDCl_3$.

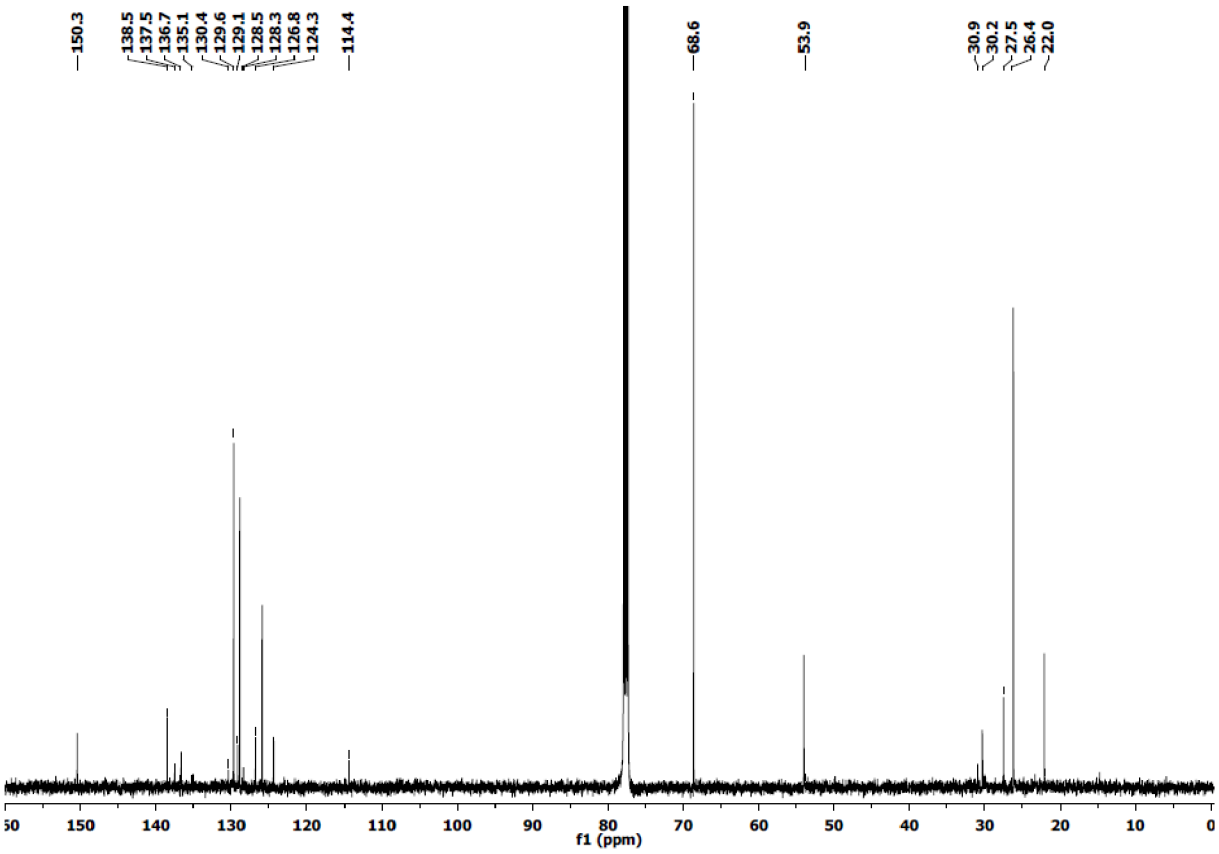

Figure S3: ^{13}C NMR Spectrum of BPH-Asx in $CDCl_3$.

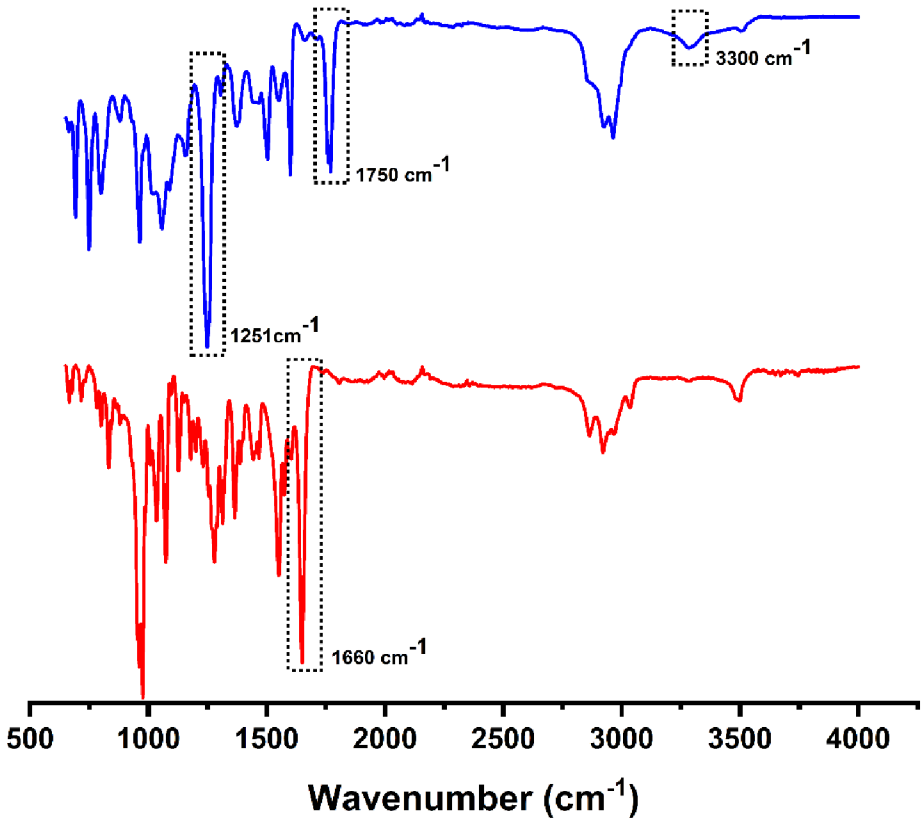

Figure S4: FT-IR Spectrum of Asx (red) and BPH-Asx (blue).

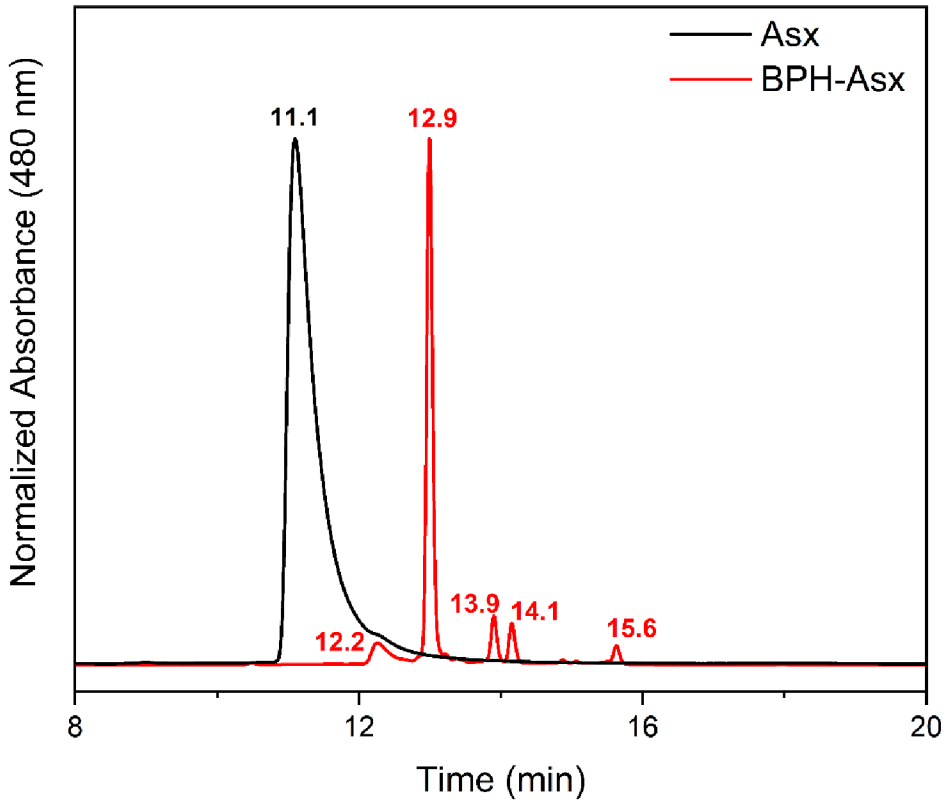

Figure S5: Normalized HPLC chromatograms of Asx (black) and BPH-Asx (red). Elution times of identified peaks are shown in the graph. The black chromatogram of Asx shows a single peak at 11.1 assigned to *all-trans* astaxanthin. For BPH-Asx, several peaks were identified at 12.2 minutes (%3), at 12.9 minutes (%81), at 13.9 minutes (%6), at 14.1 minutes (%6) and at 15.6 minutes (%4).

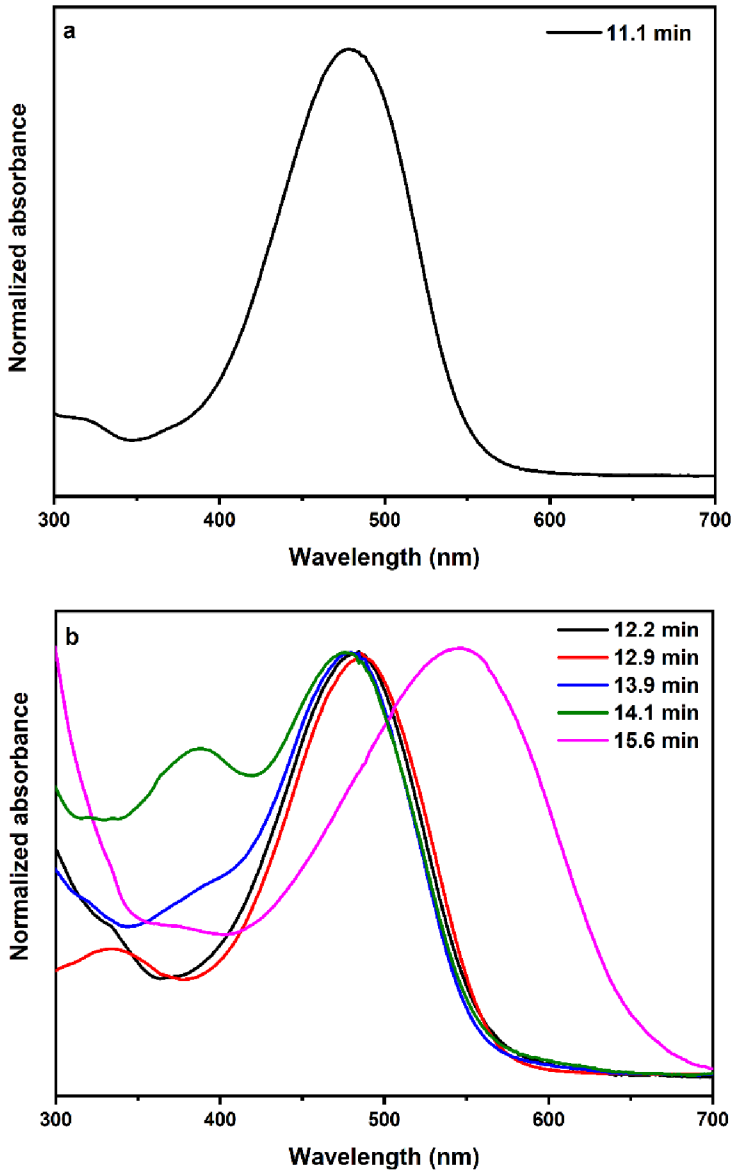

Figure S6: Normalized absorption spectra of peaks from HPLC analysis of a) Asx and b) BPH-Asx. Spectra were extracted directly from HPLC.

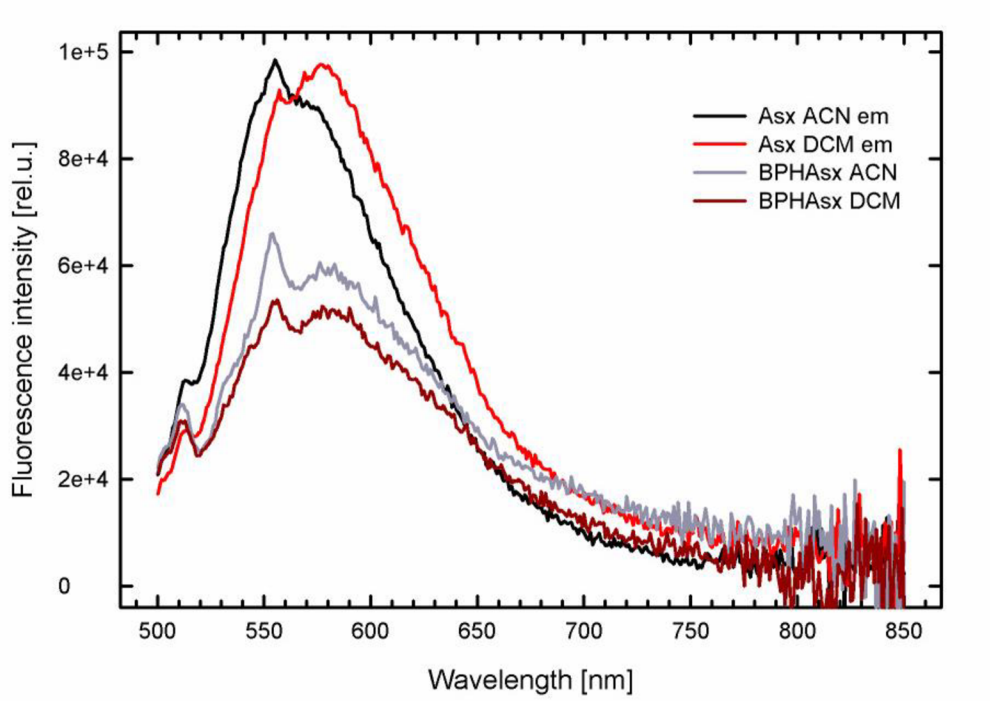

Figure S7. Fluorescence spectra of Asx and BPH-Asx in DCM and ACN. The sharp peaks are due to Raman bands. The spectra were measured with 5 nm bandpass and were corrected for instrument response. All spectra were excited at 475 nm, absorbance of the samples at this wavelength was 0.4-0.8 (3 mm path length), and the data are normalized to equal absorption at 475 nm.

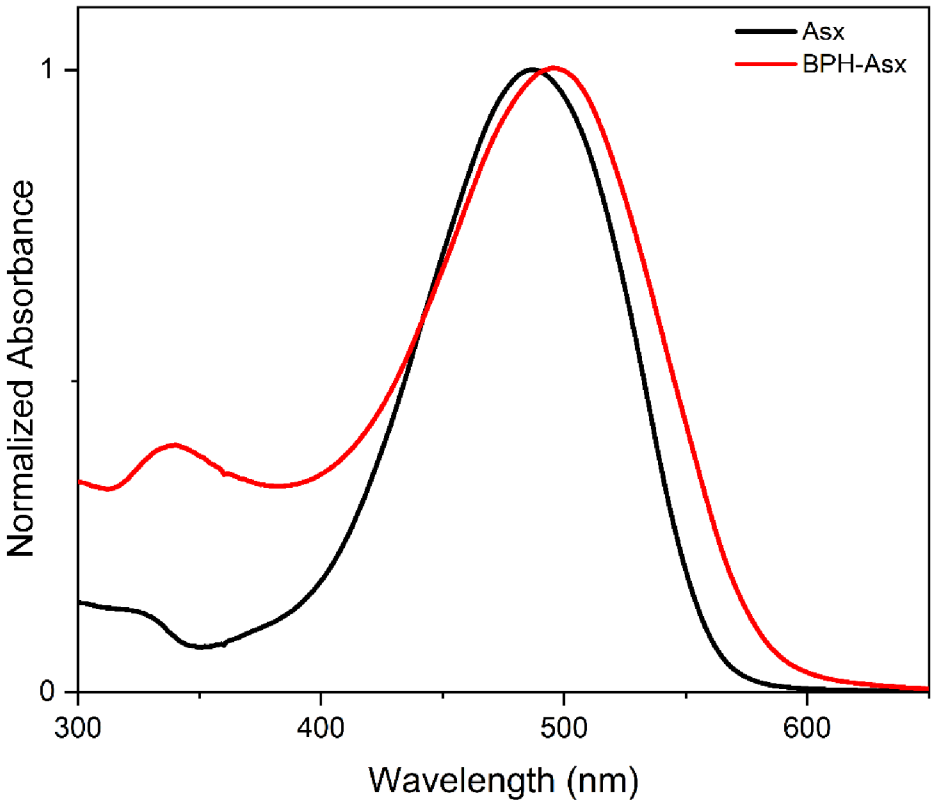

Figure S8. Steady state absorption spectra of astaxanthin (Asx) and BPH-Asx in benzene.

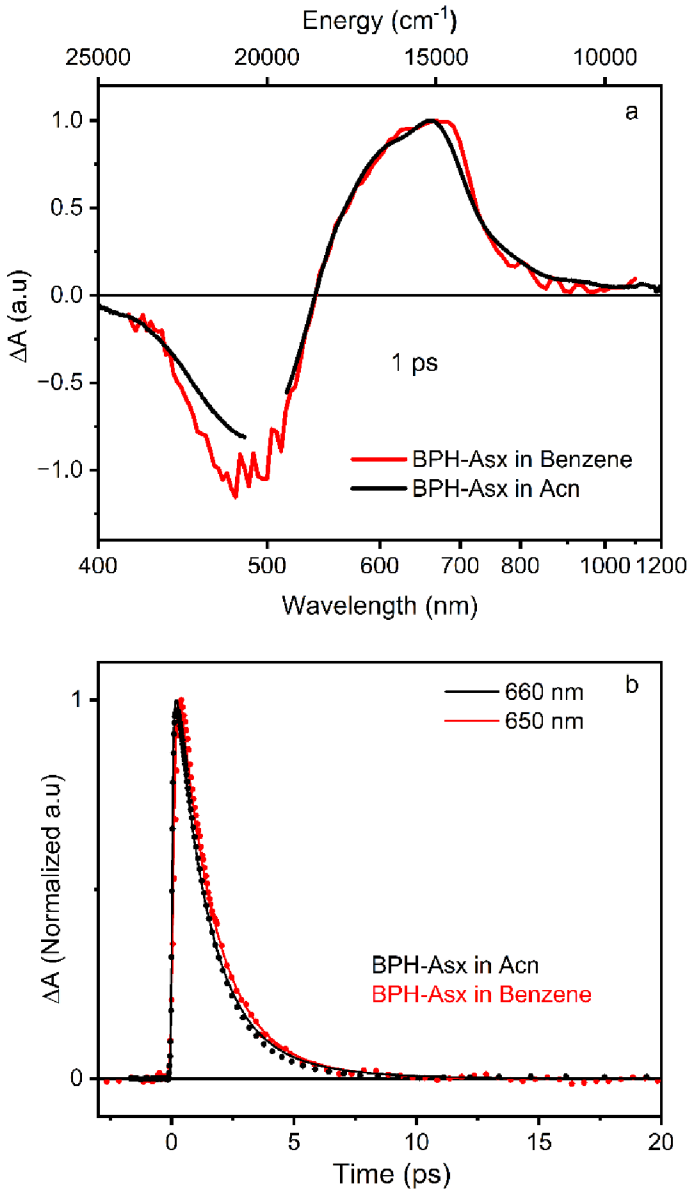

Figure S9: Normalized transient absorption spectra of a) BPH-Asx in Acn (black), and BPH-Asx in benzene (blue). The spectra were measured at 1 ps after excitation 500 nm for all compounds/solvents. Normalized kinetics b) measured at the S_1-S_n maximum of same compounds in polar and non-polar solvents. Kinetics are also normalized to maximum; the lines represent fits obtained from global fitting analysis.

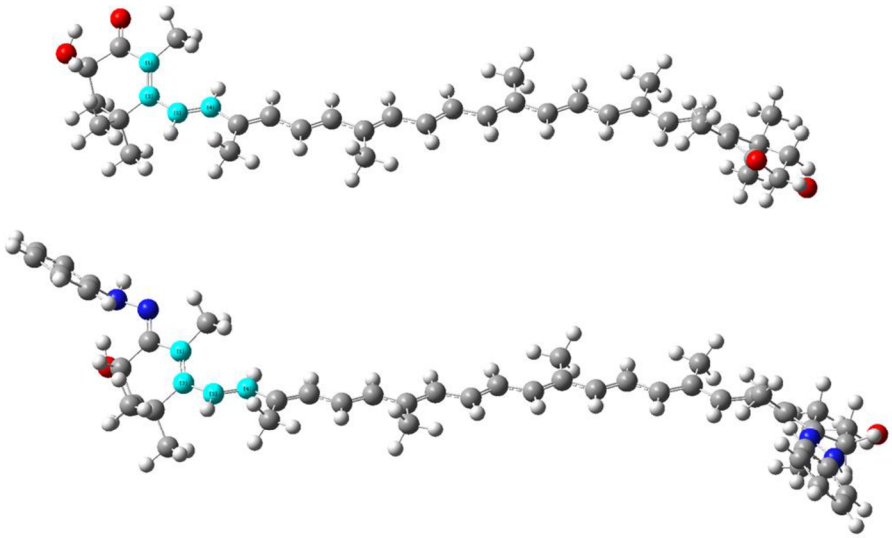

Figure S10. Relaxed ground state structures of Asx (top) and BPH-Asx (bottom). The atoms forming the dihedral angle are shown in cyan.

8.6. References

1. K. K. Namitha and P. S. Negi, Crit. Rev. Food Sci. Nutr., 2010, 50, 728-760.

2. T. Polívka and H. A. Frank, Acc. Chem. Res., 2010, 43, 1125-1134.

3. R. Croce and H. van Amerongen, Science, 2020, 369, 2058.

4. D. Zigmantas, T. Polívka, P. Persson and V. Sundström, Chem. Phys. Rev., 2022, 3, 041303.

5. A. V. Ruban, R. Berera, C. Ilioaia, I. H. van Stokkum, J. T. Kennis, A. A. Pascal, H. van Amerongen, B. Robert, P. Horton and R. van Grondelle, Nature, 2007, 450, 575-578.

6. N. E. Holt, D. Zigmantas, L. Valkunas, X. P. Li, K. K. Niyogi and G. R. Fleming, Science, 2005, 307, 433-436.

7. H. Staleva, J. Komenda, M. K. Shukla, V. Slouf, R. Kana, T. Polivka and R. Sobotka, Nat. Chem. Biol., 2015, 11, 287-291.

8. C. D. P. Duffy and A. V. Ruban, J. Photoch. and Photob. B: Biol., 2015, 152, 215-226.

9. T. G. Monger, R. J. Cogdell and W. W. Parson, Biochim. Biophys. Acta, 1976, 449, 136-153.

10. Z. Kvíčalová, J. Alster, E. Hofmann, P. Khoroshyy, R. Litvín, D. Bína, T. Polívka and J. Pšenčík, Biochim. Biophys. Acta - Bioenerg., 2016, 1857, 341-349.

11. H. A. Frank and R. J. Cogdell, Photochem. Photobiol., 1996, 63, 257-264.

12. C. S. Foote, Y. C. Chang and R. W. Denny, J. Am. Chem. Soc., 1970, 92, 5216-5218.

13. T. W. M. Boileau, A. C. Moore and J. W. Erdman, J. Antioxid. Act., 1999, 133-158.

14. S. A. R. Paiva and R. M. Russell, J. Am. Coll. Nutr., 1999, 18, 426-433.

15. N. I. Krinsky and K.-J. Yeum, Biochem. Biophys. Res. Commun., 2003, 305, 754-760.

16. M. Kobayashi and Y. Sakamoto, Biotechnol. Lett., 1999, 21, 265-269.

17. T. Polívka and V. Sundström, Chem. Rev., 2004, 104, 2021-2072.

18. T. Polívka and V. Sundström, Chem. Phys. Lett., 2009, 477, 1-11.

19. M. R. Wasielewski and L. D. Kispert, Chem. Phys. Lett., 1986, 128, 238-243.

20. H. A. Frank, J. A. Bautista, J. Josue, Z. Pendon, R. G. Hiller, F. P. Sharples, D. Gosztola and M. R. Wasielewski, J. Phys. Chem. B, 2000, 104, 4569-4577.

21. D. Zigmantas, R. G. Hiller, F. P. Sharples, H. A. Frank, V. Sundstrom and T. Polivka, Phys. Chem. Chem. Phys., 2004, 6, 3009-3016.

22. M. M. Enriquez, M. Fuciman, A. M. LaFountain, N. L. Wagner, R. R. Birge and H. A. Frank, J. Phys. Chem. B, 2010, 114, 12416-12426.

23. P. Chábera, M. Fuciman, P. Hříbek and T. Polívka, Phys. Chem. Chem. Phys., 2009, 11, 8795-8803.

24. E. Özcan, V. Kuznetsova, G. Keşan, M. Fuciman, R. Litvín and T. Polívka, J. Photochem. Photobiol. A: Chem., 2023, 441, 114737.

25. R. P. Ilagan, R. L. Christensen, T. W. Chapp, G. N. Gibson, T. Pascher, T. Polivka and H. A. Frank, J. Phys. Chem. A, 2005, 109, 3120-3127.

26. N. Christensson, T. Polivka, A. Yartsev and T. Pullerits, Phys. Rev. B, 2009, 79, 245118.

27. C. C. Gradinaru, J. T. M. Kennis, E. Papagiannakis, I. H. M. van Stokkum, R. J. Cogdell, G. R. Fleming, R. A. Niederman and R. van Grondelle, Proc. Natl. Acad. Sci. U. S. A., 2001, 98, 2364.

28. P. O. Andersson and T. Gillbro, J. Chem. Phys., 1995, 103, 2509.

29. W. Wohlleben, T. Buckup, H. Hashimoto, R. J. Cogdell, J. L. Herek and M. Motzkus, J. Phys. Chem. B, 2004, 108, 3320.

30. T. Lenzer, F. Ehlers, M. Scholz, R. Oswald and K. Oum, Phys. Chem. Chem. Phys., 2010, 12, 8832.

31. E. Papagiannakis, I. H. M. van Stokkum, M. Vengris, R. J. Cogdell, R. van Grondelle and D. S. Larsen, J. Phys. Chem. B, 2006, 110, 5727.

32. D. M. Niedzwiedzki, J. O. Sullivan, T. Polivka, R. R. Birge and H. A. Frank, J. Phys. Chem. B, 2006, 110, 22872-22885.

33. V. Balevičius, D. Abramavicius, T. Polívka, A. Galestian Pour and J. Hauer, J. Phys. Chem. Lett., 2016, 7, 3347-3352.

34. D. Kosumi, M. Fujiwara, R. Fujii, R. J. Cogdell, H. Hashimoto and M. Yoshizawa, J. Chem. Phys., 2009, 130, 214506.

35. H. Staleva, M. Zeeshan, P. Chábera, V. Partali, H. R. Sliwka and T. Polívka, J. Phys. Chem. A, 2015, 119, 11304.

36. D. M. Niedzwiedzki, T. Kajikawa, K. Aoki, S. Katsumura and H. A. Frank, J. Chem. Phys. B, 2013, 117, 6874-6887.

37. D. Kosumi, T. Kajikawa, S. Okumura, M. Sugisaki, K. Sakaguchi, S. Katsumura and H. Hashimoto, J. Phys. Chem. Lett., 2014, 5, 792-797.

38. T. Kajikawa, K. Aoki, R. S. Singh, T. Iwashita, T. Kusumoto, H. A. Frank, H. Hashimoto and S. Katsumura, Org. Biomol. Chem., 2009, 7, 3723-3733.

39. D. Kosumi, T. Kajikawa, K. Yano, S. Okumura, M. Sugisaki, K. Sakaguchi, S. Katsumura and H. Hashimoto, Chem. Phys. Lett., 2014, 602, 75-79.

40. M. M. Enriquez, S. Hananoki, S. Hasegawa, T. Kajikawa, S. Katsumura, N. L. Wagner, R. R. Birge and H. A. Frank, J. Phys. Chem. B, 2012, 116, 10748-10756.

41. H.-R. Sliwka and V. Partali, Journal, 2012, 17, 2877-2928.

42. M. P. O'Neil, M. R. Wasielewski, M. M. Khaled and L. D. Kispert, J. Chem. Phys., 1991, 95, 7212-7218.

43. P. Chábera, M. Fuciman, K. Razi Naqvi and T. Polívka, Chem. Phys., 2010, 373, 56-64.

44. H. Fukami, K. Namikawa, N. Sugiura-Tomimori, M. Sumida, K. Katano and M. Nakao, J. Oleo Sci., 2006, 55, 653-656.

45. H. L. Jackson, A. J. Cardounel, J. L. Zweier and S. F. Lockwood, Bioorg. Med. Chem. Lett., 2004, 14, 3985-3991.

46. J. Willibald, S. Rennebaum, S. Breukers, S. H. Abdel Hafez, A. Patel, C. L. Øpstad, R. Schmid, S. N. Naess, H.-R. Sliwka and V. Partali, Chem. Phys. Lipids., 2009, 161, 32-37.

47. R. Litvín, D. Bína, M. Herbstová and Z. Gardian, Photosynth. Res., 2016, 130, 137-150.

48. I. F. Sengul, K. Wood, N. Kumar and D. S. Black, Tetrahedron, 2012, 68, 9050-9055.

49. K. Holtin, M. Kuehnle, J. Rehbein, P. Schuler, G. Nicholson and K. Albert, Anal. Bioanal. Chem., 2009, 395, 1613-1622.

50 J. Kevin, H. Stapelfeldt and L. H. Skibsted, Chem. Phys. Lett., 1992, 190, 514–519.

51. T. Khan, R. Litvín, V. Šebelík and T. Polívka, Chem. Phys. Chem., 2021, 22, 471-480.

52. M. Fuciman, M. Durchan, V. Slouf, G. Kesan and T. Polivka, Chem. Phys. Lett., 2013, 568, 21-25.

53. M. Fuciman, G. Kesan, A. M. LaFountain, H. A. Frank and T. Polivka, J. Phy.s Chem. B, 2015, 119, 1457-1467.

54. H. Hashimoto, T. Yoda, T. Kobayashi and A. J. Young, J. Mol. Struct., 2002, 604, 125-146.

55. H. Staleva-Musto, V. Kuznetsova, D. Bína, R. Litvín and T. Polívka, Photosynth. Res., 2020, 144, 127-135.

9. Summary and Conclusions

This thesis is primarily focused on understanding the complex dynamics of excited states in carotenoids, with a particular emphasis on the origin and properties of some dark states. It has explored effects of different external disturbances, such as interaction with metals, pH change, applied voltage in cyclic voltammetry, or chemical modifications, on the dynamics of these states. The results clarified some of the questions but also brought up new ones. The methods used to study excited state properties as well as the obtained results could help in further research in this area and provide new approaches for studying different carotenoids.

In Paper **I**, we showed that we were able to produce astaxanthin-metal complexes with demonstrated long-term stability in methanol. The stability of these complexes allowed us to thoroughly investigate their excited states using transient absorption spectroscopy. Transient absorption spectroscopy demonstrated how interactions with Zn^{2+} and Cu^{2+} ions influenced the excited-state dynamics of the carotenoid astaxanthin. The charge transfer character of the lowest excited state (S_1/ICT) is significantly altered by the formation of astaxanthin-metal complexes. The S_1/ICT lifetime is shortened from 4.4 ps in pure astaxanthin to 3.9 ps and 2.6 ps in the astaxanthin-Zn and astaxanthin-Cu complexes, respectively. This lifetime reduction is attributed to prolonged effective conjugation caused by the interaction of metal ions with the keto oxygen in astaxanthin. Additionally, an S* signal is observed, likely resulting from a rapid population of a hot ground state, due to the significant shortening of the S_1/ICT lifetime in the astaxanthin-Cu complex. The study further demonstrates that these effects result from astaxanthin complexing with metal ions, which causes the absorption spectrum to shift red and enhances the ICT band in transient absorption spectra. The results underline the possibility of altering the excited-state properties of carotenoids through metal-ion interactions, which could improve their photoprotective capabilities in both artificial and natural light-harvesting systems.

In paper II, steady-state and ultrafast time-resolved absorption spectroscopy were used to investigate the impact of applied external voltage on the excited-state characteristics of 8′-apo-β-carotenal in acetonitrile during bulk electrolysis. The time-resolved spectroelectrochemistry method has been used with carotenoids for the first time, although it has already been applied to nanocrystals, semiconductors, thin films, and other materials. The data collected during bulk electrolysis were compared with those obtained without the applied voltage. The steady-state measurements demonstrated that although the applied voltage has changed the amplitude of the S_0-S_2 absorption band, the spectral position remains almost constant. A comparison of the transient absorption spectra reveals that, under the applied voltage of 0.5 V, the magnitude of the ICT-like band decreases during the experiment. This decrease is correlated with an extension of the S_1/ICT-like lifetime from 8 ps to 13 ps. In addition, after turning off the applied voltage, the data returned to zero voltage levels in about 30 minutes. Our results demonstrate that an external voltage can be applied to control the amplitude of the signal associated with the ICT state. As a result, our findings demonstrate that the

amplitude of the ICT state in transient absorption spectra, along with associated polarity-induced effects, can be finely adjusted by applying an external voltage.

Paper **III** explores the influence of pH-dependent effects on the excited-state behavior of crocin, a hydrophilic carotenoid that plays various roles in biological systems. The absorption and fluorescence spectra from steady-state spectroscopy indicate significant alterations, characterized by a pH-dependent blue shift and enhanced resolution of vibrational bands. These effects are further explained by transient absorption spectra, which reveal a notable blue shift in the S_1–S_n peak with increasing pH. A detailed kinetic analysis reveals the dynamics of the excited states of crocin, which depend on pH. It has been demonstrated that effective conjugation decreases at pH 11, thereby prolonging the S_1/ICT lifetime. On the other hand, our data indicate a more complicated situation at pH 9, suggesting the presence of two distinct crocin species with different relaxation patterns. This suggests structural changes in the crocin molecule, possibly due to the deprotonation of hydroxyl groups and/or saponification at high pH levels. In addition to the dynamics of excited states, crocin stability is significantly impacted by pH. Basic pH stabilizes the crocin molecule, whereas acidic pH causes rapid degradation.

In the last paper (**IV**), we present the synthesis and extensive spectroscopic investigation of bis-phenylhydrazone astaxanthin (BPH-Asx), a derivative of astaxanthin (Asx), in which a conjugated C=N bond replaces the conjugated carbonyl group of Asx. BPH-Asx was successfully synthesized and characterized using various spectroscopic techniques, revealing subtle changes in absorption spectra and significant alterations of excited-state dynamics compared to Asx. The results show that BPH-Asx has a shorter S_1 lifetime (1.4 ps) than Asx (5 ps), suggesting that its excited-state dynamics are significantly affected. The modifications caused by the conjugated C=N group result from an extension of the effective conjugation, as no polarity-induced changes were observed for BPH-Asx. Additionally, the discovery of a distinctive S* signal in BPH-Asx, with a lifetime of 3 ps, highlights the association between the effective conjugation and the presence of the S* signal, which is not detected in Asx. Additionally. The resulst have shown that astaxanthin can be modified with organic compounds using a simple synthetic pathway, adding non-native groups to its conjugated system. This modification significantly changes its photophysical properties, enabling the study of effects not present in natural carotenoids. This approach can improve our understanding of carotenoid excited states and their complex relaxation pathways.

10. Curriculum Vitae

Emrah Özcan, MSc

• Email: eozcan00@prf.jcu.cz, emrah.ozcan@gtu.edu.tr

• *ORCID ID:* 0000-0001-6325-5674 • *Researcher ID:* AAL-1301-2020 *Scopus ID:* 55874720500

Education

Ph.D. in Biophysics 01/09/2019 – present
University of South Bohemia Ceske Budejovice, Czechia

- *Ph.D. titled Carotenoid Photophysics: Influence of Environment Properties on Excited-State Dynamics under the guidance of Supervisor Prof. Tomas Polivka, Ph.D.*

Status and expected completion date: Thesis writing stage, September 2024

Ph.D. in Chemistry 01/07/2017 – 01.25.2024
Gebze Technical University Kocaeli, Türkiye

- *Ph.D. titled Photophysical Properties and Ultrafast Excited-State Dynamics of New Organoboron Derivatives under the guidance of Supervisor Prof. Bünyemin Cosut, Ph.D.*

M.Sc. in Chemistry 15/05/2015 – 01/07/2017
Gebze Technical University Kocaeli, Türkiye

- *M.Sc. titled Development and Characterization of Dendrimeric Phosphaze Core-Based Colorimetric Sensors for TNT Detection under the guidance of Supervisor Prof. Bünyemin Cosut, Ph.D.*

B.Sc. in Chemistry 06/09/2008– 06/06/2012
Black Sea Technical University Trabzon, Türkiye

Internship Program in Chemical Physics Lab 01/04/2023 – 01/05/2023
Lund University, Lund Laser Centre Lund, Sweden

- *Accepted project titled 'Ultrafast Time-Resolved Spectroelectrochemistry of Synthetic Carotenoids' by the European Laser Centre.*

Participation in Conferences, Workshops and Summer schools

- 26th Spring Symposium of the German Young Chemists Network, **poster**, Ulm, Germany, 2024
- MECAREACT Vibrational and Electronic spectroscopies applied to study of reaction mechanism, **poster,** Paris, France, 2023
- Nordic Femtochemistry Meeting, **poster,** Jyvaskyla, Finland, 2022
- Jung Chemiker Forum (JCF) Frühjahrssymposium, **poster,** Konstanz, Germany, 2018
- 13th Nanoscience & Nanotechnology Conference, **poster,** Antalya, Turkey, 2018
- 29th National Chemistry Congress, **talk,** Ankara, Turkey, 2017
- 27th National Chemistry Congress, **poster**, Canakkale, Turkey, 2015

Publications, Citations: 392, H index: 13

1. **Özcan, E.,** Keşan, G., Chabera, P., Litvín, R., & Polivka, T. (**2024**). Synthesis and spectroscopic properties of carotenoid bis-phenylhydrazone astaxanthin: Extending conjugation to a C= N group. *New Journal of Chemistry*.

2. **Özcan, E.,** Šímová, I., Bína, D., Litvín, R., & Polívka, T. (**2024**). Ultrafast spectroscopy of the hydrophilic carotenoid crocin at various pH. *Physical Chemistry Chemical Physics*, *26*(13), 10225-10233.

3. Keşan, G., **Özcan, E.,** Chábera, P., Polívka, T., & Fuciman, M. **(2023).** Time-Resolved Spectroelectrochemical Dynamics of Carotenoid 8'-apo-β Carotenal. **ChemPlusChem**, 88(11).

4. **Özcan, E.,** Kuznetsova, V., Keşan, G., Fuciman, M., Litvín, R., Polívka, T*. **(2023)**. Ultrafast excited states dynamics of metal ion complexes of the carotenoid astaxanthin. **Journal of Photochemistry & Photobiology, A: Chemistry**, 441, 114737.

5. **Özcan, E.,** Saglam, M. F., Kazan, H. H., Erol, I., Sengul, I. F., & Cosut, B. **(2023)**. Indolyl imine substituted BODIPY systems; synthesis, photophysical, and biological properties. **Tetrahedron**, 137, 133367.

6. Ayhan, M. M., **Özcan, E.,** Alkan, F., Çetin, M., Ün, I., Bardelang, D., & Çoşut, B. **(2022)**. External complexation of BODIPYs by CB [7] improves in-cell fluorescence imaging. **Materials Advances,** 3(1), 547-553.

7. **Özcan, E.,** Dedeoglu, B., Chumakov, Y., Gürek, A. G., Zorlu, Y., Coşut, B., & Menaf Ayhan, M. **(2021)**. Halogen-Bonded BODIPY Frameworks with Tunable Optical Features. **Chemistry–A European Journal**, 27(5), 1603-1608.

8. **Özcan, E.,** Dedeoglu, B., Chumakov, Y., Zorlu, Y., Çoşut, B., & Ayhan, M. M. **(2021)**. Modulation of supramolecular self-assembly of BODIPY tectons via halogen bonding. **CrystEngComm**, 23(36), 6365-6375.

9. Eçik, E. T., **Özcan, E.,** Kazan, H. H., Erol, I., Şenkuytu, E., & Çoşut, B. **(2021)**. Dual color triads: synthesis, photophysics and applications in live cell imaging. **New Journal of Chemistry**, 45(22), 9984-9994.

10. Ayhan, M. M., **Özcan, E.,** Dedeoglu, B., Chumakov, Y., Zorlu, Y., & Coşut, B. **(2021)**. Carbon (sp 3) tetrel bonding mediated BODIPY supramolecular assembly via unprecedented synergy of C sp3⋯ N and C sp3⋯ F pair interactions. **CrystEngComm**, 23(2), 268-272.

11. **Özcan, E.,** Kazan, H. H., & Çoşut, B. **(2020)**. Recent chemo-/biosensor and bioimaging studies based on indole-decorated BODIPY s. **Luminescence**, 35(2), 168-177.

12. Kazan, H. H., **Özcan, E.,** Çoşut, B., Çiftçi, G. Y., & Eçik, E. T. **(2020)**. Novel BODIPY-subphthalocyanine dyads with reasonable photodynamic therapy behaviours. **New Journal of Chemistry**, 44(32), 13738-13744.

13. **Özcan, E.,** Aksoy, B. T., Eçik, E. T., Dere, A., Karabulut, A., Yakuphanoglu, F., & Çoşut, B. **(2020)**. Fabrication of hybrid photodiode systems: BODIPY decorated cyclotriphosphazene covalently grafted graphene oxides. **Inorganic Chemistry Frontiers,** 7(16), 2920-2931.

14. Aksoy, B. T., Keşan, G., **Özcan, E.,** Eçik, E. T., Dere, A., Karabulut, A., & Çoşut, B. **(2020)**. Solution-processable BODIPY decorated triazine photodiodes and their

comprehensive photophysical evaluation. **New Journal of Chemistry,** 44(5), 2155-2165.

15. **Özcan, E.,** Tümay, S. O., Keşan, G., Yeşilot, S., & Çoşut, B. **(2019)**. The novel anthracene decorated dendrimeric cyclophosphazenes for highly selective sensing of 2, 4, 6-trinitrotoluene (TNT). **Spectrochimica Acta Part A: Molecular and Biomolecular Spectroscopy,** 220, 117115.

16. **Özcan, E.,** Ozdemir, M., Ho, D., Zorlu, Y., Ozdemir, R., Kim, C., & Cosut, B. **(2019)**. A Solution-Processable meso-Phenyl-BODIPY-Based n-Channel Semiconductor with Enhanced Fluorescence Emission. **ChemPlusChem**, 84(9), 1423-1431.

17. Keşan, G., Topaloğlu, B., **Özcan, E.,** Kazan, H. H., Eçik, E. T., Şenkuytu, E.,& Çoşut, B. **(2019)**. Azaindole-BODIPYs: Synthesis, fluorescent recognition of hydrogen sulfate anion and biological evaluation**. Spectrochimica Acta Part A: Molecular and Biomolecular Spectroscopy,** 213, 73-82.

18. **Özcan, E.,** & Çoşut, B. **(2018)**. Fluorescent Sensing of Cesium Ions by an Amide-Linked BODIPY Dye: Synthesis and Photophysical Properties**. ChemistrySelect**, 3(27), 7940-7944.

19. Kazan, H. H., **Özcan, E.,** Eçik, E. T., & Çoşut, B. **(2018)**. Novel 17α-Etinylestradiol-Substituted BODIPY Dyes: Synthesis, Photophysical Properties and Fluorescence Imaging Studies in Breast Cancer Cell Lines. **ChemistrySelect,** 3(11), 2962-2967.

20. **Özcan, E.,** Keşan, G., Topaloğlu, B., Eçik, E. T., Dere, A., Yakuphanoglu, F., & Çoşut, B. **(2018)**. Synthesis, photophysical, DFT and photodiode properties of subphthalocyanine–BODIPY dyads. **New Journal of Chemistry,** 42(7), 4972-4980.

21. Eçik, E. T., **Özcan, E.,** Kandemir, H., Sengul, I. F., & Çoşut, B. **(2017)**. Light harvesting systems composed of carbazole based subphthalocyanine-BODIPY enhanced with intramolecular fluorescence resonance energy transfer (FRET). **Dyes and Pigments,** 136, 441-449.

22. Tümay, S. O., Okutan, E., Sengul, I. F., **Özcan, E.,** Kandemir, H., Doruk, T., & Çoşut, B. **(2016)**. Naked-eye fluorescent sensor for Cu (II) based on indole conjugate BODIPY dye. **Polyhedron,** 117, 161-171.

23. **Özcan, E.,** Tümay, S. O., Alidağı, H. A., Çoşut, B., & Yeşilot, S. **(2016)**. A new cyclotriphosphazene appended phenanthroline derivative as a highly selective and sensitive OFF–ON fluorescent chemosensor for Al^{3+} ions. **Dyes and Pigments,** 132, 230-236.